

# Quantum repeaters: From quantum networks to the quantum internet

Koji Azuma<sup>\*</sup>

*NTT Basic Research Laboratories, NTT Corporation, 3-1 Morinosato-Wakamiya, Atsugi, Kanagawa 243-0198, Japan  
and NTT Research Center for Theoretical Quantum Information, NTT Corporation, 3-1 Morinosato-Wakamiya, Atsugi, Kanagawa 243-0198, Japan*

Sophia E. Economou<sup>†</sup>

*Department of Physics, Virginia Tech, Blacksburg, Virginia 24061, USA*

David Elkouss<sup>‡</sup>

*QuTech, Delft University of Technology, Lorentzweg 1, 2628 CJ Delft, The Netherlands  
and Networked Quantum Devices Unit, Okinawa Institute of Science and Technology Graduate University, Okinawa, Japan*

Paul Hilaire<sup>§</sup>

*Department of Physics, Virginia Tech, Blacksburg, Virginia 24061, USA  
and Quandela SAS, 10 Boulevard Thomas Gobert, 91120 Palaiseau, France*

Liang Jiang<sup>¶</sup>

*Pritzker School of Molecular Engineering, The University of Chicago, Chicago, Illinois 60637, USA*

Hoi-Kwong Lo<sup>\*\*</sup>

*Quantum Bridge Technologies, Inc., 100 College Street, Toronto, Ontario M5G 1L5, Canada,  
Department of Physics, University of Hong Kong, Pokfulam, Hong Kong,  
and Center for Quantum Information and Quantum Control,  
Department of Physics and Department of Electrical and Computer Engineering,  
University of Toronto, Toronto, Ontario M5S 3G4, Canada*

Ilan Tzitrin<sup>††</sup>

*Department of Physics, University of Toronto, Toronto, Ontario, Canada*



(published 20 December 2023)

A quantum internet is the holy grail of quantum information processing, enabling the deployment of a broad range of quantum technologies and protocols on a global scale. However, numerous challenges must be addressed before the quantum internet can become a reality. Perhaps the most crucial of these is the realization of a quantum repeater, an essential component in the long-distance transmission of quantum information. As the analog of a classical repeater, extender, or booster, the quantum repeater works to overcome loss and noise in the quantum channels constituting a quantum network. Here the conceptual frameworks and architectures for quantum repeaters, as well as the experimental progress toward their realization, are reviewed. Various near-term proposals to overcome the limits to the communication rates set by point-to-point quantum communication are also discussed. Finally, the manner in which quantum repeaters fit within the broader challenge of designing and implementing a quantum internet is overviewed.

DOI: [10.1103/RevModPhys.95.045006](https://doi.org/10.1103/RevModPhys.95.045006)

---

<sup>\*</sup>koji.azuma@ntt.com

<sup>†</sup>economou@vt.edu

<sup>‡</sup>david.elkouss@oist.jp

<sup>§</sup>paul.hilaire@quandela.com

<sup>¶</sup>liang.jiang@uchicago.edu

<sup>\*\*</sup>hklo@ece.utoronto.ca

<sup>††</sup>itzitrin@physics.utoronto.ca

## CONTENTS

I. Introduction	2	E. Multiqubit quantum registers and error correction	37
II. Preliminaries	5	F. Loss mitigation, quantum frequency conversion, and	38
A. Qubits	5	photonic source efficiency	38
B. Quantum no-cloning theorem	7	G. Progress toward memoryless quantum repeaters	39
C. Entanglement	7	H. Experimental realization of quantum networks	40
1. Definition and properties	7	1. Trusted large-scale repeater networks	40
2. Entanglement in bipartite states	7	2. Proof of concept of a quantum repeater	41
D. Entanglement in multipartite states	7	3. Untrusted quantum networks	42
1. Graph states	7	VI. Quantum Internet	42
E. Photonic encodings	9	A. Applications of the quantum internet	43
III. Quantum Repeaters	11	1. A set of representative communication tasks	43
A. Repeater primitives	11	2. Stages of the quantum internet	43
1. Quantum teleportation	11	B. Quantum networks	44
2. Entanglement swapping	11	1. Elements of a quantum network	44
3. Idealized quantum repeaters	11	2. Network architecture	45
4. Tools for error suppression	12	C. The fundamental limits of communications	45
a. Deterministic error suppression	13	over network	45
i. Quantum error correction	14	1. An abstract depiction of networks	45
ii. One-way entanglement distillation	14	2. Quantum network capacities	46
b. Probabilistic error suppression	14	3. Entanglement-based upper bounds	47
i. Quantum error detection	14	4. Application of the upper bounds to	49
ii. Heralded entanglement generation	14	linear networks	49
protocol	14	5. Capacity lower bounds via the aggregated	49
iii. Two-way entanglement distillation	14	repeater protocol	49
protocol	14	6. Computability of the network capacities	50
c. Comparison of deterministic and probabilistic	14	VII. Concluding Remarks	50
quantum error suppression	15	List of Symbols and Abbreviations	51
B. Generations of quantum repeaters	15	Acknowledgments	52
1. First-generation repeaters	16	References	52
2. Second-generation repeaters	18		
3. Third-generation repeaters	19		
4. Comparison of three generations of QRs	20		
C. All-optical repeaters	21		
1. Original all-photonic repeaters	21		
2. Other optical repeaters	23		
a. Modified all-photonic repeaters	23		
b. Repeaters based on encoded Bell	23		
c. Bosonic repeaters	23		
3. Repeater graph state generation	24		
a. General framework	24		
b. Dual-rail graph states	24		
i. Probabilistic (optical) generation	25		
ii. Deterministic (matter-based) generation	25		
c. GKP-encoded graph states	25		
d. Performance and overheads	26		
IV. Milestones: Outperforming Point-to-Point Optical	26		
Communication	27		
A. Adaptive measurement-device-independent QKD	27		
1. Memory-assisted implementation	28		
2. All-optical implementation	28		
3. Challenges	29		
B. Twin-field QKD	29		
C. Single sequential quantum repeater	30		
D. Postpairing measurement-device-independent QKD	30		
V. Experimental Progress Toward Repeaters	31		
A. Long-lived quantum memories	31		
B. Emission of photons entangled with the quantum	32		
memory	32		
C. Distant entanglement generation	33		
D. Entanglement distillation	33		
	34		

## I. INTRODUCTION

Following its rapid growth this century, the Internet has become an invaluable socioeconomic fixture, inextricable from almost all facets of day-to-day life. Access to high-speed Internet, the ability to send and receive digital information across the globe at almost the speed of light, has transformed from a luxury to a utility. However, the current Internet will not be sustainable or scalable without future innovation (Leon-Garcia and Steenstrup, 2021). It was estimated in 2022 that there are currently  $7 \times 10^9$  connected internet of things devices online. This number is projected to increase to  $2.54 \times 10^{10}$  by 2030 (Howarth, 2021). As the number of devices increases exponentially over time, the energy consumption in optical communication also grows exponentially, thereby contributing to climate change. The amount of local computing power needed to monitor and control network traffic also grows exponentially. The task of service and network management is thus becoming more and more complex. To move things forward, new concepts such as distributed intelligence and distributed trust (such as blockchain) are probably needed. On the other hand, in the longer term it is widely recognized that a quantum internet and distributed quantum computing will complement the classical Internet. The quantum internet will be provably secure and could provide exponentially more computational power and sensing capability for specific tasks.

Indeed, analogously to the Internet, a new system is steadily emerging in theoretical literature and early experiment: the quantum internet (Kimble, 2008), a means of transmitting quantum information globally. While serving a different

purpose from the classical Internet, this new paradigm may prove disruptive in its own way. We dedicate this review to the progress that has been made in designing and building the quantum internet, focusing largely on its main building block, quantum repeaters. In addition to the basic theoretical concepts required to understand the components of the quantum internet, we survey its more technical architectural requirements as well as the experimental advances toward its implementation.

While classical information is often encoded digitally (as sequences of 0s and 1s, usually represented in electronic signals), it can also be housed in quantum mechanical states, which abide by different rules. The quantum states encoding the bits 0 and 1, mathematically represented by vectors and denoted as  $|0\rangle$  and  $|1\rangle$  (the *computational-basis* states), can correspond to a variety of physical systems. Among the most popular and useful quantum information carriers is light, the state of the electromagnetic field associated with one or multiple photons.

Unlike the analogous classical states, quantum states can be superposed like waves. For instance, equal combinations of  $|0\rangle$  and  $|1\rangle$  include  $|+\rangle \equiv (1/\sqrt{2})(|0\rangle + |1\rangle)$  and  $|-\rangle \equiv (1/\sqrt{2})(|0\rangle - |1\rangle)$ , the *conjugate-basis* states. Measuring a conjugate-basis state in the computational basis collapses the superposition, resulting in  $|0\rangle$  or  $|1\rangle$  at random with equal probability, a manifestation of a more general postulate of quantum mechanics known as Born's rule. The fact that the outcome of this measurement is probabilistic rather than deterministic is predicted by Heisenberg's uncertainty principle.

In addition to quantum superposition, Born's rule, and Heisenberg's uncertainty principle, the formalism of quantum mechanics allows for subtle quantum correlations, named entanglement, to exist between remote physical systems. For instance, two distant photons that are entangled may be in a so-called singlet state  $(1/\sqrt{2})(|01\rangle - |10\rangle)$ , which can exhibit stronger-than-classical correlations upon measurement. Not only is it impossible to independently describe the state of each photon in the singlet, but when measured along any common axis the two photons always show opposite results. According to Schrödinger, entanglement is the essence of quantum theory, but it is far from a theoretical curiosity. The existence of nonclassical correlations associated with entangled states has been proven in several experiments via Bell tests (Brunner *et al.*, 2014; Miller, 2016), which led to three experimental physicists, Alain Aspect, John Clauser, and Anton Zeilinger, being awarded the Nobel Prize in Physics in 2022. Furthermore, in the last few decades researchers have shown that entanglement is a powerful resource in quantum information processing, enabling many unusual applications that are impossible or impractical with only classical resources.

The quantum technologies enabled by our continuously evolving ability to understand, generate, manipulate, and entangle delicate quantum systems are the premise behind what is commonly referred to as the second quantum revolution (Berry, 1998; Dowling and Milburn, 2003). In the first quantum revolution, which occurred in the last century, lasers and transistors (devices built upon the underlying principles of quantum mechanics) played a crucial role in global economic growth. Now we are already able to demonstrate primitives or complete protocols for the quintessential applications of quantum information: *quantum cryptography*, which is the unconditionally secure communication between parties, and

*quantum computation*, which is a computing method for exceeding the best-known scaling of certain classes of classical algorithms.

These and other quantum information tasks can be accessed remotely if embedded within a quantum internet: a global network of quantum information processors, namely, sources of quantum states, executors of quantum gates, and devices for quantum measurements (Wehner, Elkouss, and Hanson, 2018; Awschalom, 2020). Such a network can also provide secure access and enhance the performance of these applications of quantum information.

The security underlying the classical Internet is based on computational conjectures, which makes it vulnerable to hacking and eavesdropping. A quantum computer poses a threat to the contemporary cryptosystem because Shor's factoring algorithm (Shor, 1997) offers a way to break standard public-key encryption schemes, including Rivest-Shamir-Adleman (RSA), Diffie-Hellman, and elliptic curve cryptosystems within short timescales. Owing to the extensive experimental progress in quantum computing over the last few decades, its threat is now widely acknowledged by many governments and organizations (NIST, 2021). While certain classical solutions have been proposed to counter the threat, such as postquantum cryptographic systems, these are still conjectured to be secure only against quantum attacks. Indeed, three candidate postquantum cryptosystems in the National Institute of Standards and Technology (NIST) competition have already been easily cracked by a personal computer (Townsend, 2022). In reality, quantum key distribution (QKD) is the only known way to allow the unconditionally secure transmission of information, that is, a security founded in tested laws of physics and mathematical proofs (Bennett and Brassard, 1984; Ekert, 1991; Xu *et al.*, 2020; Curty, Azuma, and Lo, 2021). However, commercialized fiber-based point-to-point QKD is limited to a distance of less than 500 km, whereas satellite-to-ground QKD, which is intended to extend the communication distances, requires expensive components such as satellites and large telescopes. The quantum internet promises to significantly extend the range of QKD and other cryptographic protocols, thereby securing global communication and transactions.

In particular, a quantum internet will permit secure access to cloud-based quantum computing. Major information technology firms such as Google, IBM, Intel, Microsoft, and Amazon are actively constructing their own quantum processors on the way to universal, scalable, and fault-tolerant quantum computers. These companies are working toward this goal alongside dedicated quantum-computing start-up companies, which belong to a newly forming ecosystem of quantum startups. Companies such as IBM<sup>1</sup> have already put small-scale quantum processors online for external access (Castelvecchi, 2017). The history of conventional computers suggests that the first few years in the quantum-computing epoch will see only a few large-scale quantum computers in the world. This means that users will have to engage with the devices through classical

<sup>1</sup>This was followed by other companies (including ionQ, Quantinuum, Quandela, and Xanadu) proposing cloud accessible platforms based on either ion traps or photonics, which are potentially more promising platforms for remote access using quantum channels.

or quantum networks. With the help of innovative protocols for blind quantum computing (Broadbent, Fitzsimons, and Kashefi, 2009), a future quantum internet will allow users to submit their jobs anywhere in the world privately and securely.

Quantum networking is also a crucial ingredient in distributed quantum computing, which allows separate quantum computers to cooperate on an algorithm. At their early stages, quantum processors will be limited in size and complexity; to achieve greater computing power, they will likely need to be networked through quantum channels, with quantum information flowing between them. In this way, quantum networking is important even for short-distance communication between quantum computers. Other protocols enabled or improved by the quantum internet include quantum teleportation (Bennett *et al.*, 1993), quantum fingerprinting (Buhrman *et al.*, 2001), quantum sensing, clock synchronization (Jozsa *et al.*, 2000; Komar *et al.*, 2014), and the linking of distant optical telescopes for sharper images (Gottesman, Jennewein, and Croke, 2012).

Conceptually it is known that sending quantum information (i.e., qubits) can lower the amount of required communication in distributed information processing tasks, in comparison to sending classical information (bits). The study of the amount of required quantum communication is called quantum communication complexity (Brassard, 2003). Incidentally, the classical communication cost required in quantum information processing is also an important subject (Lo, 2000).

Building a quantum internet requires harnessing quantum states of light. Even in the distant future, the photon (or a state of multiple photons) will likely be the information carrier of choice in quantum communication, as it can function as a “flying” qubit (as opposed to matter-based qubits, which are fixed in space) while minimally interacting with its environment. By encoding information in photonic degrees of freedom, quantum information can be transmitted through optical fibers or in free space over long distances with little decoherence.

Despite the advantages of light, there is enough absorption and scattering of photons in the media where they propagate (processes that lead to optical attenuation) that makes loss the key physical hurdle in the construction of a quantum internet. In a standard single-mode optical fiber close to the standard telecommunication wavelength of 1550 nm, the attenuation is 0.2 dB/km (Fibre Optic Association, 2019). This means 1 of every 100 photons survives a journey of 100 km on average. Recently ultralow-loss (ULL) optical fibers were commercialized with a loss as low as 0.15 dB/km (Corning, 2021). These sorts of losses in optical channels yield fundamental limits to the rate at which two parties can establish a secret key with a point-to-point QKD protocol, given by the Takeoka-Guha-Wilde (TGW) bound (Takeoka, Guha, and Wilde, 2014a) and the Pirandola-Laurenza-Ottaviani-Banchi (PLOB) bound (Pirandola *et al.*, 2017), which are discussed in Secs. IV and VI.

Nevertheless, quantum networks based on such point-to-point QKD links have already been built all over the world. Examples of ground-based fiber networks include the Tokyo QKD network in Japan (Sasaki *et al.*, 2011), the Secure Communication Based on Quantum Cryptography (SECOQC) network in Europe (Peev *et al.*, 2009), the 2000 km Shanghai-Beijing network in China (Y.-A. Chen

*et al.*, 2021), and the European Quantum Communication Infrastructure network by the 27 European Union (EU) member states (European Commission, 2022). Additionally, ground-to-satellite quantum transmission has been performed over thousands of kilometers of free space. This line of research has demonstrated that long-distance quantum communication on a global length scale is feasible with current satellite technology; see Y.-A. Chen *et al.* (2021). Several theoretical papers envisioned a satellite-based quantum repeater network (Boone *et al.*, 2015; Gündoğan *et al.*, 2021; Khatri *et al.*, 2021). However, because their foundation is point-to-point QKD, existing quantum networks rely on trusted relay nodes to achieve information-theoretically secure communication. In these nodes, optical signals are measured to yield a classical output, and new optical signals are then generated and sent out. This classical output is vulnerable to hacking and eavesdropping, meaning security is achieved only if the nodes can be trusted.

The architectural challenge of a long-distance quantum network is therefore to overcome the fundamental limit of point-to-point quantum communication, achieving high-rate secure communication without using trusted relay nodes. Note that conventional signal boosters, repeaters, extenders, and amplifiers do not work for quantum signals because of the well-known quantum no-cloning theorem (Dieks, 1982; Wootters and Zurek, 1982), which states that an unknown quantum state cannot be reliably copied. However, it is still possible to combat loss and noise without cloning quantum states; this is achieved with the help of quantum repeaters.

In quantum repeater protocols, instead of sending quantum signals (photons) directly from one user to another, a sequence of intermediate nodes are set up. There certain strategies can be used to combat errors induced by losses and other forms of noise, including entanglement distillation or purification,<sup>2</sup> as well as quantum error detection and correction. While practical quantum repeaters are not possible with existing technology, research toward this goal is active and involves many different fields of inquiry. Several matter-based systems exist to facilitate their implementation, including atomic ensembles, which can function as quantum memories; quantum dots, which can be used as on-demand sources of a host of photonic states; and cavity QED, which can be used to enhance light-matter interactions. Since photons are often used as flying qubits and quantum memories often involve matter, the quantum interface between light and matter is regarded as a key ingredient in quantum repeaters.

In addition to the many subfields of physics involved in the effort to build quantum repeaters, the pursuit of a quantum internet more generally is an interdisciplinary theoretical and experimental endeavor involving mathematicians, computer scientists, and engineers. Classical tools from network topology, protocol design, information theory, and error correction, in addition to topics within quantum information such as state preparation, quantum channels and measurements, and quantum error correction, are all needed for investigations into the quantum internet.

<sup>2</sup>“Entanglement distillation” and “entanglement purification” are used to refer to the same operation; see Secs. III.A.4.a.ii and III.A.4.b.iii for the definition of the operation.

TABLE I. Related reviews.

Reference	Topic
Sangouard <i>et al.</i> (2011)	Quantum repeaters based on atomic ensembles and linear optics
Reiserer and Rempe (2015)	Cavity-based quantum networks with single atoms and optical photons
Heshami <i>et al.</i> (2016)	Quantum memories and applications
Atatüre <i>et al.</i> (2018)	Material platforms for spin-based photonic quantum technologies
Awschalom <i>et al.</i> (2018)	Quantum technologies with optically interfaced solid-state spins
Ruf <i>et al.</i> (2021)	Quantum networks based on color centers in diamond
Munro <i>et al.</i> (2015)	Primitives of quantum repeaters
Muralidharan <i>et al.</i> (2016)	Generations of quantum repeaters
Kimble (2008)	Introductory work to the quantum internet
Wehner, Elkouss, and Hanson (2018)	Developmental stages of the quantum internet
Xu <i>et al.</i> (2015)	Measurement-device-independent quantum cryptography
Xu <i>et al.</i> (2020)	Realistic QKD
Broadbent and Schaffner (2016)	Quantum cryptography beyond QKD
Fitzsimons (2017)	Blind quantum computing
Pirandola <i>et al.</i> (2020)	Advances in quantum cryptography
Azuma <i>et al.</i> (2021)	Tools for quantum network design

Several of the topics discussed in this review have been the focus of (or at least have gotten a mention in) previous reviews. We build on this body of work while discussing newer theoretical and experimental developments to keep pace with the dynamic field of quantum communication. For instance, the review by Sangouard *et al.* (2011) chiefly covered quantum repeaters whose memories were implemented with atomic ensembles, while Munro *et al.* (2015) focused on the primitives used in quantum repeaters. Munro *et al.* (2015) and Muralidharan *et al.* (2016) also categorized quantum repeater protocols into relevant generations that differ in performance and technological requirements. In our review we revisit this categorization, sorting repeaters based on the associated mechanisms for suppressing losses and errors. This gives us a more natural structure to understand newly emerging classes of repeaters, notably memoryless, error-corrected, and all-photonic repeaters, which have not been extensively featured in the literature. In addition to our discussion of full-fledged repeaters, we dedicate a portion of our review to simpler protocols believed to be sufficient to beat repeaterless bounds, an important milestone for long-distance quantum communication. Xu *et al.* (2020) already tackled some of these ideas with an approach centered around their security in realistic implementations; in our review, we focus on performance, chiefly in terms of key distribution metrics. Kimble (2008) and Wehner, Elkouss, and Hanson (2018) reviewed the progress toward the realization of the quantum internet. Notably Wehner, Elkouss, and Hanson (2018) introduced stages of development for the quantum internet, aligning with applications that grow in technological complexity. Here we continue this discussion but also introduce an information-theoretic framework to derive fundamental limits of quantum communication over a quantum network, with views that differ from Pirandola *et al.* (2020) and Azuma *et al.* (2021). In Table I, we provide a list of the previously mentioned reviews together with other works on applications of quantum communication that are not covered here.

The rest of this review is organized as follows. In Secs. II and III.A, we present the preliminaries required to understand quantum repeaters and the physics behind the quantum internet. In Sec. III.B, we overview the conceptual

frameworks of quantum repeaters and use them to organize the existing proposals. In Sec. III.C, we discuss an important class of memoryless repeaters that intersect with the latest generations of theoretical proposals. In Sec. IV, we review various near-term protocols, such as an adaptive version of measurement-device-independent QKD (Lo, Curty, and Qi, 2012) and twin-field QKD (Lucamarini *et al.*, 2018), which are regarded as milestones in the path to outperforming the PLOB bound en route to quantum repeaters. In Sec. V, we describe experimental advances toward optical-fiber-based quantum communication schemes featuring quantum repeaters. Section VI is dedicated to a discussion of the quantum internet, including the quantum and private capacities of quantum networks and upper bounds on the capacities. Some concluding remarks are provided in Sec. VII. For clarity, we present a [List of Symbols and Abbreviations](#).

## II. PRELIMINARIES

In this section, we summarize relevant background concepts, including qubits, entanglement, and possible photonic encodings. Repeater primitives, including teleportation and entanglement swapping, are left to Sec. III.A. Standard references, including Nielsen and Chuang (2010), can be used to supplement this part of the review.

### A. Qubits

A *qubit*, the quantum mechanical analog of the classical bit and the fundamental unit of quantum information, is another name for a two-dimensional complex Hilbert space. A pure state  $|\psi\rangle$  of any qubit can be written in the computational basis through

$$|\psi\rangle = a|0\rangle + b|1\rangle, \quad (1)$$

where  $a, b \in \mathbb{C}$  and  $|a|^2 + |b|^2 = 1$ . Setting  $a = 1/\sqrt{2}$  and  $b = \pm 1/\sqrt{2}$  gives the following states in the conjugate basis:

$$|\pm\rangle \equiv \frac{1}{\sqrt{2}}(|0\rangle \pm |1\rangle). \quad (2)$$

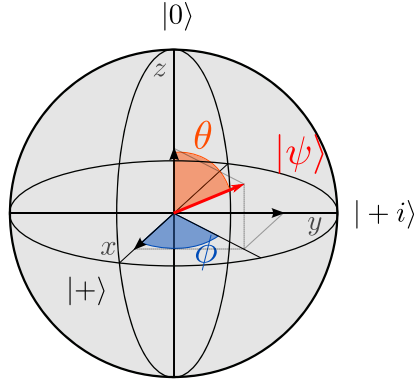


FIG. 1. Bloch sphere representation of a qubit. The  $(x, y, z)$  components of a Bloch vector (displayed as an arrow) give the expectation values of the Pauli observables  $X$ ,  $Y$ , and  $Z$ . For instance, points  $(0, 0, 1)$ ,  $(1, 0, 0)$ , and  $(0, 1, 0)$  correspond to eigenstates  $|0\rangle$ ,  $|+\rangle = (|0\rangle + |1\rangle)/\sqrt{2}$  and  $|+i\rangle = (|0\rangle + i|1\rangle)/\sqrt{2}$  of the Pauli operators  $Z$ ,  $X$ , and  $Y$  with the eigenvalue of  $+1$ , respectively.

In quantum mechanics, the global phase of a state is irrelevant; thus, one can parametrize any pure qubit through two parameters  $a = \cos(\theta/2)$  and  $b = e^{i\phi} \sin(\theta/2)$ , revealing its Bloch sphere representation (illustrated in Fig. 1), where  $\theta$  and  $\phi$  are the polar and azimuthal angles, respectively. A qubit is realized experimentally by associating it with a two-dimensional space or subspace of a physical system. Although we encounter matter (chiefly spin) qubits in this review, we are particularly interested in encodings in photonic systems, which we survey in Sec. II.E.

Interactions with the environment or preparation errors can diminish the purity of a qubit, that is, introduce classical uncertainty. In this case, we must turn to a representation of the qubit as a statistical mixture of pure quantum states. The general description of a state, which includes *mixed states*, is given by a positive operator  $\rho$  with unit trace, called a density operator. The density operator of a pure state  $|\psi\rangle$  is  $\rho = |\psi\rangle\langle\psi|$ , with  $\text{Tr}[\rho^2] = 1$ , while a density operator  $\rho$  with  $\text{Tr}[\rho^2] < 1$  describes a mixed state. In the case of a qubit, it can be written as

$$\rho = \rho_{00}|0\rangle\langle 0| + \rho_{01}|0\rangle\langle 1| + \rho_{10}|1\rangle\langle 0| + \rho_{11}|1\rangle\langle 1|, \quad (3)$$

where the populations  $\rho_{00}$  and  $\rho_{11}$  are real and add to unity ( $\rho_{00} + \rho_{11} = 1$ ), the coherences  $\rho_{01}$  and  $\rho_{10}$  are complex conjugates ( $\rho_{01} = \rho_{10}^*$ ), and  $\det[\rho] = \rho_{00}\rho_{11} - \rho_{01}\rho_{10} \geq 0$ .

Unitary transformations, operators  $U$  with  $U^\dagger U = UU^\dagger = \mathbb{1}$ , describe reversible, probability-preserving operations on qubits, i.e., quantum gates. The Pauli gates are defined through

$$X = |0\rangle\langle 1| + |1\rangle\langle 0|, \quad (4)$$

$$Y = -i|0\rangle\langle 1| + i|1\rangle\langle 0|, \quad (5)$$

$$Z = |0\rangle\langle 0| - |1\rangle\langle 1|. \quad (6)$$

$Z$ ,  $X$ , and  $Y$  effect a phase flip, a bit flip, and a combination of the two on the qubit, respectively. A unitary  $U$  is a Clifford

gate if it maps any Pauli gate  $P$  onto a Pauli gate under conjugation; that is,  $UPU^\dagger$  is also a Pauli gate. An example of a non-Pauli Clifford gate is the Hadamard gate, which is defined by

$$H = \frac{1}{\sqrt{2}}(|0\rangle\langle 0| + |0\rangle\langle 1| + |1\rangle\langle 0| - |1\rangle\langle 1|). \quad (7)$$

An example of a non-Clifford gate is the  $\pi/8$  or  $T$  gate, which is given through

$$T = |0\rangle\langle 0| + e^{i\pi/4}|1\rangle\langle 1|. \quad (8)$$

The previous discussion is generalizable to systems of multiple qubits by taking tensor products; see Sec. II.C.

A measurement process on a quantum system in a state  $\rho$  is generally described by a set of Kraus (linear) operators  $\{M_i\}_i$  satisfying  $M_i^\dagger M_i = \mathbb{1}$ . Performing the associated measurement results in an outcome  $i$  with probability  $p_i = \text{Tr}[M_i^\dagger M_i \rho]$  and leaves the state in  $M_i \rho M_i^\dagger / p_i$ . This is a formalization and generalization of Born's rule. For the particular case of a destructive Pauli measurement on a qubit, we can associate  $M_0 = \langle v_0 |$  and  $M_1 = \langle v_1 |$  with the eigenstates  $|v_0\rangle$  and  $|v_1\rangle$  of the corresponding operator;  $Z$ -basis measurements (corresponding to the Pauli  $Z$ ) are specified by the Kraus operators  $\{\langle 0 |, \langle 1 |\}$ , while  $X$ -basis measurements (corresponding to the Pauli  $X$ ) are specified by the Kraus operators  $\{\langle + |, \langle - |\}$ .

We also consider a quantum channel  $\mathcal{N}$  that deterministically converts a given state  $\rho$  into a state  $\sigma$ . This kind of transformation is useful for describing the actions of noise and transmission channels on quantum systems. Any quantum channel has an operator-sum representation  $\sigma = \mathcal{N}(\rho) = \sum_i M_i \rho M_i^\dagger$  specified by a set of Kraus operators  $\{M_i\}_i$ . Another representation is

$$\sigma_{A'} = \mathcal{N}_{A \rightarrow A'}(\rho_A) = \text{Tr}_{E'}[U_{AE}(\rho_A \otimes |0\rangle\langle 0|_E)U_{AE}^\dagger], \quad (9)$$

where  $U_{AE}$  is a unitary operator acting on Hilbert space  $\mathcal{H}_A \otimes \mathcal{H}_E = \mathcal{H}_{A'} \otimes \mathcal{H}_{E'}$  and  $|0\rangle_E$  is a state of an auxiliary system (environment)  $E$ . The map  $\mathcal{N}$  must be completely positive and trace preserving (CPTP).

Three examples of common qubit errors described by channels are phase-flip, bit-flip, and depolarizing noise, written as

$$\mathcal{N}(\rho) = (1 - p)\rho + pZ\rho Z, \quad (10)$$

$$\mathcal{N}(\rho) = (1 - p)\rho + pX\rho X, \quad (11)$$

$$\mathcal{N}(\rho) = (1 - p)\rho + \frac{p}{3}(X\rho X + Y\rho Y + Z\rho Z), \quad (12)$$

respectively, where  $0 \leq p \leq 1$  corresponds to an error probability or channel strength. A pure-loss bosonic channel is written by using a unitary operator  $U_{AE}$  defined as

$$U_{AE}a_A U_{AE}^\dagger = \sqrt{\eta}a_{A'} + \sqrt{1 - \eta}a_{E'} \quad (13)$$

in the Heisenberg representation. In Eq. (13)  $a_x$  is the annihilation operator on bosonic system  $x$  and  $0 \leq \eta \leq 1$  is the transmittance of the channel. The pure-loss bosonic channel is described as the CPTP map that is obtained by regarding  $U_{AE}$  of Eq. (9) as the one defined in Eq. (13) and  $|0\rangle_E$  of Eq. (9) as the vacuum state of the bosonic system  $E$ . The pure-loss bosonic channel is used as a model for an optical fiber: in this case, the transmittance  $\eta$  is related to the length  $L$  of the fiber through  $\eta = e^{-L/L_{\text{att}}}$ , with the constant  $L_{\text{att}}$  denoting the attenuation length.

## B. Quantum no-cloning theorem

The quantum *no-cloning theorem* (Dieks, 1982; Wootters and Zurek, 1982) entails that it is impossible to create a copy of unknown quantum states. More precisely, given an unknown state  $|\psi\rangle_A$ , the theorem states that there is no deterministic quantum operation that can copy  $|\psi\rangle_A$  onto system  $B$  to obtain  $|\psi\rangle_A \otimes |\psi\rangle_B$ . Originally demonstrated for pure states, the no-cloning theorem was later extended to mixed states through the *no-broadcasting theorem* (Barnum *et al.*, 1996). This no-go theorem has profound implications (helpful and unhelpful) for quantum information technologies. While it is at the core of the security of quantum key distribution (Bennett, Brassard, and Mermin, 1992; Koashi and Imoto, 1998, 2002), it also precludes building quantum repeaters analogously to classical signal extenders and, furthermore, creates challenges in the design and performance of quantum error-correcting codes. For example, the no-cloning theorem makes it impossible to use a classical-like repetition code to correct for errors acting on quantum states and implies an upper bound of 50% on the loss that any quantum error-correcting code can tolerate. This directly impacts the performance of quantum repeater protocols based on quantum error correction, as addressed in Sec. III.A.4.

## C. Entanglement

Here we present the formal definition of entanglement and introduce several important classes of entangled states.

### 1. Definition and properties

Entanglement [per Schrödinger, a defining feature of quantum theory (Schrödinger, 1935)] refers to the impossibility of describing certain composite quantum states through independent specifications of their constituents. The existence of entanglement, as guaranteed by the formalism and postulates of quantum theory and confirmed by many experiments, has profound physical and metaphysical repercussions, as exemplified by Einstein, Podolsky, and Rosen (EPR) (Einstein, Podolsky, and Rosen, 1935) and by Bell (Bell, 1964), and since then by numerous physicists investigating its repercussions on increasingly rigorous footing. There are several equivalent formulations of entanglement; see Horodecki *et al.* (2009). A useful formulation for our purpose is the view of entanglement as a resource for quantum information tasks. Entanglement plays a central role in virtually every primitive and application of quantum information; for us, its most relevant uses are for the protocols we describe in Sec. III.A: quantum teleportation and entanglement swapping, entanglement purification or

distillation, and quantum error correction, all of which underlie quantum repeaters. As a nontrivial resource with respect to local operations and classical communication (LOCC), entanglement cannot be increased by performing local operations (including local quantum gates and measurements), classical communication (including increase of classical correlation and adaptive schemes based on classical outputs from other parties), or a combination of the two. One can establish quantum entanglement by interacting systems via coupling Hamiltonians, physically distributing entangled states between parties (such as by sending photons over fiber channels), or performing collective measurements of observables from different parties. The entanglement generation process depends on the details of the physical system, as discussed in Sec. V.

## 2. Entanglement in bipartite states

The Hilbert space  $\mathcal{H}$  of a bipartite system is the tensor product of the subsystem spaces  $\mathcal{H} = \mathcal{H}_A \otimes \mathcal{H}_B$ . A separable bipartite pure state is a tensor product of pure states in  $\mathcal{H}_A$  and  $\mathcal{H}_B$ ,

$$|\Psi\rangle_{AB} = |\varphi\rangle_A \otimes |\phi\rangle_B \\ =: |\varphi\rangle_A |\phi\rangle_B =: |\varphi, \phi\rangle_{AB} =: |\varphi\phi\rangle_{AB}, \quad (14)$$

with reduced density operators  $\Psi_A := \text{Tr}_B[|\Psi\rangle\langle\Psi|_{AB}] = |\varphi\rangle\langle\varphi|_A$  on subsystem  $A$  and  $\Psi_B := \text{Tr}_A[|\Psi\rangle\langle\Psi|_{AB}] = |\phi\rangle\langle\phi|_B$  on subsystem  $B$ , obtained by tracing out the nonsubscripted system. By contrast, an entangled bipartite pure state cannot be described as a product of states from the individual subsystems; that is, it cannot be written in the form of Eq. (14).

Generally we can write any bipartite pure state as

$$|\Psi\rangle_{AB} = \sum_{i,j} c_{ij} |i\rangle_A \otimes |j\rangle_B, \quad (15)$$

where  $c_{ij}$  are complex numbers with  $\sum_{i,j} |c_{ij}|^2 = 1$ ,  $\{|i\rangle_A\}$ , and  $\{|j\rangle_B\}$  are orthonormal bases of the two subsystems. With the Schmidt decomposition, we can find convenient orthogonal bases  $\{|v_i\rangle_A\}$  and  $\{|w_j\rangle_B\}$  for the two subsystems such that the bipartite pure state can be expressed in a standard form with a single index,

$$|\Psi\rangle_{AB} = \sum_{j=1}^r \sqrt{p_j} |v_j\rangle_A \otimes |w_j\rangle_B, \quad (16)$$

where  $p_j > 0$  for  $j = 1, \dots, r$  and  $\sum_{j=1}^r p_j = 1$ . The integer  $r$  is called the Schmidt rank. The reduced density operators for the two subsystems are  $\Psi_A = \text{Tr}_B[|\Psi\rangle\langle\Psi|_{AB}] = \sum_{j=1}^r p_j |v_j\rangle\langle v_j|_A$  and  $\Psi_B = \text{Tr}_A[|\Psi\rangle\langle\Psi|_{AB}] = \sum_{j=1}^r p_j |w_j\rangle\langle w_j|_B$ . For  $r = 1$ , Eq. (16) reduces to a separable bipartite pure state. For  $r \geq 2$ , the state  $|\Psi\rangle_{AB}$  is entangled.

In the setting of mixed states, the definition of separability must be changed to include classical mixtures of tensor product states,

$$\rho_{AB} = \sum_j p_j \sigma_A^{(j)} \otimes \tau_B^{(j)}, \quad (17)$$

where  $\{p_j\}$  is a probability distribution and  $\sigma_A^{(j)}$  and  $\tau_B^{(j)}$  are density operators. Since  $\rho_{AB}$  can freely be generated by Alice and Bob with LOCC, the state must include only classical correlations and no entanglement. This definition includes pure-state separability as a special case; therefore, one can say that any state that cannot be written in the form of Eq. (17) (that is, as a convex combination of product states) is entangled.

Quantifying the degree of entanglement in a mixed quantum state, finding an entanglement *measure* or *monotone* that does not confuse entanglement for classical correlations and does not increase over arbitrary LOCC operations, is a difficult problem. For this purpose there is at one's disposal the Schmidt rank, concurrence, negativity, or various entropic functions of the density operator, such as the von Neumann entropy (Bennett, Bernstein *et al.*, 1996). For mixed states of two qubits, one can unambiguously compute the entanglement using one of the aforementioned tools, the concurrence (Wootters, 1998). However, characterizing entanglement for general mixed states of higher dimensions is still an important and active area of research; see Plenio and Virmani (2007) and Horodecki *et al.* (2009) for detailed discussions of the difficulties of quantifying entanglement and of existing entanglement measures.

The simplest example of useful entanglement for quantum networks is that between two qubits associated with two parties, with  $\mathcal{H}_A = \text{span}\{|0\rangle_A, |1\rangle_A\}$  and  $\mathcal{H}_B = \text{span}\{|0\rangle_B, |1\rangle_B\}$ . The space  $\mathcal{H}$  is then spanned by the four orthogonal Bell states or EPR pairs:

$$\begin{aligned} |\Phi^\pm\rangle_{AB} &= \frac{1}{\sqrt{2}}(|0\rangle_A|0\rangle_B \pm |1\rangle_A|1\rangle_B), \\ |\Psi^\pm\rangle_{AB} &= \frac{1}{\sqrt{2}}(|0\rangle_A|1\rangle_B \pm |1\rangle_A|0\rangle_B). \end{aligned} \quad (18)$$

These four Bell states are equivalent up to Pauli gates:  $|\Phi^+\rangle_{AB} = Z_B|\Phi^-\rangle_{AB} = iY_B|\Psi^-\rangle_{AB} = X_B|\Psi^+\rangle_{AB}$ . Tracing out one of the qubits from any Bell state leaves the remaining qubit in a maximally mixed state, which implies that the Bell states are maximally entangled. We often use the Bell state to calibrate the amount of entanglement shared between two parties; each Bell state counts as one entangled bit or *ebit* of entanglement, which can be used to teleport one qubit of quantum information (Bennett *et al.*, 1993); see Sec. III.A.1 for a description of quantum teleportation.

#### D. Entanglement in multipartite states

We can generalize the definitions of entanglement in Sec. II.C to systems with more than two parties. In this setting, there are several notions of separability. For example, a fully separable state defined over multiple subsystems ( $A, B, C, \dots$ ) can be written as a convex combination of product states

$$\rho_{ABC\dots} = \sum_j p_j \sigma_A^{(j)} \otimes \tau_B^{(j)} \otimes \gamma_C^{(j)} \otimes \dots \quad (19)$$

As in the bipartite case, a multipartite state is entangled when the state cannot be written in the form of Eq. (19).

Two well-known families of entangled states of  $M > 2$  parties are the Greenberger-Horne-Zeilinger (GHZ) state

$$\begin{aligned} |\text{GHZ}_M\rangle &= \frac{1}{\sqrt{2}}(\overbrace{|00\dots 0\rangle}^M + \overbrace{|11\dots 1\rangle}^M) \\ &= \frac{1}{\sqrt{2}}(|0\rangle^{\otimes M} + |1\rangle^{\otimes M}) \end{aligned} \quad (20)$$

and the *W* state

$$|W_M\rangle = \frac{1}{\sqrt{M}}(|100\dots 0\rangle + |010\dots 0\rangle + \dots + |000\dots 1\rangle). \quad (21)$$

The GHZ and *W* states cannot be transformed into each other through LOCC, thereby representing two different kinds of entanglement for three or more parties (Dür, Vidal, and Cirac, 2000); see Horodecki *et al.* (2009).

A broad and useful class of multipartite entangled states are the cluster states or, more generally, the graph states, which we now describe.

#### 1. Graph states

A graph state  $|G\rangle$  is a multipartite entangled state associated with an undirected graph  $G = (V, E)$ , with  $V$  a set of vertices and  $E$  a collection of undirected edges  $\{ij\} = \{ji\}$  for  $i, j \in V$ .  $|G\rangle$  is then defined through

$$|G\rangle \equiv \prod_{e \in E} C_e^Z \left( \bigotimes_{v \in V} |+\rangle_v \right), \quad (22)$$

where the controlled-Z (cz or controlled-phase) gate is a Clifford gate defined on qubits  $i$  and  $j$  through

$$C_{ij}^Z = |0\rangle\langle 0|_i \otimes \mathbb{1}_j + |1\rangle\langle 1|_i \otimes Z_j. \quad (23)$$

$C_{ij}^Z$  is symmetric over  $i \leftrightarrow j$ , i.e.,  $C_{ij}^Z = C_{ji}^Z = C_{\{ij\}}^Z$ , and  $C_{ij}^Z$  and  $C_{i'j'}^Z$  commute for any  $i, j, i',$  and  $j'$ .

A cluster state is a special kind of graph state whose underlying graph  $G$  forms a lattice. Performing single-qubit adaptive measurements on a cluster state allow for the execution of a measurement-based quantum computation (MBQC) (Raussendorf and Briegel, 2001). Whereas one-dimensional (linear) cluster states allow for universal operations on a single qubit, a cluster state of a minimum of two dimensions is necessary to implement a universal set of multiqubit gates, and additional dimensions are normally needed for error correction and fault tolerance (Raussendorf, Harrington, and Goyal, 2006, 2007; Raussendorf and Harrington, 2007); see Terhal (2015).

An alternative specification of the graph state is given by the *stabilizer formalism*:  $|G\rangle$  is the unique simultaneous eigenstate of all the stabilizer generator operators in  $\mathcal{S} = \{X_a \otimes Z_{N_a} | a \in V\}$  of commuting operators, where  $Z_{N_a} := \bigotimes_{v \in N_a} Z_v$  and  $N_a$  is the set of all the vertices adjacent to vertex  $a \in V$  in the graph  $G$ . We say that  $|G\rangle$  is stabilized by  $\mathcal{S}$ , making it a stabilizer state analyzable within the stabilizer formalism (Gottesman, 1997).

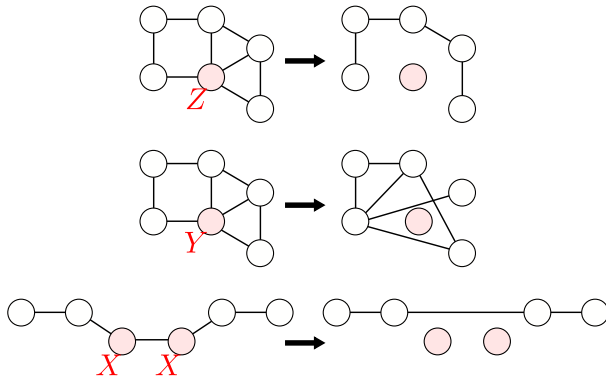


FIG. 2. Graphical rules for operations on graph states. The effects of Pauli operations on the connections in the graph states are shown.

A thorough and important review of discrete-variable qubit graph states was given by Hein, Eisert, and Briegel (2004) and Hein *et al.* (2006). We now distill their basic properties, which are illustrated in Fig. 2.

- Application of local Clifford gates to a graph state is equivalent to that of a sequence of local complementations on the underlying graph (where a local complement of a graph  $G$  at a node  $a \in V$  is obtained by complementing the subgraph of  $G$  induced by the neighborhood  $N_a$  and leaving the rest of the graph unchanged).
- Pauli Z measurement on a node decouples the node and breaks off its incident edges.
- Pauli Y measurement on a node takes the local complementation at the node and decouples the node.
- Pauli X measurement on two neighboring qubits in a linear-cluster state decouples them but connects their other neighbors with an edge.
- The entanglement in a connected graph state is *localizable*, meaning that it is possible to project any two qubits in the graph into a Bell pair by performing single-qubit (in particular, Pauli Z or X) measurements on the other qubits.

The concept of the graph state can be generalized to continuous-variable (CV) bosonic systems, describable in the phase space formalism of the quantum harmonic oscillator with position operator  $q$  and momentum operator  $p$  such that  $[q, p] = i (\hbar = 1)$ . In this case, there is a wealth of possible

encodings to choose from. For example, for a Gaussian graph state (Menicucci *et al.*, 2006) the plus state becomes the zero-momentum eigenstate of the momentum operator  $p$ ,

$$|+\rangle \rightarrow |p = 0\rangle, \quad (24)$$

while for the Gottesman-Kitaev-Preskill (GKP) encoding (Gottesman, Kitaev, and Preskill, 2000), discussed in Sec. II.E, the plus state becomes

$$|+\rangle \rightarrow |+_{\text{GKP}}\rangle = \sum_{n=-\infty}^{\infty} |p = 2n\sqrt{\pi}\rangle, \quad (25)$$

where  $|p = 2n\sqrt{\pi}\rangle$  is the eigenstate corresponding to the eigenvalue  $2n\sqrt{\pi}$  of the momentum operator  $p$ . For both of these CV encodings, the CZ gate can be written as

$$C_{ij}^Z \rightarrow e^{i(q_i \otimes q_j)}, \quad (26)$$

with the position operator  $q_i$  for bosonic system  $i$ . Clifford operations on these encodings correspond to certain Gaussian operations in phase space, which are composed of squeezing, displacements, and rotations. In either case, one uses finitely squeezed approximations of these states in practice. We give more details on these states in our discussions of photonic encodings in Sec. II.E and bosonic repeaters in Sec. III.C.2.c.

## E. Photonic encodings

There are several degrees of freedom that one can exploit when encoding quantum information into light. Each one has its advantages and challenges. In this section we review some well-known photonic encodings, summarizing some of this information in Table II.

There are a few ways to categorize photonic encodings. One is through the cardinality of the used Hilbert space. The state space of discrete-variable (DV) encodings is spanned by a finite number of orthogonal (more generally, linearly independent) states, whereas continuous-variable (CV) or bosonic encodings are spanned by infinitely (possibly countably) orthogonal (more generally, linearly independent) states. However, the line between the two kinds of encodings may not always be clear: DV systems can be viewed as finite

TABLE II. Descriptions of selected photonic encodings, including the associated gate implementations. LO here means linear optics.

	Single-rail encodings			Dual-rail encodings		
	Fock state	Coherent or cat	GKP	Time bin	Path	Polarization
Cardinality	DV	CV	CV	DV	DV	DV
Physical basis	Vacuum, single photon	Coherent states: $ \pm\alpha\rangle$	GKP 0 and 1: Eqs. (27) and (28)	Orthogonal temporal modes	Orthogonal spatial modes	Orthogonal polarizations
Entanglement w/ LO	Deterministic	Deterministic	Deterministic	Probabilistic	Probabilistic	Probabilistic
Single-mode Clifford gates w/ LO	Probabilistic	Probabilistic	Deterministic (w/ squeezing)	Deterministic	Deterministic	Deterministic
Single-mode non-Clifford gates w/ LO	Probabilistic	Probabilistic	Probabilistic	Deterministic	Deterministic	Deterministic

subspaces of CV spaces, and our interest in CV systems may chiefly be to identify two-dimensional qubit subspaces. Furthermore, in practice various imperfections and interactions with the environment increase the effective dimensionality of DV systems.

Another characterization of photonic encodings is in the number of “rails.” In the more restrictive definition, a single-rail qubit is associated with the presence or absence of a single photon in an optical (spatial or temporal) mode. More broadly, however, one can view single-rail encodings as those where each state, including states of multiple photons, occupies a single optical mode. On the other hand, a dual-rail qubit is associated with the presence of a single photon in one of two orthogonal modes. For a single-rail encoding, it is possible to generate entanglement deterministically with linear-optical resources, while linear-optical entangling operations are necessarily probabilistic in dual-rail encodings. On the other hand, single-qubit rotations for certain single-rail encoded qubits may necessitate nonlinearity (because the encoding can be based on a superposition of different photon-number states, i.e., energy eigenstates), while there are dual-rail encodings where arbitrary single-qubit rotations are possible only with linear-optical elements. See Kok *et al.* (2007).

The following photonic encodings have frequently been considered within quantum information protocols:

- *Time bin.* A photon takes one of two paths for interferometers of different lengths. Specifically,  $|0\rangle$  is associated with one path and  $|1\rangle$  is associated with the other. This encoding is suited for fiber-based communication, as it is unaffected by birefringence in optical fibers; however, it is difficult for two time-bin qubits to interact, making the encoding preferred for quantum communication over computation.
- *Polarization.* As a dual-rail encoding, a qubit is encoded into the polarization states of a single photon. Conventionally  $|0\rangle$  is associated with a horizontally polarized photon, and  $|1\rangle$  is associated with a vertically polarized photon. All single-qubit gates can be performed deterministically with wave plates and phase shifters, while linear-optical entangling gates are probabilistic, requiring beam splitters, wave plates, measurements, and postselection. As an example of a two-qubit operation, an implementation of the Bell measurement is given in Fig. 3(a). This encoding prefers free-space over fiber-based communication, as it is vulnerable to birefringence within optical fibers.
- *Path.* Computational-basis states are associated with orthogonal spatial modes. All single-qubit gates can be performed deterministically with beam splitters and phase shifters; as with the polarization encoding, entangling gates with linear-optical resources are probabilistic, requiring beam splitters, phase shifters, measurements, and postselection. As with time-bin encoding, path-encoded photons prefer fiber-based over free-space communication.
- *Fock.* A qubit is encoded into the Hilbert subspace of a single mode spanned by the vacuum state  $|0\rangle$  and the single-photon state  $|1\rangle$ , which corresponds to a single-rail qubit. With a phase shifter, we can rotate its Bloch vector along the Z axis freely, but we cannot do so along

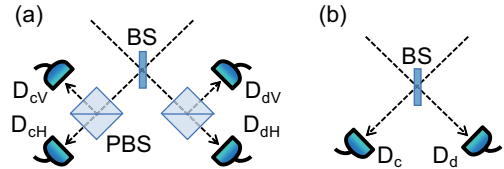


FIG. 3. Examples of implementations of Bell measurements. (a) Bell measurement for polarization-encoded qubits, spanned by horizontally and vertically polarized single-photon states  $|H\rangle$  and  $|V\rangle$ . This is implemented using the application of a 50:50 beam splitter (BS) on optical modes, followed by a polarization beam splitter (PBS) on each of the two output modes and then by photon counting at all the output modes. Clicks in detectors  $D_{ch}$  and  $D_{cv}$  or in  $D_{dH}$  and  $D_{dV}$  project the received pair of the qubits into the Bell state  $|\Psi^+\rangle = (|H\rangle|V\rangle + |V\rangle|H\rangle)/\sqrt{2}$ , while clicks in detectors  $D_{ch}$  and  $D_{dV}$  or in  $D_{cv}$  and  $D_{dH}$  project the received pair of the qubits into the Bell state  $|\Psi^-\rangle = (|H\rangle|V\rangle - |V\rangle|H\rangle)/\sqrt{2}$ . Notice that this Bell measurement can succeed only when the input two optical pulses have two or more photons in total. (b) Bell measurement for Fock-encoded qubits, spanned by the vacuum state  $|0\rangle$  and the single-photon state  $|1\rangle$ . This is implemented by the application of a 50:50 BS on optical modes, followed by photon counting at the output modes. A click in the detector  $D_c$  (or  $D_d$ ) at the constructive-interference (destructive-interference) mode projects the received pair of the qubits into the Bell state  $|\Psi^+\rangle = (|0\rangle|1\rangle + |1\rangle|0\rangle)/\sqrt{2}$  [ $|\Psi^-\rangle = (|0\rangle|1\rangle - |1\rangle|0\rangle)/\sqrt{2}$ ]. Both implementations can distinguish  $|\Psi^\pm\rangle$  from the other states only, and the success probabilities are thus 1/2 even in the ideal cases.

the  $X$  axis since  $|0\rangle$  and  $|1\rangle$  have different energies. However, a Bell state [such as  $|\Psi^\pm\rangle = (|01\rangle \pm |10\rangle)/\sqrt{2}$ ] can be deterministically obtained with a single photon incident on a 50:50 beam splitter. However, we can discriminate only Bell states  $|\Psi^\pm\rangle$  from the others, with a 50:50 beam splitter followed by two photon detectors; see Fig. 3(b). This encoding is sensitive to phase drifts in a transmission channel, and thus it is preferred in free-space over fiber-based communication.

- *Coherent or cat.* A qubit is encoded in the Hilbert subspace of a single mode spanned by coherent states  $|\alpha\rangle$  and  $|-\alpha\rangle$ , with  $\alpha > 0$ , corresponding to a single-rail qubit. The qubit basis states  $|\pm\rangle$  are associated with cat states  $(|\alpha\rangle \pm |-\alpha\rangle)/2\sqrt{p_\pm}$ , with  $p_\pm := (1 \pm \langle -\alpha|\alpha\rangle)/2$ . They are distinguished using a photon-number-resolving detector. This encoding is also sensitive to phase drifts in a transmission channel, and thus it prefers free-space over fiber-based communication.
- *GKP.* The computational-basis states are coherent superpositions of infinitely many regularly spaced position eigenfunctions (i.e., infinitely squeezed states):

$$|0_{GKP}\rangle = \sum_{n=-\infty}^{\infty} |q = 2n\sqrt{\pi}\rangle, \quad (27)$$

$$|1_{GKP}\rangle = \sum_{n=-\infty}^{\infty} |q = (2n+1)\sqrt{\pi}\rangle, \quad (28)$$

where  $|q = n\sqrt{\pi}\rangle$  is the eigenstate corresponding to the eigenvalue  $n\sqrt{\pi}$  of the position operator  $q$ . In realistic

implementations, these unphysical infinite-energy states are replaced by their normalizable, finitely squeezed counterparts. All single-qubit (many-qubit) Clifford gates, including entangling gates, are implementable deterministically through single-mode (multimode) Gaussian operations. Non-Clifford gates can be implemented with the help of ancillary states and gate teleportation, i.e., they are deterministic only conditional to the availability of the ancillae.

The aforementioned encoding schemes are “digital” because they encode a DV quantum system with a finite-dimensional Hilbert subspace of photonic modes, even if they are combined (Kwiat, 1997; Barreiro *et al.*, 2005). In contrast, we can also use the photonic modes for “analog” encoding, to store a CV analog quantum system with an infinite-dimensional Hilbert space. For example, we can encode continuous-variable quantum information using squeezed states, which can be measured via homodyne and heterodyne detectors with a continuous-variable output. For quantum communication, the continuous-variable output can be used to generate secure secret keys (Grosshans and Cerf, 2004).

One major challenge in using CV encodings for quantum repeaters is the suppression of loss errors. Because of the theorem stating that Gaussian operations are of no use for protecting Gaussian states against Gaussian errors (including loss errors) (Niset, Fiurášek, and Cerf, 2009), we have to introduce non-Gaussian operations [for instance, “quantum scissors” to truncate the number-state expansion (Pegg, Phillips, and Barnett, 1998)] or non-Gaussian ancillary resources [for instance, GKP stabilizer codes to encode an oscillator in many oscillators assisted by GKP ancillae (Noh, Girvin, and Jiang, 2020)] to overcome loss errors.

### III. QUANTUM REPEATERS

This section begins with a review of primitives for quantum repeaters. This is followed by an explanation of quantum repeater protocols through a conceptual classification based on methods to suppress loss and operation errors. We also review all-optical implementations of quantum repeaters.

#### A. Repeater primitives

Here we review quantum teleportation and entanglement swapping as primitives for quantum repeaters. We also summarize various tools for error suppression that are necessary for quantum repeaters.

##### 1. Quantum teleportation

Quantum teleportation is a procedure for transferring quantum information from a sender to a distant receiver without transferring the physical system in which it is encoded (Bennett *et al.*, 1993). To accomplish this, the two parties must establish a classical communication link and preshare a maximally entangled state. The teleportation consists of two steps. First, the sender locally performs a joint measurement between the state that she wants to transfer and her portion of the preshared entangled state. Second, she communicates the measurement outcome via the classical channel to the receiver, who must apply a local unitary operation to his

quantum state to recover the original state. There are quantum teleportation protocols for qudits<sup>3</sup> (Werner, 2001) and CV systems (Braunstein and Kimble, 1998); here we focus on qubits to illustrate the concept.

Suppose that Alice has a qubit in an arbitrary state  $|\psi\rangle_{A_1}$  that she wants to send to Bob. Suppose also that she has already shared a Bell state  $|\Phi^+\rangle_{A_2B}$  with Bob from Eq. (18). By performing a Bell-state measurement on her two qubits  $A_1$  and  $A_2$ , that is, a projection onto one of the Bell states of Eq. (18), she will project Bob’s qubit onto some state. This state of Bob’s qubit  $B$  is equal to the initial state  $|\psi\rangle$  up to local rotations that are determined by the random outcome of Alice’s measurement as

$$\begin{aligned} |\Phi^+\rangle_{A_1A_2} &\rightarrow |\psi\rangle_B, \\ |\Phi^-\rangle_{A_1A_2} &\rightarrow Z_B|\psi\rangle_B, \\ |\Psi^+\rangle_{A_1A_2} &\rightarrow X_B|\psi\rangle_B, \\ |\Psi^-\rangle_{A_1A_2} &\rightarrow Z_BX_B|\psi\rangle_B. \end{aligned} \quad (29)$$

To conclude the teleportation, Alice must transfer the outcome of her measurement to Bob through a classical channel so that Bob can undo the Pauli by-product and recover the original state  $|\psi\rangle$ . Even though Bob has a state that is locally equivalent to Alice’s immediately after the Bell measurement, his ignorance at that point of the precise Pauli gate he has to apply means that Alice cannot transfer quantum information instantly to Bob. The quantum teleportation protocol therefore crucially needs classical communication, making it limited by the speed of light. This impossibility of faster-than-light communication assisted by quantum entanglement is known as the no-signaling principle (Eberhard and Ross, 1989).

Quantum teleportation allows a sender to send arbitrary quantum information encoded into a qubit by consuming an ebit (preshared with the receiver) and by sending 2 bits of classical information to the receiver. This implies that distributing ebits efficiently or quickly using a quantum communication network is a fundamental question.

##### 2. Entanglement swapping

Entanglement swapping (Zukowski *et al.*, 1993) can be thought of as an extension of quantum teleportation where Alice and Bob each share a two-qubit maximally entangled state with Charlie:  $|\Phi^+\rangle_{AC_1}$  and  $|\Phi^+\rangle_{C_2B}$ . After Charlie performs a Bell measurement on his systems  $C_1$  and  $C_2$ , Alice’s and Bob’s qubits end up in one of the four Bell states, depending on the measurement outcome, as

$$\begin{aligned} |\Phi^+\rangle_{C_1C_2} &\rightarrow |\Phi^+\rangle_{AB}, \\ |\Phi^-\rangle_{C_1C_2} &\rightarrow |\Phi^-\rangle_{AB} = Z_B|\Phi^+\rangle_{AB}, \\ |\Psi^+\rangle_{C_1C_2} &\rightarrow |\Psi^+\rangle_{AB} = X_B|\Phi^+\rangle_{AB}, \\ |\Psi^-\rangle_{C_1C_2} &\rightarrow |\Psi^-\rangle_{AB} = Z_BX_B|\Phi^+\rangle_{AB}. \end{aligned} \quad (30)$$

Although their qubits have not directly interacted, Alice and Bob have established a maximally entangled state. This is

<sup>3</sup>Recently such high-dimensional teleportation is refocused in the context of quantum networks (Bacco *et al.*, 2021) thanks to experimental progress (Luo *et al.*, 2019; Hu *et al.*, 2020).

particularly useful in the context of quantum communication, as it means that entanglement can be propagated through a quantum network even between stationary nodes. Indeed, entanglement swapping is the crux of quantum repeater schemes based on heralded entanglement generation<sup>4</sup>; see Secs. III.A.3, III.B.1, and III.B.2.

### 3. Idealized quantum repeaters

As shown in the quantum teleportation protocol of Sec. III.A.1, once Alice and Bob share a Bell pair (an ebit), Alice can send an unknown state of a qubit to Bob by LOCC; i.e., they can achieve quantum communication. Thus, the challenge of quantum communication reduces mainly to how to distribute a Bell pair between Alice and Bob in practice. Flying qubits (photons) appear to be the medium of choice for this. However, the transmittance  $\eta$  of an optical fiber (and hence the ratio of photons sent to photons received) decreases exponentially with its length  $L$  according to  $\eta = e^{-L/L_{\text{att}}}$  of Eq. (13). In fact, the transmittance decreases as though it is multiplied by 0.1 every 50 km in the case of typical optical fibers with an attenuation length  $L_{\text{att}} = 22$  km [and even the quantum and private capacities of the pure-loss bosonic channel (13) are now known to both be described by  $-\log_2(1 - \eta)$  ( $\approx \eta$  for  $\eta \ll 1$ ) (Pirandola *et al.*, 2017); see Secs. IV and VI]. Hence, simply linking Alice and Bob directly with an optical fiber is not enough to achieve efficient quantum communication, especially if they are far apart.<sup>5</sup>

Here we introduce a simple example to show how a quantum repeater protocol overcomes such an exponential increase of photon loss with the length of an optical fiber. The example is based on heralded entanglement generation and entanglement swapping; it is a simplified protocol designed to capture the main concept of the first-generation quantum repeater protocols (Briegel *et al.*, 1998; Duan *et al.*, 2001; Sangouard *et al.*, 2011), which appears in Sec. III.B.1. The technique is based on a concatenation allowed by the entanglement swapping of Sec. III.A.2 that is similar to the Duan-Lukin-Cirac-Zoller (DLCZ) protocol (Duan *et al.*, 2001). For simplicity, we assume that the fiber attenuation is the only error and that all other operations are perfect.

Suppose that we have a quantum memory  $X$  that can establish a Bell state  $|\Phi^+\rangle_{Xx} := (|0\rangle_X|H\rangle_x + |1\rangle_X|V\rangle_x)/\sqrt{2}$  with an optical pulse  $x$ , where  $\{|0\rangle_X, |1\rangle_X\}$  is the computational basis of the quantum memory, while  $|H\rangle_x$  and  $|V\rangle_x$  are

<sup>4</sup>Entanglement swapping was first experimentally demonstrated by Pan *et al.* (1998); see Sec. V.H.3 for an up-to-date demonstration. The entanglement swapping operation can also be achieved using quantum Zeno effect, with no controlled gates required (Bayrakci and Ozaydin, 2022).

<sup>5</sup>Note that the transmittance  $\eta$  of a typical fiber with a length of 500 km is about  $10^{-10}$ . Therefore, even if the system is designed to achieve a private capacity  $-\log_2(1 - \eta)$  per mode with a clock rate of 10 GHz, the possible key rate is of the order of 1 bit/s, which seems to be slow for practical applications. For instance, by consuming a secret key obtained by running this system for 24 hours, we can send a secret email with a size of 20 kbytes, securely, at best. Hence, about 500 km is sometimes said to be a practical distance limit of a fiber-based point-to-point quantum communication.

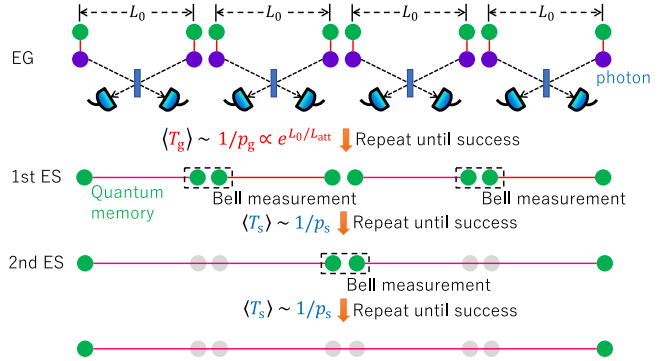


FIG. 4. Idealized quantum repeater protocol. Three quantum repeater nodes (corresponding to the case of  $N_{\text{QR}} = 3$ ) are located at regular intervals between Alice and Bob, who are separated by a distance  $L$ , with  $L_0 = L/4$ . The protocol starts by entanglement generation (EG) based on the application of the linear-optical Bell measurement of Fig. 3(a) to polarized single photons from adjacent repeater nodes with success probability  $p_g(L_0) = e^{-L_0/L_{\text{att}}}/2$ , followed by entanglement swapping (ES) with success probability  $p_s$ . The EG protocol establishes a Bell pair between adjacent repeater nodes after a number of trials of the order of  $\langle T_g(L_0) \rangle = p_g^{-1}(L_0)$ . Given halves of a pair of Bell states, the ES protocol succeeds in swapping the entanglement after a number of trials of the order of  $\langle T_s \rangle = p_s^{-1}$ . If a trial of ES fails, we need to start again from EG to go back to the trial. Therefore, in this figure the average of the total number of trials  $T_{\text{tot}}^{(3)}$  needed to establish a Bell pair between Alice and Bob is  $\langle T_{\text{tot}}^{(3)} \rangle \sim \langle T_g(L_0) \rangle \langle T_s \rangle^2 = p_s^{-2} p_g^{-1}(L_0) = 2p_s^{-2} e^{L/(4L_{\text{att}})}$ . This is of the order of the square root of  $\langle T_{\text{tot}}^{(1)} \rangle$ , which is further of the order of the square root of  $\langle T_{\text{tot}}^{(0)} \rangle$ .

horizontally polarized and vertically polarized single-photon states of the pulse  $x$ , respectively. We also assume that an arbitrary state  $a|0\rangle + b|1\rangle$  of the quantum memory can be converted into the state  $a|H\rangle + b|V\rangle$  of a polarization qubit if needed. This kind of memory is an idealized version of a quantum memory, which can be realized using two atomic ensembles (Sangouard *et al.*, 2011) (for example, we ignore any multiphoton excitations that arise in practice). We also use a linear-optical Bell measurement for polarization-encoded qubits in Fig. 3(a). This implementation works as a probabilistic Bell measurement.

We can generate a Bell state between stations  $X$  and  $Y$ , separated by a distance  $l$ , by combining such a quantum memory, the Bell measurement, and optical fibers. To achieve this, the party  $X$  (as well as the party  $Y$ ) first establishes a Bell state  $|\Phi^+\rangle_{Xx}$  ( $|\Phi^+\rangle_{Yy}$ ) between her own (his own) quantum memory  $X$  ( $Y$ ) and an optical pulse  $x$  ( $y$ ) locally and then sends the single photon  $x$  ( $y$ ) to a measuring station in the middle of the parties over an optical fiber [modeled by Eq. (13)]; see the schematic for entanglement generation (EG) in Fig. 4. On receiving the pulses from the separated parties, the measuring station performs the linear-optical Bell measurement of Fig. 3(a) on those pulses. This Bell measurement succeeds when both single photons  $x$  and  $y$  from the separated parties arrive at the measuring station without having been lost (during their travel over the lossy optical fiber), and the surviving photons are projected into a Bell state  $|\Psi^+\rangle_{xy}$  or  $|\Psi^-\rangle_{xy}$ , which occurs with the probability

$p_g(l) = e^{-l/L_{\text{att}}}/2$ . This success event entangles the quantum memories  $XY$  of the separated parties into  $|\Psi^+\rangle_{XY}$  or  $|\Psi^-\rangle_{XY}$  according to Eq. (30). This is called a heralded entanglement generation protocol.

If Alice and Bob, separated by distance  $L$ , run this entanglement generation protocol between them without any quantum repeater, the average of the number  $T_g(L)$  of trials needed to obtain a Bell pair will be

$$\langle T_{\text{tot}}^{(0)} \rangle := \langle T_g(L) \rangle = p_g^{-1}(L) = 2e^{L/L_{\text{att}}}, \quad (31)$$

which grows exponentially with the distance  $L$ .

We now introduce an entanglement swapping protocol. For simplicity, suppose that a single quantum repeater node  $C$  is located at the midpoint between Alice and Bob, and that it runs the aforementioned entanglement generation protocols in parallel with Alice and Bob. Each of these entanglement generation protocols then gives a Bell pair after trials of the order of  $\langle T_g(L/2) \rangle = 2e^{L/(2L_{\text{att}})}$ . Once it succeeds, the obtained Bell pair can be kept in quantum memories until both of the parallel protocols succeed. Thus, they can obtain Bell pairs not only between Alice and the node  $C$  but also between the node  $C$  and Bob, after trials of the order of  $\langle T_g(L/2) \rangle = 2e^{L/(2L_{\text{att}})}$ , thanks to the parallelization. After receiving a classical signal to herald this successful sharing of Bell pairs, the node  $C$  converts states of local quantum memories into polarization qubits and then implements the linear-optical Bell measurement of Fig. 3(a) [corresponding to a schematic for entanglement swapping (ES) in Fig. 4]. This works as entanglement swapping to provide a Bell state between Alice and Bob with a success probability  $p_s = 1/2$  of the Bell measurement (in the ideal case). Hence, the average of the number  $T_s$  of trials needed for the entanglement swapping to succeed (after the success of the entanglement generation protocols) is  $\langle T_s \rangle = p_s^{-1}$ . However, if the Bell measurement fails, Alice and Bob start from scratch, i.e., from the parallel entanglement generation protocols. Thus, the average of the total number of trials  $T_{\text{tot}}^{(1)}$  needed to establish a Bell pair between Alice and Bob is

$$\langle T_{\text{tot}}^{(1)} \rangle \sim \langle T_g(L/2) \rangle \langle T_s \rangle = p_s^{-1} p_g^{-1}(L/2) = 2^2 e^{L/(2L_{\text{att}})}. \quad (32)$$

See [Sangouard \*et al.\* \(2011\)](#) and [Azuma \*et al.\* \(2021\)](#) for discussions on the validity of this approximation. Therefore, by comparing Eqs. (32) and (31), we can conclude that, for a large distance  $L$ , the existence of a single quantum repeater node  $C$  can provide a square-root improvement over the direct entanglement generation between Alice and Bob in the number of trials needed.

The process for achieving this square-root improvement with entanglement swapping can be concatenated. If Alice and Bob use three equally spaced quantum repeater nodes, they can achieve further square-root improvement (see Fig. 4); if they use seven, they can have further square-root improvement, etc. In particular, if Alice and Bob have  $N_{\text{QR}} = 2^n - 1$  quantum repeater nodes equally spaced between them, the average of the total number  $T_{\text{tot}}^{(N_{\text{QR}})}$  of trials needed to have a Bell pair between Alice and Bob will be

$$\begin{aligned} \langle T_{\text{tot}}^{(N_{\text{QR}})} \rangle &\sim p_s^{-n} p_g^{-1}(L/2^n) = 2p_s^{-n} e^{L/(2^n L_{\text{att}})} \\ &= 2^{1+\log_2(N_{\text{QR}}+1)} e^{\frac{L}{(N_{\text{QR}}+1)L_{\text{att}}}} \end{aligned} \quad (33)$$

[see again [Sangouard \*et al.\* \(2011\)](#) and [Azuma \*et al.\* \(2021\)](#) for details regarding this approximation]. This shows the ultimate advantage of utilizing quantum repeaters: the exponential improvement in the number of trials needed to establish entanglement with the number of quantum repeater nodes  $N_{\text{QR}}$ . Even if  $p_s < 1/2$  for practical reasons, as long as  $p_s$  is independent of the distance  $L$ , namely, constant, this exponential improvement holds, which enables Alice and Bob to perform quantum communication efficiently over long distances.

This simple model does not include realistic imperfections such as memory errors and imperfect entanglement generation and swapping operations. In practice, these errors will accumulate and become non-negligible over longer distances. However, thanks to the existence of error suppression mechanisms explained in Sec. III.A.4, we can devise several kinds of quantum repeaters that work in the presence of not only loss but also other such imperfections.

#### 4. Tools for error suppression

As shown in Sec. III.A.3, there is a quantum repeater protocol that enables Alice and Bob to achieve efficient long-distance quantum communication, even with the use of optical fibers impacted by photon loss. However, this protocol was idealized; we assumed that the optical attenuation in fiber is the only source of error and that all other operations are perfect. In practice, there are many physical imperfections that compromise the quality of the resulting entanglement. Therefore, quantum repeater protocols need to be equipped with error suppression mechanisms, which we discuss in this section.

It is helpful to classify error suppression techniques into two categories: those employing deterministic error suppression [including quantum error correction ([Lidar and Brun, 2013](#)) and one-way entanglement distillation ([Bennett, DiVincenzo \*et al.\*, 1996](#))] and those leveraging probabilistic error suppression [including quantum error detection ([Lidar and Brun, 2013](#)) and two-way entanglement purification ([Bennett, Brassard \*et al.\*, 1996; Deutsch \*et al.\*, 1996; Briegel \*et al.\*, 1998](#))]. The former class of techniques succeed deterministically, meaning they do not require users to share a heralding signal alerting each other of the success or failure of the error suppression; note that the probabilistic nature of the latter class necessitates users to alert each other of success or failure via classical communication and discard the failed instances. For networks with large spatial separation between the nodes, the time delay associated with this classical heralding signaling is highly relevant to the performance of the network; for reference, a photon takes roughly 0.5 ms to travel 100 km in an optical fiber. While deterministic error suppression has an advantage in this regard, probabilistic error suppression works even for states that are too noisy to be recovered through deterministic techniques. That is, the probabilistic techniques tend to have higher thresholds on tolerable error or loss probabilities ([Bennett, DiVincenzo \*et al.\*, 1996](#)). We now summarize these two types of approaches for suppressing errors.

*a. Deterministic error suppression*

*i. Quantum error correction*

The essence of quantum error correction (QEC) is to use the redundancy in the entanglement of many physical qubits to encode a logical state and correct for errors. In particular, a qubit is encoded into a two-dimensional subspace of a large Hilbert space composed of many physical qubits rather than directly into a single physical system. Quantum error correction is a deterministic process; it is not impacted by the delays associated with classical heralding signals. For large-scale quantum networks, having this determinism favorably affects communication rates; however, physical implementations of QEC codes are demanding due their complexity and exhibit lower thresholds (to work) on the errors affecting the physical qubits. These thresholds become more stringent as the variety and magnitude of errors increase.

*ii. One-way entanglement distillation*

The purpose of one-way entanglement distillation protocol (1EDP) for two distant parties is to obtain an almost maximally entangled Bell pair from a set of noisier entangled pairs by applying direct one-way LOCC between them. Here *one-way* means that only one party has to communicate the results during the distillation process via classical communication; there is no backward classical communication. 1EDP is closely connected to quantum error correction (Horodecki *et al.*, 2009). Since there is a direct mapping from a one-way hashing protocol (Bennett, DiVincenzo *et al.*, 1996) [or a one-way breeding protocol (Bennett, Brassard *et al.*, 1996)] to a quantum error-correcting code, we treat them as equivalent at the protocol level. In practice, there may be subtle differences in the error accumulation and resource counts between one-way hashing protocols and quantum error correction.

*b. Probabilistic error suppression*

*i. Quantum error detection*

QEC codes can also be used simply to detect errors: that is, to herald the presence of error and discard the state without correcting the error. Quantum error detection is a probabilistic process; as a result, it takes time to inform the relevant parties, through a classical signal, about the outcome of the error detection, causing additional delay.

*ii. Heralded entanglement generation protocol*

A widely used error detection scheme is the heralded entanglement generation protocol (HEGP), which can generate entanglement on success and detect loss errors on failure. Since entanglement cannot be generated under LOCC, a party needs to generate an entangled state between a local qubit and a flying qubit locally and to then send the flying qubit over a quantum channel. A typical choice of a flying qubit is a bosonic system such as a photonic state; its quantum channel (a bosonic channel) has loss as the dominant noise process. The goal of HEGP, then, is to generate high-quality entanglement between separated parties in a heralded manner, notwithstanding losses in the channel.

Depending on how the quantum information is encoded in the optical modes or how the local stationary qubits are entangled with the optical modes, one ought to choose appropriate schemes to detect loss errors. For dual-rail

(single-rail) discrete-variable encodings, one generates entanglement using two-photon (single-photon) interference of incoming optical modes from neighboring stations while detecting loss errors according to the click patterns of the photon detection (Duan *et al.*, 2001; Barrett and Kok, 2005; Childress, Taylor *et al.*, 2006; Sangouard *et al.*, 2011; Azuma and Kato, 2012; Azuma *et al.*, 2012) after the interference; see examples in Secs. III.A.3, IV.B, and V.C. For continuous-variable [for instance, GKP (Gottesman, Kitaev, and Preskill, 2000)] encoding, one can generate entanglement by combining the two incoming optical modes from neighboring stations followed by homodyne measurements at the output ports. The outcomes from the homodyne measurements provide information about the likelihood of loss errors, which can be used to determine whether or not the entanglement generation is successful (Fukui, Alexander, and Van Loock, 2021).

If loss errors are detected, the heralded entanglement generation procedure is simply repeated until the two adjacent stations receive the confirmation of certain successful detection patterns via two-way classical signaling. Instead of using this time multiplexing, we could use spatial or frequency multiplexing to run the heralded entanglement generation protocol in parallel so that one of the multiplexed trials will succeed with a high probability within a constant time (Sinclair *et al.*, 2014).

*iii. Two-way entanglement distillation protocol*

The purpose of two-way entanglement distillation protocol (2EDP) or purification protocol for two distant parties is to produce an almost maximally entangled pair from noisier entangled pairs by using two-way LOCC between them. 2EDP allows both parties to communicate with each other using a classical channel, which enables them to compare measurement results or adaptively perform operations conditioned on the outcomes from the other party. For example, if the Bell states suffer from bit-flip errors,  $\rho_{AB} = (1 - \epsilon)|\Phi^+\rangle\langle\Phi^+|_{AB} + \epsilon|\Psi^+\rangle\langle\Psi^+|_{AB}$ , separated parties can use two copies of the states to obtain one pair with a suppressed error of  $O(\epsilon^2)$  by comparing measurement outcomes of a parity-check measurement on their own halves (Bennett, DiVincenzo *et al.*, 1996; Deutsch *et al.*, 1996; Briegel *et al.*, 1998). We can also extend the result to suppress dephasing errors. For general depolarization errors, we can use twirling (Bennett, Brassard *et al.*, 1996) or switching between phase and bit errors (Deutsch *et al.*, 1996) to suppress the errors.

For ideal operations, we can quickly converge to perfect Bell pairs. In principle, we can extract entanglement with a rate limited by the two-way distillable entanglement (Bennett, DiVincenzo *et al.*, 1996). In practice, however, operation errors limit the ultimate fidelity of the distilled Bell pairs. Various protocols have been proposed to distill entanglement (Bennett, Brassard *et al.*, 1996; Deutsch *et al.*, 1996; Jiang, Taylor, Sørensen, and Lukin, 2007; Fujii and Yamamoto, 2009; Nickerson, Li, and Benjamin, 2013; Krastanov, Albert, and Jiang, 2019; Zhou, Zhong, and Sheng, 2020; Riera-Sàbat *et al.*, 2021). For example, one can use multiple copies of imperfect Bell pairs to purify a Bell pair (Fujii and Yamamoto, 2009; Nickerson, Li, and Benjamin, 2013). One can also use a genetic algorithm to find the optimal 2EDP (Krastanov, Albert, and Jiang, 2019). Existing entanglement can also enhance the performance of 2EDP (Riera-Sàbat *et al.*, 2021).

TABLE III. Comparison between deterministic and probabilistic error suppression protocols.

	Deterministic error suppression	Probabilistic error suppression
Schemes	Quantum error correction One-way entanglement distillation	Quantum error detection Two-way entanglement distillation
Signaling	No delay	Delay
Threshold to work	$\eta > 1/2$ for loss of qubits or bosons $p < 1/4$ at least for depolarization of qubits	$\eta > 0$ for loss of qubits or bosons $p < 1/2$ for depolarization of qubits

Since there is a direct mapping from 2EDP to quantum error detection (Dür and Briegel, 2007), we can treat them as equivalent at the protocol level. In practice, just as in the relationship between QEC and 1EDP, there may be subtle differences in error accumulation and resource counts between quantum error detection and 2EDP.

For CV encoding, due to the Gaussian entanglement distillation no-go theorem (Eisert, Scheel, and Plenio, 2002; Fiurášek, 2002; Giedke and Cirac, 2002), the CV repeaters use non-Gaussian operations in the entanglement distillation protocols (Ralph and Lund, 2009; Fiurášek, 2010) to suppress loss errors. Instead, we can distill entanglement using non-deterministic noiseless linear amplification (NLA) with quantum scissors (Pegg, Phillips, and Barnett, 1998; Ralph and Lund, 2009) or other non-Gaussian filtering with single-photon addition and subtraction operations (Fiurášek, 2010).

#### c. Comparison of deterministic and probabilistic quantum error suppression

Deterministic error suppression has no corresponding classical signaling delay. However, it imposes a threshold of 50% on the loss of qubits or bosonic systems [associated with the transmittance  $\eta$  as  $\eta > 1/2$  if they are sent over a pure-loss channel, as in Eq. (13)] (Bennett, DiVincenzo *et al.*, 1996; Bennett, DiVincenzo, and Smolin, 1997; Giovannetti *et al.*, 2003a, 2003b). Furthermore, this category of protocols will not work at all for qubits sent over a depolarizing channel [Eq. (12)] with a strength  $p > 1/4$  (Bennett, DiVincenzo *et al.*, 1996; Bennett, DiVincenzo, and Smolin, 1997; Knill and Laflamme, 1997), although they work for  $p \lesssim 0.18929$  with the hashing protocol (Bennett, DiVincenzo *et al.*, 1996), and even for  $p \lesssim 0.19130$  with a concatenated coding scheme (Fern and Birgitta Whaley, 2008). Probabilistic error suppression has an associated classical signaling delay, but it can tolerate larger errors. In principle, it works if the transmission probability of qubits or bosonic systems is nonzero (Bennett, DiVincenzo, and Smolin, 1997; Pirandola *et al.*, 2017) or if qubits are sent over a depolarizing channel with  $p < 1/2$  (Bennett, DiVincenzo *et al.*, 1996; Deutsch *et al.*, 1996). We summarize and compare the properties of deterministic and probabilistic error suppression protocols in Table III.

## B. Generations of quantum repeaters

There are two major challenges for fiber-based quantum communication over long distances. First, as pointed out in Sec. III.A.3, fiber attenuation during transmission leads to an exponential decrease in the entangled-pair generation rate. Second, several operational errors, such as channel errors, gate errors, measurement errors, and quantum memory errors,

severely degrade the quality of the obtained entanglement. Unlike classical information, quantum information is encoded as quantum states that cannot be amplified or duplicated deterministically due to the quantum no-cloning theorem; see Sec. II.B.

To overcome these challenges, quantum repeaters (QRs) have been proposed for the faithful realization of long-distance quantum communication (Briegel *et al.*, 1998). As exemplified in Sec. III.A.3, the essence of QRs is to divide the total distance of communication into shorter intermediate segments connected by QR stations, in which loss errors from fiber attenuation can be corrected. Active error suppression schemes are also employed at every repeater station to correct operation errors, i.e., imperfections induced by the channel, measurements, and gate operations. In the following, we classify quantum repeaters according to how one suppresses loss and operation errors [using probabilistic error suppression (Sec. III.A.4.b) or deterministic error suppression (Sec. III.A.4.a)], which will lead to a different scaling of quantum communication rates.

For probabilistic error suppression protocols, we need two-way classical signaling to inform relevant repeater nodes whether to proceed to the next step (if error suppression succeeds) or to make another attempt (if error suppression fails). A widely used error detection scheme to suppress loss errors is the HEGP, as exemplified by dual-rail photonic encoding in Sec. III.A.3. For single-rail or CV encoding, photon click patterns or other non-Gaussian operations [such as non-deterministic NLA with quantum scissors (Pegg, Phillips, and Barnett, 1998; Ralph and Lund, 2009)] may not immediately identify loss events, but they inform us of successful sharing of high-quality entanglement with suppression of loss errors. If loss errors are detected or not suppressed, one simply repeats the heralded entanglement generation procedure until the two adjacent stations receive the confirmation of certain successful detection patterns via two-way classical signaling. Similarly, to achieve probabilistic suppression of operation errors, a popular error detection scheme is the 2EDP, which consumes several low-fidelity Bell pairs to probabilistically generate a smaller number of higher-fidelity Bell pairs (Deutsch *et al.*, 1996; Dür *et al.*, 1999). As in the HEGP, to confirm the success of distillation or purification two-way classical signaling between repeater stations for exchanging measurement results is required. The time delays from the two-way classical signaling may decrease the communication rates.

To achieve deterministic error suppression of loss errors or operation errors, we can use quantum error correction (Jiang *et al.*, 2009; Fowler *et al.*, 2010; Munro *et al.*, 2010; Li *et al.*, 2013; Muralidharan *et al.*, 2014; Azuma, Tamaki, and Lo, 2015) or one-way entanglement distillation (Bennett, DiVincenzo *et al.*, 1996; Zwerger *et al.*, 2018). The

TABLE IV. Three generations of quantum repeaters classified according to probabilistic or deterministic suppression of loss and operation errors. The timescale (key generation rate) and cost coefficient scale differently with the total distance  $L$ , repeater spacing  $L_0$ , and gate time  $t_0$ .

Errors	Error suppression	1G	2G	3G
Loss error	Probabilistic	✓	✓	✓
	Deterministic			
Operation error	Probabilistic	✓	✓	✓
	Deterministic			
Timescale		$\max(L/c, t_0)$	$\max(L_0/c, t_0)$	$t_0$
Cost coefficient		$\text{poly}(L)$	$\text{polylog}(L)$	$\text{polylog}(L)$

key idea is to encode a logical qubit into a block of physical qubits that are sent through the lossy channel, and then to use quantum error correction to restore the logical qubit. One can also include one-way classical signaling to assist the deterministic one-way entanglement distillation protocols (Bennett, Brassard *et al.*, 1996; Bennett, DiVincenzo *et al.*, 1996), but the additional one-way (forward) classical signaling from the sender does not affect the quantum channel capacity. Hence, all the deterministic error suppression (even when assisted by one-way forward signaling) can correct no more than a 50% loss, which is consistent with the no-cloning theorem (Stace, Barrett, and Doherty, 2009; Muralidharan *et al.*, 2014), and not more than 25% depolarizing errors; see Table III. The existence of these finite thresholds itself implies the need for quantum repeater nodes in the case using deterministic error suppression, as such errors tend to depend on the communication distance (Briegel *et al.*, 1998).

Based on the methods adopted to suppress loss and operation errors, we can classify various QRs into three categories, as shown schematically in Table IV. We refer to these as first, second, and third generations of QRs (Muralidharan *et al.*, 2014, 2016; Munro *et al.*, 2015) to imply the increasing difficulty in technology with improved performance.<sup>6</sup> Note that the combination of deterministic suppression of loss errors and probabilistic suppression for operation errors, which does not appear in Table IV, is suboptimal compared to the other three combinations.

Each generation of QRs performs best for a specific regime of operational parameters, such as local gate speed, gate fidelity, and coupling efficiency. We consider both the temporal and physical resources consumed by the three generations of QRs and identify the most efficient architectures for different parameter regimes. The results can guide the design of efficient long-distance quantum communication links that act as elementary building blocks for future quantum networks.

### 1. First-generation repeaters

The first generation of QRs uses probabilistic error suppression to overcome practical imperfections; for example, HEGP can herald successful entanglement generation while overcoming loss errors, and 2EDP can use two-way classical

signaling to recognize successful entanglement distillation to suppress operation errors (Briegel *et al.*, 1998; Kok, Williams, and Dowling, 2003; Childress, Taylor *et al.*, 2006; Van Loock *et al.*, 2006; Munro *et al.*, 2008; Sangouard *et al.*, 2011; Azuma *et al.*, 2012). Since we have explained the principle of QRs by exemplifying a simplified first-generation QR protocol in Sec. III.A.3, here we start by summarizing how QRs from this generation can be used to correct losses with a simple example in which we assume there are no operation errors. Alice and Bob, separated by a distance  $L_{\text{tot}}$ , want to share a maximally entangled qubit pair that they can use, for instance, to teleport a quantum state or to distill a private key. They are connected by a lossy medium such as a telecommunication (telecom) fiber, having the typical loss of 0.2 dB/km (that is, an attenuation length  $L_{\text{att}} \approx 22$  km). Supposing that  $L_{\text{tot}} \gg L_{\text{att}}$ , the direct transmission of a photon between Alice and Bob succeeds with a vanishingly small probability of the order of  $e^{-L_{\text{tot}}/L_{\text{att}}} \ll 1$ .

The solution provided by first-generation QRs is to divide the total distance  $L$  between Alice and Bob into smaller lengths with the help of  $N_{\text{QR}} = L_{\text{tot}}/L_0 - 1$  quantum repeater nodes. Here we assume that the nodes are evenly separated by an internodal distance  $L_0$ , with  $L_0 = L_{\text{tot}}/2^n$  for simplicity. The role of each QR node is to share entanglement with its adjacent nodes: we use an HEGP strategy to create high-quality entanglement between a quantum memory and its counterpart to the immediate left, and between another memory and its counterpart in the adjacent QR node to the right. Each HEGP trial also takes a time  $T_{\text{trial}} = t_{\text{op}} + t_{\text{c}}$ , which depends on the total time  $t_{\text{op}}$  of operations and on the time  $t_{\text{c}} = L_0/c$  for photons to arrive at the central measuring station and the classical signaling back to the QR node.

A typical HEGP procedure has a success probability  $P_{\text{ent}}$  that depends on the photon collection efficiency, fiber transmission efficiency, and photon detection efficiency. For the dual-rail encoding, without ancillary photons  $P_{\text{ent}} \leq 1/2$  even in the lossless limit, limited by linear optics and by the photon loss probability (Calsamiglia and Lütkenhaus, 2001). However, we can use more advanced encoding to achieve a higher success probability ( $P_{\text{ent}} > 1/2$ ) (Azuma *et al.*, 2009, 2012; Martin and Whaley, 2019). In any case, if it succeeds, the HEGP tends to present high-quality entanglement between nearest-neighbor nodes, even under the existence of photon loss. Owing to the probabilistic nature of the HEGP, for the first-generation QR protocol to proceed, it is necessary to inform the adjacent nodes whether the HEGP has succeeded or not. In the case of a failure, the process is repeated until it succeeds. The entanglement generation

<sup>6</sup>We can also classify QRs using other criteria, such as the physical platforms and different operations; see Razavi (2018). We discuss various physical platforms and implementations in Sec. V.

procedure therefore succeeds in an average time  $\langle T_{\text{ent}} \rangle = P_{\text{ent}}^{-1} T_{\text{trial}} = P_{\text{ent}}^{-1} (L_0/c + t_{\text{op}})$ . In a successful case, the entanglement can be stored in the quantum memories.

At each QR node, we can store entangled qubit pairs shared with an adjacent node, say, the node on the immediate left, during the time required to produce an entangled pair with the adjacent QR node on the right. Thanks to this functionality of quantum memories, we see that not all of the entanglement needs to be generated at the same time throughout the network; this is why this strategy can outperform direct photon transmission and a quantum relay protocol (Jacobs, Pittman, and Franson, 2002; Waks, Zeevi, and Yamamoto, 2002; de Riedmatten *et al.*, 2004) (which uses repeater nodes but distributes photonic Bell pairs only from sending repeater nodes to their adjacent receiver nodes, in which Bell measurement is performed soon after receiving halves of the Bell pairs). When a QR node finally shares an entangled pair of qubits with each of its adjacent nodes, it performs entanglement swapping between its two quantum memories such that if it succeeds, a high-quality entangled pair is now shared between its two adjacent nodes. After repeating these entanglement swapping steps at each QR node, Alice and Bob end up with a high-quality entangled pair at a rate much higher than what is achievable with direct fiber transmission; see Sec. III.A.3 for details.

Thus far we have considered only loss errors and have thus assumed that information can be manipulated, transferred, and stored faithfully. In practice, this is not the case: we ought to also handle operation errors, which eventually reduce the fidelity of the two qubits shared by Alice and Bob. This is achieved through an entanglement distillation scheme, which can be incorporated into first-generation QRs, for example, using a nested purification QR scheme, which we now introduce.

As illustrated in Fig. 5, we start with distilled high-fidelity entangled pairs with separation  $L_0 = L_{\text{tot}}/2^n$ , created and stored in adjacent stations. At the  $k$ th nesting level ( $k = 1, 2, \dots, n$ ), two entangled pairs of distance  $L_{k-1} = 2^{k-1}L_0$  are connected by entanglement swapping to extend entanglement to a distance  $L_k = 2^kL_0$  (Zukowski *et al.*, 1993). As practical gate operations and entanglement swapping [Figs. 5(b)–5(d)] inevitably cause the fidelity of entangled pairs to drop, 2EDP may be incorporated at each level of entanglement extension [Figs. 5(e)–5(g)] (Deutsch *et al.*, 1996; Dür *et al.*, 1999). With  $n$  nesting levels of connection and distillation, a high-fidelity entangled pair over distance  $L_n = L_{\text{tot}}$  can be obtained. Suppose that  $T_{k-1}$  is the average time needed to prepare a distilled entangled pair over distance  $L_{k-1}$ , the average time to prepare a distilled entangled pair over distance  $L_k$  is

$$T_k = \alpha_k T_{k-1} + \beta_k L_k/c = \alpha_k T_{k-1} + \beta_k 2^k t_c, \quad (34)$$

where  $t_c = L_0/c$  is the communication time between neighboring repeater stations,  $\alpha_k$  and  $\beta_k$  are dimensionless numbers capturing the time overhead associated with the entanglement swapping, distillation, and multiple rounds of classical communication. For simplicity, we assume that each nesting level has similar overheads  $\alpha_k \approx \alpha$  and  $\beta_k \approx \beta$  for  $k \geq 1$ . The

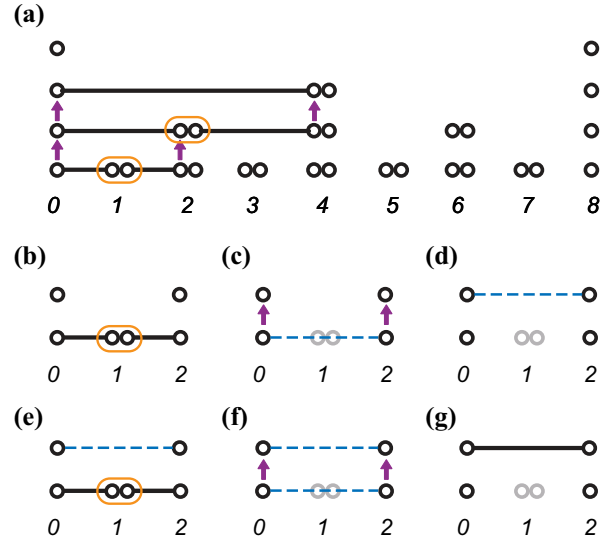


FIG. 5. First-generation repeater protocol [BDCZ scheme (Briegel *et al.*, 1998)]. (a) In a realization based on the pumping protocol with  $N + 1 = 9$  nodes, the number of qubits per node is bounded by  $2 \log_2 2N = 8$ . Each orange oval surrounding two vertices (or two qubits) describes an application of a Bell measurement to the two qubits for entanglement swapping. (b)–(d) Two entangled pairs with distance 1 are connected through entanglement swapping (orange oval) at node 1 to produce an entangled state with distance 2 that is stored in the qubits (as described by the purple arrows) at a higher level. (e)–(g) Another entangled state with distance 2 is produced to purify the entangled state (as described by purple arrows) stored in qubits at a higher level. Similarly, entangled states with distance  $2^n$  can be connected to produce entangled states with distance  $2^{n+1}$ , which can be further purified, as indicated in (a). From Jiang, Taylor, Khaneja, and Lukin, 2007.

average time to generate distilled entangled pairs between neighboring repeaters is  $T_0 = \beta_0 t_c$ , with the time overhead  $\beta_0$  associated with photon efficiency, entanglement generation, and purification between neighboring repeater stations. From the recursive relation, we can obtain the average time to generate a distilled entangled pair over distance  $L_n = L_{\text{tot}}$  is

$$T_{\text{tot}} = T_n \sim (L_{\text{tot}}/L_0)^{\log_2 [\max(\alpha, 2)]} \max(\beta, \beta_0) t_c, \quad (35)$$

which increases polynomially with  $L_{\text{tot}}$ , depending on the value of  $\alpha$ .

For the simple mode of a loss-only channel  $\alpha \approx (3/2)(1/P_{\text{swap}})$  with prefactor 3/2 for the time overhead associated with the requirement that two entangled pairs on both sides should be ready for entanglement swapping (Jiang, Taylor, Khaneja, and Lukin, 2007; Sangouard *et al.*, 2011; Azuma *et al.*, 2021), and  $P_{\text{swap}}$  for the success probability of entanglement swapping. For example,  $P_{\text{swap}} \leq 1/2$  for the Duan-Lukin-Cirac-Zoller quantum repeater protocol based on atomic ensembles and linear optics (Duan *et al.*, 2001). To overcome operation errors, we need entanglement distillation from at least two copies of entangled pairs, and hence  $\alpha \geq 2$  for all entanglement distillation schemes [for instance, the Briegel-Dür-Cirac-Zoller (BDCZ) protocol (Briegel *et al.*,

1998) and the Childress-Taylor-Sørensen-Lukin protocol (Childress, Taylor *et al.*, 2006)], unless we use multiplexing in generating entangled pairs (Dür *et al.*, 1999).

The first generation of QRs reduces the exponential overhead in direct state transfer to only polynomial overhead, which is limited by the two-way classical signaling required by the HEGP between nonadjacent repeater stations. The communication rate still decreases polynomially with distance and thus becomes slow for long-distance quantum communication. The communication rate of first-generation QRs can be boosted using temporal, spatial, and/or frequency multiplexing associated with the internal degrees of freedom for the quantum memory (Bonarota, Le Gouët, and Chanelière, 2011; Sangouard *et al.*, 2011).

The first generation of QRs can also be efficient in entanglement resources. As shown in Fig. 5, the BDCZ protocol (Briegel *et al.*, 1998; Dür *et al.*, 1999) has a self-similar structure with  $n = \log_2(L_{\text{tot}}/L_0)$  nesting levels. We start with the elementary entangled pairs with initial fidelity<sup>7</sup>  $F$  and distance  $L_0$  between neighboring repeater nodes. In the  $j$ th nesting level (with  $j = 1, 2, \dots, n$ ), a repeater node performs entanglement swapping to convert two initial entangled pairs with fidelity  $F$  and length  $2^{j-1}L_0$  into an entangled pair with fidelity  $F'$  ( $\leq F$  in general) and length  $2^jL_0$ . The extended entangled pairs with fidelity  $F'$  are collected, and  $M$  pairs of them are used to distill a purified entangled pair with an initial fidelity  $F$  and length  $2^jL_0$  through an entanglement distillation protocol. These imply that each purified entangled pair with fidelity  $F$  and length  $2^jL_0$  can be regarded as having been made from  $2M$  entangled pairs with fidelity  $F$  and length  $2^{j-1}L_0$ . Therefore, an entangled pair with fidelity  $F$  and length  $L_{\text{tot}} = 2^nL_0$  can be made up from  $(2M)^n = (L_{\text{tot}}/L_0)^{1+\log_2 M}$  elementary entangled pairs.

In addition, the first generation of QRs can be highly efficient, even in terms of quantum memory resources, if the purification of an unpurified entangled pair with length  $2^jL_0$  ( $j = n, n-1, \dots, 0$ ) can be done using a sequential application of the pumping protocol that “pumps” entanglement to the entangled pair out of a fixed unpurified auxiliary entangled pair with the same length ( $2^jL_0$ ); see Fig. 5 (Briegel *et al.*, 1998; Dür *et al.*, 1999). Here how much entanglement is purified depends on both the initial fidelity and the shape of the fixed auxiliary pair. During the purification, we need only two pairs of memories, one for storing the entangled pair to be pumped and the other for storing the auxiliary entangled pair for each round, and the purification is regarded as having started from two unpurified pairs with length  $2^jL_0$ . One of these two unpurified pairs, as the auxiliary entangled pair, should be prepared repeatedly during the pumping purification, and it can be regarded as having been obtained by connecting two purified entangled pairs with length  $2^{j-1}L_0$

through entanglement swapping. As a result, a purified entangled pair with the length of  $2^jL_0$  can be regarded as having been made from an unpurified entangled pair (to be pumped at the  $j$ th nesting level) with length  $2^jL_0$  and from two purified pairs with length  $2^{j-1}L_0$ . By considering this recursively from  $j = n$  to  $j = 1$ , a purified entangled pair with length  $2^nL_0 (= L_{\text{tot}})$  is regarded as having been made from one unpurified entangled pair (to be pumped at the  $n$ th nesting level) with length  $2^nL_0$ , two unpurified pairs [to be pumped at the  $(n-1)$ th nesting level] with length  $2^{n-1}L_0, \dots, 2^1L_0$  unpurified pairs (to be pumped at the second nesting level) with the length of  $2L_0$ , and  $2^n$  purified pairs with length  $L_0$ . Since each of these entangled pairs needs two quantum memories, the maximum number of memories  $N_{\text{tot}}$  required during the protocol is  $N_{\text{tot}} = 2\sum_{j=0}^n 2^j = 2(2^{n+1} - 1) = 2(2L_{\text{tot}}/L_0 - 1) = 4L_{\text{tot}}/L_0 - 2$ . For example, we have  $n = 3$  in Fig. 5(a), where 30 quantum memories are written, corresponding to  $N_{\text{tot}}$  memories.

There are different variations of the BDCZ protocol. Its measurement-based implementation using graph states was given by Zwerger, Dür, and Briegel (2012). The DLCZ protocol simplifies it with the use of atomic ensembles and linear optics (Duan *et al.*, 2001). Room-temperature quantum repeaters have also been proposed using nitrogen-vacancy defect centers in diamond (Childress, Taylor *et al.*, 2006; Ji *et al.*, 2022). Sangouard *et al.* (2011) provided a review on various first-generation quantum repeaters based on atomic ensembles and linear optics, where HEGPs are based on Fock-state encoding, polarization encoding, and time-bin encoding. The concept of nested purification in the BDCZ protocol, as well as the concatenation of quantum error-correcting codes (Knill and Laflamme, 1997), is generalized to distribute entangled pairs with fixed error to clients in a quantum network with arbitrary topology, regardless of their distance, across its multiple subnetworks (Azuma, 2023).

We can further generalize the BDCZ protocol by introducing CV encoding. For example, we can take a hybrid CV-DV approach by interfering optical coherent-state signals to generate DV entanglement between repeater stations (Childress, Taylor *et al.*, 2006; Van Loock *et al.*, 2006; Munro *et al.*, 2008; Azuma *et al.*, 2012). Moreover, we can design CV quantum repeaters to efficiently distribute CV entangled states with high fidelity over long distances (Dias and Ralph, 2017; Furrer and Munro, 2018; Seshadreesan, Krovi, and Guha, 2020). Owing to the Gaussian entanglement distillation no-go theorem (Eisert, Scheel, and Plenio, 2002; Fiurášek, 2002; Giedke and Cirac, 2002), CV repeaters use non-Gaussian operations in entanglement distillation protocols (Ralph and Lund, 2009; Fiurášek, 2010) to suppress loss errors.

## 2. Second-generation repeaters

The second generation of QRs uses probabilistic error suppression (see Sec. III.A.4.b) for loss errors and deterministic error suppression (see Sec. III.A.4.a) for operation errors (Jiang *et al.*, 2009; Munro *et al.*, 2010; Li *et al.*, 2013; Mazurek *et al.*, 2014). For example, we can first prepare the encoded states  $|0\rangle_L$  and  $|+\rangle_L$  using Calderbank-Shor-Steane (CSS) codes and then store them at two adjacent stations. CSS

<sup>7</sup>A general definition of the fidelity between states  $\rho$  and  $\sigma$  is given by  $F(\rho, \sigma) := \|\sqrt{\rho}\sqrt{\sigma}\|^2$ , where  $\|X\| := \text{Tr}\sqrt{X^\dagger X}$  is the trace norm (Jozsa, 1994). The “initial fidelity” here means the fidelity of an initial state  $\rho$  to a Bell state  $|\Phi^+\rangle$ , i.e.,  $F = F(\rho, |\Phi^+\rangle) = \langle\Phi^+|\rho|\Phi^+\rangle$ .

codes are considered because of their fault-tolerant implementation of preparation, measurement, and encoded CNOT gates (Jiang *et al.*, 2009; Nielsen and Chuang, 2010). An encoded Bell pair  $|\Phi^+\rangle_L = (1/\sqrt{2})(|0,0\rangle_L + |1,1\rangle_L)$  between adjacent stations can then be created via teleportation-based nonlocal CNOT gates (Gottesman and Chuang, 1999; Jiang *et al.*, 2009) applied to each physical qubit in the encoded block using the entangled pairs generated through the HEGP process. Finally, QEC is carried out when entanglement swapping at the encoded level is performed to extend the range of entanglement. Second-generation QRs use QEC to replace 2EDP and therefore avoid the time-consuming two-way classical signaling between nonadjacent stations. The communication rate is then limited by the time delay associated with two-way classical signaling between adjacent stations and local gate operations. If the probability of accumulated operation errors over all repeater stations is sufficiently small, we can simply use the second generation of QRs without encoding. For instance, proposals based on single ion qubits, to which we can apply deterministic Bell measurements, fall into this category (Sangouard, Dubessy, and Simon, 2009; Kimiae Asadi *et al.*, 2018; Asadi, Wein, and Simon, 2020).

We can generate entangled pairs through an HEGP process that is adapted for different photonic encoding schemes; see Sec. II.E. For dual-rail photonic encoding (time bin, polarization, or path), we can use linear optics and photon detectors to herald the successful Bell measurement and also detect photon loss errors [Fig. 3(a)]. The potential limitation is that the success probability of the Bell measurement will be upper bounded by 50% for dual-rail encoding. Alternatively, we can use bosonic encodings such as GKP states for the HEGP (Fukui, Alexander, and Van Loock, 2021). Unlike the dual-rail encoding schemes, GKP encoding can achieve deterministic Bell measurements with linear optics and homodyne detection (Gottesman, Kitaev, and Preskill, 2001). In the presence of loss errors, there will be vacuum noise added to the system, which can be detected by the homodyne measurement. GKP encoding can correct small added vacuum noise up to certain level, above which it is better to report the presence of large noise and restart the process.

As with the first-generation repeaters, we can also give bounds on the achievable communication rate for the second-generation repeaters, which is limited by the HEGP and 2EDP between neighboring repeater stations. For example, for the case of dual-rail encoding, we have  $R \leq \langle T_{\text{ent}} \rangle^{-1} \leq [2(L_0/c + t_{\text{op}})]^{-1}$ . By reducing the distance  $L_0$  to zero and neglecting  $t_{\text{op}}$ , we see that this bound can in principle go to infinity. Yet, assuming  $L_0 \rightarrow 0$  would require infinitely many QR nodes ( $N_{\text{QR}} \rightarrow \infty$ ), and thus an infinite amount of resources (quantum memories).

The physical resources required for the second generation of QRs depend on the size of the CSS code  $n_{\text{code}}$ . At each repeater station, we need at least  $2n_{\text{code}}$  qubits for storing the encoded states  $|0\rangle_L$  and  $|+\rangle_L$ , and we also need additional memory qubits to store and purify entanglement between neighboring repeater stations (Jiang *et al.*, 2009). Hence, the total number of quantum memory qubits is  $N_{\text{tot}} \sim n_{\text{code}}L_{\text{tot}}/L_0$ .

The size of the encoding block  $n_{\text{code}}$  only needs to increase polylogarithmically with the total distance  $L_{\text{tot}}$ . Asymptotically there are CSS codes with  $n_{\text{code}} \leq 19t$  that can correct up to  $t$  bit-flip and dephasing errors [obtained from the Gilbert-Varsharov bound; see Eq. (30) of Calderbank and Shor (1996)]. This implies that we only need a result for  $n_{\text{code}} \propto t \sim \ln(L_{\text{tot}}/L_0)$  that increases logarithmically with  $L_{\text{tot}}$  (Jiang *et al.*, 2009). In practice, however, it might be challenging to initialize large CSS encoding blocks fault tolerantly with imperfect local operations. To avoid complicated initialization, we can construct larger CSS codes by concatenating smaller codes with  $r$  nesting levels, and the code size scales polynomially with the code distance  $n_{\text{code}} \propto t^r \sim [\ln(L_{\text{tot}}/L_0)]^r$ . Alternatively, we can consider the Bacon-Shor code (Bacon, 2006); the encoding block scales quadratically with the code distance  $n_{\text{code}} = (2t+1)^2 \sim [\ln(L_{\text{tot}}/L_0)]^2$ , and the initialization can be reduced to the preparation of  $(2t+1)$ -qubit GHZ states. For finite total distance  $L_{\text{tot}}$ , a more useful performance metric for comparing the QR protocols should quantify both the amount of physical resources and the communication rate; see Sec. III.B.4.

### 3. Third-generation repeaters

The third generation of QRs relies on deterministic error suppression, such as QEC and one-way hashing (see Sec. III.A.4.a), to correct both loss and operation errors (Fowler *et al.*, 2010; Munro *et al.*, 2012; Muralidharan *et al.*, 2014). The quantum information can be directly encoded in a block of physical qubits that is sent through the lossy channel. If the loss and operation errors are sufficiently small, the received physical qubits can be used to restore the entire encoding block, which is retransmitted to the next repeater station. The third generation of QRs only needs one-way signaling and thus can achieve high communication rates, just like classical repeaters that are limited only by local operation delays.

Various choices of quantum error-correcting codes can be used for the third generation of QRs (Knill and Laflamme, 1996). For qubit-based quantum error correction, we can use quantum parity codes (Ralph, Hayes, and Gilchrist, 2005) with moderate coding blocks ( $\sim 200$  qubits) to efficiently overcome both loss and operation errors (Munro *et al.*, 2012; Muralidharan *et al.*, 2014). The surface code (Raussendorf and Harrington, 2007; Raussendorf, Harrington, and Goyal, 2007) or the tree-cluster code (Varnava, Browne, and Rudolph, 2006) can suppress more loss errors (up to 50%) with larger encoding blocks. For quantum codes based on  $d$ -level quantum systems (for instance, based on time-bin encoding), we can implement quantum polynomial codes (Cleve, Gottesman, and Lo, 1999) to approach loss tolerances of up to 50% (Muralidharan *et al.*, 2017) and quantum Reed-Solomon codes (Li, Xing, and Wang, 2008) to further improve the key generation rate (Muralidharan *et al.*, 2018). If we treat each optical mode as a continuous-variable system, we can use bosonic quantum error-correcting codes [such as cat codes (Leghtas *et al.*, 2013; Mirrahimi *et al.*, 2014), binomial codes (Michael *et al.*, 2016), and GKP codes (Gottesman, Kitaev, and Preskill, 2001; Albert *et al.*, 2018; Noh, Albert, and Jiang, 2019)] to correct the loss

errors. The advantage of bosonic codes is that they can efficiently use the large Hilbert space of bosonic systems and reduce the number of bosonic modes, which might be advantageous for maximizing the usage of our optical quantum channel bandwidth (Li *et al.*, 2017). To further suppress the residual errors from the first-level bosonic codes, we can concatenate it with a second-level DV encoding, which leads to a concatenated CV-DV encoding scheme. To reduce the resource cost with respect to an architecture for which all repeaters are the same, we can introduce two different types of repeaters, correcting errors at two different levels (Rozpedek *et al.*, 2021).

Note that the second and third generations of QRs can achieve communication rates much faster than the first generation over long distances, but they are technologically more demanding. For example, they require high-fidelity quantum gates, as QEC works well only when operation errors are below the fault-tolerance threshold. The repeater spacing for the third generation of QRs is smaller than that of the first two generations of QRs because error correction can correct only a finite amount of loss errors deterministically [up only to 50% loss error rates deterministically (Stace, Barrett, and Doherty, 2009; Muralidharan *et al.*, 2014)].

As with the second generation of QRs, the physical resources required for the third generation of QRs depend on the size of the quantum error-correcting code. We can use  $n_{\text{code}}$  to characterize the size of the encoding blocks based on qubits or bosonic modes. At each repeater station, we need  $O(n_{\text{code}})$  quantum memories to perform error correction suppressing not only operation errors but also loss errors. The total number of quantum memories (in terms of qubits or bosonic modes) needed is  $N_{\text{tot}} \sim n_{\text{code}} L_{\text{tot}} / L_0$ . In principle we can use QEC over optical modes to fully replace the need for traditional atomic or solid-state quantum memory, which inspires the design of all-photonic quantum repeaters, as discussed in Sec. III.C.

For the specific application of quantum key distribution, we can use QRs to generate random secret classical bits shared by remote parties. Since the ultimate goal is to generate secret keys rather than the entangled states, we might slightly relax the requirement of quantum memories. In particular, in this case, even for first- and second-generation repeaters, there is no need for long-lived quantum memories to store the entangled states at the end stations because they can be measured simultaneously and immediately after starting the protocol (Jiang *et al.*, 2009); see Secs. III.C.1 and VI.A.2. However, notice that first- and second-generation QRs still need quantum memories at repeater nodes, whose required memory time is longer than that of third-generation QRs.

#### 4. Comparison of three generations of QRs

To present a systematic comparison of different QRs in terms of efficiency, we need to consider both temporal and physical resources. The temporal resource depends on the rate, which is limited by the time delay from the two-way classical signaling (in first- and second-generation repeaters) and the local gate operation (in the second and third generations)

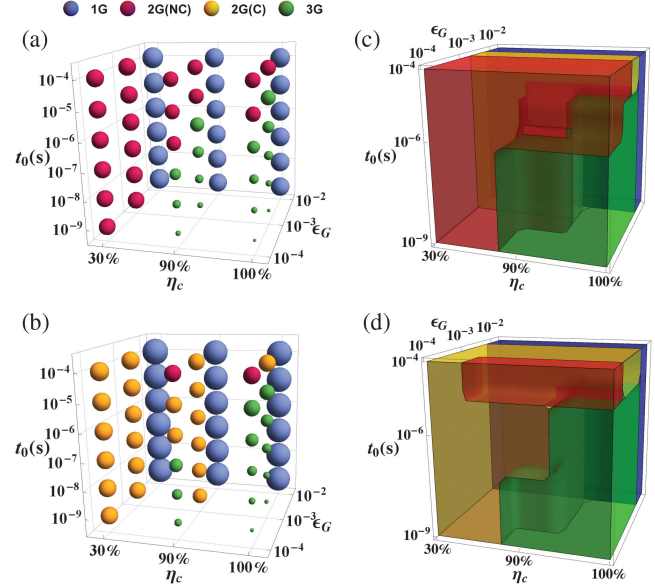


FIG. 6. Bubble plot comparing various QR protocols in the three-dimensional parameter space spanned by coupling efficiency  $\eta_c$ , gate error probability  $\epsilon_G$ , and gate time  $t_0$  for (a)  $L_{\text{tot}} = 1000$  km and (b)  $L_{\text{tot}} = 10000$  km. The bubble color indicates the associated optimized QR protocol, and the bubble diameter is proportional to the cost coefficient. Region plots show the distribution of different optimized QR protocols in the three-dimensional parameter space for (c)  $L_{\text{tot}} = 1000$  km and (d)  $L_{\text{tot}} = 10000$  km. A yellow region of the second generation with encoding is contained in (c), which can be verified in a bubble plot with a finer discretization of  $\epsilon_G$ . From Muralidharan *et al.*, 2016.

(Jiang, Taylor, Khaneja, and Lukin, 2007). The physical resources depend on the total number of qubits needed for the HEGP (first and second generations) and QEC (second and third generations) (Bratzik, Kampermann, and Bruss, 2014; Muralidharan *et al.*, 2014). One can quantitatively compare the three generations of QRs using a cost function (Muralidharan *et al.*, 2014) related to the required number of qubit memories to achieve a given transmission rate. If a total of  $N_{\text{tot}}$  qubits are needed to generate secure keys at  $R$  bits per second, a cost function is defined as

$$C(L_{\text{tot}}) = \frac{N_{\text{tot}}}{R} = \frac{N_s}{R} \frac{L_{\text{tot}}}{L_0}, \quad (36)$$

where  $N_s$  is the number of qubits needed per repeater station,  $L_{\text{tot}}$  is the total communication distance, and  $L_0$  is the spacing between neighboring stations. Since the cost function scales at least linearly with  $L_{\text{tot}}$ , to demonstrate the additional overhead associated with  $L_{\text{tot}}$  a cost coefficient can be introduced as

$$C'(L_{\text{tot}}) = \frac{C(L_{\text{tot}})}{L_{\text{tot}}}, \quad (37)$$

which can be interpreted as the resource overhead (qubits times time) for the creation of one secret bit over 1 km (with the target distance  $L_{\text{tot}}$ ). Besides the fiber attenuation [which is chosen as  $L_{\text{att}} = 20$  km in Fig. 6 by Muralidharan *et al.*

(2016)], the cost coefficient also depends on other experimental parameters, in particular, the coupling efficiency  $\eta_c$ , the gate error probability  $\epsilon_G$ , and the gate time  $t_0$ .

We can summarize the analysis of QRs based on the cost coefficient (Muralidharan *et al.*, 2016) using bubble and region plots in the three-dimensional parameter space, as shown in Fig. 6, which compares representative protocols from three generations of quantum repeaters (Briegel *et al.*, 1998; Jiang *et al.*, 2009; Muralidharan *et al.*, 2017).<sup>8</sup> The bubble color indicates the associated optimized QR protocol, and the bubble diameter is proportional to the cost coefficient. The parameter space can be divided into the following regions: (I) For high gate error probability ( $\epsilon_G \gtrsim 1\%$ ), the first generation dominates. (II.A) For intermediate gate error probability but poor coupling efficiency or slow local operation ( $0.1L_{\text{att}}/L_{\text{tot}} \lesssim \epsilon_G \lesssim 1\%$  and  $\eta_c \lesssim 90\%$  or  $t_0 \gtrsim 1\ \mu\text{s}$ ), the second generation with encoding is more favorable. (II.B) For low gate error probability but low coupling efficiency or slow local operation ( $\epsilon_G \lesssim 0.1L_{\text{att}}/L_{\text{tot}}$  and  $\eta_c \lesssim 90\%$  or  $t_0 \gtrsim 1\ \mu\text{s}$ ), the second generation without encoding is more favorable. (III) For high coupling efficiency, fast local operation, and low gate error probability ( $\eta_c \gtrsim 90\%$ ,  $t_0 \lesssim 1\ \mu\text{s}$ , and  $\epsilon_G \lesssim 1\%$ ), the third generation becomes the most favorable scheme in terms of the cost coefficient.

### C. All-optical repeaters

While the traditional repeater protocol necessitates physical memories (stationary quantum systems) to store quantum information during the long waits associated with long-distance entanglement generation, it is fairly nontrivial whether the protocol can be implemented all optically solely by replacing the memories with all-optical memories like those proposed by Leung and Ralph (2006). Note, however, that repeaters featuring QEC codes could preclude the necessity of such memories, as QEC codes can instead deterministically suppress the noise and loss affecting qubits. Indeed, error-corrected repeaters, which intersect with the previously discussed second and third generations, are shown to be implementable all optically; in this case, the significant differences in analysis and implementation compared to matter-based repeaters warrant special attention, which we now provide.

To better understand all-optical or all-photonic repeaters, we first review the operating principle of another quantum information protocol MBQC (sometimes referred to as one-way computation<sup>9</sup>), which is especially relevant for optical implementations. In a measurement-based quantum computer (Raussendorf and Briegel, 2001), in contrast to a gate-based computer, an entangled resource state, namely, a cluster (or graph) state (Sec. II.D.1), is initially prepared and the computation proceeds by way of adaptive single-qubit

measurements on this state. For physical platforms suffering from probabilistic entangling gates, among them discrete-variable dual-rail photonics (see Sec. II.E), this type of computer has the advantage that such probabilistic gates are involved only in the preparation of the initial resource states and are not necessary during the computation. This circumvents the exponential decay of the computational success with the number of entangling operations and dramatically reduces the resource costs (Nielsen, 2004; Browne and Rudolph, 2005; Kok *et al.*, 2007) compared to the gate-based scheme (Knill, Laflamme, and Milburn, 2001). Furthermore, the measurement-based approach allows for fixed-depth circuits where a physical qubit undergoes only a finite (and generally small) number of gate operations before being consumed by a single-qubit measurement. This approach therefore accords well with flying qubits; it helps to overcome the weakness of probabilistic entangling gates for certain photonic encodings and drastically cuts down on the amount of loss each photon experiences.

In measurement-based computation, universality (the ability to approximate any unitary on any number of data qubits arbitrarily well) is achieved through an appropriate choice of cluster state (Briegel and Raussendorf, 2001), as well as access to non-Clifford operations. Fault tolerance (the exponential suppression of state preparation and gate and measurement errors) is obtained through an error-correcting code (Sec. III.A.4.a.1), which translates to a cluster state with a special shape and structure (the encoding); a prescription for implementing logical operations through adaptive single-qubit measurements; and a means of detecting and correcting the error, including an algorithm for extracting the outcomes of logical measurements (the decoding and recovery).

A common feature of recent architectures of all-optical repeaters is that they are realizable through measurement-based implementations of QEC codes. A measurement-based quantum repeater operates in much the same way as a measurement-based computer; however, there is a handful of salient distinctions, which is emblematic of the differences between computation and communication. First, gate-set universality is not necessary for communication, meaning that Clifford operations suffice. Second, the dominant source of errors for the photonic states constituting optical repeaters, namely, loss, is an even larger threat. Third, in contrast to computation, which can be done locally, the goal of communication is inherently nonlocal: to entangle spatially distant objects. Since noise for physical qubits generally increases with time, it is important to take the classical communication time into account.

With these general notions out of the way, in Secs. III.C.1–III.C.3 we overview the workings of several protocols for all-optical repeaters and describe promising schemes for the preparation of repeater graph states. We begin with a summary of the first all-photonic repeater proposal (Azuma, Tamaki, and Lo, 2015) as an instructive example.

#### 1. Original all-photonic repeaters

The review of the all-photonic repeaters by Azuma, Tamaki, and Lo (2015) begins with a description of the repeater graph state (RGS). The ideal RGS that they proposed has two layers.

<sup>8</sup>The communication rate for the first generation of QRs can be boosted using temporal, spatial, and/or frequency multiplexing associated with the internal degrees of freedom for the quantum memory (Afzelius *et al.*, 2009; Sanguard *et al.*, 2011).

<sup>9</sup>“One-way” has a special meaning in quantum communication, so we forego this terminology.

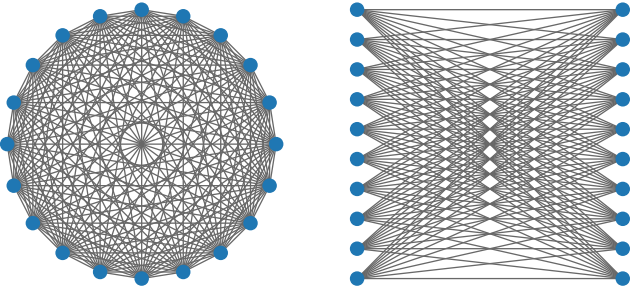


FIG. 7. Left graphic: clique. Right graphic: biclique. In the clique, each vertex is connected with every other. In the biclique, each vertex from the left set is connected with a vertex on the right, but the sets are internally disconnected. These graphs can underlie repeater graph states. See Sec. II.D.1 for more on graph states.

The inner or core layer is a complete graph or clique (Fig. 7) that is locally equivalent to a GHZ state of  $n$  qubits from Eq. (20). The qubits in the inner layer are tailored to play the same role as quantum memories in a second-generation quantum repeater protocol. Recall the (implicit) assumption of the second-generation QR protocol about quantum memories that allows us to apply deterministic Bell measurements on quantum memories that have successfully shared entanglement with adjacent repeater nodes; see III.B.2. To make photonic qubits play this role, the core qubits in the RGS of Fig. 8 are prepared in a complete-graph state<sup>10</sup> as in Fig. 7 (to overcome the probabilistic nature of the linear-optical Bell measurements). In particular, if we apply  $X$ -basis measurements to two of them and  $Z$ -basis measurements to the other qubits, it works as the Bell measurement on the two qubits and decouples the others (although we only use single-qubit measurements). To achieve these  $X$ -basis or  $Z$ -basis measurements deterministically even under photon loss, the qubits in the inner layer are encoded into a larger graph state with sufficient redundancy. Azuma, Tamaki, and Lo (2015) considered a tree-graph QEC code proposed by Varnava, Browne, and Rudolph (2006) for this purpose, as demonstrated schematically in the right graphic of Fig. 8. This code places a qubit to be encoded at the root of a tree-graph state composed of physical qubits. It then allows one to execute an arbitrary logical single-qubit measurement on the encoded qubit deterministically, even under loss, via single-qubit measurements on the physical qubits. Increasing the size of the tree-graph state with increasing losses will ensure that the correction succeeds as long as the loss probability per physical qubit is less than 50%, a threshold consistent with the no-cloning theorem.

The other layer of the RGS consists of outer qubits or leaves appended to the vertices of the core graph (Fig. 8); these are analogous to photons entangled with quantum memories for the purpose of the HEGP in the second-generation QR protocol. In fact, a pair of outer qubits, each of which belongs

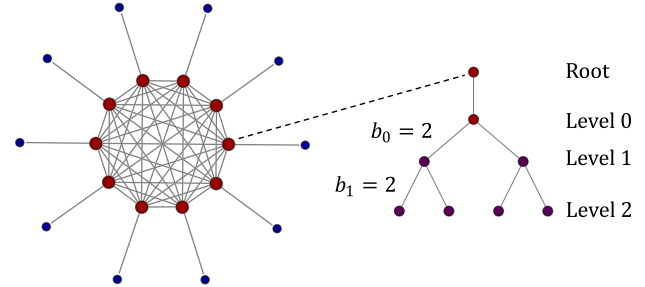


FIG. 8. Encoded RGS proposed by Azuma, Tamaki, and Lo (2015). Left graphic: the two layers of the RGS. The inner layer is composed of core qubits (large red vertices, closer to the center), while the outer layer is composed of outer qubits (or leaves) (small blue vertices, farther from the center). Each vertex in the clique (left graphic) is a logical qubit, which can be encoded in, for instance, the Varnava tree code (right graphic) (Varnava, Browne, and Rudolph, 2006) to protect itself from loss (as well as general errors under the restriction of Pauli measurements). Displayed are the levels and branching parameters  $\{b_0, b_1, \dots, b_{d-1}\}$  of the tree ( $d = 2$  here). Note the root and zeroth-level qubits (the two upper red qubits) in the tree will be measured out in the  $X$  basis, connecting the qubits in the first level with all of the neighbors of the root qubit. The inner logical qubits, which are conduits for the entanglement swapping, are connected to outer unencoded physical leaf qubits, which help effect the entanglement generation.

to a different RGS, will be subject to a linear-optical Bell measurement in order to entangle their neighboring core qubits. Combining these layers of the RGS, the final state proposed by Azuma, Tamaki, and Lo (2015) is shown in Fig. 8.

With an understanding of the RGS, we can now overview the precise operations required for Alice and Bob to establish an entangled pair in a given clock cycle of the all-photonic repeater protocol. The scheme is illustrated in Fig. 9. We use the notation from before:  $L$  is the total channel length;  $N$  is the number of repeater stations (sources or major nodes), not including Alice and Bob; and  $m$  is the number of parallel pulses. This means that there are  $N + 1$  measurement stations (receivers or minor nodes), and  $M = 2m$  is the number of core qubits of the RGS if it is symmetric.

We assume that an RGS is available at each source node (leaving the various preparation mechanisms for Sec. III.C.3). Each of the two (minor) nodes neighboring the source node receives half of the photons in the RGS prepared and sent by the source. Upon arrival of the photons, every receiver first conducts simultaneous Bell-state measurements (BSMs) [Fig. 3(a)] on  $m$  pairs of leaf photons of RGSs from different source nodes; this connects their adjacent inner qubits. Although each such BSM can succeed with a probability of at most only 1/2 (and it is less than 1/2 in practice because of the losses experienced by the leaves), with  $m$  large enough at least one BSM per station would be guaranteed to have succeeded. Depending on the outcomes of the BSMs, every receiver node applies  $X$ -basis measurements on a pair of the inner qubits whose adjacent leaves have been subject to a successful BSM, and  $Z$ -basis measurements on the other inner qubits. Since inner qubits are encoded in the tree-graph code, these single-qubit measurements succeed almost

<sup>10</sup>However, Russo, Barnes, and Economou (2018) and Tzitrin (2018) showed that some of the connections in the clique composing the RGS are unnecessary, so some variant, such as the biclique in Fig. 7, is sufficient as core qubits.

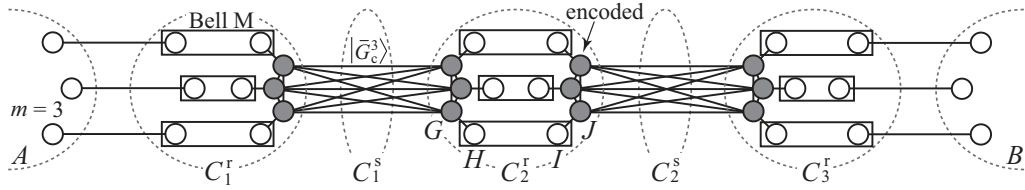


FIG. 9. Summary of the original all-photonic repeater scheme (Azuma, Tamaki, and Lo, 2015). Alice (A) and Bob (B) want to establish one entangled pair; each prepares  $m$  Bell pairs ( $m = 3$  here) and sends them to a nearby receiver. Repeater graph states are created at  $C_1^s$  and  $C_2^s$  and their qubits are sent to adjacent receivers  $C_1^r$  and  $C_2^r$  and the ones  $C_3^r$  and  $C_3^s$ , respectively. The receivers perform  $m$  simultaneous Bell-state measurements on the outer qubits. In every receiver node, X-basis measurements are performed on a pair of inner qubits adjacent to outer qubits, to which the Bell measurement is successfully applied, while Z-basis measurements are conducted on the other inner qubits. From Azuma, Tamaki, and Lo, 2015.

deterministically (as long as the loss is below the threshold of 50%). Effectively, the Z-basis measurements transform the total state into a linear-cluster state between Alice and Bob, which is then converted into a Bell pair between them by the X-basis measurements, according to the effects detailed in Sec. II.D.1.

Note that the choice of the measurement on an inner encoded qubit, and accordingly on the physical qubits composing the tree cluster, depends on the measurement outcomes from the outer qubits. This means that it is necessary to convey classical information from the outer qubits to the inner qubits. However, this can be done locally at each receiver node (that is, simply by using a local active-feed-forward technique), as the inner qubits are transmitted together with their adjacent outer qubits. Therefore, the amount of necessary signaling is designed to be minimal, reducing time-dependent loss and errors for the photons.

Although loss is the dominant source of noise, one cannot dismiss other sources of error. Aided by a majority vote protocol, the tree-graph code of Varnava *et al.* was robust against general errors under the restriction of X-basis or Z-basis measurements on the encoded qubit, in contrast to other single-qubit measurements. In Sec. III.C.2, we overview an optical repeater protocol that instead makes use of parity codes (Ewert, Bergmann, and Van Loock, 2016). The existence of a better code specifically suited to an all-photonic repeater (in terms of error tolerance and overheads) is an important open question.

The all-optical protocol needs no quantum memories, including qubits held by Alice and Bob, for the applications in which entanglement for Alice and Bob, once generated, is consumed immediately to generate classical output strings such as QKD (Bennett, Brassard, and Mermin, 1992; Lo and Chau, 1999; Shor and Preskill, 2000; Mayers, 2001; Renner, 2008; Koashi, 2009; Portmann and Renner, 2022), nonlocal measurements (Vaidman, 2003; Clerk *et al.*, 2010), and cheating strategies in position-based quantum cryptography (Buhrman *et al.*, 2011; Kent, Munro, and Spiller, 2011; Lau and Lo, 2011). However, for applications that demand a strictly quantum output state to Alice and Bob, such as quantum teleportation and distributed quantum computation (Gottesman, 1999; Eisert *et al.*, 2000; Collins, Linden, and Popescu, 2001), the applications themselves require Alice and Bob to have quantum memories with memory time on the order of classical communication time between Alice and Bob

because of the necessity of classical signaling. See Sec. VI.A.2 or Azuma, Tamaki, and Lo (2015) for details.

## 2. Other optical repeaters

### a. Modified all-photonic repeaters

Although Pant *et al.* (2017) aimed to analyze the performance of the all-photonic repeaters of Azuma, Tamaki, and Lo (2015), they made several modifications that warrant discussion.

First, so-called boosted Bell-state measurements (BBSMs) were employed by Pant *et al.* (2017). The previously cited maximal linear-optical Bell measurement success rate of 1/2 can be increased with additional resources, such as ancillary photons in separable (Ewert and Van Loock, 2014) or entangled states (Grice, 2011), weak nonlinearities (Barrett *et al.*, 2005), and predetection squeezing (Zaidi *et al.*, 2015; Kilmer and Guha, 2019). However, BBSMs are no panacea: they increase experimental complexity and overhead, and infinite resources are still needed for unity success probability, which is in line with a no-go theorem (Lütkenhaus, Calsamiglia, and Suominen, 1999). The specific BBSMs (Ewert and Van Loock, 2014) employed by Pant *et al.* (2017) succeed 3/4 of the time. The analysis shows that they result in a net improvement to the overheads.

A more crucial design change is in the treatment of the inner qubits. In the original proposal, photons forming the clique of the RGS (the encoded inner qubits) are sent to neighboring receiver nodes together with their adjacent leaves, while Pant *et al.* (2017) assumed that they are stored locally at the source nodes in fiber spools. In the original proposal, signaling from the leaves to the inner qubits can be done via local active feed forward; however, all the physical qubits in the encoding must be sent, necessitating a large number of fiber connections. While resulting in fewer fiber connections, the approach of Pant *et al.* comes at the expense of an increased loss, which stems from the necessity of signaling from the leaves to the inner qubits over the associated distance. Finally, there is also a modification of the original scheme in Pant *et al.* with regard to the multiplexing strategy in state generation, which is discussed in Sec. III.C.3.

### b. Repeaters based on encoded Bell measurements

Ewert, Bergmann, and Van Loock (2016) and Lee, Ralph, and Jeong (2019) presented all-optical repeater protocols

based on parity codes (Ralph, Hayes, and Gilchrist, 2005). Specifically, Ewert, Bergmann, and Van Loock (2016) made use of Bell states with parity encoding. The graph states locally equivalent to the encoded Bell states look much like the RGS from the original protocol: they are bicliques (complete bipartite graphs) with multiple leaves per node (Ewert and Van Loock, 2017). However, the protocol of Ewert *et al.* itself is conceptually different from the all-photonic repeaters of Azuma, Tamaki, and Lo (2015), as also mentioned by Zwerger, Briegel, and Dür (2016); it sends an encoded qubit directly from a sender to a receiver, which makes it closer to the third-generation schemes of Knill and Laflamme (1996), Varnava, Browne, and Rudolph (2007), Muralidharan *et al.* (2014), Zwerger, Briegel, and Dür (2014), and Munro *et al.* (2015) based on quantum error correction than the protocol of Azuma, Tamaki, and Lo (2015), which can be regarded as a time-reversed version of a second-generation quantum repeater protocol. In their protocol (Ewert, Bergmann, and Van Loock, 2016), Bell measurement efficiency and loss tolerance improves as the size of the parity code increases. Furthermore, their scheme does not require active-feed-forward techniques, lowering local operation times, reducing losses, and facilitating on-chip integration. The concatenated Bell measurement scheme of Lee, Ralph, and Jeong (2019) reached the fundamental limits for Bell measurement efficiency and loss tolerance under the constraints of linear optics and the no-cloning theorem. Regarding loss tolerance, this scheme also saturates the fundamental loss-tolerance limits for logical Bell measurements based on adaptive linear-optical physical Bell measurements (Hilaire, Castor *et al.*, 2023). However, recent Bell measurement schemes (Hilaire *et al.*, 2021; Bell, Pettersson, and Paesani, 2023), based on an adaptive combination of physical two-photon Bell measurements and single-qubit measurements, exhibit an even stronger loss tolerance (saturating the no-cloning limit). The performances of these new logical Bell measurement schemes remain to be evaluated in a quantum repeater scheme. In a recent development (Niu *et al.*, 2023), the all-photonic quantum repeater concept has been expanded to low-density-parity-check codes with linear encoding rates. The consequential linear scaling of logical transmitted qubits with code size was to significantly enhance end-to-end communication rates.

#### c. Bosonic repeaters

Certain repeaters based on continuous-variable states have been proposed (Fukui, Alexander, and Van Loock, 2021; Rozpędek *et al.*, 2021). They leverage the inherent error-correction properties of bosonic encodings along with higher-level qubit codes to create what can be viewed as concatenated CV-DV error-correcting codes. Recall from Sec. II.E that there are several advantages to the GKP encoding, in particular. For one, it can tolerate small displacement errors; since any continuous error can be decomposed into displacements, it can natively treat loss errors as well. In fact, it was discovered that GKP states fare better against loss errors in certain settings than codes tailored to handle losses (Albert *et al.*, 2018). Furthermore, for GKP states entangling gates and Bell measurements are deterministic contingent on the availability of Gaussian resources, with the only probabilistic component being state generation. Finally,

additional analog information obtained from GKP-level error correction can be used to improve the logical error rates at the qubit code level (Fukui, Tomita, and Okamoto, 2017; Noh and Chamberland, 2020).

The repeater architecture given by Rozpędek *et al.* (2021) leveraged the aforementioned advantages of GKP encodings and used two types of repeaters: those consisting purely of GKP states, which can correct small displacement errors, and those comprising GKP states concatenated with small qubit-level codes. In a related work, Fukui, Alexander, and Van Loock (2021) compared the use of GKP encoding on its own, in a one- or two-way scheme, and with higher-level encodings.

### 3. Repeater graph state generation

Producing a large, high-quality optical graph state for measurement-based quantum information protocols is a tall order. In all-optical approaches, the stochasticity of entangling operations in some encodings (such as dual-rail ones) and of state preparation in others (such as GKP states) can result in large overheads; in matter-based approaches, effects like decoherence and inhomogeneity between emitters can result in a significant decay of entanglement with the size of the target state. Nevertheless, there has been steady theoretical and experimental progress toward high-probability, high-fidelity cluster state generation. We now discuss some promising ways of preparing optical graph states.

#### a. General framework

Optical graph state generation can be understood in a general framework that involves the “stitching” of smaller resource states into iteratively larger states. Measurement-based entangling operations, such as those used for dual-rail encodings, are more formally referred to as fusion gates (Browne and Rudolph, 2005); they were introduced by Pittman, Jacobs, and Franson (2001). Fusion gates on two spatial modes, each of which may have a single photon in the polarization or path degrees of freedom, come in two varieties: type-I fusions, which consume a single photon to create larger one-dimensional cluster states, and type-II fusions (essentially, rotated Bell measurements), which consume two photons to grow cluster states in higher dimensions. As with BSMs, fusion probabilities may also be boosted with additional resources, a fact that was exploited for RGS generation by Pant *et al.* (2017); as before, this introduces trade-offs with experimental complexity and overheads (Gimeno-Segovia, 2016). For completeness, we also mention fusion-based quantum computation (Bartolucci *et al.*, 2023), a proposed alternative framework to MBQC where the fusion operations serve to both create entanglement and perform logical operations.

The schema for generating optical graph states is as follows:

- (1) *Unit resource production.* First, an optical circuit produces the smallest unit states. These can be single-qubit states or small entangled states such as Bell pairs,  $n$ -partite GHZ states for  $n \geq 3$ , and few-qubit linear-cluster states.
- (2) *Growth into metaunits.* As an optional intermediary step, the unit resources can be combined into larger metaunits. The utility of this extra step is to leave open the possibility, for example, of generating dual-rail  $n$ -partite GHZ states directly from single photons, or

instead from photonic Bell pairs; see [Gimeno-Segovia \(2016\)](#).

(3) *Stitching.* Units or metaunits are entangled iteratively until the desired graph state is created. For dual-rail encodings, this can be achieved with type-II fusions; for GKP states, this can be done with continuous-variable CZ gates.

A few notes are in order. First, the framework accommodates matter-based optical graph state generation; in this case, the entanglement in the growth or stitching stages can be achieved either directly at the optical level or with the assistance of the interaction between emitters. Second, each step carries an associated probability and fidelity that depends on the choice of encoding, the scheme for generating and entangling the resources, and the particular hardware implementation. Other considerations that will affect the architectural design include how much of the state can be made spatially (i.e., with the state composed of single photons generated at the same time but spread over space) or temporally (i.e., with the state composed of single photons generated at different time steps). This is related to the question of how much of the graph state (for instance, how many layers in a regular cluster state) must exist at one time.

#### *b. Dual-rail graph states*

We review two different approaches to produce a graph state of dual-rail encoded qubits: one all optical but probabilistic, the other relying on matter qubits but deterministic.

#### *i. Probabilistic (optical) generation*

The original all-photonic repeater proposal ([Azuma, Tamaki, and Lo, 2015](#)) relies on the approach taken by [Varnava, Browne, and Rudolph \(2007, 2008\)](#) for generating a tree-graph state specified by a branching parameter  $\{b_0, b_1, \dots, b_{d-1}\}$  (Fig. 8), where the root qubit of the tree-graph state is connected to a zeroth-level qubit, the zeroth-level qubit is connected to  $b_0$  first-level qubits by edges and every  $i$ th-level qubit is connected to  $b_i$  ( $i+1$ )th-level qubits by edges ( $i = 0, 1, \dots, d-1$ ). As the encoding, the root and the zeroth-level qubits are measured off line in the  $X$  basis. The tree-graph state can be transformed into an RGS. The protocol of [Varnava \*et al.\*](#) proceeds as follows.

To begin, six single photons are prepared with single-photon sources. The photons are then sent to an optical circuit composed of beam splitters, a type-I fusion gate, and a type-II fusion gate, which produces a tripartite GHZ state with probability  $1/32$ . Thanks to the design of this circuit, even if single-photon sources and detectors do not have unity efficiency, the generated tripartite GHZ state is affected only by individual (uncorrelated) loss ([Varnava, Browne, and Rudolph, 2008](#)). This GHZ state then becomes the unit resource to produce the RGS. In particular, two tripartite GHZ states are converted to a four-partite GHZ state by a type-II fusion gate, and this four-partite GHZ state corresponds to a three-qubit tree, i.e., a  $\{2\}$  tree, with a redundant root qubit composed of two qubits. From these elementary  $\{2\}$  trees, one can efficiently generate an arbitrary  $\{b_0, b_1, \dots, b_{d-1}\}$  tree from the bottom ( $d$ th level) to the top (zeroth level) with the help of type-II fusion gates.

Several generalizations or modifications are possible for this procedure. [Pant \*et al.\* \(2017\)](#) chose the more efficient generation scheme of [Li \*et al.\* \(2015\)](#), considered boosted fusion gates, improved the multiplexing strategy, and reordered the local measurements unconditioned on BSM outcomes. Furthermore, it is possible to create  $n$ -partite GHZ resource states with probability  $1/2^{2n-1}$ , and this number can theoretically be increased with Bell-state inputs rather than single-photon inputs, as well as boosted BSMs ([Joo \*et al.\*, 2007; Varnava, Browne, and Rudolph, 2008; Zhang \*et al.\*, 2008; Gimeno-Segovia, 2016](#)). For optical repeaters based on other error-correcting codes, which correspond to other graph states, these resource states can be stitched according to the different, tailored procedures.

#### *ii. Deterministic (matter-based) generation*

Unlike fusion-based approaches, which are fundamentally probabilistic, the protocol of [Buterakos, Barnes, and Economou \(2017\)](#), which uses emitter and ancilla qubits to generate the RGS, is (at least in principle) deterministic. The generation of linear-cluster states from a single emitter was proposed by [Schön \*et al.\* \(2005\)](#) for atomic systems and by [Lindner and Rudolph \(2009\)](#) for quantum dots (QDs). More complex graph states, including a 2D square lattice cluster state, can be created by a linear chain of emitters with nearest-neighbor coupling ([Economou, Lindner, and Rudolph, 2010; Gimeno-Segovia, Rudolph, and Economou, 2019](#)). Indeed, any graph state can be created with these ingredients ([Russo, Barnes, and Economou, 2019](#)). [Buterakos, Barnes, and Economou \(2017\)](#) found that the key mechanism for generating the RGS is to entangle the emitter with an ancilla and pump it to produce one arm of the RGS, which emerges entangled to both the emitter and the ancilla. The emitter is then measured and thus removed from the graph, and the process is repeated until all the photonic arms are connected to the ancilla, which is assumed to have a longer coherence time than the emitter. Measurement on the ancilla in the  $Y$  basis disentangles it from the graph and connects all the inner photons to each other, completing the RGS.

An attractive feature of the protocol of [Buterakos, Barnes, and Economou \(2017\)](#) is that it is economical in terms of resources, which are quantified by the number of required matter qubits: To generate the unencoded version of the RGS, only one emitter and one ancilla are needed, regardless of the size of the graph. In addition to the unencoded version, [Buterakos, Barnes, and Economou \(2017\)](#) provided a recipe for the deterministic creation of arbitrarily large encoded RGSs in which the inner qubits are encoded using trees of depth 2 or 3. These protocols require only three matter qubits, including two emitters and one ancilla. [Hilaire, Barnes, and Economou \(2021\)](#) gave a more general recipe for generating RGSs with arbitrarily deep tree encodings of the core photons in which the requisite number of matter qubits scaled linearly with the tree depth  $d$  ( $d-1$  emitters and two ancilla qubits). In this case, the number of required CZ gates is  $2m(2 + \sum_{k=0}^{d-2} \prod_{j=0}^k b_j)$ , where  $b_j$  denotes the branching vector component of the tree at level  $j$  and  $2m$  is the number of arms in the RGS. These ideas for the deterministic generation of entangled photonic states were generalized by [Li, Economou, and Barnes \(2022\)](#), who

provided a recipe for the generation of an arbitrary graph using the minimal number of emitters.

Buterakos, Barnes, and Economou (2017) also introduced a recipe for producing tree graphs of arbitrary depth  $d$  with  $k$  arms at each vertex using  $d - 1$  emitters and one ancilla. The number of CZ gates required in this case is  $[b^d + (-1)^{d+1}]/(k + 1) - 1$ . This approach for creating tree-encoded photonic qubits is a powerful capability in its own right and can be applied to quantum repeaters of any generation. For example, Borregaard *et al.* (2020) employed this tree generation procedure in their proposed scheme to implement third-generation repeaters using silicon-vacancy (Si-V) defects in diamond as memory qubits.

The deterministic RGS protocol can be applied to any type of dual-rail encoding. Many of the proposals for graph state generation, especially with quantum dots, consider photon polarization encoding, but time-bin encoding has also been proposed in these systems (Lee *et al.*, 2019). In the case of time-bin encoding, an alternative deterministic way of generating graph states is to use a single emitter and time-delayed feedback, as proposed by Pichler *et al.* (2017) and as adapted for RGS generation by Zhan and Sun (2020). To implement a maximally entangling gate, however, these approaches require the experimentally challenging capability of strong coupling between the emitter and the photonic waveguide where the photons propagate.

For the physical implementation of deterministic RGS generation schemes, modest-sized registers of well-controlled emitters and ancilla qubits are needed. The emitters need to be of high quality, especially in terms of brightness, so that the photon is emitted in the desired mode and successfully collected. This is critical for the protocol to be classified as deterministic. The register should also feature ancilla qubits with long coherence times, albeit not as long as what is required for quantum memories in first- and second-generation repeaters, along with the ability to perform high-fidelity gates between emitters and ancillae.

Self-assembled QDs are leading contenders for RGS generation. Indeed, the first experimental demonstration of an emitter-based cluster state generation protocol (Schwartz *et al.*, 2016) employed exciton-biexciton transitions in these systems. QDs are excellent photon emitters. They have an efficient optical (excitonic) transition with a timescale of 1 ns (100 ps) without (with) coupling to a cavity. The QD community has made rapid progress over the last several years to improve the brightness, indistinguishability, and purity of QD photon sources (Senellart, Solomon, and White, 2017). Note, however, that QDs have relatively low coherence times compared to point defects and atomic qubits and lack a long-lived quantum memory to act as the ancilla. Nevertheless, promising recent work (Gangloff *et al.*, 2019; Jackson *et al.*, 2021) suggests that the dense nuclear spin environment (more than  $10^4$  spinful nuclei) could potentially be cooled and controlled enough to play this role.

Other candidates for deterministic RGS generation are optically active point defects in wide band gap materials, such as the nitrogen-vacancy or silicon-vacancy centers in diamond and the silicon-carbon divacancy or silicon vacancy in silicon carbide. These systems have longer coherence times

than quantum dots and feature a small number of nuclear spins (natural abundance  $\sim 1\%$  in C and  $\sim 4\%$  in Si), which can be isolated and controlled well and are thus already being explored as memory registers for quantum repeater nodes (Taminiau *et al.*, 2012; Nguyen *et al.*, 2019a; Bourassa *et al.*, 2020). However, defects are not as efficient and bright as QDs, and they tend to emit into unwanted modes a large fraction of the time. Atomic systems, such as trapped ions and atoms in optical lattices or cavities, have long coherence times and can be controlled with high fidelity. While their photon emission is not as fast, their other attractive properties could possibly compensate for the lower rates (Thomas *et al.*, 2022). Hybrid strategies combining deterministic generation based on quantum emitters and linear-optical fusion are particularly appealing when quantum emitters cannot interact with each other (Herrera-Martí *et al.*, 2010; Hilaire, Vidro *et al.*, 2023). In that setting, we can use quantum emitters to generate one-dimensional clusters and GHZ states deterministically and fuse them probabilistically using linear-optical boosted fusion gates to generate graph states of arbitrarily complex topologies.

#### c. GKP-encoded graph states

While entangling gates for GKP encodings are deterministic and readily accessible experimentally, state preparation is a greater challenge. There are several existing proposals to this end, with a recent focus on modified Gaussian boson sampling devices, which use Gaussian optics combined with photon-number-resolving detection (Quesada *et al.*, 2019; Sabapathy *et al.*, 2019; Su, Myers, and Sabapathy, 2019; Tzitrin *et al.*, 2020). Once the GKP states are produced, they can be stitched together deterministically with passive and static optical resources, namely, beam splitters, phase shifters, and delay lines (Tzitrin *et al.*, 2021).

#### d. Performance and overheads

The overheads of the various optical repeater protocols are highly sensitive to the chosen state generation scheme. Here we review the resource requirements and performances of the repeaters discussed in this section.

In the original all-photonic repeater protocol (Azuma, Tamaki, and Lo, 2015), the total number of photons consumed to produce an entangled pair between Alice and Bob scales polynomially with the total distance. The average rate to produce an entangled pair with a single-repeater system is on the order of the repetition rate of the slowest device among single-photon sources, photon detectors, and active-feed-forward techniques. The resource costs for the repeaters discussed by Ewert, Bergmann, and Van Loock (2016) and Ewert and Van Loock (2017) scale linearly or less than quadratically per the number of photons per encoded qubit.

Hilaire, Barnes, and Economou (2021) analyzed the performance of repeaters based on the deterministic RGS generation of Buterakos, Barnes, and Economou (2017) by calculating a bound on the secret key rate per matter qubit and comparing it to direct transmission and to “memory-based” (i.e., first- and second-generation) repeaters. To compare to the latter, the figure of merit is defined as the rate of a Bell-state generation between the end nodes (Alice and Bob) divided by the number of matter qubits per node. In the case of

memory-based repeaters, there is an upper bound on this quantity that originates from the need for classical heralding between nodes and that is given by  $c/4L$ . This bound is used by [Hilaire, Barnes, and Economou \(2021\)](#) for memory-based repeaters; further reductions in the rate originating from SWAP gates between the emitter and memory qubits are ignored.

The deterministic RGS generation based on matter qubits discussed by [Buterakos, Barnes, and Economou \(2017\)](#) relies on entangling CZ gates between emitter and ancilla qubits, which enable us to create complicated photonic graph states. For realistic systems, the longest timescale in the deterministic RGS generation is the duration of these gates  $T_{\text{CZ}}$ , compared to which the photon generation and single-qubit gate times are negligible. It is therefore  $T_{\text{CZ}}$  that sets the bound for the secret key rate for repeaters based on deterministic RGS generation. [Hilaire, Barnes, and Economou \(2021\)](#) fixed the tree encoding depth to 2 for the inner RGS photons and optimize over the RGS size (number of arms), the branching vector  $b_0, b_1$  of the tree encoding, and the number of nodes to maximize the key rate for a total distance of  $10^3$  km. For these distances, it is found that for  $T_{\text{CZ}} \leq 60$  ns the RGS approach always outperforms memory-based repeaters. In this case, the distance between adjacent nodes is approximately 3.5 km. These are most likely conservative estimates since memory-based repeaters also require entangling gates between matter qubits, which will further lower their rates. More research into quantifying the performance of deterministic RGS protocols is needed. For example, [Hilaire, Barnes, and Economou \(2021\)](#) kept the tree encoding depth fixed throughout their treatment ( $d = 2$ ). While deeper trees offer higher protection against photon loss, contributing to an increase of the rate, they also require a larger number of emitter-ancilla CZ gates, thus decreasing the rate. An analysis of optimal encoding depths is an open problem associated with deterministic RGS generation.

Sometimes one is limited not by the number of photons but rather by the number of optical modes available for communicating between neighboring repeater stations (i.e., by the optical channel bandwidth, as in classical communication). Thus, it is important to choose good mode-efficient encoding schemes. In the low-loss regime, we can use continuous-variable codes to encode multiple qubits per bosonic mode; for example, the GKP encoding can almost approach the quantum channel capacity of the one-way pure-loss channel ([Noh, Girvin, and Jiang, 2020](#)). In addition, other CV codes, like cat codes, can also boost the secure communication rate per mode when compared to DV encodings ([Li \*et al.\*, 2017](#)). Moreover, for CV-DV concatenated encoding we can further reduce the resource overhead by optimizing the distribution of two different types of repeaters associated with CV and DV error correction, respectively ([Rozpędek \*et al.\*, 2021](#)).

#### IV. MILESTONES: OUTPERFORMING POINT-TO-POINT OPTICAL COMMUNICATION

Point-to-point communication schemes allow for quantum communication over intracity distances even with the use of a standard optical fiber, and they are ready for practical use; see [Lo, Curty, and Tamaki \(2014\)](#) and [Xu \*et al.\* \(2020\)](#). However, those schemes have a fundamental limitation on

their achievable distances [which are about 500 km in practice, i.e., in the case of the use of a standard optical fiber ([Boaron \*et al.\*, 2018](#); see Sec. III.A.3)]. This limitation is now explicitly given as the form of upper bounds ([Takeoka, Guha, and Wilde, 2014a; Pirandola \*et al.\*, 2017](#)) on the two-way private and quantum capacities of a lossy bosonic channel, which are proportional to the transmittance  $\eta$  of the channel for small  $\eta$ . The two-way private (quantum) capacity represents how many private bits (ebits) can be obtained, in principle, per use of a given channel, in an asymptotically faithful manner, with the free use of LOCC. In the case of the lossy bosonic channel of Eq. (13), these quantities are given by the PLOB bound  $-\log_2(1 - \eta)$  ([Pirandola \*et al.\*, 2017](#)); see Sec. VI.

As one can see from Sec. III, a quantum repeater scheme has no fundamental limitation on its achievable distances. Indeed, it enables us to perform quantum communication efficiently even over intercontinental distances, but its realization is still challenging. This means that there is a technological gap between quantum repeater schemes for intercontinental distances and point-to-point communication schemes for intracity distances.

To bridge the gap, intermediate quantum communication schemes, especially for the application to QKD, for intercity distances have been proposed ([Abruzzo, Kampermann, and Bruß, 2014; Panayi \*et al.\*, 2014; Azuma, Tamaki, and Munro, 2015; Bäuml \*et al.\*, 2015; Luong \*et al.\*, 2016; Lucamarini \*et al.\*, 2018; Rozpędek \*et al.\*, 2019; Xie \*et al.\*, 2022](#)). In particular, the schemes use only a single node  $C$  that is located at the center between a sender Alice and a receiver Bob and is connected to them with optical fibers. The goal of the schemes is basically to double the achievable distances of point-to-point QKD schemes by making the secret key rate proportional to  $\sqrt{\eta}$ , outperforming the two-way private and quantum capacities proportional to  $\eta$  (for small  $\eta$ ), where  $\eta$  is the transmittance of a pure-loss channel between Alice and Bob [see also [Curty, Azuma, and Lo \(2021\)](#), who contextualized this approach from the viewpoint of security for QKD]. This expected secret key rate has the same scaling as the private capacity of single-repeater communication schemes with the use of pure-loss channels ([Azuma, Mizutani, and Lo, 2016; Azuma and Kato, 2017; Rigovacca \*et al.\*, 2018; Pirandola, 2019](#)); see Sec. VI for details. The schemes are divided into three categories: one is based on two-photon interference with dual-rail encoded qubits (Secs. IV.A and IV.D) at the central node  $C$ , another is based on single-photon interference with single-rail encoded qubits (Sec. IV.B), and the third one is a time-reversed version of these (Sec. IV.C) that works without optical Bell measurements. In this section, we review these schemes, whose realizations are regarded as good and natural milestones toward quantum repeaters.

##### A. Adaptive measurement-device-independent QKD

To double the communication distance by utilizing a central node  $C$  between communicators, an adaptive measurement-device-independent (MDI) QKD scheme was proposed with matter quantum memories ([Abruzzo, Kampermann, and Bruß, 2014; Panayi \*et al.\*, 2014](#)) and with all-optical quantum

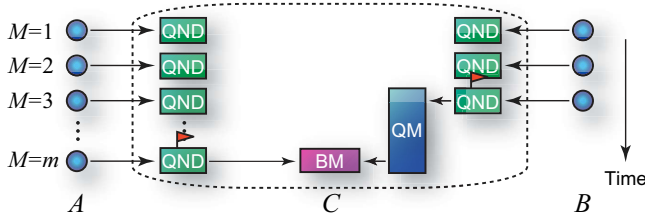


FIG. 10. The concept of memory-assisted MDI QKD. In this protocol, once node  $C$  confirms the arrival of an optical polarization qubit either from Alice's side or from Bob's side with QND measurement (which is indicated by a red flag on a box labeled "QND"), it keeps it in a quantum memory (QM) until an optical polarization qubit arrives at node  $C$  from the other side, followed by its release to be subjected to Bell measurement (BM).

nondemolition (QND) measurements (Azuma, Tamaki, and Munro, 2015) based on a dual-rail encoding. Although these schemes were originally proposed to perform QKD, its use as an entanglement generation protocol (or a coherent version) can be summarized as follows (Figs. 10 and 12): (i) Both Alice and Bob send  $m$  optical polarization qubits (using  $2m$  bosonic modes), each of which is maximally entangled with a local qubit, to the central node  $C$ . (ii) Upon receiving the pulses, node  $C$  essentially performs QND measurements to the pulses to confirm the arrival of single photons over lossy channels. (iii) Qubits of single photons that have successfully arrived from Alice are then paired with ones from Bob at node  $C$ . (iv) Node  $C$  then performs a linear-optical Bell measurement of Fig. 3(a) relying on two-photon interference on each of these pairs. (v) Node  $C$  then announces the pairings and the measurement outcomes of the Bell measurements. (vi) Finally, Alice and Bob keep their local qubits, which are supposed to be entangled with each other according to the announcement of step (v). The essence of this protocol is to perform the Bell measurement only on pairs of pulses that still have single photons even after the travel over the lossy optical channels.

If the protocol is used for QKD as in the original proposals (Abruzzo, Kampermann, and Bruß, 2014; Panayi *et al.*, 2014; Azuma, Tamaki, and Munro, 2015), Alice and Bob perform at random a Z-basis or X-basis measurement on each of their local qubits just after step (i), and their measurement outcomes are regarded as their choice of random bits in QKD. Step (i) is then replaced by the random preparation of BB84 signals  $\{|0\rangle, |1\rangle, |+\rangle, |-\rangle\}$  (Bennett and Brassard, 1984). This also implies that Alice and Bob could use phase-randomized weak coherent states emitted by lasers, instead of single-photon sources, using the decoy-state method (Hwang, 2003; Lo, Ma, and Chen, 2005; Wang, 2005). The security simply follows from that for the original MDI QKD (Lo, Curty, and Qi, 2012; Curty *et al.*, 2014) because it relies only on the trust of Alice and Bob.

The communication efficiency of the aforementioned protocol scales with  $\sqrt{\eta}$  rather than  $\eta$ , where  $\eta$  is the transmittance of a direct lossy bosonic channel between Alice and Bob. This can be understood as follows. Notice first that the success probability of the QND measurement in step (ii) is proportional to  $\sqrt{\eta}$  because the polarization qubit emitted by Alice (or Bob) simply travels over a lossy bosonic channel

connecting the central node  $C$  to Alice (between the central node  $C$  and Bob), rather than between Alice and Bob. This means that if the number  $m$  of multiplexing, defined in step (i), is of the order of  $(\sqrt{\eta})^{-1}$ , the probability with which the QND measurement in step (ii) finds the arrival of nonzero single photons from Alice and Bob is fairly high. Node  $C$  can have nonzero pairs in step (iii), to which the Bell measurements are applied in step (iv). Thus, as long as the inherent success probabilities of the QND measurement and the Bell measurement are constant (or, precisely, independent of the transmittance  $\sqrt{\eta}$  of the channels), Alice and Bob would have an entangled pair with a finite probability through steps (v) and (vi). Therefore,  $m \sim (\sqrt{\eta})^{-1}$  is enough to present an entangled pair to Alice and Bob, implying that the communication efficiency, that is, the secret key rate per pulse,<sup>11</sup> of the protocol scales with  $\sqrt{\eta}$ .

## 1. Memory-assisted implementation

The memory-assisted MDI QKD protocol (Abruzzo, Kampermann, and Bruß, 2014; Panayi *et al.*, 2014) corresponds to an implementation of the protocol mentioned in Sec. IV.A by utilizing the functionality of matter quantum memories (Fig. 10). In particular, the protocol assumes that the central node  $C$  uses matter quantum memories to achieve steps (ii)–(iv), and  $m$  optical polarization qubits in step (i) are sent by Alice and Bob in a time-multiplexing manner. If we can use a matter quantum memory that heralds the successful storing of a received optical polarization qubit, this heralding signal is regarded as the signal of the success of the QND measurement in step (ii). To achieve step (iii), the node  $C$  simply uses one memory for Alice and one memory for Bob. Each of these memories receives optical pulses from Alice or Bob until it successfully stores a single photon. Once this storage succeeds, each memory keeps the qubit information until the other memory heralds the successful storage. If both memories herald the successful storage of a single photon, they load the stored photons to perform the linear-optics-based Bell measurement of Fig. 3(a) on them as step (iv). The secret key rate of this protocol is exemplified in Fig. 11, which shows  $\sqrt{\eta}$  scaling when the required memory time in the protocol is shorter than the coherence time of the quantum memories.

Although we have assumed that the matter quantum memories have a function of heralding the storage, this method works even with a matter quantum memory that can only compose a Bell state with an optical polarization qubit. In particular, in this case, as in step (ii), node  $C$  simply needs to perform the linear-optical Bell measurement of Fig. 3(a) on this polarization qubit emitted by a quantum memory and a received pulse from Alice (or Bob). Since this

<sup>11</sup>Notice that an optical pulse here is regarded as being composed of two bosonic modes, i.e., a mode for horizontally polarized photons and a mode for vertically polarized photons. Hence, for this optical pulse the PLOB (upper) bound on achievable secret key rates of point-to-point QKD between Alice and Bob per pulse (composed of the two bosonic modes) is  $-2 \log_2(1 - \eta)$ , which is approximated as  $2\eta / \ln 2 \approx 2.89\eta$  for small  $\eta$ .

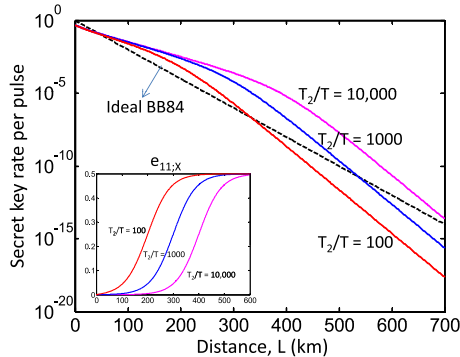


FIG. 11. Secret key rate (per pulse) of an adaptive MDI QKD protocol based on matter quantum memories with heralding storage and on Alice’s and Bob’s use of ideal single-photon sources. The secret key rate of the ideal BB84, which scales linearly with  $\eta = e^{-L/L_{\text{att}}}$  ( $L_{\text{att}} = 22$  km), is also shown as a reference.  $T_2$  is the dephasing time for the matter quantum memories,  $1/T$  is the pulse generation rate of Alice and Bob, and  $e_{11;X}$  is the phase error rate for Alice’s and Bob’s raw keys.  $T_2/T$  corresponds to how many attempts, each of which needs time  $T$ , are possible for the matter quantum memory to successfully store a single photon within its coherence time  $T_2$ , that is, the allowed number  $m$  of time multiplexing in the protocol. The secret key rate scales linearly with  $\sqrt{\eta}$  as long as  $T_2/T \geq (\sqrt{\eta})^{-1}$ , but it then converges to  $\eta$  as  $\eta$  decreases. This is because the increase of phase error  $e_{11;X}$  for the case of  $T_2/T \leq (\sqrt{\eta})^{-1}$  nullifies the benefit of time multiplexing from the use of matter quantum memories, as shown. From Panayi *et al.*, 2014.

Bell measurement provides the signal of the success only when it receives two or more photons, the signal of the success of this Bell measurement implies that the qubit information held by the pulse from Alice (or Bob) is successfully teleported into the other half of the Bell state, i.e., into the matter quantum memory. That is, this is essentially the success of the QND measurement required in step (ii). Hence, a matter quantum memory that can compose a Bell state with an optical polarization qubit allows node  $C$  to implement the QND measurement in an indirect manner, which is also enough to implement the memory-assisted MDI QKD protocol.

This memory-assisted implementation uses time multiplexing by utilizing matter quantum memories. The dominant noise of matter quantum memories is dephasing and/or amplitude damping (which is sometimes treated as a depolarizing channel to simplify theoretical treatment), both of which increase exponentially with time. Therefore, the noise would significantly limit the allowed number  $m$  of time multiplexing in the memory-assisted MDI QKD protocols.

In fact, the secret key rate of a memory-assisted MDI QKD protocol using matter quantum memories with dephasing is limited by the allowed number  $m$  of multiplexing, that is, by  $T_2/T$  in Fig. 11, which corresponds to how many attempts (each of which needs time  $T$ ) are possible for the matter quantum memory to successfully store a single photon within its coherence time  $T_2$ . In the figure, as  $\eta$  decreases the secret key rate scales linearly with  $\sqrt{\eta}$  as long as  $T_2/T \geq (\sqrt{\eta})^{-1}$ , but it then converges to  $\eta$ . This implies that the required coherence time  $T_2$  is of the order of  $(\sqrt{\eta})^{-1}T = e^{L/(2L_{\text{att}})}T$

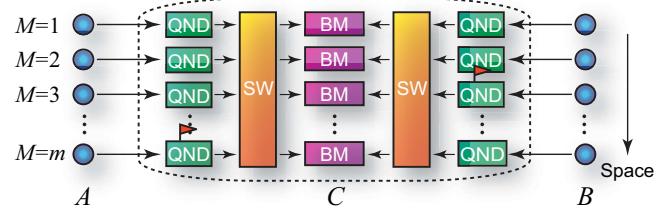


FIG. 12. The concept of all-photonic adaptive MDI QKD. In this protocol, node  $C$  first performs QND measurements to confirm the successful arrival of single photons (which is indicated by a red flag on a box labeled QND in the figure), followed by optical switches (SWs) to send the surviving photons to BM modules. Adapted from Azuma, Tamaki, and Munro, 2015.

with  $\eta = e^{-L/L_{\text{att}}}$  ( $L_{\text{att}} = 22$  km), and thus it scales exponentially with  $L/2$ . However, as long as the period  $T$  of Alice’s and Bob’s pulse generation can be taken to be small, the required coherence time could be smaller (Panayi *et al.*, 2014) than even the minimum coherence time  $L/c$  required by multiplexed first-generation quantum repeaters (Razavi, Piani, and Lutkenhaus, 2009).

## 2. All-optical implementation

The all-photonic adaptive MDI QKD protocol could be understood as an all-optical implementation of the aforementioned protocol in Sec. IV.A (Fig. 12) (Azuma, Tamaki, and Munro, 2015). In the protocol, the QND measurement in step (ii) is assumed to be performed using a quantum teleportation, as in the memory-assisted MDI QKD protocol, but it is implemented using only optical devices.<sup>12</sup> In particular, to achieve the QND measurement in step (ii), node  $C$  first prepares optical polarization qubits in a Bell state locally, then applies the linear-optical Bell measurement of Fig. 3(a) on the half of this Bell pair and the optical pulse sent by Alice or Bob. The success of this Bell measurement teleports the qubit information of the surviving single photon into the other half of the Bell pair, corresponding to the success of the QND measurement. Since this protocol does not assume the use of matter quantum memories,  $m$  optical polarization qubits in step (i) of this protocol are assumed to be sent by Alice and Bob simultaneously in a spatial-multiplexing manner. Thus, the all-optical QND measurements referenced in step (ii) are performed at the same time on all the pulses sent by Alice and Bob, and the pairing in step (iii) is then made using an optical switch. The performance of this protocol is exemplified in Fig. 13, which shows  $\sqrt{\eta}$  scaling of the secret key rate.

This all-optical implementation uses spatial multiplexing by utilizing optical switches. The dominant noise of optical switches is the photon loss. However, in contrast to memory-assisted implementation, this loss increases only logarithmically with the number  $m$  of spatial multiplexing

<sup>12</sup>An idea similar to this, called a qubit amplifier, is also used in the context of the device-independent QKD in order to close the detection loophole problem (Gisin, Pironio, and Sangouard, 2010; Curty and Moroder, 2011).

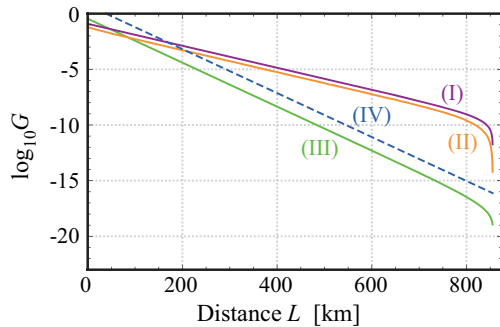


FIG. 13. Secret key rate (per pulse)  $G$  of an all-photonic adaptive MDI QKD protocol.  $\eta$  is rephrased by the distance  $L$  between Alice and Bob, with  $\eta = e^{-L/L_{\text{att}}}$  ( $L_{\text{att}} = 22$  km) and  $c = 2.0 \times 10^8$  m/s. Lines (I)–(IV) represent the performance of the protocol with active optical switches, that of the protocol with a passive Hadamard linear-optical circuit, that of the original MDI QKD protocol (Lo, Curty, and Qi, 2012), and that of the TGW bound, respectively (Takeoka, Guha, and Wilde, 2014a). This graph is described under the following assumptions (Azuma, Tamaki, and Munro, 2015): a single active feed forward can be completed within time  $\tau_a$ , during which photons run in optical fibers and are subject to the corresponding photon loss; heralded single-photon sources emit pulses with duration  $\tau_s$  and efficiency  $\eta_s$ , and they are multiplexed (Migdall, Branning, and Castelletto, 2002; Ma *et al.*, 2011; Christ and Silberhorn, 2012; Collins *et al.*, 2013; Bonneau *et al.*, 2015) to produce high-fidelity telecom single photons with the repetition rate of the slowest optical device at the expense of the use of at least one active feed forward; single-photon detectors have a quantum efficiency  $\eta_d$  and a dark count rate  $\nu_d$ ; Bell pairs for the all-photonic QND measurements can be generated in a constant time  $\tau_a$  with single-photon sources rather than a Bell-pair photon source by paralleling a probabilistic procedure (Browne and Rudolph, 2005) with the active-feed-forward technique. In particular, they are assumed to be  $\eta_s = 0.90$  (Migdall, Branning, and Castelletto, 2002; Christensen *et al.*, 2013; Giustina *et al.*, 2013),  $\tau_s = 100$  ps (Shibata, Honjo, and Shimizu, 2014),  $\eta_d = 0.93$  (Marsili *et al.*, 2013),  $\nu_d = 1$  s<sup>-1</sup> (Shibata *et al.*, 2010; Marsili *et al.*, 2013), and  $\tau_a = 67$  ns (Ma *et al.*, 2011). From Azuma, Tamaki, and Munro, 2015.

(Azuma, Tamaki, and Munro, 2015). Note that the all-optical protocol can achieve the  $\sqrt{\eta}$  scaling even if it uses only an  $m \times 1$  optical switch and a Bell measurement module at the middle node  $C$ . Thus, if we implement an  $m \times 1$  optical switch by concatenating  $2 \times 1$  optical switches with transmittance  $\eta_{\text{sw}}$  in a knockout tournament manner with depth  $\lceil \log_2 m \rceil$ , the transmittance of the  $m \times 1$  optical switch decreases as  $\eta_{\text{sw}}^{\lceil \log_2 m \rceil}$ , and it thus scales only logarithmically with the number  $m$ . This is a merit of using spatial multiplexing rather than time multiplexing. This combination of an  $m \times 1$  optical switch and a Bell measurement module is also implementable without using such a large-scale optical switch, that is, using only single-mode on-off switches, a passive Hadamard linear-optical circuit, and single-photon detectors (Azuma, Tamaki, and Munro, 2015). The performance in this case is also described in Fig. 13.

### 3. Challenges

The question as to whether a two-mode squeezed state, which can be produced with practical systems, can be directly used as the Bell state to implement the teleportation-based QND measurement in step (ii) has been answered in the negative thus far. For instance, if we use atomic-ensemble quantum memories for the memory-assisted MDI QKD protocol, the memory can naturally compose a two-mode squeezed state with an optical pulse (Duan *et al.*, 2001; Sangouard *et al.*, 2011). However, this entanglement cannot be directly used as a resource to implement the teleportation-based QND measurement in step (ii) (Piparo, Razavi, and Panayi, 2015), because the multiphoton component of the two-mode squeezed state makes the success probability of the QND measurement dependent on the transmittance  $\sqrt{\eta}$  of the channels. This result is made stronger by assuming that node  $C$  is allowed to use photon-number-resolving detectors (Trényi, Azuma, and Curty, 2019) rather than the threshold detectors assumed by Piparo, Razavi, and Panayi (2015). In particular, they showed, by deriving necessary conditions on photon-number statistics of the entanglement photon sources, that the polarization entanglement produced by a spontaneous parametric down-conversion process cannot be directly used to implement the QND measurement in step (ii) of the all-photonic adaptive MDI QKD protocol.

As a result, a single matter qubit, such as a single ion, a quantum dot, or a nitrogen-vacancy center in a diamond, inside a cavity has been proposed as a candidate for the memory to realize the memory-assisted MDI QKD protocol (Piparo, Razavi, and Munro, 2017a, 2017b), while a source emitting an entangled photon pair with a low multiphoton component, such as one assumed in the original paper (see the caption of Fig. 13) (Azuma, Tamaki, and Munro, 2015) or an entanglement photon source (Eisaman *et al.*, 2011), is needed to implement the all-photonic adaptive MDI QKD protocol. In the case where multiphoton emission is highly suppressed, threshold detectors without the function of photon-number resolving are sufficient for implementing the teleportation-based QND measurement.

As for the all-photonic adaptive MDI QKD protocol, since it needs only QND measurements on the photon number, it could adopt different types of QND measurements, such as the one proposed by Imoto, Haus, and Yamamoto (1985) based on an optical Kerr effect and the type proposed by Brune *et al.* (1990) based on a dispersive atom-field coupling; see Scully and Suhail Zubairy (1997) and Walls and Milburn (2007). It is thus an important open question as to whether the all-photonic adaptive MDI QKD keeps its merit on communication efficiency even if we replace the teleportation-based QND measurement with an alternative one. As for the memory-assisted MDI QKD, a proof-of-principle experiment of the key element has been performed with a single solid-state spin memory integrated into a nanophotonic diamond resonator (Bhaskar *et al.*, 2020), based on an encoding on the phase difference between two sequential pulses [like one used in a differential phase shift QKD (Inoue, Waks, and Yamamoto, 2002; Sasaki, Yamamoto, and Koashi, 2014)]; see also Sec. V.H.2.

## B. Twin-field QKD

To double the communication distance by utilizing a central node  $C$  between communicators, another idea is also focused on, especially in the field of QKD, thanks to the proposal of a twin-field (TF) QKD protocol based on a single-rail encoding (Lucamarini *et al.*, 2018). The scaling improvement of the TF QKD protocol is essentially explained by the following point: like entanglement generation processes in quantum repeater protocols (Duan *et al.*, 2001; Childress, Taylor *et al.*, 2006; Azuma *et al.*, 2012), the protocol makes node  $C$  use a simple linear-optical Bell measurement of Fig. 3(b) based on single-photon interference rather than the two-photon interference used in the original MDI QKD (Lo, Curty, and Qi, 2012), and Alice and Bob encode their qubit information into a single optical mode (i.e., a single-rail encoding), rather than two modes (i.e., a dual-rail encoding such as a polarization or a time bin). This aims to utilize the feature that this Bell measurement [to project a given state into a Bell state  $(|0\rangle|1\rangle \pm |1\rangle|0\rangle)/\sqrt{2}$  with the vacuum state  $|0\rangle$  and the single-photon state  $|1\rangle$  as shown in Fig. 3(b)] succeeds if a single photon reaches node  $C$  either from Alice or from Bob. For instance, in the case of the DLCZ protocol (Duan *et al.*, 2001), states of each local memory of Alice and Bob are entangled with the number states (i.e., the Fock states) of a single optical mode, while in the case of hybrid quantum repeater protocols (Childress, Taylor *et al.*, 2006; Azuma *et al.*, 2012) the computational-basis states of each of Alice's and Bob's local qubits are entangled with two coherent states of a single optical mode (corresponding to a cat-state encoding). As a result, the efficiency of this type of entanglement generation scheme (Duan *et al.*, 2001; Childress, Taylor *et al.*, 2006; Azuma *et al.*, 2012) scales with  $\sqrt{\eta}$  rather than  $\eta$  without requiring any challenging devices at node  $C$  thanks to the use of single-photon interference. This scaling improvement in entanglement generation might be reasonable because it relies on the following technical challenges:

- (a) Those entanglement generation schemes need intense phase stabilization regarding the channels between Alice and node  $C$  and between Bob and node  $C$ , in contrast to ones based on two-photon interference at node  $C$ .
- (b) Those schemes require Alice and Bob to use matter quantum memories that could be used to prepare nontrivial optical states, such as number states (Duan *et al.*, 2001) and cat states (Childress, Taylor *et al.*, 2006; Azuma *et al.*, 2012).

A bold claim was given in the original proposal of the TF QKD protocol (Lucamarini *et al.*, 2018). It argued that, if we borrow the idea of the decoy-state method (Hwang, 2003; Lo, Ma, and Chen, 2005; Wang, 2005), coherent states are enough to achieve QKD with  $\sqrt{\eta}$  scaling without requiring any device that has the potential to prepare nontrivial optical states [in contrast to the entanglement generation schemes having requirement (b)]. The idea (Lucamarini *et al.*, 2018) stemmed from making a decoy-state phase-encoding BB84 protocol be in the form of an MDI QKD setup, namely, attaching the decoy-state method to a phase-encoding MDI QKD protocol (Tamaki *et al.*, 2012). However, despite this extremely appealing claim, a rigorous security proof against the most

general type of eavesdropping strategies was missing in the original proposal (Lucamarini *et al.*, 2018): only security over restricted eavesdropping was proven. This triggered much interest in developing variants of the TF QKD protocol, as well as their security proofs over arbitrary eavesdropping attacks in asymptotic scenarios (Lin and Lütkenhaus, 2018; Ma, Zeng, and Zhou, 2018; Tamaki *et al.*, 2018; Wang, Yu, and Hu, 2018; Cui *et al.*, 2019; Curty, Azuma, and Lo, 2019) and in finite-size scenarios (Jiang *et al.*, 2019; Maeda, Sasaki, and Koashi, 2019; Yu *et al.*, 2019; Xu *et al.*, 2020; Currás-Lorenzo *et al.*, 2021). Here we focus on a variant (Curty, Azuma, and Lo, 2019) of the TF QKD protocol, as it is explicitly related to entanglement generation protocols in quantum repeaters, to see why coherent states are enough to achieve QKD.

Before introducing the variant protocol, we introduce its coherent version, which is essentially equivalent to an entanglement generation protocol (Azuma *et al.*, 2012). The coherent version is described as follows. (i) Both Alice and Bob prepare an optical pulse entangled with a local qubit, whose state is described as  $(|0\rangle|\alpha\rangle + |1\rangle|-\alpha\rangle)/\sqrt{2}$ , where  $|0\rangle$  and  $|1\rangle$  are orthogonal states of the local qubit and  $|\pm\alpha\rangle$  are coherent states of the optical pulse with an amplitude  $\alpha > 0$ . (ii) Each of them sends the prepared optical pulse to node  $C$  over a lossy bosonic channel [Eq. (13)] with the transmittance  $\sqrt{\eta}$ . (iii) Upon receiving the pulse  $a$  in coherent states  $|\pm\eta^{1/4}\alpha\rangle_a$  from Alice and the pulse  $b$  in coherent states  $|\pm\eta^{1/4}\alpha\rangle_b$  from Bob, node  $C$  performs a linear-optical Bell measurement of Fig. 3(b) relying on single-photon interference on them. (iv) Node  $C$  then announces the measurement outcome of the Bell measurement. (v) Finally, Alice and Bob keep their local qubits if they know that one of two detectors for the Bell measurement announces arrival of photons through the announcement in step (iv).

Notice that the 50:50 beam splitter of the Bell measurement in step (iii) [Fig. 3(b)] converts received states  $|\pm\eta^{1/4}\alpha\rangle_a|\pm\eta^{1/4}\alpha\rangle_b$  into coherent states  $|\pm\sqrt{2}\eta^{1/4}\alpha\rangle_c|0\rangle_d$  and  $|\pm\eta^{1/4}\alpha\rangle_a|\mp\eta^{1/4}\alpha\rangle_b$  into coherent states  $|0\rangle_c|\pm\sqrt{2}\eta^{1/4}\alpha\rangle_d$ , respectively, where  $c$  and  $d$  are the outputs having received constructive interference and destructive interference, respectively. Since the detection of photons in the number basis erases the phase information  $\pm$  of the coherent states  $|\pm\sqrt{2}\eta^{1/4}\alpha\rangle$ , the successful detection of photons defined in step (v) effectively works as the nondestructive parity measurement, i.e., projection measurement  $|00\rangle\langle 00| + |11\rangle\langle 11|$  or  $|01\rangle\langle 01| + |10\rangle\langle 10|$  on Alice's and Bob's local qubits (with phase errors in the case of  $\eta < 1$ ) (Azuma *et al.*, 2012), which entangles their local qubits in the protocol.

To see the scaling, suppose that the Bell measurement is performed using ideal threshold detectors, for simplicity. The success probability of the Bell measurement is  $r = 1 - e^{-2\sqrt{\eta}\alpha^2}$ , while the Bell pair obtained at step (iv) includes only the phase error with probability  $e_Z = (1 - e^{-2\alpha^2(2-\sqrt{\eta})})/2$  (Azuma *et al.*, 2012). This performance as entanglement generation has been shown to be optimal in various scenarios (Azuma *et al.*, 2009, 2010; Azuma and Kato, 2012; Azuma, Imoto, and Koashi, 2022). If we maximize an asymptotic key rate formula  $G = r[1 - h(e_Z)]$

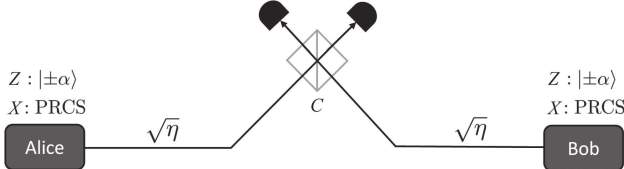


FIG. 14. Schematic of a TF-type QKD protocol (Curty, Azuma, and Lo, 2019). Both Alice and Bob choose the  $Z$  or  $X$  basis randomly. If the  $Z$  basis is selected, Alice and Bob prepare coherent state  $|\alpha\rangle$  or  $|-\alpha\rangle$  at random and send it to the central node  $C$ . If the  $X$  basis is selected, Alice and Bob prepare a phase-randomized coherent state (PRCS) whose intensity is chosen randomly from a predefined set [so as to be able to use the decoy-state method (Hwang, 2003; Lo, Ma, and Chen, 2005; Wang, 2005)] and send it to the central node  $C$ . Upon receiving pulses from Alice and Bob, the central node  $C$  performs the Bell measurement based on single-photon interference [Fig. 3(b)]. The secret key is distilled only from instances where both Alice and Bob choose the  $Z$  basis and the Bell measurement at node  $C$  succeeds. Adapted from Currás-Lorenzo *et al.*, 2021.

with the binary entropy function  $h$  over  $\alpha$ , we can easily confirm that  $G$  scales with  $\sqrt{\eta}$ . However, this merely means that the key rate  $G$  could scale  $\sqrt{\eta}$  when Alice and Bob use matter quantum memories to realize their local qubits, as considered by Azuma *et al.* (2012).

To make the protocol composed of steps (i)–(iv) a prepare-and-measure scheme, Alice and Bob are supposed to perform  $Z$ -basis or  $X$ -basis measurements randomly on each of their local qubits just after step (i) and before step (ii). Here the  $Z$ -basis measurement prepares the optical pulse in coherent state  $|\alpha\rangle$  or  $|-\alpha\rangle$  at random, while the  $X$ -basis measurement prepares it in cat state  $|C_+\rangle := (|\alpha\rangle + |-\alpha\rangle)/2\sqrt{p_+}$  with probability  $p_+$  or  $|C_-\rangle := (|\alpha\rangle - |-\alpha\rangle)/2\sqrt{p_-}$  with probability  $p_-$ , where  $p_{\pm} = (1 \pm \langle -\alpha|\alpha \rangle)/2$ . The random preparation of coherent states  $|\pm\alpha\rangle$  regarding the  $Z$ -basis measurement can be easily done. In contrast, the preparation

of cat states  $|C_{\pm}\rangle$  regarding the  $X$ -basis measurement is problematic because it requires a challenging device in practice. However, this preparation is not necessary if Alice and Bob will distill a key only from the outcomes of the  $Z$ -basis measurements. In particular, in the case of this QKD the  $X$ -basis measurements are used only to estimate the actual phase error rate  $e_Z$  for privacy amplification, and estimation of its upper bound by Alice and Bob through a protocol is enough to prove the security (Bennett, Brassard, and Mermin, 1992; Lo and Chau, 1999; Shor and Preskill, 2000; Mayers, 2001; Renner, 2008; Koashi, 2009; Tamaki *et al.*, 2014; Portmann and Renner, 2022). In fact, it turns out that the estimation of an upper bound on the phase error  $e_Z$  can be done simply by sending phase-randomized coherent states in the case of the choice of  $X$  basis and by invoking a decoy-state method without preparing the cat states  $|C_{\pm}\rangle$  (Curty, Azuma, and Lo, 2019). As a result, the protocol is described in Fig. 14, and the conjecture in the original proposal that the coherent states (and their phase-randomized ones) are enough to achieve QKD with  $\sqrt{\eta}$  scaling is concluded to be true, as shown in Fig. 15.

The TF QKD protocol and its secure variants omit technical challenge (b) as unnecessary for QKD, but they still include technical challenge (a). Nonetheless, various experiments (Minder *et al.*, 2019; S. Wang *et al.*, 2019; Zhong *et al.*, 2019, 2021, 2022; Chen *et al.*, 2020; J.-P. Chen *et al.*, 2021; Pittaluga *et al.*, 2021; Clivati *et al.*, 2022; Wang *et al.*, 2022) to overcome this have been performed toward the full implementation of the TF-type QKD protocols in practical scenarios. These trials are important even for quantum repeaters because they represent a good milestone toward the realization of a quantum repeater protocol based on single-photon interference, which involves the same technical challenge (a) (Duan *et al.*, 2001; Childress, Taylor *et al.*, 2006; Azuma *et al.*, 2012).

In TF QKD, to achieve the phase stability required for entanglement swapping based on single-photon interference, there are two general strategies. The first strategy is to use only one laser and employ autocompensation with a Sagnac loop where optical signals go through the same path either clockwise or counterclockwise (Zhong *et al.*, 2019, 2021, 2022). The second strategy allows two independent lasers to be used but may require a combination of techniques including, for example, frequency locking, using a reference pulse for compensation, and ensuring that the optical path lengths of the two optical fibers do not differ too drastically (Minder *et al.*, 2019; S. Wang *et al.*, 2019; Chen *et al.*, 2020; J.-P. Chen *et al.*, 2021; Pittaluga *et al.*, 2021; Clivati *et al.*, 2022; Li *et al.*, 2023).

### C. Single sequential quantum repeater

A third alternative is to invert the previous schemes and place a quantum device with a quantum memory in the central node and two detectors in the end nodes. This scheme was proposed by Luong *et al.* (2016).

In this scheme, the central node sends a photon entangled with a memory qubit to one of the end nodes until the end node confirms successful detection of the photon. The central node then repeats the same process with the other end node and thus emits a photon entangled with a memory qubit until

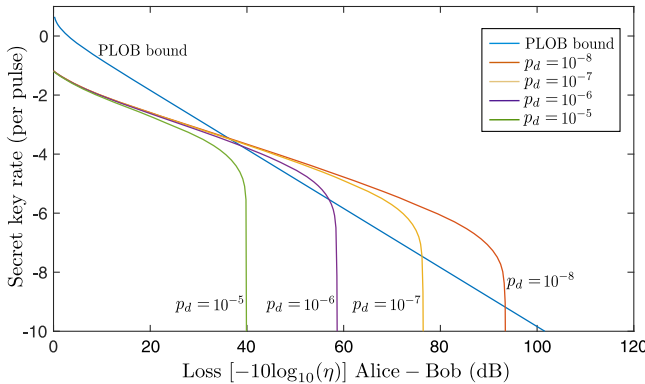


FIG. 15. Secret key rates (per pulse) of a TF-type QKD protocol for different dark count rates  $p_d$  in logarithmic scale as a function of the overall loss between Alice and Bob. The PLOB bound is the private capacity of a lossy bosonic channel (Pirandola *et al.*, 2017). Assume a misalignment of 2% in each of the channels between Alice and the central node  $C$  and between Bob and  $C$ , and also the inefficiency function for the error-correction process  $f = 1.16$ . Adapted from Curty, Azuma, and Lo, 2019.

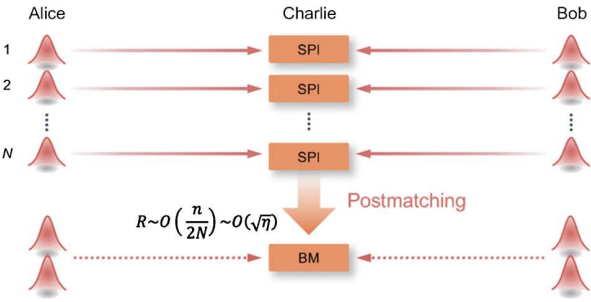


FIG. 16. Postpairing measurement-device-independent QKD. In this protocol, Alice and Bob send  $N$  pulses to the middle node  $C$  (Charlie) to perform the linear-optical Bell measurement of Fig. 3(b) based on single-photon interference (SPI), and a two-photon Bell state is obtained by postmatching two successful SPI events. Here  $n$  represents the number of successes of the Bell measurement based on SPI and  $\sqrt{\eta}$  represents the transmittance of pure-loss channels between Alice and Charlie and between Charlie and Bob. Adapted from [Xie \*et al.\*, 2022](#).

success. Once the second end node confirms the successful detection of a photon, the central node performs a Bell measurement and heralds the measurement outcome to the two end nodes.

The advantage of this scheme is the simplicity of the setup, requiring a single node holding two memory qubits and no optical Bell measurement. However, this setup is not measurement-device independent and it requires qualitatively long coherence times compared to memory-based adaptive MDI QKD. In particular, the coherence time should be large compared to the sum of the travel time of a photon from the center node to an end node plus the corresponding heralding signal, multiplied by the average number of times required for a successful event.

The feasibility of this setup for outperforming the point-to-point limits was analyzed for different hardware parameters by [Luong \*et al.\* \(2016\)](#) and [Rozpędek \*et al.\* \(2018, 2019\)](#). An experimental demonstration of the setup was recently reported by [Langenfeld \*et al.\* \(2021\)](#) with rubidium atoms in an optical cavity. While below the fundamental limit for direct transmission, the scaling of the key rate in the experiment was shown to be proportional to the square root of the transmittance of an optical fiber connecting two end parties.

#### D. Postpairing measurement-device-independent QKD

Recently [Xie \*et al.\* \(2022\)](#) and [Zeng \*et al.\* \(2022\)](#) proposed a variant of the MDI QKD protocol that can be conceptually intermediate between adaptive MDI QKD and TF QKD and whose secret key rate can scale with  $\sqrt{\eta}$  rather than  $\eta$ , where  $\eta$  is the transmittance of a pure-loss channel between Alice and Bob. In this protocol (Fig. 16), the middle node  $C$  still uses the linear-optical Bell measurement of Fig. 3(b) based on single-photon interference like TF QKD, while Alice and Bob send  $N$  optical pulses in coherent states to the middle node sequentially, that is, in a time-multiplexing manner like adaptive MDI QKD. The main aim here is to make a protocol rely on the application of a Bell measurement to project onto

Bell states  $(|01\rangle_{a_ia_j}|10\rangle_{b_ib_j} \pm |10\rangle_{a_ia_j}|01\rangle_{b_ib_j})/\sqrt{2}$  based on two-photon interference between  $i$ th and  $j$ th time bins ( $i, j = 1, 2, \dots, N$  and  $i \neq j$ ) at the middle node  $C$ , where  $a_i$  and  $b_i$  are  $i$ th time bins sent by Alice and Bob, respectively. This is implemented by postselecting time slots  $i$  and  $j$ , to which the Bell measurements based on single-photon interference at node  $C$  are successfully applied, under the assumption that the phase correlation between such possibly long-time separated  $i$ th and  $j$ th time bins is kept in the implementation. This keeping of the phase correlation is a technological challenging part if the number  $N$  of multiplexing is large. Nonetheless, since this protocol can be regarded as relying on two-photon interference at the middle node  $C$  rather than single-photon interference (like adaptive MDI QKD), an intense phase stabilization regarding the channels between Alice and node  $C$  and between Bob and node  $C$  could be unnecessary, in contrast to the case of TF QKD. In the protocol, Alice and Bob send Charlie optical pulses in coherent states whose phases are chosen randomly from  $[0, 2\pi)$  and whose intensities are chosen randomly from a predefined set. This is designed so that time bins  $a_ia_j$  and  $b_ib_j$ , postselected by the middle node  $C$ , can be regarded as a BB84 signal and a decoy state, that is, a signal used in the normal MDI QKD with time-bin encoding ([Ma and Razavi, 2012](#)). This postselection includes the matching between Alice's and Bob's random choices of phases in some cases [although, in contrast, it was shown to be unnecessary in the case of TF QKD ([Lin and Lütkenhaus, 2018](#); [Cui \*et al.\*, 2019](#); [Curty, Azuma, and Lo, 2019](#); [Maeda, Sasaki, and Koashi, 2019](#); [Currás-Lorenzo \*et al.\*, 2021](#))].

For a large number  $N$  of the multiplexing  $n = \mathcal{O}(N\sqrt{\eta})$ , where  $\sqrt{\eta}$  represents the transmittance of pure-loss channels between Alice and the middle node  $C$  and between the middle node  $C$  and Bob, Bell measurements based on single-photon interference would succeed. Hence, there would be  $\mathcal{O}(n/2) = \mathcal{O}(N\sqrt{\eta}/2)$  instances to which the target Bell measurements based on two-photon interference are deemed to be successfully applied. Since the success of the target Bell measurement could produce an entangled state between Alice's virtual qubit and Bob's virtual qubit, the secret key rate of the protocol could scale with  $\sqrt{\eta}$ .

According to the proposals, called mode-pairing QKD ([Zeng \*et al.\*, 2022](#)) and asynchronous MDI QKD ([Xie \*et al.\*, 2022](#)), experimental demonstrations were performed by [Zhu \*et al.\* \(2023\)](#) and [Zhou \*et al.\* \(2023\)](#), respectively.

## V. EXPERIMENTAL PROGRESS TOWARD REPEATERS

Long-distance quantum communication is enabled by low-loss media for photon transfer. Free-space communication ([Ursin \*et al.\*, 2007](#)) and satellite-based communication ([Liao \*et al.\*, 2017](#); [Yin \*et al.\*, 2017](#)) have unique experimental challenges; in this section, we chiefly describe the practical advances toward optical-fiber-based quantum communication schemes featuring quantum repeaters. We organize our discussion roughly according to the requirements of each generation of repeaters from Sec. III.B and of memoryless repeaters from Sec. III.C.

Almost all quantum repeater architectures require the implementation of efficient interfaces between quantum memories and photons. In first-generation repeaters, a quantum memory must be capable of storing quantum information for a long time (Sec. V.A) and of emitting photons that are entangled with the memory degrees of freedom (Sec. V.B). These photons are then coupled into optical fibers that connect distant repeater nodes. The intermediate entanglement between distant quantum memories (Sec. V.C) is finally used to create end-to-end entanglement links between Alice and Bob with a rate ideally much higher than direct transmission over fibers.

In first-generation repeaters, unavoidable memory errors are dealt with through entanglement distillation (Sec. V.D). In the second generation of quantum repeaters, memory errors are corrected through quantum error correction. Therefore, quantum registers of many quantum memories are required at each repeater node to encode logical memory qubits (Sec. V.E). In the third generation of repeaters, loss errors are also dealt with through QEC. Since any QEC code can tolerate a probability of erasure (a common model for loss) of only 50% (see Secs. II.B and V.E), advanced engineering is required to obtain high transmissivities as well as collection, coupling, and detection efficiencies for the photons (Sec. V.F). In addition to the experimental progress aligning with the three generations, we review the headway that has been made toward memoryless repeaters (Sec. V.G), whose all-photonic implementations require the efficient generation of highly entangled states of many photons. Finally, we overview the experimental demonstrations of trusted QKD networks and small quantum networks (Sec. V.H) that exist as important milestones on the way to a quantum internet.

### A. Long-lived quantum memories

The success of most quantum repeater schemes critically relies on the performance of their quantum memories. The coherence time  $T_2$  of the memory (sometimes called the memory time) is the relevant figure of merit: it characterizes the time during which quantum information can be stored in the memory before being degraded by the environment. For example, when generating entanglement between two quantum memories at nodes separated by a distance  $L_0$  in a heralded manner (Sec. III.A.4.b.2), high entanglement fidelities can be achieved only if  $L_0 \ll cT_2$ , with  $c$  the speed of light in fiber. A quantum memory also needs to have characteristics beyond the coherence time, namely, fast, efficient, and high-fidelity initialization, gate application, and photon retrieval and readout. For brevity we restrict our discussion to the coherence time and refer interested readers to Lvovsky, Sanders, and Tittel (2009), Simon *et al.* (2010), and Heshami *et al.* (2016) for discussions of other important features of quantum memories.

Several candidates for quantum memories are under development, among them atomic ensembles [ $T_2 = 0.2\text{--}16$  s (Dudin, Li, and Kuzmich, 2013; Yang *et al.*, 2016)] including Bose-Einstein condensates (Riedl *et al.*, 2012) and single natural or artificial atomic systems such as cold atoms, trapped ions [ $T_2 = 4$  ms for  $^{128}\text{Ba}^+$  (Inlek *et al.*, 2017)], color centers

in diamond [ $T_2 = 1$  s (Bar-Gill *et al.*, 2013; Abobehi *et al.*, 2018)], and quantum dots [ $T_2 = 3$   $\mu\text{s}$  (Greilich *et al.*, 2007)]. All of these platforms are also quantum emitters, making them suitable candidates for atom-photon interfaces; other systems may have superior coherence times but cannot emit photons. To benefit from these extremely long-lived memories, hybrid strategies can be chosen in which the quantum memory is indirectly interfaced with photons through its coupling to an efficient quantum emitter. This occurs naturally in nitrogen-vacancy (N-V) centers, for example, where the electron spin is coupled via hyperfine interaction with nearby  $^{13}\text{C}$  nuclear spins ( $T_2 = 75$  s) (Bradley *et al.*, 2019). The same strategy is also taken with trapped ions, where ionic species with good emission properties, such as  $^{128}\text{Ba}^+$ , are interfaced at the same quantum node with  $^{171}\text{Yb}^+$ , the latter of which has much longer coherence times [ $T_2 > 1$  h (Wang *et al.*, 2017, 2021)]. Using these ions, Hucul *et al.* (2015) showed two-ion entanglement that persists over more than 1 s. Recent results have also shown that a typically short-lived quantum dot spin can be efficiently coupled to a single magnon excitation of its nuclear environment, which consists of  $10^4\text{--}10^5$  nuclear spins that behave as a long-lived memory [ $T_2^* \approx 1$   $\mu\text{s}$  (Gangloff *et al.*, 2019; Jackson *et al.*, 2021)], compared to  $T_2^* = 39$  ns for the electron spin (Éthier-Majcher *et al.*, 2017)]. Rare-earth  $\text{Eu}^{3+}$  ions in  $\text{Y}_2\text{SiO}_5$  crystals have the longest coherence time experimentally observed with  $T_2 = 6$  h (Zhong, Hedges *et al.*, 2015). This platform has an optical memory that can store a time-bin-encoded photonic qubit for 1 h (Ma *et al.*, 2021).

Another important criterion for these platforms is the temperature at which they operate. It potentially implies the use of different cooling strategies that can be technologically demanding, from dilution refrigerator or liquid helium temperature cryostats to laser cooling. Several studies proposed softening this requirement through the use of “room-temperature” quantum repeaters based on either hybrid optomechanical systems with N-V centers (Ji *et al.*, 2022) or warm atomic vapors (Borregaard *et al.*, 2016; Katz and Firstenberg, 2018; Pang *et al.*, 2020; Dideriksen *et al.*, 2021; Li *et al.*, 2021; Shaham, Katz, and Firstenberg, 2022).

In Table V, we summarize the experimental performance of long-lived quantum memories together with their emission properties. In addition to the coherence time, several other figures of merit are also important for quantum repeater applications. These include the quantum emitter control gate fidelity ( $F$ ) and dephasing and relaxation times ( $T_2^*, T_1$ ), as well as the availability of an additional quantum register and its properties. The photonic properties of the quantum emitters are also important, namely, the photon collection efficiency ( $\eta_{\text{eff}}$ ), the Debye-Waller factor in the case of solid-state defect qubits (i.e., the probability of emitting a photon into the zero-phonon line)  $\eta_{\text{DW}}$ , the indistinguishability  $\iota$ , and the quality of the spin-photon entanglement [ $F$  (atom-phot)]. The photon wavelength also plays a crucial role in quantum communication since the best transmission rates are achieved for telecom wavelengths. We include well-established quantum emitters alongside more recent but promising systems, such as rare-earth ions and new defects in diamond and silicon.

TABLE V. Properties of selected memory qubits for quantum repeater applications. Results for most systems were generally obtained in separate experiments. We distinguish the properties of the qubit emitters from those of the potential  $N$ -qubit registers they are coupled to. Also included are the properties of the systems as single-photon emitters, including the emission time  $T_1$ , the end-to-end collection efficiency  $\eta_{\text{eff}}$ , the photon indistinguishability  $\iota$ , the Debye-Waller factor  $\eta_{\text{DW}}$ , the fidelity  $F$  of the atom-photon entanglement, and the emission wavelength  $\lambda_{\text{QE}}$ . The asterisk indicates heralded entanglement generation fidelity between two quantum memories. The footnotes cited in the final column indicate the references to each row entry.

Quantum emitter	Quantum memory				Quantum register				Emitting properties		
	$T_2$	$T_2^*$	$F$ (gate)	$N$	$T_2$	$T_1$	$\eta_{\text{eff}}$	$\iota$	$\eta_{\text{DW}}$	$F$ (atom-phot)	$\lambda_{\text{QE}}$ (nm)
Atomic ensemble	$^{87}\text{Rb}$	16 s					87%				780 <sup>a</sup>
Single atoms or trapped ions	$^{87}\text{Rb}$ $^{171}\text{Yb}^+$ $^{128}\text{Ba}^+$	2.6 ms $> 1$ h 4 ms	400 $\mu\text{s}$	$\geq 97.5\%$		300 ns	60%			89% 90% 369 <sup>c</sup>	780 <sup>b</sup> 369 <sup>c</sup>
Quantum dot				$\geq 4$ ( $^{171}\text{Yb}^+$ )	$> 1$ h						493 <sup>d</sup>
Defects (diamond)	N-V Si-V Ge-V Sn-V	3 $\mu\text{s}$ 0.6 s 10 ms 540 ns	39 ns 5–36 $\mu\text{s}$ 115 ns	95% $> 99\%$	1 9 1	1 $\mu\text{s}$ 75 s 100 ms	0.6–0.8 ns 13 ns 1.6 ns	57% 37% 85% 72%	90% 99.5% 98.6% 75%	$\geq 80\%$ 96% 94% 60%	900–1565 <sup>e</sup> 637 <sup>f</sup> 737 <sup>g</sup> 602 <sup>h</sup>
Defects (in Si)	$V_{\text{Si}}$ $V_{\text{Si}}V_{\text{C}}$ $V_{4+}$ N-V	0.8–20 ms 64 ms	375 $\mu\text{s}$	99.98%	$\geq 1$		4.5 ns				620 <sup>i</sup>
Defects (in Si)	$G$ $T$					37 ns	69%				862–917 <sup>j</sup>
Rare-earth ions	$\text{Eu}^{3+}$ $\text{Er}^{3+}$ $\text{Pr}^{3+}$ $\text{Nd}^{3+}$	8.1 ms 880 $\mu\text{s}$			$\geq 1$	6 h 1.2 s 1.5–8.7 ms $\geq 1$	0.8–1.2 ms 1.2 s 1.5–8.7 ms $\geq 1$				1078–1132 <sup>k</sup> 1278–1388 <sup>l</sup> 1180–1468 <sup>m</sup>
						34 ns	15%				1269 <sup>k</sup>
						802 ns	23%				1326 <sup>l</sup>
											579 <sup>m</sup>
											1532 <sup>n</sup>
											606 <sup>o</sup>
								80%			883 <sup>p</sup>

<sup>a</sup>See Hosseini *et al.* (2011), Dudin, Li, and Kuzmich (2013), Xu *et al.* (2013), and Park, Kim, and Moon (2019).

<sup>b</sup>See Ebert *et al.* (2015), Levine *et al.* (2019), Langenfeld *et al.* (2020), Van Leent *et al.* (2020), and Daiss *et al.* (2021).

<sup>c</sup>See Wang *et al.* (2021).

<sup>d</sup>See Inlek *et al.* (2017).

<sup>e</sup>See De Greve *et al.* (2011), Matthiesen *et al.* (2013), Bechhold *et al.* (2015), Somaschi *et al.* (2016), Éthier-Majcher *et al.* (2017), Olbrich *et al.* (2017), Gangloff *et al.* (2019), Jackson *et al.* (2021), and Tomm *et al.* (2021).

<sup>f</sup>See Aharonovich *et al.* (2011), Bar-Gill *et al.* (2013), Arroyo-Camejo *et al.* (2014), Hensen *et al.* (2015), Bauch *et al.* (2018), Bradley *et al.* (2019), Pompili *et al.* (2021), and Ruf *et al.* (2021).

<sup>g</sup>See Neu, Fischer *et al.* (2011), Neu, Steinmetz *et al.* (2011), Sipahigil *et al.* (2014), Pingault *et al.* (2017), Sukachev *et al.* (2017), Becker *et al.* (2018), Nguyen *et al.* (2019a), Bhaskar *et al.* (2020), and Ruf *et al.* (2021).

<sup>h</sup>See Iwasaki *et al.* (2015), Palyanov *et al.* (2015), Wan *et al.* (2020), and Ruf *et al.* (2021).

<sup>i</sup>See Görlitz *et al.* (2020), Trusheim *et al.* (2020), and Ruf *et al.* (2021).

<sup>j</sup>See Lukin, Guidry, and Vučković (2020) and references therein.

<sup>k</sup>See Durand *et al.* (2021).

<sup>l</sup>See Bergeron *et al.* (2020) and Higginbottom *et al.* (2022).

<sup>m</sup>See Zhong, Hedges *et al.* (2015) and Zhong and Goldner (2019).

<sup>n</sup>See Rančić *et al.* (2018) and Zhong and Goldner (2019).

<sup>o</sup>See Zhong and Goldner (2019) and Lago-Rivera *et al.* (2021).

<sup>p</sup>See Zhong, Kindem *et al.* (2015) and Liu *et al.* (2021).

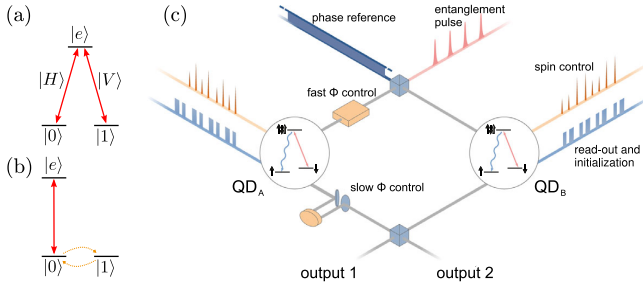


FIG. 17. Level structure and heralded entanglement generation. (a) Lambda-level structure with states  $|e\rangle$  (excited),  $|0\rangle$  (connected to  $|e\rangle$  by horizontally polarized light  $|H\rangle$ ), and  $|1\rangle$  (connected to  $|e\rangle$  by vertically polarized light  $|V\rangle$ ). (b) Level structure for time-bin entanglement, where  $|e\rangle$  is connected only to  $|0\rangle$ ; control of the qubit states is required. (c) Setup for spin-spin heralded entanglement generation. From Stockill *et al.*, 2017.

### B. Emission of photons entangled with the quantum memory

Quantum memories should have (or should be coupled to quantum emitters that have) optical transitions that allow the emission of photons entangled with the memory qubits. The emitted photonic qubits are to be encoded in one of the degrees of freedom discussed in Sec. II E. The emission of spin-entangled qubits encoded in photonic frequency, polarization, emission time-bin, and spatial modes has already been experimentally demonstrated with the help of trapped ions, N-V centers, and quantum dots. Many schemes exist for the production of photons entangled with the memory's degrees of freedom, varying in details depending on the photonic encoding and the energy-level structure of the emitter. For concreteness, we review two of the most common examples of such schemes here.

Polarization-entangled photons can be produced in a system with a  $\Lambda$ -shaped level structure (that is, a  $\Lambda$  system), where the qubit ground states  $|0\rangle$  and  $|1\rangle$  are both optically coupled to a single excited state  $|e\rangle$  by orthogonally polarized transitions (say, horizontally polarized and vertically polarized photons, respectively). This type of level structure is present in most quantum emitters, including some species of trapped ions (Blinov *et al.*, 2004) and atoms (Volz *et al.*, 2006), in atomic ensembles (Chen *et al.*, 2007), N-V centers (Togan *et al.*, 2010), and in quantum dots when a transverse magnetic field is applied (De Greve *et al.*, 2012; Gao *et al.*, 2012; Schaibley *et al.*, 2013). A quantum memory prepared in the excited state will spontaneously emit a single photon with either horizontal or vertical polarization ( $|H\rangle$  or  $|V\rangle$ ), as shown in Fig. 17(a). After this emission, the total memory-photon system is in the entangled state  $|0, H\rangle + |1, V\rangle$ . For this scheme to successfully produce such a maximally entangled state, the coupling strength of the two optical transitions ought to be the same. If the transitions differ in energy ( $E_H \neq E_V$ ), as in quantum dots, the final state might instead be  $|0, (H, E_H)\rangle + |1, (V, E_V)\rangle$ , where  $|(A, E_A)\rangle$  for  $A = H$  and  $V$  denotes the redundant encoding of the photonic qubit on its polarization and frequency degrees of freedom. The demonstration of bipartite entanglement is therefore challenging in this case since it

requires that this redundancy be erased. Such a quantum erasure of the photon frequency was demonstrated by Yu *et al.* (2015).

Despite its relative simplicity, the previous scheme may not be available for all quantum memories, as it requires a lambda-level structure. There is an alternative approach (Hensen *et al.*, 2015; Lee *et al.*, 2019; Tchebotareva *et al.*, 2019; Vasconcelos *et al.*, 2020) requiring only one strong optical transition that results in a photon whose emission time bin is entangled with the memory qubit. The minimal-level structure required for this scheme is illustrated in Fig. 17(b); it corresponds to a three-level system ( $|0\rangle$ ,  $|1\rangle$ , and  $|e\rangle$ ) where only one state of the qubit states, for instance,  $|0\rangle$ , is optically coupled to the excited state  $|e\rangle$ . The memory is initialized in a superposition state  $|0\rangle + |1\rangle$ , and the optical transition  $0 \leftrightarrow e$  is then excited by a  $\pi$  pulse such that the system ends up in  $|e\rangle + |1\rangle$ . If in the excited state the memory emits a photon in the early time bin  $|t_1\rangle$ ; otherwise, it emits no photons, resulting in the state  $|\text{vac}\rangle$ :  $|0, t_1\rangle + |1, \text{vac}\rangle$ . The memory qubit is then flipped in its qubit subspace (yielding  $|1, t_1\rangle + |0, \text{vac}\rangle$ ) and the  $0 \leftrightarrow e$  transition is excited again, leading to the emission of a photon in the time bin  $t_0$  if the excited state is populated:  $|1, t_1\rangle + |0, t_0\rangle$ . We see that a single photon is always emitted, and that its emission time bin is indeed entangled with the quantum memory. This strategy requires the preparation of the memory in a superposition state and more control pulses; however, it has the advantage of operating with only a single optical transition, making it particularly convenient in cases such as N-V centers (Bernien *et al.*, 2013) in which one specific optical transition has better properties than the others. This approach has also been demonstrated for quantum dots, where a certain transition is made more favorable through cavity (Purcell) enhancement (Lee *et al.*, 2018).

### C. Distant entanglement generation

It is possible to generate heralded entanglement between distant qubits mediated by the detection of photons. The implementation of these schemes is usually based on the interference of photons within a linear-optical setup. To optimally interfere and hence create high-quality entanglement, the photons emitted by two distant quantum memories should be perfectly indistinguishable (Aharonovich, Englund, and Toth, 2016; Senellart, Solomon, and White, 2017).

The scheme of Cabrillo *et al.* (1999) based on single-photon interference [see Bose *et al.* (1999) for a similar proposal] for distant entanglement generation has been demonstrated with trapped ions (Slodička *et al.*, 2013), quantum dots (Deleteil *et al.*, 2016; Stockill *et al.*, 2017), N-V centers in diamond (Humphreys *et al.*, 2018), and atomic ensembles (Chou *et al.*, 2007). The experiment conducted by Stockill *et al.* (2017), which was based on two quantum dot spins separated by a few meters, resulted in a postselected entanglement generation rate of 7.3 kHz (Stockill *et al.*, 2017).

We now illustrate how the scheme works experimentally. Two quantum dots  $A$  and  $B$  situated at two separated nodes are prepared in a Voigt configuration (in-plane magnetic field) to exhibit a  $\Lambda$ -level structure with similar optical transition energies. The two quantum dots are prepared initially in the state  $|\downarrow_A, \downarrow_B\rangle$  and are excited by the same weak

phase-stabilized laser such that a photon can be produced by each quantum dot through Raman scattering with a probability  $p \ll 1$ ; see Fig. 17(c). The photonic modes are then mixed on a 50:50 beam splitter at a central node to erase the which-path information: that is, to make it impossible to tell which quantum dot emitted the photon [essentially to perform the Bell measurement of Fig. 3(b)]. The state before the photon detection is

$$\begin{aligned} |\Psi\rangle = & (1-p)|\downarrow_A, \downarrow_B\rangle|0_1, 0_2\rangle \\ & + \sqrt{p(1-p)/2}(e^{i\Phi_A}|\uparrow_A, \downarrow_B\rangle + e^{i\Phi_B}|\downarrow_A, \uparrow_B\rangle)|1_1, 0_2\rangle \\ & + \sqrt{p(1-p)/2}(e^{i\Phi_A}|\uparrow_A, \downarrow_B\rangle - e^{i\Phi_B}|\downarrow_A, \uparrow_B\rangle)|0_1, 1_2\rangle \\ & + p/\sqrt{2}e^{i(\Phi_A+\Phi_B)}|\uparrow_A, \uparrow_B\rangle(|0_1, 2_2\rangle - |2_1, 0_2\rangle), \end{aligned} \quad (38)$$

where  $|i_1, j_2\rangle$  (with  $i$  and  $j$  integers) corresponds to the number of photons in the first and second output modes of the beam splitter and  $\Phi_A$  and  $\Phi_B$  are the optical phases along the different optical paths corresponding to qubits  $A$  and  $B$ . If a single photon is detected, the quantum dot system is projected with a probability  $\approx p$  onto the maximally entangled state  $e^{i\Phi_A}|\uparrow_A, \downarrow_B\rangle \pm e^{i\Phi_B}|\downarrow_A, \uparrow_B\rangle$ , with the sign depending on the output mode of the beam splitter in which the photon was detected. In practice  $p$  cannot be as high as desired, because the quantum dot spins undergo two spin flip processes with probability  $p^2$ , resulting in the emission of two photons. In that case, if only one of the two photons is detected (due to either imperfect collection and detection efficiencies or transmission losses) the heralding single-photon process leads to a state with fidelity that decreases with higher  $p$ . Stockill *et al.* (2017), Yu *et al.* (2020), Lago-Rivera *et al.* (2021), and Pompili *et al.* (2021) used this method to demonstrate heralded entanglement generation. Stockill *et al.* (2017) demonstrated the highest rate for distant spin-spin entanglement with postselection, and Yu *et al.* (2020) demonstrated the longest fiber distance between two remotely entangled quantum memories using atomic ensembles. However, while the two memories were separated by 50 km of fiber, this was achieved using a spooled fiber of that length; the actual distance between the systems was a meter.

There are other methods for generating distant heralded entanglement, namely, the Barrett and Kok scheme (Barrett and Kok, 2005) based on two-photon detection. This scheme has been demonstrated with N-V centers (Bernien *et al.*, 2013) and trapped ions (Moehring *et al.*, 2007). The longest-distance entanglement between separated systems reached using this approach (1.3 km) was also achieved with N-V centers, in a loophole-free Bell test experiment (Hensen *et al.*, 2015). Yu *et al.* (2020) also demonstrated a field-deployed heralded entanglement generation between two atomic ensembles separated by 11 km (22 km of fibers) using two-photon interference. The latter was achieved by increasing the collection and detection efficiencies of the photons as well as converting the optical photons to the telecommunication frequency, which enjoys the highest transmissivity in optical fibers; see Sec. V.F for more details.

The scheme of Cabrillo *et al.* (1999) is required to operate in the low photon emission probability regime to obtain high-fidelity heralded entanglement. In comparison, Barrett and Kok's scheme can operate in the high-fidelity regime even

with high emission probability. Therefore, it should be better suited for efficient quantum emitters and a short distance between the nodes. However, for longer distances the fiber losses becomes dominant and having a single-photon heralding like the protocol of Cabrillo *et al.* leads to a better scaling with distance than the two-photon heralding of the Barrett and Kok scheme (in alignment with the relationship discussed in Sec. IV.B between TF QKD and the original MDI QKD).

#### D. Entanglement distillation

During the generation of entanglement between remote nodes, operation errors or the decoherence of quantum memories can lead to a reduced fidelity of Bell states shared between distant nodes. For first-generation quantum repeaters, the fidelity of Bell pairs can be increased through entanglement distillation (Sec. III.B.1). Starting with two imperfect copies of a Bell pair, it is possible to produce a single Bell pair with an improved fidelity with a success probability of at best 50%. Entanglement distillation has been demonstrated with photonic Bell pairs (Pan *et al.*, 2001, 2003; Yamamoto, Koashi, and Imoto, 2001; Yamamoto *et al.*, 2003), atoms (Reichle *et al.*, 2006), and N-V centers (Kalb *et al.*, 2017).

Photonic realizations differ in success rate because it is impossible to perform a deterministic CNOT gate with linear optics. Instead, the entanglement distillation protocols are performed using solely linear optics with a success rate limited to 25% at best (Pan *et al.*, 2001; Yamamoto, Koashi, and Imoto, 2001). Reichle *et al.* (2006) demonstrated the first experimental entanglement distillation with quantum memories. They distilled two Bell pairs of  ${}^9\text{Be}^+$  ions, confined in the same Paul trap, with an overall success probability above 35%. Yet, because the pairs of entangled atoms were not spatially separated, this scheme is not particularly useful to enable long-distance quantum communication applications. Using two N-V centers with two  ${}^{13}\text{C}$  nuclear spins, Kalb *et al.* (2017) demonstrated entanglement distillation of a  $(65 \pm 3\%)$ -fidelity Bell state in N-V centers that were spatially separated by 2 m. The highest reported heralded entanglement rate was 182 Hz (Stephenson *et al.*, 2020), with trapped ions separated by 2 m using a two-photon interference scheme. Stephenson *et al.* expected a distilled Bell-pair fidelity of 99% is within experimental reach.

There are also distillation schemes (Sheng and Deng, 2010; Sheng, Zhou, and Long, 2013) that utilize specific properties of encodings. For instance, Hu *et al.* (2021) demonstrated entanglement distillation by utilizing hyperentanglement (Kwiat, 1997; Barreiro *et al.*, 2005).

#### E. Multiqubit quantum registers and error correction

Multiple memory qubits will be required per repeater node, either for increasing the communication rate via multiplexing (Collins *et al.*, 2007) or for enabling error correction in repeaters beyond the first generation. A quantum register extends the architecture from Sec. V.A to a quantum emitter with good optical properties coupled to a large number of long-lived quantum memory qubits. This arrangement naturally occurs in color centers in diamond, where the defect is coupled by hyperfine interaction to tens of  ${}^{13}\text{C}$  nuclear spins (Bradley *et al.*, 2019), forming the register of qubits. There

have been several advances in this line of research, such as in experiments where the nuclear spins are individually controlled using the electron spin (Childress, Gurudev Dutt *et al.*, 2006; Gurudev Dutt *et al.*, 2006; Balasubramanian *et al.*, 2009; Fuchs *et al.*, 2011; Taminiau *et al.*, 2012; Bradley *et al.*, 2019). Similarly, in the trapped ion setting a quantum register of many qubits has been realized using one quantum emitter coupled to many memory qubits in the same optical trap. For example, dual species quantum nodes based on pairs of different ionic species such as  $^{128}\text{Ba}^+$ - $^{171}\text{Yb}^+$  (Inlek *et al.*, 2017) and  $^{25}\text{Mg}^+$ - $^9\text{Be}^+$  (Tan *et al.*, 2015) are being investigated. In a quantum dot, however, the spin is coupled to only one (or potentially two) different magnon species (Jackson *et al.*, 2021), imposing limits on the size of the register. An alternative strategy for obtaining more qubits at each repeater node could be to vertically stack quantum dots (Stinaff *et al.*, 2006).

For repeaters from the second and third generation, a quantum register at each node can be seen as a quantum processor used to logically encode the quantum information transferred between nodes and to correct errors. A QEC code was recently implemented in trapped ions (Egan *et al.*, 2021). Here nine physical  $^{171}\text{Yb}^+$  qubits (with four additional qubits for stabilizer measurements) are associated with one logical qubit of the Bacon-Shor code in a fault-tolerant design. A recent experiment using superconducting qubits (Google Quantum AI, 2023) demonstrated a logical error rate reduction through increasing the size of the QEC code being used. There is also an effort to pursue error-corrected repeater nodes with solid-state spins (Walther *et al.*, 2014; Cramer *et al.*, 2016). In particular, with defects in diamond (Aboobehi *et al.*, 2022) it was recently shown the experimental fault-tolerant operation of a logical qubit using the five-qubit code together with a flag protocol (Chamberland and Beverland, 2018; Chao and Reichardt, 2018) requiring a total of seven qubits. Yet, this proof-of-principle demonstration remains above the break-even point for which logical qubit operations have higher fidelities than physical qubit operations.

The logical qubits in error-corrected repeaters must be interfaced optically. For several platforms investigated for the realization of multiqubit processors, such as superconducting circuits, a major challenge for quantum communication applications revolves around the emission of optical photons, which requires quantum transduction from microwave to optical energies (Lauk *et al.*, 2020; Mirhosseini *et al.*, 2020; Ang *et al.*, 2022).

The realization of logical photonic qubits is also being pursued; they are required in the third generation of repeaters and in all-photonic quantum repeaters in order to correct for loss errors. Error detection has been demonstrated on a photonic platform (Bell *et al.*, 2014), and recently a proof-of-concept photonic nine-qubit Shor code was experimentally implemented together with an all-photonic quantum repeater proposal (Zhang, Liu *et al.*, 2022).

#### F. Loss mitigation, quantum frequency conversion, and photonic source efficiency

A stringent requirement on correcting photonic errors is imposed by the no-cloning theorem (Sec. II.B), which implies that it is impossible to correct physical qubit losses of more

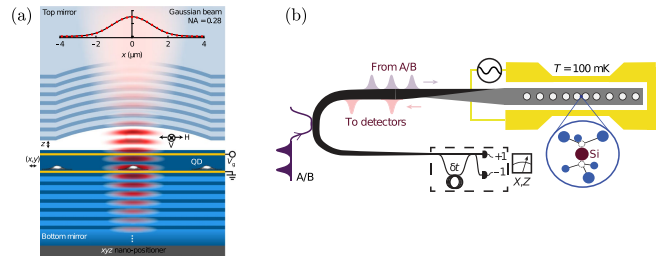


FIG. 18. State-of-the-art cavity-QED devices. (a) A quantum dot coupled deterministically to an open Fabry-Perot cavity. From Tomm *et al.*, 2021. (b) A silicon-vacancy center in diamond in a photonic crystal cavity evanescently coupled to a fiber. From Bhaskar *et al.*, 2020.

than 50% with QEC. In light of this, reducing the photon losses throughout a quantum network is critical for the implementation of repeaters where the loss is handled via QEC. Loss occurs at every optical component, with the main sources being propagation and coupling losses due to the intrinsic properties of fibers and photonic chips. Loss also occurs at the detectors and during the collection of photons produced by quantum emitters.

Losses in fibers are caused chiefly by infrared absorption and Rayleigh scattering, as well as imperfections introduced in manufacturing. Minimal loss is obtained at the telecom wavelength (1550 nm), where the loss coefficient is 0.2 dB/km, with few prospects for improvement. Even though there are ultralow-loss fibers with losses of 0.16 dB/km (Boaron *et al.*, 2018), they are not widely available and would require complete modification of the existing infrastructure. It is therefore crucial to use quantum emitters that emit at the telecom wavelength, such as some engineered quantum dots (Benyoucef *et al.*, 2013) or rare-earth ions (Zhong *et al.*, 2019) and color centers in silicon (Bergeron *et al.*, 2020; Redjem *et al.*, 2020).

An alternative strategy consists of using a quantum frequency converter. The objective is to change the frequency of the photonic qubits while preserving the quantum information encoded into them (and the single-photon statistics if they are required for the scheme) (Tanzilli *et al.*, 2005; McGuinness *et al.*, 2010; Ikuta *et al.*, 2011). Frequency converters are generally based on a nonlinear  $\chi^{(2)}$  crystal (or possibly  $\chi^{(3)}$ ) pumped by a laser pulse with frequency  $\omega_l$  chosen such that the frequency  $\omega_i$  of an input photon is modified into  $\omega_f = \omega_i - \omega_l$ . This strategy has been used to convert the frequency to a telecom wavelength of photons emitted by N-V centers (Tchekhovareva *et al.*, 2019), quantum dots (De Greve *et al.*, 2012; Zaske *et al.*, 2012), single atoms (Van Leent *et al.*, 2020, 2022), ions (Bock *et al.*, 2018; Krutyanskiy *et al.*, 2019, 2023), rare-earth-doped crystals (Maring *et al.*, 2017), and atomic ensembles (Dudin *et al.*, 2010; Ikuta *et al.*, 2018; Yu *et al.*, 2020).

The efficient collection of light produced by quantum emitters is another important technological challenge. Since spontaneous emission is nondirectional, photon collection efficiencies tend to be low. To obtain a high efficiency source of single photons, the electromagnetic environment of the quantum emitter ought to be engineered to force its emission into one specific mode, which can then be coupled into a fiber.

This can be achieved using waveguides, which inhibit the emission outside of the waveguide mode (Arcari *et al.*, 2014), or with microcavities, which enhance the coupling between the quantum emitter and the electromagnetic mode confined in the cavity. In these two cases, the emission of a single photon is much more probable inside a particular mode (of the cavity or the waveguide) than in all the others. This photonic mode can then be efficiently coupled to the transmission fiber. Cavity enhancement also has the important advantage of increasing the probability of emission of indistinguishable coherent photons (Riedel *et al.*, 2017) as compared to incoherent phonon-assisted emission. Two examples of state-of-the-art cavity-QED devices are reviewed in Fig. 18. The single-photon collection efficiency has drastically improved over the years for all quantum emitters through technological and material improvement of cavity-QED devices (Barros *et al.*, 2009; Maiwald *et al.*, 2012; Somaschi *et al.*, 2016; H. Wang *et al.*, 2019; Bhaskar *et al.*, 2020; Uppu *et al.*, 2020; Tomm *et al.*, 2021); in quantum dots, trapped ions, and defects in diamond, the collection efficiency has now risen above the 50% threshold.

While it does not make use of quantum emitters, note that spontaneous parametric down-conversion sources have seen their effective collection efficiency increase to 67% through large-scale multiplexing and active switching (Kaneda and Kwiat, 2019). Although it is not possible to use these sources to realize an efficient light-matter interface in quantum repeater protocol based on matter qubits, they nevertheless show great potential for all-photonic approaches, as detailed in Sec. V.G.

The single-photon detection efficiency (Hadfield, 2009) has also been significantly increased through the development of superconducting nanowire single-photon detectors. Devices with detection efficiencies as high as 95% are now commercially available, and superconducting nanowire detectors with efficiencies as high as 99% have been demonstrated at telecom frequencies (Hu, Li *et al.*, 2020; Chang *et al.*, 2021). Transition edge sensors also enjoy high detection efficiencies, with the added benefit that they can resolve photon numbers (Lita, Miller, and Nam, 2008), which can be useful for some heralded entanglement generation schemes.

## G. Progress toward memoryless quantum repeaters

In all-photonic quantum repeaters, error correction and loss tolerance should be achieved through photonic codes, instead of using quantum memories. The technological requirements of such repeaters are therefore considerably different than the other approaches. The primary challenge revolves around the creation of large, highly entangled photonic states, namely, graph states.

Several different approaches have been suggested for photonic graph state generation. Until recently, the largest entangled states of photons were produced experimentally using spontaneous parametric down-conversion sources and fusion gates (Browne and Rudolph, 2005). The probabilistic nature of fusion gates is the main limitation to the number of photons in the graph state that can be produced using this approach, with the current maximum being 12 (Zhong *et al.*, 2018).

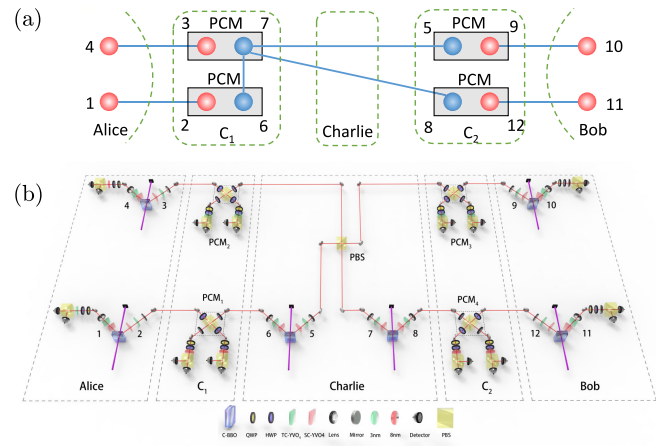


FIG. 19. A proof-of-principle experiment for an all-photonic quantum repeater. Passive choice measurement (PCM) automatically performs an entangling Bell measurement (in the case of a coincidence detection) or a disentangling local  $X$  measurement (in the case of a single-photon detection or the failure of the Bell measurement). From Li *et al.*, 2019.

Proof-of-principle experiments of all-photonic quantum repeaters have already been realized (Hasegawa *et al.*, 2019; Li *et al.*, 2019). In both cases, the original protocol given by Azuma, Tamaki, and Lo (2015) was replaced by a variant in order to facilitate its experimental realization. In this new all-photonic communication scheme, which was introduced by Hasegawa *et al.* (2019), Alice and Bob prepare  $n$  photonic Bell pairs each, sending half of every one of them through a lossy fiber to a central node (Charlie). Prior to the arrival of the photons, Charlie prepares a  $2n$ -qubit GHZ state (equivalent to the complete-graph state in Sec. III.C.1 under local unitaries) and performs photonic Bell-state measurements between the incoming photons and the corresponding photons in the GHZ state. The first key concept behind this scheme is a time-reversed adaptive Bell measurement, which Li *et al.* (2019) referred to as a passive choice measurement. If the photon  $a_i$  ( $i = 1, 2, \dots, n$ ) emerging from Alice arrives at Charlie's node and the joint measurement with photon  $c_i$  from Charlie's GHZ state is successful, then Charlie achieves a Bell-state projection. However, if the photon  $a_i$  does not make it to Charlie's node or if the measurement is unsuccessful, the Bell-state analyzer passively adapts to an  $X$ -basis measurement on  $c_i$  that disconnects photon  $c_i$  from the GHZ state. This leads to the second important idea given by Hasegawa *et al.* (2019): the outer qubits from the original repeater graph state given by Azuma, Tamaki, and Lo (2015) can be removed, leaving a bare GHZ state in its place.

Li *et al.* (2019) demonstrated the aforementioned scheme with a four-qubit GHZ state and  $n = 2$  multiplexed communication channels. We now examine the experiment in Fig. 19. Alice, Bob, and Charlie each prepare two Bell pairs using spontaneous parametric down-conversion sources. Alice and Bob send one qubit from each Bell pair (each corresponding to transmission over a communication channel) to Charlie's node. Charlie mixes his two Bell pairs to produce a four-qubit GHZ state and the protocol proceeds as previously explained with  $n = 2$ . Although the experiment did not surpass the PLOB bound (Pirandola *et al.*, 2017), Li *et al.*

demonstrated an enhancement in communication rates between Alice and Bob compared to the case where Charlie uses a Bell pair for each communication channel (that is, does not multiplex the channels). These results attested to the interest and experimental feasibility of all-photonic solutions for quantum communication.

In principle, the aforementioned modifications simplify the original all-photonic repeater, making it attainable with current technology. However, the protocol works only if a single QR node is used, consequently leading to an  $\eta^{1/2}$  scaling at best, and limiting the communication distances to at most about 1000 km in practice<sup>13</sup> (in the sense explained in footnote 5). Going beyond this limit would require one to cascade multiple QR nodes and use photonic states with many more photons, such as the RGS in the original protocol (Sec. III.C.1). Furthermore, the protocol is particularly sensitive to local losses at Charlie's node, as demonstrated by Hasegawa *et al.* (2019). Delaying the preparation of the GHZ state only partially mitigates this issue, with a more complete scheme requiring loss-tolerant error correction. Recently Zhang, Liu *et al.* (2022) demonstrated a nine-qubit Shor code, with a new all-photonic quantum repeater approach that could be cascaded. They also showed its tolerance to single-photon losses. Among the steps remaining for it to be fully operable, this Shor code should be generated in a heralded fashion rather than being postselected.

To move to higher photon numbers, the all-optical strategy requires probabilistic fusion gates combined with high-speed feed forward (Sec. III.C.3) to grow larger and larger graphs based on small graph resources. Having efficient feed forward techniques is thus crucial (Zanin *et al.*, 2021). This is achievable only with ultrafast optical switches and electronics.

The technological challenges of bosonic repeaters (Sec. III.C.2.c) are somewhat different than the discrete-variable repeater that we have focused on. For the particular case of encoding qubits into momentum-squeezed or GKP states, one can deterministically combine modes into large graph states with Gaussian operations (linear optics and squeezing). However, the production of GKP states is challenging, with only a single early demonstration in the photonic platform (Konno *et al.*, 2023). However, Gaussian states of light are now a well-mastered technology (Asavanant *et al.*, 2019).

An alternative strategy for producing photonic graph states is to use light-matter interfaces in generation procedures in the manner of Buterakos, Barnes, and Economou (2017) or Pichler *et al.* (2017), Zhan and Sun (2020), and Zhan *et al.* (2023), whose approach was based on the initial work of Schön *et al.* (2005), Lindner and Rudolph (2009), and Economou, Lindner, and Rudolph (2010). This strategy is more demanding experimentally but has the advantage of being deterministic in principle. Indeed, with unity collection efficiency of the photons and perfect control of the quantum emitters, the generation procedure does become completely

deterministic: the entanglement between photons is produced through the control of the quantum emitter rather than through probabilistic fusion gates. A proof-of-concept experiment was realized by Schwartz *et al.* (2016), who produced a linear-cluster state by manipulating and optically pumping the spin of a quantum dot. They produced a three-qubit linear-cluster state and showed that entanglement persists for up to five photons. More recently Cogan *et al.* (2023) showed that entanglement persists over ten photons, with indistinguishability above 90%, also using the deterministic generation from a hole spin quantum dot emitter. Quantum-dot-based sources of entangled photons have also been inserted inside microcavities to generate linear-cluster states at much higher rates (Coste *et al.*, 2023). A similar generation scheme using a single atom trapped in a cavity was used to demonstrate a 12-photon linear-cluster state and a 14-photon GHZ state (Thomas *et al.*, 2022), which to date constitutes the record largest experimentally demonstrated entangled photonic state. In those experiments the emitters produced polarization-entangled photons, but strategies involving time-bin entanglement have also been explored (Lee *et al.*, 2018; Vasconcelos *et al.*, 2020; Appel *et al.*, 2022; Vezvaei *et al.*, 2022).

To go beyond linear-cluster state generation, one can use either multiple solid-state qubits or the strong nonlinear interaction induced by atoms for light to effect entangling gates. For the generation procedures of Pichler *et al.* (2017) and Zhan and Sun (2020), one needs to implement spin-photon CZ gates, where a phase shift is induced in a photon that depends on the spin state. Cavity-QED devices increase the spin-photon interaction such that such spin-photon gates are within reach with many cavity-QED platforms (Arnold *et al.*, 2014; Reiserer *et al.*, 2014; Sun *et al.*, 2016; Javadi *et al.*, 2018; Androvitsaneas *et al.*, 2019; Wells *et al.*, 2019; Bhaskar *et al.*, 2020).

## H. Experimental realization of quantum networks

In this section, we review experiments that go beyond two-node quantum communication to inch closer to the quantum internet. We start by presenting the experimental realizations of trusted large-scale repeater networks for QKD applications based on trusted relays. We then discuss experimental progress toward the realization of quantum repeaters to actualize long-distance quantum communication over untrusted nodes. Finally, we discuss the experimental realization of untrusted quantum networks.

### 1. Trusted large-scale repeater networks

Several intercity QKD networks have already been realized, such as the SECOQC network in Austria (Peev *et al.*, 2009), the Tokyo QKD network in Japan (Sasaki *et al.*, 2011), the SwissQuantum network in Switzerland (Stucki *et al.*, 2011), the Illinois Express Quantum network in the U.S. (Chung *et al.*, 2021), and the Shanghai-Beijing QKD network in China (Y.-A. Chen *et al.*, 2021). In all of these networks, cryptographic keys are distributed between nodes separated by long distances using relay nodes. Assuming that the relay nodes are trusted, a secure key can be established at rates much higher than are possible through direct fiber

<sup>13</sup>For instance, with a twin-field-type QKD protocol that utilizes a single node between communicators, Wang *et al.* (2022) successfully generated a secret key with  $4.572 \times 10^{-1}$  secret bits per second over 786.67 km of fiber, and  $1.399 \times 10^{-2}$  secret bits per second over 833.80 km of fiber experimentally.

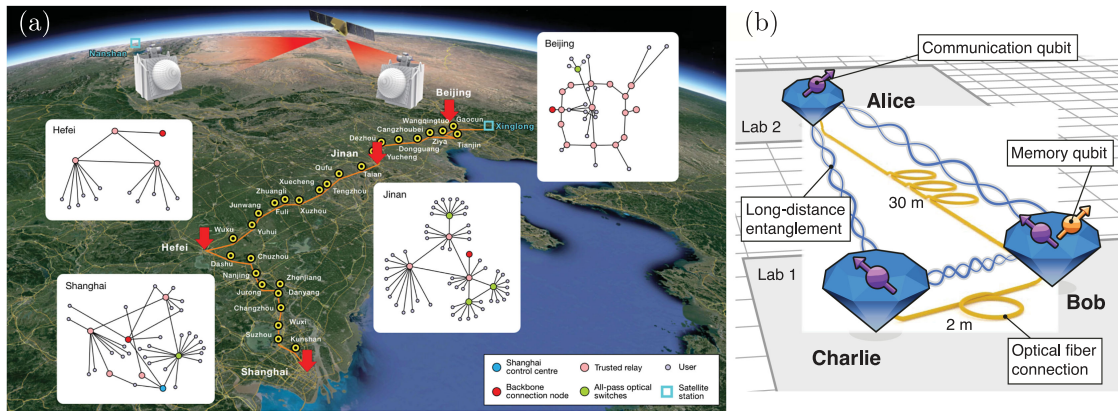


FIG. 20. Quantum networks. (a) Shanghai-Beijing QKD network. From Y.-A. Chen *et al.*, 2021. (b) Experimental quantum network composed of N-V centers acting as quantum memories. From Pompili *et al.*, 2021.

transmission (Pirandola *et al.*, 2017), thereby enabling efficient QKD over long distances.

In Fig. 20(a), we illustrate the Shanghai-Beijing QKD network, the largest QKD network to date. This network links four metropolitan areas (Shanghai, Hefei, Jinan, and Beijing) using a backbone of 32 trusted relays in a linear topology. If any one of the 32 relay nodes is compromised, the generated key may be insecure. The trusted relays allow for efficient long-distance QKD between these metropolitan areas. Each of these cities comprises small QKD networks with different topologies, where end users with reduced capabilities (requiring only a QKD source) can connect to the network. This network incorporates both fiber- and satellite-based communication: the nodes at Nanshan and Xinglong are separated by 2600 km, communicating through free space via a satellite node that also acts as a trusted relay. A similar strategy has been used to distribute a secret key over intercontinental distances: between Graz in Austria and Nanshan and Xinglong in China, covering a total distance of 7600 km (Liao *et al.*, 2018). Thanks to this combination of fiber- and satellite-based quantum communication, the Shanghai-Beijing QKD network covers a total distance of 4600 km and provides a typical secret rate between each node of 50 kbit/s and a minimum internode secret key rate of 28 kbit/s in the entire network. The large key rates achieved at such distances are completely out of reach for direct transmission over a fiber. Given its covered distance, complex topology, and the different quantum channels used, this QKD network can be considered a genuine prototype of the quantum internet for QKD applications, albeit at the cost of having to trust the network provider.

## 2. Proof of concept of a quantum repeater

Improving on a trusted repeater network is required to implement device-independent QKD, which can be realized through the distribution of Bell pairs to the end nodes. Recent experimental demonstrations of fibered device-independent QKD based on quantum memories [single  $^{87}\text{Rb}$  atoms (Zhang *et al.*, 2022) and  $^{88}\text{Sr}^+$  ions (Nadlinger *et al.*, 2022)] constituted significant improvements as they closed the detection loophole in the violation of Bell's inequality. In an experiment using an untrusted satellite node to share

private keys with the help of the Ekert 91 protocol (Ekert, 1991), Yin *et al.* (2017) set the record distance of 1200 km for a distribution of entangled photons. Realizing a long-distance device-independent multinode network would also crucially require the practical implementation of efficient quantum repeaters in real networks. However, this major milestone is the subject of active research and remains to be demonstrated. Note, however, that device-independent QKD still suffers from attacks<sup>14</sup> such as memory attacks (Barrett, Colbeck, and Kent, 2013) and covert channels (Curty and Lo, 2019).

Bhaskar *et al.* (2020) demonstrated that the use of a single-repeater node in an experiment increases the communication rate of MDI QKD compared to repeaterless communication. Like Li *et al.* (2019), Bhaskar *et al.* used a repeater scheme with a single-repeater node; however, they were able to demonstrate improvement over the PLOB bound in terms of a key rate in bits per channel use versus an effective channel transmission: a fourfold secret key rate increase over the original MDI QKD (Lo, Curty, and Qi, 2012). The repeater node consists of a single silicon-vacancy center embedded in a diamond photonic crystal cavity. The cavity mode of this device is efficiently evanescently coupled to a fiber to minimize the photonic losses. A significant improvement toward the photon collection efficiency was also demonstrated, reaching 85%. The silicon-vacancy system is positioned in a dilution refrigerator to achieve a coherence time  $T_2 = 0.2$  ms. In their experiment, the quantum memory at Charlie's node does not emit photons but receives weak coherent time-bin-encoded pulses from Alice and Bob. Using electromagnetically induced transparency of their cavity-QED device, these weak pulses are reflected or not depending on the electronic spin state. The reflected photonic pulses are then detected by superconducting single-photon

<sup>14</sup>This is because once a key has been generated it is classical, and as such is subject to copying. Therefore, if a QKD system is reused in future QKD sessions, then the key generated in a previous session might be stored in some memories and be leaked. Moreover, not only the QKD devices but also the conventional computers used in the classical postprocessing (for instance, error correction and privacy amplification) can leak key information via covert channels.

detectors. If a photonic pulse coming from Bob is detected shortly after a pulse from Alice, a key bit can be distributed between Alice and Bob when Charlie communicates the two-photon and spin measurement results. With these experiments it is possible to achieve a  $\sqrt{\eta}$  scaling because the two coherent pulses do not need to arrive simultaneously at the repeater node, thanks to the quantum memory; see Sec. IV for details. The role of the memory is to store the information of the first pulse during the time it remains coherent while waiting for the second pulse to be detected. While operating with only one quantum memory per node for the moment, these results foresee a promising route toward long-distance quantum communication. Indeed, a silicon-vacancy color center can in principle make use of their  $^{13}\text{C}$  neighbors to effect a quantum register of long-lived memories (Nguyen *et al.*, 2019b). This may increase the performance of the protocol by enabling longer storage times as well as the concatenation of multiple repeater nodes, in principle paving the way to obtain a polynomial scaling of the rate with the communication distance. This Si-V-center system will be integrated in the future 50-km-long Boston quantum network (Bersin *et al.*, 2023).

In a more recent experiment, Langenfeld *et al.* (2021) demonstrated a memory-enhanced quantum repeater node based on two  $^{87}\text{Rb}$  atoms in an atomic cavity. This node can in principle be cascaded at the core of a quantum repeater scheme that overcomes the previous  $\sqrt{\eta}$  limits of a repeater node with a single memory such as that discussed by Bhaskar *et al.* (2020). Moreover, the single-qubit error rate was below 11%, ensuring that a secure key can indeed be transferred using this repeater node. Such a memory-enhanced repeater has also been demonstrated by performing entanglement swapping with two  $^{87}\text{Rb}$  atomic-ensemble memories (Pu *et al.*, 2021).

### 3. Untrusted quantum networks

Since a quantum internet for applications beyond QKD may look like a multinode network where quantum information is stored and processed by quantum memories, a complementary route toward the development of long-distance multinode networks is to create multiqubit quantum networks at a small distance and to progressively increase their size when the quantum repeater technology becomes more mature. The work of Pompili *et al.* (2021) is the first realization of such a small quantum network, where each node includes a quantum memory to process quantum information locally. This network is based on three nodes, with an internode distance of a maximum of 7 m; see Fig. 20(b). Each node includes one or two quantum memories based on an N-V center electron spin, and potentially another proximal  $^{13}\text{C}$  nuclear spin.

Pompili *et al.* (2021) used their network to perform non-trivial multinode operations such as the generation of a three-qubit GHZ state with a memory qubit at each node and the generation of a Bell pair between quantum memories situated at nodes that were not directly connected. After the generation of heralded entanglement between an N-V electron spin at Alice's node and the electron spin at Charlie's node, the information encoded in Charlie's electron spin qubit was swapped to a  $^{13}\text{C}$  nuclear spin so that the electron spin could be used again to generate entanglement with Bob's N-V

center. This entanglement generation step could be realized with the strategies introduced in Sec. V.C. The entanglement was swapped by performing a Bell measurement between the electron and the nuclear spins at Charlie's node. This was the first demonstration of deterministic entanglement swapping in a heralded fashion between distant nodes that were not originally connected. The work required the cooperation of a multitude of experimental components. Pompili *et al.* (2021) used the single-photon detection scheme proposed by Cabrillo *et al.* (1999) to herald entanglement generation between distant spins with 80% fidelity and at rates of 7 and 9 Hz, using phase-stabilized links between the three nodes. The quantum information initially stored in Charlie's electron spin qubit needed to be swapped into one of its proximal nuclear spins, thereby requiring a nuclear spin register and a high level of control. In addition, since the entanglement ought to be stored for the time the three nodes were connected, dynamical decoupling sequences were used to further isolate the spins from their environment. Finally, an electron-nuclear spin Bell state was used to swap the entanglement at the central node and produce a Bell state between Alice's and Bob's spin qubits at a rate of 25 mHz. This protocol had an overall fidelity of 55%, which could potentially be improved by using better photonic interfaces, spin control, and readout techniques, as well as by reducing the infidelities and increasing the rate of the distant spin-spin entanglement generation. Such a network has also been used to teleport quantum information between two nodes that are not immediate neighbors (Hermans *et al.*, 2022).

The interest of these results is also to provide a test bed for real-life applications and to prepare the other technological aspects of the implementation of a quantum network, such as the communication protocols. There is also a considerable development of quantum network simulator software (Matsuo, Durand, and Meter, 2019; Coopmans *et al.*, 2021; Wallnöfer *et al.*, 2022) to assist in this goal, for example, to envision a city-scale network (Yehia *et al.*, 2022).

## VI. QUANTUM INTERNET

The goal of this section is to look beyond linear networks, i.e., chains of quantum repeaters, and discuss how they blend into the vision of a future quantum internet. First, we present a set of communication tasks that can be implemented over a quantum network, and we link these sample communication tasks with experimental requirements and associate the tasks with a taxonomy of stages of the quantum internet that summarizes the discussion of Wehner, Elkouss, and Hanson (2018). Second, we introduce the elements of a quantum network and place repeaters in the larger context of a quantum network architecture. Finally, we investigate how to evaluate the usefulness of quantum networks for these different tasks. For this we introduce a simplified model of a network in terms of a graph. The evaluation is phrased in the form of network capacities, quantities that can be achieved in an idealized situation. We observe that, in spite of the apparent additional difficulty of dealing with a network, in this abstract setting many of the tools from point-to-point links carry to the network setting; see Azuma *et al.* (2021) for a review on tools for predicting quantum network performance.

## A. Applications of the quantum internet

### 1. A set of representative communication tasks

Before we discuss how to quantify the usefulness of a quantum network, it is relevant to discuss the potential applications of quantum networks and more generally of the quantum internet. In the following we discuss a representative set of the applications that we know today divided by area. However, as in the early days of the Internet, we should expect many new applications to be found as the number of users increases.

First, a quantum internet can be used for transmitting information. The nodes in the network might want to transmit classical information or quantum information. The latter is not possible without a quantum network, but for the former the quantum internet can offer an advantage with respect to a classical network. In particular, both entangled channel inputs (Hastings, 2009) and joint quantum measurements (Sasaki *et al.*, 1998; Guha, 2011) can enhance the transmission rate of classical communication. A quantum internet can also be used to transmit classical information between two parties that is kept secret from any third party (Devetak, 2005). In turn this enables secret key distribution, a task that is possible with classical means only if the parties are willing to make assumptions on the communication channel [for example, wireless physical layer security relies on a model of the conditional probability distribution associated with the wireless channel (Bloch *et al.*, 2008)] or on the capabilities of a potential eavesdropper [for example, the security of the RSA cryptosystem (Rivest, Shamir, and Adleman, 1978) relies on the difficulty of the factoring problem].

Second, a quantum network can be used to implement several cryptographic tasks beyond private communication, with qualitative advantages with respect to classical networks. The best-known one is QKD. Some other tasks are byzantine agreement (Ben-Or and Hassidim, 2005), certified deletion (Broadbent and Islam, 2020), conference key agreement (Chen and Lo, 2007; Augusiak and Horodecki, 2009; Murta *et al.*, 2020), distribution of money (Wiesner, 1983), leader election (Tani, Kobayashi, and Matsumoto, 2005), and secret sharing (Cleve, Gottesman, and Lo, 1999; Hillery, Bužek, and Berthiaume, 1999). There are some important cryptographic tasks that cannot be implemented either with classical or with quantum resources, such as information-theoretically secure quantum bit commitment and two-party secure computation (Lo, 1997; Lo and Chau, 1997; Mayers, 1997; Lo and Chau, 1998). But, if one is willing to make an assumption on the amount of storage (Damgård *et al.*, 2008) or on the quality (Konig, Wehner, and Wullschleger, 2012) of the storage of a potential attacker, then implementing these tasks with quantum resources is advantageous. In this category fall quantum protocols for bit commitment (Kent, 2011; Konig, Wehner, and Wullschleger, 2012), oblivious transfer (Schaffner, 2010; Wehner *et al.*, 2010), and secure identification (Damgård *et al.*, 2007; Dupuis, Fawzi, and Wehner, 2015). Strikingly, a quantum network offers the possibility of implementing most of these cryptographic tasks without making any assumptions on the behavior of the devices held

by the legitimate parties (Mayers and Yao, 1998). In consequence, these so-called device-independent implementations close by construction one of the most important sources of side channel attacks.

Third, as noted in Sec. I, the study of quantum communication complexity tells us that by sending quantum information (qubits) we can dramatically lower the amount of communication required compared to sending classical information (bits). Quantum fingerprinting (Buhrman *et al.*, 2001) is an example of the quantum advantage in communication.

Fourth, another important application of quantum networks is computation. In its more direct sense, an alternative paradigm to the monolithic construction of a quantum computer is the so-called modular or distributed quantum computer (Nickerson, Fitzsimons, and Benjamin, 2014). In this paradigm high-quality small quantum computers are linked via entanglement to build a larger quantum computer. A quantum network can also be used to perform quantum computation on a remote quantum computer without revealing information about the computation or the underlying data (Childs, 2005; Broadbent, Fitzsimons, and Kashefi, 2009; Aharonov *et al.*, 2017), to perform multipartite computation (Cleve and Buhrman, 1997), or to obtain a computational advantage in distributed computation tasks (Le Gall, Nishimura, and Rosmanis, 2019).

Finally, the entanglement distributed by a quantum network can boost the performance of sensing applications (Degen, Reinhard, and Cappellaro, 2017). Notable examples in this domain are in clock synchronization (Komar *et al.*, 2014) and in interferometry, where entanglement can be used to extend the baseline of telescopes (Gottesman, Jennewein, and Croke, 2012; Khabiboulline *et al.*, 2019).

### 2. Stages of the quantum internet

The path to building the quantum internet will be long and difficult. The current standard viewpoint is that the quantum internet will probably develop in stages. There are different ways to divide it into stages. The classification proposed by Wehner, Elkouss, and Hanson (2018) is based on the network functionality available to the end nodes.

Quantum networks where nodes have limited functionality are already useful for applications, and new tasks can be implemented as the functionality of the end nodes increases. This means that, even at the early stages of development, we expect quantum networks to be useful. We later recap the discussion given by Wehner, Elkouss, and Hanson (2018), linking the communication tasks introduced in Sec. VI.A.1 to development stages.

In the first stage *trusted repeater networks* are built. In this stage, the nodes can prepare and transmit quantum states to adjacent nodes in the network. This functionality allows one to implement prepare-and-measure quantum key distribution protocols between adjacent nodes. In this way, it is possible to construct a network of individual quantum key distribution links, but it is not a fully quantum network in the sense that quantum information cannot be transmitted to nonadjacent nodes. This limited functionality is nonetheless useful: in such a network, if two end nodes trust the behavior of the nodes in a

path connecting them, then they can exchange keys that are secure under this assumption (Salvail *et al.*, 2010). Existing quantum networks such as the Tokyo QKD network (Sasaki *et al.*, 2011), the SECOQC network (Peev *et al.*, 2009), and the Shanghai-Beijing network (Y.-A. Chen *et al.*, 2021) are at this stage; see Sec. V.H.1.

In the second stage, end-to-end *prepare-and-measure networks* are built. In this stage, the nodes can prepare single qubits and transmit them to any other node in the network without any trust assumption and on the receiving side, nodes can measure incoming qubits. A potential price to pay is the postselection of the transmitted signals. Nonetheless, prepare-and-measure networks can still be useful for various additional applications, including secure identification in two-party cryptography with noisy quantum memories and key distribution. This includes protocols where entanglement is used as a proof technique in the virtual protocol to guarantee security but the nodes do not share an entangled state at any moment. Instead, it is sufficient that the nodes can confirm whether entanglement could have been shared if the end nodes had run a coherent version of a prepare-and-measure protocol. For instance, communicators in a time-reversed entanglement distribution protocol (Biham, Huttner, and Mor, 1996), a measurement-device-independent quantum key distribution (MDI-QKD) (Lo, Curty, and Qi, 2012), and a TF QKD (Lucamarini *et al.*, 2018) fall into this category, which removes assumptions about the measurement devices and highly limits the feasibility of side channel attacks; see Curty, Azuma, and Lo (2021).

In the third stage, *entanglement distribution networks* are achieved where two users can obtain end-to-end quantum entanglement in either a deterministic or a heralded fashion. In this stage, the end nodes require no quantum memories. This added functionality enables, for example, device-independent QKD when the loss is sufficiently low.

In the following we discuss the final three stages. These stages differ in regard to the quality of the quantum computational capabilities of the nodes.

In the fourth stage, *quantum memory networks* are built. In this stage, the end users can store quantum information in their memories and teleport quantum information to each other. The minimum storage time is determined by the transit time between the two end nodes. Note that in this stage the operations are done directly on the physical qubits. There is no fault tolerance. This functionality enables some blind quantum computation schemes provided that there is a remote quantum computer (Broadbent, Fitzsimons, and Kashefi, 2009; Aharonov *et al.*, 2017). It also enables protocols for extending the baseline of telescopes (Gottesman, Jennewein, and Croke, 2012; Khabiboulline *et al.*, 2019); protocols for cryptographic tasks such as anonymous quantum communication (Christandl and Wehner, 2005), secret sharing (Cleve, Gottesman, and Lo, 1999; Hillery, Bužek, and Berthiaume, 1999), and simple leader election (Ambainis *et al.*, 2004); and some protocols for clock synchronization (Komar *et al.*, 2014).

In the fifth stage, *few-qubit fault-tolerant networks* are built. Here the end nodes can perform local quantum operations fault tolerantly on a few logical qubits. This ability allows more complex protocols to be executed. More concretely an

end node can perform a fault-tolerant execution of a universal gate set on  $q$  logical qubits such that the number  $q \geq 1$  is small enough that the local quantum processors can still be simulated efficiently by a conventional computer. Since conventional computing power tends to increase exponentially with time, which value of  $q$  remains simulatable is a function of time and technology. This functionality enables the implementation of a distributed quantum computer by linking the end nodes.

In the sixth and final stage, *quantum-computing networks* are built and large-scale fault-tolerant quantum computation can be performed. The end node can perform large-scale quantum computation that cannot be simulated efficiently by any conventional computer. This will be the ultimate quantum internet. With this functionality it is possible to implement protocols for leader election (Tani, Kobayashi, and Matsumoto, 2005), fast Byzantine agreement (Ben-Or and Hassidim, 2005), quantum money (Gavinsky, 2012), and weak coin flipping with arbitrarily small bias (Mochon, 2007; Chailloux and Kerenidis, 2009).

We end the recap of the stages by noting that the placement of the tasks in a stage given by Wehner, Elkouss, and Hanson (2018) corresponds to the current theoretical state of the art. Future protocol proposals might allow one to reduce the requirements to implement a given task. For a more thorough description of existing protocols and their relation to the development stages, investigate the quantum protocol zoo (Quantum Protocol Zoo, 2019).

## B. Quantum networks

### 1. Elements of a quantum network

The Internet connects user devices that we call end systems or hosts. These devices are linked by communication channels to other nodes in the network. However, the hosts are not directly linked. Instead, they are connected via intermediate devices that are called routers. Routers in the Internet receive packets of information on incoming links and, depending on the content of the packet, forward it through one outgoing link. Devices situated in a communication link that passively amplifies the signal and does not take routing decisions are called relays.

Similarly, a quantum network (Van Meter, 2014) connects end systems linked by quantum channels. Intermediate nodes in quantum networks, in addition to taking routing decisions, participate in the generation of long-distance entanglement. The responsibilities associated with entanglement generation depend on the technology; see Sec. III.B. They might include generating entanglement with adjacent nodes, implementing a purification protocol, swapping entanglement, or processing encoded quantum information. Moreover, quantum networks will also require classical nodes and links for their operation.

In this review, we have used the term quantum repeaters to denote all intermediate nodes in a quantum network. However, it is possible to make a finer classification. In analogy with classical networks, Munro *et al.* (2022) differentiated between quantum relays and quantum repeaters depending on whether they processed quantum information passively or actively. Another distinction can be made, depending on whether or not

the intermediate nodes participate in network management and decide how to swap entanglement. The former are called quantum routers and the latter are referred to as automated quantum nodes (Dahlberg *et al.*, 2019; Kozlowski *et al.*, 2020).

## 2. Network architecture

The Internet provides an information-transmission service to the end systems. To implement this service, most communication networks rely on a layered approach. Each layer of the so-called network stack uses the service from the layer below without requiring any knowledge about how it is implemented or what hardware components it relies upon and provides a more complex service to the layer above.

*A priori* the main service of the quantum internet will be the delivery of remote bipartite entanglement, which can then be used as a resource for applications (Van Meter, 2014). Other proposals posit that the delivery of graph states will be the fundamental primitive of the quantum internet (Pirker and Dür, 2019). Independently of the main service, for the quantum internet we can expect a layered architecture similar to that of the Internet (Van Meter *et al.*, 2009; Van Meter and Touch, 2013; Dahlberg *et al.*, 2019; Pirker and Dür, 2019; Cacciapuoti *et al.*, 2020; Kozlowski, Dahlberg, and Wehner, 2020; Kozlowski *et al.*, 2020); see Illiano *et al.* (2022) for a survey on protocol stack proposals. Recently Pompili *et al.* (2022) experimentally demonstrated entanglement delivery using a network stack.

The quantum internet architecture will not be independent of the Internet since it is clear that the quantum internet will rely on classical communication for its functionality. However, the quantum internet could also support the functionality of the classical Internet, thereby creating a complex interplay (Cacciapuoti *et al.*, 2022).

## C. The fundamental limits of communications over network

In the following we discuss the usefulness of quantum networks from an information-theoretic point of view. First, we introduce a model of a network in terms of a graph and the relevant notation. We then define the quantities that characterize the fundamental limits for communicating over quantum networks, i.e., the quantum network capacities. In the network setting there is a richer set of quantities than with direct transmission, depending, for instance, on how the communication rates are defined or whether several sets of users concurrently want to perform a communications task.

Second, we show how to bound the network capacities both from above and from below. These bounds take a particularly simple form in some relevant cases, for instance, for general linear networks (Pirandola, 2019) or for bounding the performance of DLCZ-like protocols (like the one in Sec. III.A.3) in the presence of noisy memories (Azuma, Mizutani, and Lo, 2016). We end by discussing the computability of these bounds and show that, given bounds on the individual channel capacities, the bounds on the network capacities can be efficiently derived.

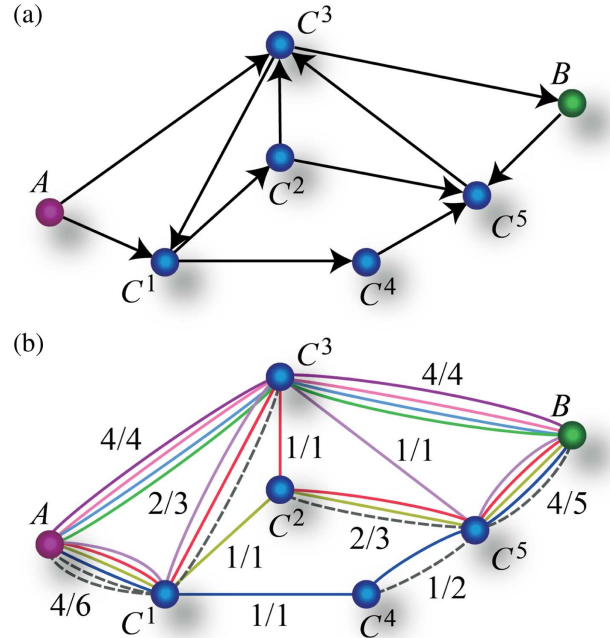


FIG. 21. Quantum and Bell-pair networks. (a) A quantum network as a graph. A quantum network can be abstracted using a directed graph  $G = (V, E)$ , with  $V$  and  $E$  the sets of vertices and edges. We associate with each vertex  $v \in V$  a node in the quantum network, and with each edge  $e \in E$  a quantum channel  $\mathcal{N}_e$ . In this example, Alice's node  $A$  and Bob's node  $B$  are part of a network with seven nodes that also include the intermediary nodes  $C^1, C^2, C^3, C^4$ , and  $C^5$ . (b) A network of maximally entangled states. One approach to entanglement distribution between distant parties in a quantum network is the aggregated repeater protocol (Azuma and Kato, 2017). In this protocol, adjacent nodes prepare maximally entangled states that can then be transformed into end-to-end entanglement between two distant parties by swapping the entanglement. The quantum network in (a) has been used to generate entanglement between adjacent nodes. Each edge is annotated with a fraction  $x/y$ , where the denominator  $y$  denotes the number of entangled pairs, while the numerator  $x$  denotes the number of entangled states used to establish entanglement between the end parties  $A$  and  $B$ . In this example, the minimum cut  $\Delta(\mathcal{V})$  over  $y$  is given for the choice of  $\mathcal{V} = \{A, C_1, C_3\} \subset V_{A:B}$ , and a total of eight Bell pairs could be distributed between  $A$  and  $B$ . Adapted from Azuma and Kato, 2017.

### 1. An abstract depiction of networks

Like classical networks, quantum networks consist of many different components: end nodes, communication channels, routers, switches, multiplexers, etc. However, for analysis purposes it is more convenient to restrict networks to two different components: nodes and communication channels.

We can represent this abstract network by  $\mathcal{G} = (G, g)$ , where  $G = (V, E)$  is a directed graph [see Fig. 21(a)] and  $g$  is a map from edges in the graph to quantum channels, i.e., CPTP maps.

We denote by  $V$  the set of nodes in the graph and by  $E$  the set of edges. Letting  $e \in E$  be a directed edge from node  $u$  to

node  $v$ , we say that the tail and head of the directed edge  $e$  are  $u$  and  $v$ , respectively. We denote the edge by  $uv$  whenever it is useful to specify the tail and head of the edge.

We associate with each node  $v \in V$  a quantum information processing device. The capabilities of the quantum information processing devices sitting at network nodes can range from a source that can prepare a predefined set of quantum states to a fully fledged universal quantum computer. For the rest of the section, we assume that nodes can perform noiselessly arbitrary local operations (LOs). Since classical communication is qualitatively cheaper than quantum communication, it is common to assume free classical communication between nodes connected by a quantum channel, and sometimes between any two nodes in the network. With this additional assumption, the nodes in the network can implement LOCC without cost.

Finally, we associate with each edge  $uv$  a quantum channel that receives a quantum system as the input from node  $u$  and outputs a quantum system to node  $v$  via the map:  $g(uv) = \mathcal{N}_{u \rightarrow v}$ . To simplify the notation, when possible we denote the channel at edge  $e$  by  $\mathcal{N}_e$ .

This abstract depiction of a network as a graph allows us to leverage tools from graph and network theory. One concept that is useful in the following is a cut. Given a bipartition of the vertex set  $V$ , i.e., two sets  $V' \subset V$  and  $V'' = V \setminus V'$ , the associated cut set or cut  $\Delta(V')$  is the set of edges connecting  $V'$  with  $V''$ . In particular, the cut associated with  $V'$  is given by

$$\Delta(V') := \Delta^+(V') \cup \Delta^-(V'), \quad (39)$$

with the outcut  $\Delta^+(V')$  associated with  $V'$ ,

$$\Delta^+(V') := \{uv \in E : u \in V', v \in V \setminus V'\}, \quad (40)$$

and with the incut  $\Delta^-(V')$  associated with  $V'$ ,

$$\Delta^-(V') := \{uv \in E : u \in V \setminus V', v \in V'\}. \quad (41)$$

Given two different vertices  $A, B \in V$ , we denote by  $V_{A;B}$  the set of all bipartitions of  $V$  separating  $A$  and  $B$ , i.e., the set of all the subsets of  $V$  that include node  $A$  but not node  $B$ .

## 2. Quantum network capacities

While the applications of the quantum internet are much different, most of them can be implemented if the relevant nodes in the network share an appropriate entangled state. For instance, to transmit a  $d$ -dimensional quantum state, it is sufficient to distribute a  $d$ -dimensional bipartite maximally entangled state,

$$|\Phi_d\rangle \equiv \frac{1}{\sqrt{d}} \sum_{i=1}^d |ii\rangle, \quad (42)$$

called an edit (called an ebit when  $d = 2$ ), which then can be consumed to teleport the desired state; see Sec. III.A.1.

Similarly, to secretly transmit a message from a set of  $d$  possible messages, it suffices to distribute a  $d$ -dimensional bipartite private state (Horodecki *et al.*, 2005) or pdit (called a pbit when  $d = 2$ ). The family of private states consists of the

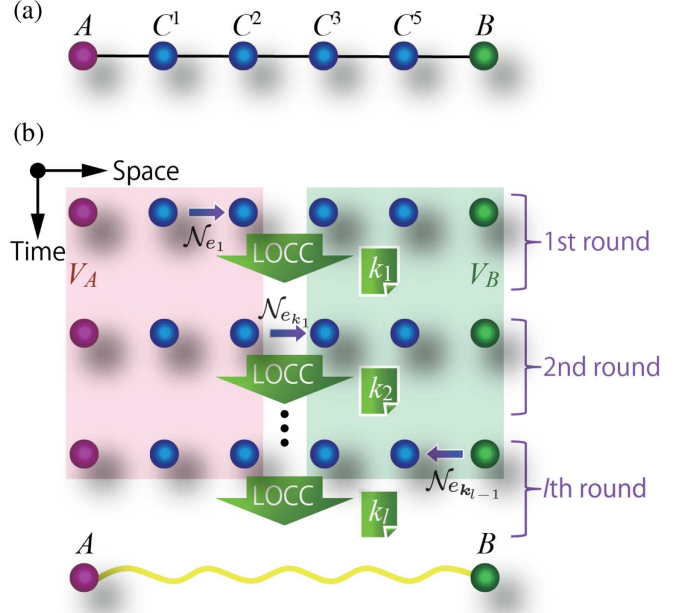


FIG. 22. Linear network and general protocol. (a) A repeater chain or linear quantum network is associated with a linear graph, i.e., a graph that can be described by a sequence of edges connecting distinct nodes. The linear network in the panel may be a subnetwork of the network shown in Fig. 21(a). (b) General adaptive protocol illustrated over the linear network in (a). The goal of the protocol is to distribute Bell pairs between  $A$  and  $B$ . The protocol begins with the network joint state represented by a separable state and proceeds iteratively until meeting a termination condition. On each round a node transmits a local subsystem through a quantum channel. All nodes then perform an LOCC operation. The LOCC operation, the choice of channel, and the transmitted subsystem can depend on the history of the measurement outcomes [such as  $k_1$  and  $k_2$  in (b)] of the protocol. The nodes of the linear network can be divided into two disjoint virtual nodes:  $V_A$  [nodes in the left (pink) box] including  $A$  and  $V_B$  [nodes in the right (green) box] including  $B$ . The intuition behind the capacity upper bounds in Eqs. (47) and (49) is that distributing entanglement between these two virtual nodes is an easier task than distributing entanglement between  $A$  and  $B$  over the network. Adapted from Azuma, Mizutani, and Lo, 2016.

states that can be used to generate a  $d$ -dimensional secret key, i.e., a uniform probability distribution over  $d$  values shared between two honest parties Alice and Bob and secret to any other user. The class of private states includes the class of maximally entangled states but is strictly larger. In fact, there are states that cannot be distilled into a maximally entangled state but nonetheless can be used to distill a pdit (Horodecki *et al.*, 2005).

Formally, a pdit is a state shared between Alice, who holds the systems  $a_1 a_2$ , and Bob, who holds  $b_1 b_2$ , in the following form:

$$\gamma_d \equiv U_{\text{twist}}(|\Phi_d\rangle\langle\Phi_d|_{a_1 b_1} \otimes \sigma_{a_2 b_2}) U_{\text{twist}}^\dagger, \quad (43)$$

where  $\sigma_{a_2 b_2}$  is an arbitrary bipartite state and  $U_{\text{twist}} = \sum_{i=1}^d |ij\rangle\langle ij|_{a_1 b_1} \otimes U_{a_2 b_2}^{(ij)}$  is a so-called twisting controlled

unitary: the systems  $a_1b_1$  control the application of  $U_{a_2b_2}^{(ij)}$ , arbitrary unitary operators on the systems  $a_2b_2$ .

GHZ states and multipartite private states (Augusiak and Horodecki, 2009) play a similar role as a resource for multiuser tasks such as secret sharing and conference key agreement. Hence, to study the usefulness of a quantum network for a given application, it suffices to study the rate at which the network can produce the desired resource state. In fact for many tasks of interest both problems are equivalent.

For simplicity, we restrict the following discussion to bipartite target states, which we denote by  $\theta_{AB}^{(d)}$ . Typically the target state is a maximally entangled state or a private state:  $\theta_{AB}^{(d)} = |\Phi_d\rangle\langle\Phi_d|_{AB}$  or  $\theta_{AB}^{(d)} = \gamma_d$ .

As mentioned, we assume that the nodes can noiselessly apply any LOCC operation. We now discuss a general protocol for distributing entanglement in a quantum network between nodes  $A$  and  $B$ ; see Fig. 22. Before the protocol, there is no entanglement between different nodes in the network. Therefore, the joint state is represented by a separable state as in Eq. (19). Iteratively, first a node transmits a local subsystem through a quantum channel and then all nodes perform an LOCC operation. The LOCC operation, the choice of a channel, and the transmitted subsystem can depend on the history of the protocol, for instance, on the measurement outcomes obtained through LOCC in previous rounds.

We denote the reduced state between  $A$  and  $B$  at the end of the protocol by  $\sigma_{AB}$ . It will be within a trace distance  $\epsilon(\geq 0)$  from a target state  $\theta_{AB}^{(d)}$ , i.e.,  $\|\sigma_{AB} - \theta_{AB}^{(d)}\|_1 \leq \epsilon$ , where  $\|X\|_1 = \text{Tr}(\sqrt{X^\dagger X})$ . We say that a protocol is a  $P_{\{n_e\}_{e \in E, e}}$  adaptive protocol if the average number of uses of channel  $\mathcal{N}_e$  is upper bounded by  $n_e$  for all edges and the protocol produces a state at most at a distance  $\epsilon$  from a target state  $\theta_{AB}^{(d)}$ , where  $d(\geq 1)$  can depend on the outcome of the protocol.

The figure of merit of  $P_{\{n_e\}_{e \in E, e}}$  protocols is the average amount of the target entanglement produced, which is quantified by  $\log_2 d$  for the mentioned states. From an operational point of view, a  $d$ -dimensional maximally entangled state or private state enables, respectively, the transmission of  $\log_2 d$  qubits or the private communication of  $\log_2 d$  bits. We denote the average entanglement produced (it might vary from round to round) by  $\langle \log_2 d \rangle$ .

We obtain the rate by dividing the average entanglement (produced by the protocol) by the appropriate quantity of resources used; as this quantity, in contrast with the single channel case, one can consider several metrics: the number of channels used, the number of full uses of the network, or the number of times a path of channels connecting  $A$  with  $B$  was used. These metrics could be related to time, which is for engineering purposes a more convenient figure of merit; see Azuma and Kato (2017), Bäuml *et al.* (2020), and Azuma *et al.* (2021) for details.

The capacity of the quantum network is the optimal asymptotic rate for producing a target entangled state  $\theta$  at which the error parameter  $\epsilon$  can be made arbitrarily small. Following our previous discussion on the rate, each choice of rates gives rise to a different type of network capacity.

We denote by  $n = \sum_e n_e$  an upper bound on the total number of channel uses and by  $p_e = n_e/n$  the frequency that the protocol uses channel  $\mathcal{N}_e$ . Given a fixed set of frequencies,

we define the capacity per channel use (Azuma, Mizutani, and Lo, 2016) as

$$C_c^\theta(\mathcal{G}, \{p_e\}_{e \in E}) = \lim_{\epsilon \rightarrow 0} \lim_{n \rightarrow \infty} \frac{1}{n} \sup_{P_{\{n_e\}_{e \in E, e}}} \langle \log_2 d \rangle. \quad (44)$$

Depending on the network scenario, the usage frequencies of the channels in the network can be free parameters. In this case, Eq. (44) can be maximized over the set  $\{p_e\}_{e \in E}$  of frequencies to give a unique network capacity per channel use (Bäuml *et al.*, 2020),

$$C_c^\theta(\mathcal{G}) = \max_{p_e \geq 0, \sum_e p_e = 1} C_c^\theta(\mathcal{G}, \{p_e\}_{e \in E}). \quad (45)$$

To capture the capacity per network use, which we denote by  $C_n^\theta(\mathcal{G})$ , we let all upper bounds on the average number of channel uses be equal ( $n_e = n_{e'} \forall e, e' \in E$ ), and we let  $m$  denote the number of network uses; i.e., we let  $m = n_e$ , which then implies  $C_n^\theta(\mathcal{G}) = |E|C_c^\theta(\mathcal{G}, \{p_e = 1/|E|\}_{e \in E})$  (because  $n = |E|m$ ). This quantity corresponds to the notion introduced by Pirandola (2019) to capture the limits of so-called flooding protocols. A third important scenario is to be able to use only a single path among possible paths between nodes  $A$  and  $B$  (Pirandola, 2019), where the goal is to find the maximum possible rate per use of a single path, called the single-path capacity. This quantity can be obtained by maximizing  $C_n^\theta(\mathcal{P})$  over arbitrary paths  $\mathcal{P}$  in  $G$  between nodes  $A$  and  $B$ , where  $\mathcal{P} = (P, g)$  and  $g$  is the same map from edges to quantum channels as for  $\mathcal{G}$ ; see Sec. VI.C.1.

If the target state  $\theta$  is a maximally entangled state [see Eq. (42)], then each of these expressions represents a quantum capacity of the quantum network  $\mathcal{G}$ . If  $\theta$  is a private state [see Eq. (43)] it represents a private capacity.

The distribution of entanglement between a single set of users is but one of many possible measures of usefulness of a quantum network. Networks typically serve many users and one might be interested in understanding the capacity of the network for distributing entanglement to multiple sets of users. Equation (44) can be adapted to capture multiuser setups by modifying appropriately the figure of merit of the protocol  $\langle \log_2 d \rangle$  and the definition of  $P_{\{n_e\}_{e \in E, e}}$  protocol (Bäuml *et al.*, 2020). For instance, given  $m$  sets of users and letting  $\langle \log_2 d^{(i)} \rangle$  be the average amount of entanglement that a  $P_{\{n_e\}_{e \in E, e}}$  protocol produces for set  $i$  of users, then the maximization of  $\min_{i=1}^m \langle \log_2 d^{(i)} \rangle$  leads to the maximum rate that can be guaranteed to all sets of users, called the worst-case network capacity, while the maximization of  $\sum_{i=1}^m \langle \log_2 d^{(i)} \rangle$  leads to the maximum total rate, which is called the total network capacity.

We end the discussion by noting that it is possible to consider more general models and capacities of a network (Townsend, 1997; Fröhlich *et al.*, 2013; Seshadreesan, Takeoka, and Wilde, 2016; Bäuml and Azuma, 2017; Laurenza and Pirandola, 2017; Takeoka, Seshadreesan, and Wilde, 2017; Bäuml, Das, and Wilde, 2018; Das, Bäuml, and Wilde, 2020). For instance, it is possible to consider multiple input and multiple output channels connecting an arbitrary number of parties (Das *et al.*, 2021).

### 3. Entanglement-based upper bounds

While in general there is no known procedure for computing these capacities, there are several tools for bounding them

both from above and from below, leveraging the relation between the communication task and the distillation of the appropriate entangled state.

In the following, we present a formulation by Rigovacca *et al.* (2018) for abstract entanglement measures. This formulation generalizes earlier work by Pirandola (2016, 2019) for quantum networks composed of a specific type of channels [called teleportation-simulable channels (discussed later)] with the relative entropy of entanglement and by Azuma, Mizutani, and Lo (2016) for arbitrary quantum networks with the squashed entanglement. In particular, these two results build, respectively, on the PLOB (Pirandola *et al.*, 2017) and TGW bounds (Takeoka, Guha, and Wilde, 2014a) on the private capacity of an individual channel; see Secs. III.A.3 and IV.

In particular, let  $\mathcal{E}$  be a measure of bipartite entanglement. That is,  $\mathcal{E}$  is a function from the set of bipartite states into the positive real numbers that satisfy several requirements (Horodecki *et al.*, 2009). In particular, it is not increasing on average under LOCC. We define the entanglement of channel  $\mathcal{N}_{A \rightarrow B}$  as

$$\mathcal{E}(\mathcal{N}_{A \rightarrow B}) \equiv \sup_{\rho_{AA'}} \mathcal{E}[\mathcal{N}_{A \rightarrow B}(\rho_{AA'})], \quad (46)$$

where  $\rho_{AA'}$  is a bipartite state between systems  $A$  and  $A'$ . We note that it is sufficient to optimize the right-hand side of Eq. (46) over pure states on  $A$  and  $A'$ . This follows from the monotonicity of entanglement measures under LOCC operations (Khatri and Wilde, 2020).

Now let  $\mathcal{E}$  be a bipartite entanglement measure that satisfies the following two inequalities:

- P1 *Continuity.* If a bipartite state  $\rho_{AB}$  is at epsilon distance from the target state  $\theta_{AB}^{(d)}$ , i.e.,  $\|\rho_{AB} - \theta_{AB}^{(d)}\|_1 \leq \epsilon$ , then  $\mathcal{E}(\rho_{AB}) \geq g(\epsilon) \log d - f(\epsilon)$ , with  $f$  and  $g$  being two real valued continuous functions that verify  $\lim_{\epsilon \rightarrow 0} f(\epsilon) = 0$  and  $\lim_{\epsilon \rightarrow 0} g(\epsilon) = 1$ .
- P2 *Subadditivity.* Given a bipartite state  $\rho_{A_1 A_2 B_1}$ , the entanglement in the  $AB$  cut after sending the system  $A_2$  through channel  $\mathcal{N}_{A \rightarrow B}$  is not larger than the original entanglement in the  $AB$  cut plus the entanglement of the channel:  $\mathcal{E}(\sigma_{A_1 B_2 B_1}) \leq \mathcal{E}(\rho_{A_1 A_2 B_1}) + \mathcal{E}(\mathcal{N}_{A \rightarrow B})$ , where  $\sigma_{A_1 B_2 B_1} = \mathcal{N}_{A_2 \rightarrow B_2}(\rho_{A_1 A_2 B_1})$ .

The capacity of the network for distributing some target state  $\theta$  (i.e., ebits or pbits) between two nodes  $A$  and  $B$  can be bounded from above by the following optimization formulas (Rigovacca *et al.*, 2018):

$$C_c^\theta(\mathcal{G}, \{p_e\}_{e \in E}) \leq \min_{\mathcal{V} \in V_{A:B}} \sum_{e \in \Delta(\mathcal{V})} p_e \mathcal{E}(\mathcal{N}_e), \quad (47)$$

$$C_c^\theta(\mathcal{G}) \leq \max_{\sum_e p_e \geq 0} \min_{\mathcal{V} \in V_{A:B}} \sum_{e \in \Delta(\mathcal{V})} p_e \mathcal{E}(\mathcal{N}_e), \quad (48)$$

$$C_n^\theta(\mathcal{G}) \leq \min_{\mathcal{V} \in V_{A:B}} \sum_{e \in \Delta(\mathcal{V})} \mathcal{E}(\mathcal{N}_e). \quad (49)$$

Note that Eqs. (47)–(49) do not depend on any functional of more than one channel: Eqs. (47) and (48) depend only on the entanglement of each of the channels individually and the channel usage frequencies, while Eq. (49) depends only on the entanglement of the channels. The minimization is

performed over  $V_{A:B}$ , the set of all cuts between  $A$  and  $B$ . The intuition for this formula is that we could join all the nodes of the network into two virtual nodes, one including  $A$  and one including  $B$ ; see Fig. 22(b). Distributing entanglement between these two virtual nodes is an easier task and can be done at a rate no larger than the entanglement of all the channels connecting the two virtual nodes. Since this argument provides a valid upper bound for any bipartition, the minimum provides the best upper bound of this form.

Note that there are several entanglement measures that verify P1 and P2 for private states (and in consequence also for maximally entangled states). In particular, the squashed entanglement (Takeoka, Guha, and Wilde, 2014a, 2014b) and the max-relative entropy of entanglement (Christandl and Müller-Hermes, 2017) satisfy both properties for arbitrary channels, while the relative entropy of entanglement is known to satisfy both properties only for a family of channels known as teleportation-simulable, Choi-simulable, or stretchable channels (Bennett, DiVincenzo *et al.*, 1996; Gottesman and Chuang, 1999; Horodecki, Horodecki, and Horodecki, 1999; Wolf, Pérez-García, and Giedke, 2007; Pirandola *et al.*, 2017).

Leveraging an inequality from Christandl and Müller-Hermes (2017), Rigovacca *et al.* (2018) proved a hybrid relative entropy upper bound, where the entanglement measure in the upper bounds in Eqs. (47)–(49) is the relative entropy of entanglement for teleportation-simulable channels and the max-relative entropy of entanglement for the other channels. Therefore, the best current option to give upper bounds in the form of Eq. (47), (48), or (49) to a given arbitrary quantum network is to use this hybrid relative-entropy bound or the squashed-entanglement bound. Many relevant channels, such as the amplitude damping channel, are not teleportation simulable. However, several channels of particular interest are teleportation simulable; this includes the depolarizing and dephasing channels, more generally mixed Pauli channels, the erasure channel, and lossy bosonic channels. For the lossy bosonic channels, which model optical fibers, the relative entropy of entanglement-based upper bound is tight (Pirandola *et al.*, 2017). In the following we define Choi-simulable channels.

A channel  $\mathcal{N}_{A \rightarrow B}$  is teleportation simulable if, given a state  $\rho_A$  that one wants to transmit through channel  $\mathcal{N}_{A \rightarrow B}$  and the Choi state of the channel  $\Gamma_{A'B} = \mathcal{N}_{A \rightarrow B}(|\Phi_d\rangle\langle\Phi_d|_{A'A})$ , there is an LOCC protocol  $\Lambda$  that simulates the action of the channel on any input state  $\rho_A$ ,

$$\mathcal{N}_{A \rightarrow B}(\rho_A) = \Lambda(\Gamma_{A'B} \otimes \rho_{A''}). \quad (50)$$

To gain intuition about Eq. (50), one can think of the identity channel from  $A$  to  $B$ . Since  $\Gamma_{A'B}$  is then an edit, the simulation can be obtained by teleportation; i.e.,  $\Lambda$  consists of a joint generalized Bell measurement on systems  $A'A''$  and applying the appropriate correction to system  $B$ . More generally, this strategy works for any channel whose action commutes with the receiver's corrections of quantum teleportation (Bennett *et al.*, 1993) because, in this case, the correction to system  $B$  can be regarded as a correction for system  $A$  before entering the channel  $\mathcal{N}_{A \rightarrow B}$ . Thus, this is merely a local teleportation to send a quantum state  $\rho_{A''}$  to system  $A$ .

#### 4. Application of the upper bounds to linear networks

In the following we focus on a particular use case: linear networks; see Fig. 22. This use case of the upper bounds is of particular relevance to quantum repeater protocols. In this case, the cut sets are the individual channels, highly simplifying the upper bounds. The bounds on the capacities per channel (47), (48) and, per network, (49) take the form

$$C_c^\theta(\mathcal{G}, \{p_e\}_{e \in E}) \leq \min_{e \in E} p_e \mathcal{E}(\mathcal{N}_e), \quad (51)$$

$$C_c^\theta(\mathcal{G}) \leq \frac{1}{\sum_{e \in E} [\mathcal{E}(\mathcal{N}_e)]^{-1}}, \quad (52)$$

$$C_n^\theta(\mathcal{G}) \leq \min_{e \in E} \mathcal{E}(\mathcal{N}_e). \quad (53)$$

The upper bound on the network capacity per channel use (52) was derived by [Azuma, Mizutani, and Lo \(2016\)](#).

As a first example, we consider a linear network connected by lossy bosonic channels. For these channels, the choice of the relative entropy of entanglement (i.e.,  $\mathcal{E} = E_R$ ) gives tight bounds. In particular, it was shown by [Pirandola \*et al.\* \(2017\)](#) that  $E_R(\mathcal{N}_e) = -\log_2(1 - \eta_e)$ , where  $\eta_e$  is the transmittance of the lossy bosonic channel  $\mathcal{N}_e$  of Eq. (13). If we then insert this relation into Eqs. (51)–(53), we obtain the following expressions for the capacities of the network:

$$C_c^\theta(\mathcal{G}, \{p_e\}_{e \in E}) = \min_{e \in E} -p_e \log_2(1 - \eta_e), \quad (54)$$

$$C_c^\theta(\mathcal{G}) = \frac{1}{\sum_{e \in E} [-\log_2(1 - \eta_e)]^{-1}}, \quad (55)$$

$$C_n^\theta(\mathcal{G}) = \min_{e \in E} [-\log_2(1 - \eta_e)], \quad (56)$$

where Eq. (56) was derived by [Pirandola \(2019\)](#).

As a second example, we consider the performance of a DLCZ-type quantum repeater protocol (like the one in Sec. III.A.3) ([Duan \*et al.\*, 2001](#)) where the memory in the nodes is subject to decoherence and taking into account the time required to exchange classical communication between distant nodes. [Razavi \*et al.\* \(2009\)](#) noticed that, in contrast to the polynomial scaling with the total distance  $L$  predicted by the DLCZ protocol, the performance with finite coherence times of quantum memories degrades exponentially with  $\sqrt{L}$ . [Azuma, Mizutani, and Lo \(2016\)](#) strengthened the results and showed that polynomial scalings for a large class of DLCZ-type protocols could be possible only above a threshold coherence time. In particular, the performance of any DLCZ-type repeater scheme with a memory coherence time below  $1.0 \times 10^{-4}$  s is upper bounded by an exponential on the square root of the total distance, irrespective of how many repeater nodes are available; see Fig. 23. This kind of performance is achievable as described in Sec. IV. The key idea to apply upper bound (52) is that the memory noise can be modeled by a noisy quantum channel between the memory at the time when it stores a state and the memory at the moment that it releases the state for probabilistic entanglement swapping. In consequence, the performance of any protocol using the noisy memory is bounded by the performance of an induced linear network [i.e., by using Eq. (52)].

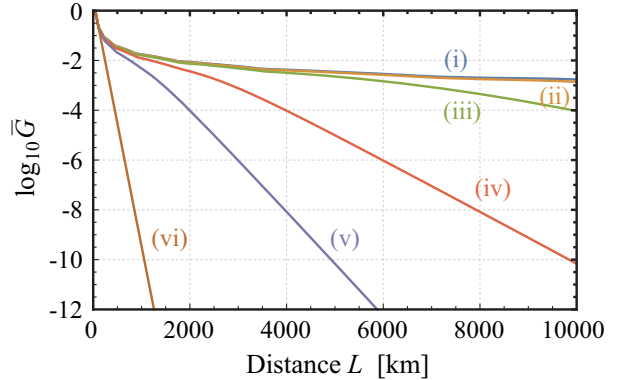


FIG. 23. Upper bound on the secret key rate achievable with a noisy linear network. In particular, the upper bound applies to a wide range of protocols that includes DLCZ ([Duan \*et al.\*, 2001](#)) and others ([Kok, Williams, and Dowling, 2003](#); [Sangouard \*et al.\*, 2011](#); [Azuma \*et al.\*, 2012](#)) when implemented with matter quantum memories in the presence of dephasing noise. The linear network consists of a chain of repeaters equally separated and connected by an optical fiber with attenuation length 22 km and spanning a total distance of  $L$  (km). The coupling efficiency to an optical fiber is assumed to be 90%. In the calculation, the number of repeater nodes is optimized. The curves labeled (i)–(vi), respectively, correspond with the following coherence times:  $1.0 \times 10^{-2}$ ,  $5.0 \times 10^{-3}$ ,  $2.5 \times 10^{-3}$ ,  $1.0 \times 10^{-3}$ ,  $5.0 \times 10^{-4}$ , and  $1.0 \times 10^{-4}$  s. The upper bound in (vi) scales better than direct transmission and is roughly proportional to the square root of the PLOB bound but equivalent to the intercity QKD protocols in Sec. IV. In consequence, with a coherence time of  $1.0 \times 10^{-4}$  s there can be no advantage for a DLCZ-type repeater scheme over the simpler intercity QKD protocols. From [Azuma, Mizutani, and Lo, 2016](#).

#### 5. Capacity lower bounds via the aggregated repeater protocol

We now look at a general lower bound on the capacity of quantum networks ([Azuma and Kato, 2017](#)). This lower bound, based on the aggregated quantum repeater protocol, matches the general upper bounds given in Eqs. (47) and (49) up to a prefactor. Moreover, the aggregation even of existing protocols ([Duan \*et al.\*, 2001](#); [Jiang \*et al.\*, 2009](#); [Sangouard \*et al.\*, 2011](#); [Li \*et al.\*, 2013](#); [Mazurek \*et al.\*, 2014](#)) matches the lower bound on the capacity up to another prefactor for the case of optical quantum networks composed of lossy bosonic channels. This implies that the upper bounds have no scaling gap and yield good measures of the usefulness of a network. We note that while we have exemplified the upper bounds with a linear network of repeaters in Sec. VI.C.4, they can be applied to any quantum network with an arbitrary topology, including distributed quantum computation setups.

In the following, we discuss the lower bound that corresponds to the achievable rate of the aggregated quantum repeater protocol introduced by [Azuma and Kato \(2017\)](#); see Fig. 21(b). The goal of this protocol is to distribute entanglement between targeted nodes in the network that is later consumed to perform the appropriate communications task.

For each of the quantum channels in a given quantum network, we consider a protocol that produces entangled states that are  $\epsilon$  close to a maximally entangled state at a rate  $R_e$  that can be different for each channel. This is possible for all

channels provided that  $R_e < Q(\mathcal{N}_e)$ , i.e., provided that the rate is below the maximal rate of the channel for distributing maximally entangled states for a large enough number of channel uses (called the quantum capacity of the channel  $\mathcal{N}_e$ ). If each of the channels is used  $n_e$  times, the entire network will be in a tensor product of entangled states and the entire network can then be regarded as a multigraph with  $n_e R_e$  edges per edge in the original graph, where each edge in the multigraph corresponds to a qubit maximally entangled state  $|\Phi_2\rangle$ .

We can use the resulting state to create maximally entangled states between Alice at node  $A$  and Bob at node  $B$ . For each state it is necessary to perform entanglement swapping over a path of maximally entangled states connecting Alice with Bob. The number of maximally entangled states that can be distributed between Alice and Bob is then equivalent to the maximum number of edge disjoint paths connecting Alice with Bob in the multigraph. This maximum number of paths is by Menger's theorem (Jungnickel, 2005) equivalent to the value of the minimum cut of the graph:

$$M = \min_{\mathcal{V} \in V_{A,B}} \sum_{e \in \Delta(\mathcal{V})} n_e R_e. \quad (57)$$

This minimization can be solved in time proportional to a polynomial in the number of edges. However, since the number of edges grows with the number of uses, the full optimization is *a priori* intractable. If we consider the achievable rate per channel use with the aggregated repeater protocol, Eq. (57) becomes  $\min_{\mathcal{V} \in V_{A,B}} \sum_{e \in \Delta(\mathcal{V})} (n_e/n) R_e$ . Moreover, for a number of uses  $n$  large enough, any rate below the capacity of each channel is achievable. Consequently, the right-hand side of the following expression is achievable:

$$C_c^\theta(\mathcal{G}, \{p_e\}_{e \in E}) \geq \min_{\mathcal{V} \in V_{A,B}} \sum_{e \in \Delta(\mathcal{V})} p_e Q(\mathcal{N}_e), \quad (58)$$

$$C_c^\theta(\mathcal{G}) \geq \max_{\sum_e p_e = 1} \min_{\mathcal{V} \in V_{A,B}} \sum_{e \in \Delta(\mathcal{V})} p_e Q(\mathcal{N}_e), \quad (59)$$

$$C_n^\theta(\mathcal{G}) \geq \min_{\mathcal{V} \in V_{A,B}} \sum_{e \in \Delta(\mathcal{V})} Q(\mathcal{N}_e), \quad (60)$$

where  $p_e = n_e/n$ . We note that the lower bounds are of the same form as the respective upper bounds in Eqs. (47)–(49), where the entanglement of the channel is replaced by the quantum capacity. Therefore, if  $\mathcal{E}(\mathcal{N}_e) = Q(\mathcal{N}_e)$  holds for any  $e$ , these lower bounds (58), (59), and (60) coincide with upper bounds (47), (48), and (49). This is indeed the case for quantum networks composed only of lossy bosonic channels.

The aggregation of quantum repeaters is also possible while minimizing cost (Azuma, 2023). The cost here is a general notion like a price to pay for presenting ebits between two targeted nodes in a quantum network.

## 6. Computability of the network capacities

We now discuss how to compute both the lower and upper bounds in Eqs. (47)–(49) and (58)–(60). This is indeed important in practice, for instance, to determine how a network provider should distribute entanglement to clients according to their requests. All six equations depend only on the values of the entanglement of the individual channels.

Equations (47), (49), (58), and (60) are expressed as the solution of the minimum cut over an undirected graph, while Eqs. (48) and (59) maximize the minimum cut over all possible edge distributions. All of these optimization problems, including the latter cases (Bäuml *et al.*, 2020), can be solved by a linear program in time polynomial in the number of nodes in the graph (Jungnickel, 2005). Similar arguments allow one to find efficiently lower and upper bounds not only on the previously described capacities for two-party communication but also on the worst-case and total quantum network capacities (see Sec. VI.C.2) and for distributing GHZ states (Bäuml *et al.*, 2020).

## VII. CONCLUDING REMARKS

The quantum internet will have important applications in sensor networks, upscaling quantum computing and secure quantum communication (Awschalom, 2020). To build the quantum internet, quantum repeaters have been proposed and extensively studied. This review has focused on the various generations of quantum repeaters as well as all-photonic quantum repeaters; we have seen that quantum repeaters are essential for realizing an efficient quantum internet. Nonetheless, our discussion has been largely limited to a fiber-optical setting connecting two end nodes Alice and Bob.

In this concluding section, we take a step back to think more about how to build a quantum internet. We discuss a few alternative designs and important issues facing the quantum internet: not only its efficiency but also its cost and the uncertainty in the technology it would leverage.

Cost can be a critical issue in realizing any technology. Although the conventional Internet is believed to contribute trillions of U.S. dollars each year to the U.S. economy, simply upgrading the existing fiber-optical network in the U.S. to cover many, say, 90%, of the households there would take an additional investment of over  $10^{11}$  U.S. dollars; see (Cartesian, 2021). This figure is for a single country and for an upgrade to the existing, extensively developed Internet. Therefore, it is reasonable to predict that the construction and operation of a global quantum internet would ultimately take decades and require investments of trillions of U.S. dollars. This is an astonishing number. Such an enormous investment would almost certainly come not only from governments but also from for-profit commercial corporations. For a comparison, the LIGO and LHC projects (endeavors admittedly more localized in scope) required only  $1.1 \times 10^9$  and  $4.75 \times 10^9$  dollars, respectively (Horgan, 2016; Roche, 2022). We have not even begun to estimate the cost of building various generations of quantum repeater structures on a global scale. Some detailed calculations, aided by a quantum network simulator, would be needed to address the cost issue more seriously.

In addition, as mentioned in Sec. I, the Internet consumes a lot of energy through the transmission of optical signals. Furthermore, the sensing, monitoring, and routing of the Internet require tremendous amounts of local computational power. As the Internet grows, scalability becomes a challenge. A quantum internet could operate at the single-photon level. It may well be interesting to explore whether a quantum internet could lead to large savings in energy consumption. Similarly, it may be worthwhile to investigate whether quantum computing and quantum information processing could contribute to the management of the Internet.

Next we imagine a world (sometime in the distant future) where quantum memories with long-term stability become widely available at low cost. In this case, to distribute entanglement one could simply ship those stable quantum memories all over the world, physically, in the same way that we currently dispatch hard drives and mail; see [Devitt \*et al.\* \(2016\)](#). The apparent drawback would be latency, which refers to the delay before a transfer of data begins following an instruction for its transfer; however, this shipment could be done off line, and entanglement swapping could be used to connect users via intermediate nodes instantaneously in the same way that a telephone network can connect the users. In this way, the latency issue could be alleviated. With the physical shipment of quantum memory devices, the requirements of quantum repeaters could be reduced. This is just one way in which our design of the quantum internet is highly dependent on the available technology, in addition to the cost.

Currently quantum memories often operate at cryogenic temperatures and their lifetimes are often limited. If this is the case, quantum repeater nodes will need refrigerators. Notice that all-photonic quantum repeaters may also require refrigerators (in either photonic graph-state generation devices or measurement devices). Suppose that we wanted to connect someone in New York with another person in Tokyo (10 845 km away) through undersea optical fibers. Optimistically, we would then need to place a quantum repeater node every few hundred kilometers under the sea. In this case, hundreds of repeater nodes would be needed. Placing cryogenic repeater nodes in undersea optical fibers, maintaining them, and providing the energy to operate them reliably are no easy feats and would likely prove to be costly.

As an alternative solution, ground-to-satellite quantum communication is a serious candidate. By preparing an entangled source of photons in a satellite Charlie and sending photon pairs to two ground stations Alice and Bob, Charlie can act as an untrusted relay to connect two distant locations on the globe. Currently the line of sight is a serious restriction in ground-to-satellite communication. However, we can envision a future where space-grade long-lifetime quantum memories are available. By first sending one half of an entangled pair to Alice, storing the other half in the quantum memory on a rapidly moving quantum satellite, and later sending it to Bob, Charlie can connect any two ground stations that have a line of sight to any point on the satellite's orbit. Besides this, a constellation of orbiting satellites could provide a continuous, on-demand entanglement distribution service to ground stations ([Khatri \*et al.\*, 2021](#)). In principle, one could put quantum repeaters even on satellites to run a quantum repeater protocol ([Liorni, Kampermann, and Bruß, 2021](#)). However, this can be challenging if the repeaters require a cryogenic environment.

As mentioned (see Sec. [III](#)), the probabilistic nature of a Bell-state measurement in linear optics (for certain photonic encodings) is a key limiting factor in the design of both matter-based and all-photonic quantum repeaters. Indeed, without using additional ancillae or a different encoding, the success probability of a linear-optical Bell measurement is upper bounded by  $1/2$ . A game changer for the efficiency of quantum repeaters would therefore be a near-deterministic, high-fidelity entangling gate on photons. This could be based

on an enhancement by quantum memories ([Munro \*et al.\*, 2012; Bhaskar \*et al.\*, 2020; Borregaard \*et al.\*, 2020](#)).

For all-photonic repeaters, in particular, a game changer would be the deterministic generation of photonic graph states based on coupled quantum emitters such as quantum dots; see [Li, Economou, and Barnes \(2022\)](#). Alternatively, a hybrid approach with a single quantum emitter and subsequent fusions would also dramatically lower the resource requirements ([Hilaire, Vidro \*et al.\*, 2023](#)). There is another possibility for development based purely on all photonics beginning with all-photonic intercity QKD (Sec. [IV](#)), proceeding to all-photonic quantum repeaters (Sec. [III.C](#)), and ending with a linkage of fault-tolerant photonic quantum computers ([Knill, Laflamme, and Milburn, 2001](#)).

Another important area of research is the quantum interconnect; see [Awschalom \*et al.\* \(2021\)](#). Indeed, the ability to convert and transfer quantum information across different platforms will enhance the interoperability of the future quantum internet.

In this review, we have focused on the distribution of bipartite entanglement. However, for many applications, including quantum sensing, it is often advantageous to use multipartite entangled states. Conceptually we can build up multipartite states through successive teleportations. However, were we to do it with linear optics, the probabilistic nature of a Bell measurement would make the success probability of constructing an  $n$ -partite entangled state decrease exponentially with  $n$ . Therefore, there is value in further exploring the preparation and distribution of multipartite entanglement.

To conclude, we stress that a truly global quantum internet requires seamless operation across continents. As different countries are currently pursuing different approaches and strategies for the quantum internet, there will be a need for cooperation and standardization in the design, construction, and operation of this major technology.

## LIST OF SYMBOLS AND ABBREVIATIONS

BBSM	boosted Bell-state measurement
BDCZ	Briegel-Dür-Cirac-Zoller
BM	Bell measurement
BSM	Bell-state measurement
CPTP	completely positive and trace preserving
CSS	Calderbank-Shor-Steane
CV	continuous variable
DLCZ	Duan-Lukin-Cirac-Zoller
DV	discrete variable
EG	entanglement generation
ES	entanglement swapping
GHZ	Greenberger-Horne-Zeilinger
GKP	Gottesman-Kitaev-Preskill
HEGP	heralded entanglement generation protocol
LHC	Large Hadron Collider
LIGO	Laser Interferometer Gravitational-Wave Observatory
LOCC	local operations and classical communication

MBQC	measurement-based quantum computing
MDI	measurement device independent
MIT	Massachusetts Institute of Technology
NISQ	noisy intermediate scale quantum
NIST	National Institute for Standards in Technology
N-V	nitrogen vacancy
PBS	polarizing beam splitter
PLOB	Pirandola-Laurenza-Ottaviani-Banchi
PNR	photon-number-resolving detector
PRCS	phase-randomized coherent state
QD	quantum dot
QED	quantum electrodynamics
QKD	quantum key distribution
QM	quantum memory
QND	quantum non-demolition
QR	quantum repeater
RGS	repeater graph state
RSA	Rivest-Shamir-Adleman
SECOQC	secure communication based on quantum cryptography
SPD	single-photon detector
SW	(optical) switch
TF QKD	twin-field quantum key distribution
TGW	Takeoka-Guha-Wilde
ULL	ultralow loss

## ACKNOWLEDGMENTS

We thank Stefan Bäuml, Johannes Borregaard, Ronald Hanson, Tomoyuki Horikiri, Rikizo Ikuta, Jessica Illiano, Norbert Lütkenhaus, Mattia Montagna, William J. Munro, Shoichi Murakami, Fatih Ozaydin, Stefano Pirandola, John Preskill, Mohsen Razavi, Tim Taminiau, Wolfgang Tittel, Takashi Yamamoto, Qiang Zhou, and Val Zwiller for their helpful comments and suggestions on different versions of this manuscript. K. A. is thankful for the support, in part, from the CREST program of JST (Grant No. JP-MJCR1671), from the PREST program of JST (Grant No. JP-MJPR1861), from Moonshot R&D of JST (Grant No. JP-MJMS2061), from the JSPS KAKENHI program (Grant No. 21H05183 JP), and from R&D of ICT Priority Technology (Grant No. JPMI00316). S. E. E. was supported by the NSF (Grant No. 1741656), the EU Horizon 2020 program (Grant No. GA 862035 QLUSTER), and the ARO (MURI Grant No. W911NF2120214). D. E. was supported by the Netherlands Organization for Scientific Research (NWO/OCW) as part of the Quantum Software Consortium program (Project No. 024.003.037/3368), and partially supported by the JST Moonshot R&D program under Grant No. JPMJMS226C. L. J. was supported by the ARO (Grants No. W911NF-18-1-0020, No. W911NF-18-1-0212, and MURI Grant No. W911NF-16-1-0349), AFOSR (MURI Grants No. FA9550-19-1-0399 and No. FA9550-21-1-0209), U.S. DOE Q-NEXT, the NSF

(Grants No. EFMA-1640959, No. OMA-1936118, and No. EEC-1941583), NTT Research, and the Packard Foundation (2013-39273). H.-K. L. was supported by NSERC, Connaught Innovation, CFI, ORF, Mitacs Accelerate, Huawei Canada, Royal Bank of Canada (RBC), a start-up grant from the University of Hong Kong, the U.S. Air Force, the NRC CSTIP program, and the Innovative Solutions Canada program. I. T. was supported by an Ontario Graduate Scholarship.

## REFERENCES

Abobeih, M. H., Y. Wang, J. Randall, S. J. H. Loenen, C. E. Bradley, M. Markham, D. J. Twitchen, B. M. Terhal, and T. H. Taminiau, 2022, “Fault-tolerant operation of a logical qubit in a diamond quantum processor,” *Nature (London)* **606**, 884–889.

Abobeih, Mohamed H., Julia Cramer, Michiel A. Bakker, Norbert Kalb, Matthew Markham, Daniel J. Twitchen, and Tim H. Taminiau, 2018, “One-second coherence for a single electron spin coupled to a multi-qubit nuclear-spin environment,” *Nat. Commun.* **9**, 2552.

Abruzzo, Silvestre, Hermann Kampermann, and Dagmar Bruß, 2014, “Measurement-device-independent quantum key distribution with quantum memories,” *Phys. Rev. A* **89**, 012301.

Afzelius, Mikael, Christoph Simon, Hugues de Riedmatten, and Nicolas Gisin, 2009, “Multimode quantum memory based on atomic frequency combs,” *Phys. Rev. A* **79**, 052329.

Aharonov, Dorit, Michael Ben-Or, Elad Eban, and Urmila Mahadev, 2017, “Interactive proofs for quantum computations,” *arXiv:1704.04487*.

Aharonovich, I., S. Castelletto, D. A. Simpson, C.-H. Su, A. D. Greentree, and S. Prawer, 2011, “Diamond-based single-photon emitters,” *Rep. Prog. Phys.* **74**, 076501.

Aharonovich, Igor, Dirk Englund, and Milos Toth, 2016, “Solid-state single-photon emitters,” *Nat. Photonics* **10**, 631–641.

Albert, Victor V., *et al.*, 2018, “Performance and structure of single-mode bosonic codes,” *Phys. Rev. A* **97**, 032346.

Ambainis, Andris, Harry Buhrman, Yevgeniy Dodis, and Hein Rohrig, 2004, “Multiparty quantum coin flipping,” in *Proceedings of the 19th IEEE Annual Conference on Computational Complexity, Amherst, MA, 2004* (IEEE, New York), pp. 250–259, **10.1109/CCC.2004.1313848**.

Androvitsaneas, Petros, *et al.*, 2019, “Efficient quantum photonic phase shift in a low  $Q$ -factor regime,” *ACS Photonics* **6**, 429–435.

Ang, James, *et al.*, 2022, “Architectures for multinode superconducting quantum computers,” *arXiv:2212.06167*.

Appel, Martin Hayhurst, *et al.*, 2022, “Entangling a Hole Spin with a Time-Bin Photon: A Waveguide Approach for Quantum Dot Sources of Multiphoton Entanglement,” *Phys. Rev. Lett.* **128**, 233602.

Arcari, Marta, Immo Söllner, Alisa Javadi, S. Lindskov Hansen, Sahand Mahmoodian, Jin Liu, Henri Thyrrstrup, Eun Hye Lee, Jin Dong Song, and Søren Stobbe, *et al.* 2014, “Near-Unity Coupling Efficiency of a Quantum Emitter to a Photonic Crystal Waveguide,” *Phys. Rev. Lett.* **113**, 093603.

Arnold, C., V. Loo, A. Lemaître, I. Sagnes, O. Krebs, P. Voisin, P. Senellart, and L. Lanço, 2014, “Cavity-Enhanced Real-Time Monitoring of Single-Charge Jumps at the Microsecond Time Scale,” *Phys. Rev. X* **4**, 021004.

Arroyo-Camejo, Silvia, Andrii Lazariev, Stefan W. Hell, and Gopalakrishnan Balasubramanian, 2014, “Room temperature high-fidelity holonomic single-qubit gate on a solid-state spin,” *Nat. Commun.* **5**, 4870.

Asadi, F Kimiae, S. C. Wein, and C. Simon, 2020, “Protocols for long-distance quantum communication with single  $^{167}\text{Er}$  ions,” *Quantum Sci. Technol.* **5**, 045015.

Asavanant, Warit, *et al.*, 2019, “Generation of time-domain-multiplexed two-dimensional cluster state,” *Science* **366**, 373–376.

Atatüre, Mete, Dirk Englund, Nick Vamivakas, Sang-Yun Lee, and Joerg Wrachtrup, 2018, “Material platforms for spin-based photonic quantum technologies,” *Nat. Rev. Mater.* **3**, 38–51.

Augusiak, Remigiusz, and Paweł Horodecki, 2009, “Multipartite secret key distillation and bound entanglement,” *Phys. Rev. A* **80**, 042307.

Awschalom, David, 2020, “From long-distance entanglement to building a nationwide quantum internet: Report of the DOE Quantum Internet Blueprint workshop,” Brookhaven National Laboratory Technical Report No. BNL-216179-2020-FORE, 10.2172/1638794.

Awschalom, David, *et al.*, 2021, “Development of quantum interconnects (QuICs) for next-generation information technologies,” *PRX Quantum* **2**, 017002.

Awschalom, David D., Ronald Hanson, Jörg Wrachtrup, and Brian B. Zhou, 2018, “Quantum technologies with optically interfaced solid-state spins,” *Nat. Photonics* **12**, 516–527.

Azuma, Koji, 2023, “Networking quantum networks with minimum cost aggregation,” *arXiv:2304.08921*.

Azuma, Koji, Stefan Bäuml, Tim Coopmans, David Elkouss, and Boxi Li, 2021, “Tools for quantum network design,” *AVS Quantum Sci.* **3**, 014101.

Azuma, Koji, Nobuyuki Imoto, and Masato Koashi, 2022, “Optimal supplier of single-error-type entanglement via coherent-state transmission,” *Phys. Rev. A* **105**, 062432.

Azuma, Koji, and Go Kato, 2012, “Optimal entanglement manipulation via coherent-state transmission,” *Phys. Rev. A* **85**, 060303.

Azuma, Koji, and Go Kato, 2017, “Aggregating quantum repeaters for the quantum internet,” *Phys. Rev. A* **96**, 032332.

Azuma, Koji, Akihiro Mizutani, and Hoi-kwong Lo, 2016, “Fundamental rate-loss trade-off for the quantum internet,” *Nat. Commun.* **7**, 13523.

Azuma, Koji, Naoya Sota, Masato Koashi, and Nobuyuki Imoto, 2010, “Tight bound on coherent-state-based entanglement generation over lossy channels,” *Phys. Rev. A* **81**, 022325.

Azuma, Koji, Naoya Sota, Ryo Namiki, Şahin Kaya Özdemir, Takashi Yamamoto, Masato Koashi, and Nobuyuki Imoto, 2009, “Optimal entanglement generation for efficient hybrid quantum repeaters,” *Phys. Rev. A* **80**, 060303.

Azuma, Koji, Hitoshi Takeda, Masato Koashi, and Nobuyuki Imoto, 2012, “Quantum repeaters and computation by a single module: Remote nondestructive parity measurement,” *Phys. Rev. A* **85**, 062309.

Azuma, Koji, Kiyoshi Tamaki, and Hoi-Kwong Lo, 2015, “All-photonic quantum repeaters,” *Nat. Commun.* **6**, 6787.

Azuma, Koji, Kiyoshi Tamaki, and William J. Munro, 2015, “All-photonic intercity quantum key distribution,” *Nat. Commun.* **6**, 10171.

Bacco, Davide, Jacob F. F. Bulmer, Manuel Erhard, Marcus Huber, and Stefano Paesani, 2021, “Proposal for practical multidimensional quantum networks,” *Phys. Rev. A* **104**, 052618.

Bacon, Dave, 2006, “Operator quantum error-correcting subsystems for self-correcting quantum memories,” *Phys. Rev. A* **73**, 012340.

Balasubramanian, Gopalakrishnan, *et al.*, 2009, “Ulralong spin coherence time in isotopically engineered diamond,” *Nat. Mater.* **8**, 383–387.

Bar-Gill, Nir, Linh M. Pham, Andrejs Jarmola, Dmitry Budker, and Ronald L. Walsworth, 2013, “Solid-state electronic spin coherence time approaching one second,” *Nat. Commun.* **4**, 1743.

Barnum, Howard, Carlton M. Caves, Christopher A. Fuchs, Richard Jozsa, and Benjamin Schumacher, 1996, “Noncommuting Mixed States Cannot Be Broadcast,” *Phys. Rev. Lett.* **76**, 2818.

Barreiro, J. T., N. K. Langford, N. A. Peters, and P. G. Kwiat, 2005, “Generation of Hyperentangled Photon Pairs,” *Phys. Rev. Lett.* **95**, 260501.

Barrett, Jonathan, Roger Colbeck, and Adrian Kent, 2013, “Memory Attacks on Device-Independent Quantum Cryptography,” *Phys. Rev. Lett.* **110**, 010503.

Barrett, S. D., Pieter Kok, Kae Nemoto, R. G. Beausoleil, W. J. Munro, and T. P. Spiller, 2005, “Symmetry analyzer for nondestructive Bell-state detection using weak nonlinearities,” *Phys. Rev. A* **71**, 060302.

Barrett, Sean D., and Pieter Kok, 2005, “Efficient high-fidelity quantum computation using matter qubits and linear optics,” *Phys. Rev. A* **71**, 060310.

Barros, H. G., A. Stute, T. E. Northup, C. Russo, P. O. Schmidt, and R. Blatt, 2009, “Deterministic single-photon source from a single ion,” *New J. Phys.* **11**, 103004.

Bartolucci, Sara, *et al.*, 2023, “Fusion-based quantum computation,” *Nat. Commun.* **14**, 912.

Bauch, Erik, Connor A. Hart, Jennifer M. Schloss, Matthew J. Turner, John F. Barry, Pauli Kehayias, Swati Singh, and Ronald L. Walsworth, 2018, “Ulralong Dephasing Times in Solid-State Spin Ensembles via Quantum Control,” *Phys. Rev. X* **8**, 031025.

Bäuml, Stefan, and Koji Azuma, 2017, “Fundamental limitation on quantum broadcast networks,” *Quantum Sci. Technol.* **2**, 024004.

Bäuml, Stefan, Koji Azuma, Go Kato, and David Elkouss, 2020, “Linear programs for entanglement and key distribution in the quantum internet,” *Commun. Phys.* **3**, 55.

Bäuml, Stefan, Matthias Christandl, Karol Horodecki, and Andreas Winter, 2015, “Limitations on quantum key repeaters,” *Nat. Commun.* **6**, 6908.

Bäuml, Stefan, Siddhartha Das, and Mark M. Wilde, 2018, “Fundamental Limits on the Capacities of Bipartite Quantum Interactions,” *Phys. Rev. Lett.* **121**, 250504.

Bayrakci, Veysel, and Fatih Ozaydin, 2022, “Quantum zeno repeaters,” *Sci. Rep.* **12**, 15302.

Bechtold, Alexander, Dominik Rauch, Fuxiang Li, Tobias Simmet, Per-Lennart Ardel, Armin Regler, Kai Müller, Nikolai A. Sinitzyn, and Jonathan J. Finley, 2015, “Three-stage decoherence dynamics of an electron spin qubit in an optically active quantum dot,” *Nat. Phys.* **11**, 1005–1008.

Becker, Jonas N., Benjamin Pingault, David Groß, Mustafa Gündoğan, Nadezhda Kukharchyk, Matthew Markham, Andrew Edmonds, Mete Atatüre, Pavel Bushev, and Christoph Becher, 2018, “All-Optical Control of the Silicon-Vacancy Spin in Diamond at Millikelvin Temperatures,” *Phys. Rev. Lett.* **120**, 053603.

Bell, B. A., D. A. Herrera-Martí, M. S. Tame, D. Markham, W. J. Wadsworth, and J. G. Rarity, 2014, “Experimental demonstration of a graph state quantum error-correction code,” *Nat. Commun.* **5**, 3658.

Bell, J. S., 1964, “On the Einstein Podolsky Rosen paradox,” *Phys. Phys. Fiz.* **1**, 195–200.

Bell, Tom J., Love A. Pettersson, and Stefano Paesani, 2023, “Optimizing graph codes for measurement-based loss tolerance,” *PRX Quantum* **4**, 020328.

Bennett, C. H., and G. Brassard, 1984, “Quantum cryptography: Public key distribution and coin tossing,” in *Proceedings of IEEE International Conference on Computers, Systems, and Signal Processing, Bangalore, India, 1984* (IEEE, New York), pp. 175–179, [10.1109/j.tcs.2014.05.025](https://doi.org/10.1109/j.tcs.2014.05.025).

Bennett, C. H., G. Brassard, C. Crepeau, R. Jozsa, A. Peres, and W. K. Wootters, 1993, “Teleporting an Unknown Quantum State via Dual Classical and Einstein-Podolsky-Rosen Channels,” *Phys. Rev. Lett.* **70**, 1895.

Bennett, C. H., G. Brassard, S. Popescu, B. Schumacher, J. A. Smolin, and W. K. Wootters, 1996, “Purification of Noisy Entanglement and Faithful Teleportation via Noisy Channels,” *Phys. Rev. Lett.* **76**, 722–725.

Bennett, Charles H., Herbert J. Bernstein, Sandu Popescu, and Benjamin Schumacher, 1996, “Concentrating partial entanglement by local operations,” *Phys. Rev. A* **53**, 2046.

Bennett, Charles H., Gilles Brassard, and N. David Mermin, 1992, “Quantum Cryptography without Bell’s Theorem,” *Phys. Rev. Lett.* **68**, 557–559.

Bennett, Charles H., David P. DiVincenzo, and John A. Smolin, 1997, “Capacities of Quantum Erasure Channels,” *Phys. Rev. Lett.* **78**, 3217.

Bennett, Charles H., David P. DiVincenzo, John A. Smolin, and William K. Wootters, 1996, “Mixed-state entanglement and quantum error correction,” *Phys. Rev. A* **54**, 3824–3851.

Ben-Or, Michael, and Avinatan Hassidim, 2005, “Fast quantum byzantine agreement,” in *Proceedings of the Thirty-Seventh Annual ACM Symposium on Theory of Computing, Baltimore, 2005*, edited by H. Gabow and Ronald Fagin (Association for Computing Machinery, New York), pp. 481–485, [10.1145/1060590.1060662](https://doi.org/10.1145/1060590.1060662).

Benyoucef, M., M. Yacob, J.P. Reithmaier, J. Kettler, and P. Michler, 2013, “Telecom-wavelength (1.5 μm) single-photon emission from inp-based quantum dots,” *Appl. Phys. Lett.* **103**, 162101.

Bergeron, L., C. Chartrand, A. T. K. Kurkjian, K. J. Morse, H. Riemann, N. V. Abrosimov, P. Becker, H.-J. Pohl, M. L. W. Thewalt, and S. Simmons, 2020, “Silicon-integrated telecommunications photon-spin interface,” *PRX Quantum* **1**, 020301.

Bernien, Hannes, *et al.*, 2013, “Heralded entanglement between solid-state qubits separated by three metres,” *Nature (London)* **497**, 86–90.

Berry, Michael, 1998, *Introduction to Quantum Computation and Information*, edited by Hoi-Kwong Lo, Sandu Popescu, and Tim Spiller (World Scientific, Singapore).

Bersin, E., *et al.*, 2023, “Development of a Boston-area 50-km fiber quantum network testbed,” [arXiv:2307.15696](https://arxiv.org/abs/2307.15696).

Bhaskar, Mihir K., *et al.*, 2020, “Experimental demonstration of memory-enhanced quantum communication,” *Nature (London)* **580**, 60–64.

Biham, Eli, Bruno Huttner, and Tal Mor, 1996, “Quantum cryptographic network based on quantum memories,” *Phys. Rev. A* **54**, 2651.

Blinov, B. B., D. L. Moehring, L.-M. Duan, and Chris Monroe, 2004, “Observation of entanglement between a single trapped atom and a single photon,” *Nature (London)* **428**, 153–157.

Bloch, Matthieu, João Barros, Miguel R. D. Rodrigues, and Steven W. McLaughlin, 2008, “Wireless information-theoretic security,” *IEEE Trans. Inf. Theory* **54**, 2515–2534.

Boaron, Alberto, *et al.*, 2018, “Secure Quantum Key Distribution over 421 km of Optical Fiber,” *Phys. Rev. Lett.* **121**, 190502.

Bock, Matthias, Pascal Eich, Stephan Kucera, Matthias Kreis, Andreas Lenhard, Christoph Becher, and Jürgen Eschner, 2018, “High-fidelity entanglement between a trapped ion and a telecom photon via quantum frequency conversion,” *Nat. Commun.* **9**, 1998.

Bonarota, M., J. L. Le Gouët, and T. Chanelière, 2011, “Highly multimode storage in a crystal,” *New J. Phys.* **13**, 013013.

Bonneau, Damien, Gabriel J. Mendoza, Jeremy L O’Brien, and Mark G. Thompson, 2015, “Effect of loss on multiplexed single-photon sources,” *New J. Phys.* **17**, 043057.

Boone, K., J.-P. Bourgoin, E. Meyer-Scott, K. Heshami, T. Jennewein, and C. Simon, 2015, “Entanglement over global distances via quantum repeaters with satellite links,” *Phys. Rev. A* **91**, 052325.

Borregaard, J., M. Zugenmaier, J. M. Petersen, H. Shen, G. Vasilakis, K. Jensen, E. S. Polzik, and A. S. Sørensen, 2016, “Scalable photonic network architecture based on motional averaging in room temperature gas,” *Nat. Commun.* **7**, 11356.

Borregaard, Johannes, Hannes Pichler, Tim Schröder, Mikhail D. Lukin, Peter Lodahl, and Anders S. Sørensen, 2020, “One-Way Quantum Repeater Based on Near-Deterministic Photon-Emitter Interfaces,” *Phys. Rev. X* **10**, 021071.

Bose, S., P. L. Knight, M. B. Plenio, and V. Vedral, 1999, “Proposal for Teleportation of an Atomic State via Cavity Decay,” *Phys. Rev. Lett.* **83**, 5158.

Bourassa, A., *et al.*, 2020, “Entanglement and control of single nuclear spins in isotopically engineered silicon carbide,” *Nat. Mater.* **19**, 1319.

Bradley, C. E., J. Randall, M. H. Abobeih, R. C. Berrevoets, M. J. Degen, M. A. Bakker, M. Markham, D. J. Twitchen, and T. H. Taminiau, 2019, “A Ten-Qubit Solid-State Spin Register with Quantum Memory up to One Minute,” *Phys. Rev. X* **9**, 031045.

Brassard, Gilles, 2003, “Quantum communication complexity,” *Found. Phys.* **33**, 1593–1616.

Bratzik, S., H. Kampermann, and D. Bruss, 2014, “Secret key rates for an encoded quantum repeater,” *Phys. Rev. A* **89**, 032335.

Braunstein, Samuel L., and H. Jeff Kimble, 1998, “Teleportation of Continuous Quantum Variables,” *Phys. Rev. Lett.* **80**, 869.

Briegel, H.-J., W. Dür, J. I. Cirac, and P. Zoller, 1998, “Quantum Repeater: The Role of Imperfect Local Operations in Quantum Communication,” *Phys. Rev. Lett.* **81**, 5932–5935.

Briegel, Hans J., and Robert Raussendorf, 2001, “Persistent Entanglement in Arrays of Interacting Particles,” *Phys. Rev. Lett.* **86**, 910–913.

Broadbent, Anne, Joseph Fitzsimons, and Elham Kashefi, 2009, “Universal blind quantum computation,” in *Proceedings of the 50th Annual IEEE Symposium on Foundations of Computer Science, Atlanta, 2009* (IEEE, New York), pp. 517–526, [10.1109/FOCS.2009.36](https://doi.org/10.1109/FOCS.2009.36).

Broadbent, Anne, and Rabib Islam, 2020, “Quantum encryption with certified deletion,” in *Theory of Cryptography Conference* (Springer, New York), pp. 92–122, [10.1007/978-3-030-64381-2\\_4](https://doi.org/10.1007/978-3-030-64381-2_4).

Broadbent, Anne, and Christian Schaffner, 2016, “Quantum cryptography beyond quantum key distribution,” *Des. Codes Cryptogr.* **78**, 351–382.

Browne, Daniel E., and Terry Rudolph, 2005, “Resource-Efficient Linear Optical Quantum Computation,” *Phys. Rev. Lett.* **95**, 010501.

Brune, M., S. Haroche, V. Lefevre, J. M. Raimond, and N. Zagury, 1990, “Quantum Nondemolition Measurement of Small Photon Numbers by Rydberg-Atom Phase-Sensitive Detection,” *Phys. Rev. Lett.* **65**, 976.

Brunner, Nicolas, Daniel Cavalcanti, Stefano Pironio, Valerio Scarani, and Stephanie Wehner, 2014, “Bell nonlocality,” *Rev. Mod. Phys.* **86**, 419–478.

Buhrman, Harry, Nishanth Chandran, Serge Fehr, Ran Gelles, Vipul Goyal, Rafail Ostrovsky, and Christian Schaffner, 2011, “Position-based quantum cryptography: Impossibility and constructions,” in *Advances in Cryptology—CRYPTO 2011*, edited by Phillip Rogaway (Springer, Berlin), pp. 429–446, [10.1007/978-3-642-22792-9\\_24](https://doi.org/10.1007/978-3-642-22792-9_24).

Buhrman, Harry, Richard Cleve, John Watrous, and Ronald de Wolf, 2001, “Quantum Fingerprinting,” *Phys. Rev. Lett.* **87**, 167902.

Buterakos, Donovan, Edwin Barnes, and Sophia E. Economou, 2017, “Deterministic Generation of All-Photonic Quantum Repeaters from Solid-State Emitters,” *Phys. Rev. X* **7**, 041023.

Cabrillo, C., J. I. Cirac, P. Garcia-Fernandez, and P. Zoller, 1999, “Creation of entangled states of distant atoms by interference,” *Phys. Rev. A* **59**, 1025.

Cacciapuoti, Angela Sara, Marcello Caleffi, Francesco Tafuri, Francesco Saverio Cataliotti, Stefano Gherardini, and Giuseppe Bianchi, 2020, “Quantum internet: Networking challenges in distributed quantum computing,” *IEEE Network* **34**, 137–143.

Cacciapuoti, Angela Sara, Jessica Illiano, Seid Koudia, Kyrylo Simonov, and Marcello Caleffi, 2022, “The quantum internet: Enhancing classical Internet services one qubit at a time,” *IEEE Network* **36**, 6–12.

Calderbank, A. R., and Peter W. Shor, 1996, “Good quantum error-correcting codes exist,” *Phys. Rev. A* **54**, 1098.

Calsamiglia, John, and Norbert Lütkenhaus, 2001, “Maximum efficiency of a linear-optical Bell-state analyzer,” *Appl. Phys. B* **72**, 67–71.

Cartesian, 2021, “Addressing gaps in broadband infrastructure availability and service adoption,” <https://www.cartesian.com/addressing-gaps-in-broadband-infrastructure-availability-and-service-adoption/>.

Castelvecchi, Davide, 2017, “IBM’s quantum cloud computer goes commercial,” *Nature (London)* **543**, 159.

Chailloux, André, and Iordanis Kerenidis, 2009, “Optimal quantum strong coin flipping,” in *Proceedings of the 50th Annual IEEE Symposium on Foundations of Computer Science, Atlanta, 2009* (IEEE, New York), pp. 527–533, [10.1109/FOCS.2009.71](https://doi.org/10.1109/FOCS.2009.71).

Chamberland, Christopher, and Michael E. Beverland, 2018, “Flag fault-tolerant error correction with arbitrary distance codes,” *Quantum* **2**, 53.

Chang, J., *et al.*, 2021, “Detecting telecom single photons with  $(99.5^{+0.5}_{-2.07})$  system detection efficiency and high time resolution,” *APL Photonics* **6**, 036114.

Chao, Rui, and Ben W. Reichardt, 2018, “Quantum Error Correction with Only Two Extra Qubits,” *Phys. Rev. Lett.* **121**, 050502.

Chen, Jiu-Peng, *et al.*, 2020, “Sending-or-Not-Sending with Independent Lasers: Secure Twin-Field Quantum Key Distribution over 509 km,” *Phys. Rev. Lett.* **124**, 070501.

Chen, Jiu-Peng, *et al.*, 2021, “Twin-field quantum key distribution over a 511 km optical fibre linking two distant metropolitan areas,” *Nat. Photonics* **15**, 570–575.

Chen, Kai, and Hoi-Kwong Lo, 2007, “Multi-partite quantum cryptographic protocols with noisy GHZ states,” *Quantum Inf. Comput.* **7**, 689–715.

Chen, Shuai, Yu-Ao Chen, Bo Zhao, Zhen-Sheng Yuan, Jörg Schmiedmayer, and Jian-Wei Pan, 2007, “Demonstration of a Stable Atom-Photon Entanglement Source for Quantum Repeaters,” *Phys. Rev. Lett.* **99**, 180505.

Chen, Yu-Ao, *et al.*, 2021, “An integrated space-to-ground quantum communication network over 4,600 kilometres,” *Nature (London)* **589**, 214–219.

Childress, L., M. V. Gurudev Dutt, J. M. Taylor, A. S. Zibrov, F. Jelezko, J. Wrachtrup, P. R. Hemmer, and M. D. Lukin, 2006, “Coherent dynamics of coupled electron and nuclear spin qubits in diamond,” *Science* **314**, 281–285.

Childress, L., J. M. Taylor, A. S. Sørensen, and M. D. Lukin, 2006, “Fault-Tolerant Quantum Communication Based on Solid-State Photon Emitters,” *Phys. Rev. Lett.* **96**, 070504.

Childs, Andrew M., 2005, “Secure assisted quantum computation,” *Quantum Inf. Comput.* **5**, 456–466.

Chou, Chin-Wen, Julien Laurat, Hui Deng, Kyung Soo Choi, Hugues De Riedmatten, Daniel Felinto, and H. Jeff Kimble, 2007, “Functional quantum nodes for entanglement distribution over scalable quantum networks,” *Science* **316**, 1316–1320.

Christ, Andreas, and Christine Silberhorn, 2012, “Limits on the deterministic creation of pure single-photon states using parametric down-conversion,” *Phys. Rev. A* **85**, 023829.

Christandl, Matthias, and Alexander Müller-Hermes, 2017, “Relative entropy bounds on quantum, private and repeater capacities,” *Commun. Math. Phys.* **353**, 821–852.

Christandl, Matthias, and Stephanie Wehner, 2005, “Quantum anonymous transmissions,” in *Proceedings of the International Conference on the Theory and Application of Cryptology and Information Security, Chennai, India, 2005*, edited by Bimal Roy (Springer, New York), pp. 217–235, [10.1007/11593447\\_12](https://doi.org/10.1007/11593447_12).

Christensen, Brad G., *et al.*, 2013, “Detection-Loophole-Free Test of Quantum Nonlocality, and Applications,” *Phys. Rev. Lett.* **111**, 130406.

Chung, Joaquin, *et al.*, 2021, “Illinois Express Quantum Network (IEQNET): Metropolitan-scale experimental quantum networking over deployed optical fiber,” in *Quantum Information Science, Sensing, and Computation XIII*, edited by Eric Donkor and Michael Hayduk, SPIE Proceedings Vol. 11726 (SPIE—International Society for Optical Engineering, Bellingham, WA), p. 1172602, [10.1117/12.2588007](https://doi.org/10.1117/12.2588007).

Clerk, A. A., M. H. Devoret, S. M. Girvin, Florian Marquardt, and R. J. Schoelkopf, 2010, “Introduction to quantum noise, measurement, and amplification,” *Rev. Mod. Phys.* **82**, 1155–1208.

Cleve, Richard, and Harry Buhrman, 1997, “Substituting quantum entanglement for communication,” *Phys. Rev. A* **56**, 1201.

Cleve, Richard, Daniel Gottesman, and Hoi-Kwong Lo, 1999, “How to Share a Quantum Secret,” *Phys. Rev. Lett.* **83**, 648.

Clivati, Cecilia, *et al.*, 2022, “Coherent phase transfer for real-world twin-field quantum key distribution,” *Nat. Commun.* **13**, 157.

Cogan, Dan, Zu-En Su, Oded Kenneth, and David Gershoni, 2023, “Deterministic generation of indistinguishable photons in a cluster state,” *Nat. Photonics* **17**, 324–329.

Collins, Daniel, Noah Linden, and Sandu Popescu, 2001, “Nonlocal content of quantum operations,” *Phys. Rev. A* **64**, 032302.

Collins, Matthew J., *et al.*, 2013, “Integrated spatial multiplexing of heralded single-photon sources,” *Nat. Commun.* **4**, 2582.

Collins, O. A., S. D. Jenkins, A. Kuzmich, and T. A. B. Kennedy, 2007, “Multiplexed Memory-Insensitive Quantum Repeaters,” *Phys. Rev. Lett.* **98**, 060502.

Coopmans, Tim, *et al.*, 2021, “NetSquid, a discrete-event simulation platform for quantum networks,” *Commun. Phys.* **4**, 164.

Corning, 2021, “Corning SMF-28 ULL optical fiber portfolio,” <https://www.corning.com/optical-communications/worldwide/en/home/products/fiber/optical-fiber-products/smf-28-ull.html>.

Coste, N., *et al.*, 2023, “High-rate entanglement between a semiconductor spin and indistinguishable photons,” *Nat. Photonics* **17**, 582–587.

Cramer, J., N. Kalb, M. A. Rol, B. Hensen, M. S. Blok, M. Markham, D. J. Twitchen, R. Hanson, and T. H. Taminiau, 2016, “Repeated quantum error correction on a continuously encoded qubit by real-time feedback,” *Nat. Commun.* **7**, 11526.

Cui, Chaohan, Zhen-Qiang Yin, Rong Wang, Wei Chen, Shuang Wang, Guang-Can Guo, and Zheng-Fu Han, 2019, “Twin-Field Quantum Key Distribution without Phase Postselection,” *Phys. Rev. Appl.* **11**, 034053.

Currá-Lorenzo, Guillermo, Álvaro Navarrete, Koji Azuma, Go Kato, Marcos Curty, and Mohsen Razavi, 2021, “Tight finite-key security for twin-field quantum key distribution,” *npj Quantum Inf.* **7**, 22.

Curty, Marcos, Koji Azuma, and Hoi-Kwong Lo, 2019, “Simple security proof of twin-field type quantum key distribution protocol,” *npj Quantum Inf.* **5**, 64.

Curty, Marcos, Koji Azuma, and Hoi-Kwong Lo, 2021, “A quantum leap in security,” *Phys. Today* **74**, No. 3, 36.

Curty, Marcos, and Hoi-Kwong Lo, 2019, “Foiling covert channels and malicious classical post-processing units in quantum key distribution,” *npj Quantum Inf.* **5**, 14.

Curty, Marcos, and Tobias Moroder, 2011, “Heralded-qubit amplifiers for practical device-independent quantum key distribution,” *Phys. Rev. A* **84**, 010304.

Curty, Marcos, Feihu Xu, Wei Cui, Charles Ci Wen Lim, Kiyoshi Tamaki, and Hoi-Kwong Lo, 2014, “Finite-key analysis for measurement-device-independent quantum key distribution,” *Nat. Commun.* **5**, 3732.

Dahlberg, Axel, *et al.*, 2019, “A link layer protocol for quantum networks,” in *Proceedings of the ACM Special Interest Group on Data Communication, Beijing, 2009* (Association for Computing Machinery, New York), pp. 159–173, [10.1145/3341302.3342070](https://doi.org/10.1145/3341302.3342070).

Daiss, Severin, Stefan Langenfeld, Stephan Welte, Emanuele Distante, Philip Thomas, Lukas Hartung, Olivier Morin, and Gerhard Rempe, 2021, “A quantum-logic gate between distant quantum-network modules,” *Science* **371**, 614–617.

Damgård, Ivan B., Serge Fehr, Louis Salvail, and Christian Schaffner, 2007, “Secure identification and QKD in the bounded-quantum-storage model,” in *Advances in Cryptology—CRYPTO 2007, Lecture Notes in Physics Vol. 4622*, edited by Alfred Menezes (Springer, New York), pp. 342–359, [10.1007/978-3-540-74143-5\\_19](https://doi.org/10.1007/978-3-540-74143-5_19).

Damgård, Ivan B., Serge Fehr, Louis Salvail, and Christian Schaffner, 2008, “Cryptography in the bounded-quantum-storage model,” *SIAM J. Comput.* **37**, 1865–1890.

Das, Siddhartha, Stefan Bäuml, and Mark M. Wilde, 2020, “Entanglement and secret-key-agreement capacities of bipartite quantum interactions and read-only memory devices,” *Phys. Rev. A* **101**, 012344.

Das, Siddhartha, Stefan Bäuml, Marek Winczewski, and Karol Horodecki, 2021, “Universal Limitations on Quantum Key Distribution over a Network,” *Phys. Rev. X* **11**, 041016.

Degen, C. L., F. Reinhard, and P. Cappellaro, 2017, “Quantum sensing,” *Rev. Mod. Phys.* **89**, 035002.

De Greve, Kristiaan, *et al.*, 2011, “Ultrafast coherent control and suppressed nuclear feedback of a single quantum dot hole qubit,” *Nat. Phys.* **7**, 872–878.

De Greve, Kristiaan, *et al.*, 2012, “Quantum-dot spin-photon entanglement via frequency downconversion to telecom wavelength,” *Nature (London)* **491**, 421–425.

Delteil, Aymeric, Zhe Sun, Wei-bo Gao, Emre Togan, Stefan Faelt, and Atac Imamoglu, 2016, “Generation of heralded entanglement between distant hole spins,” *Nat. Phys.* **12**, 218–223.

de Riedmatten, Hugues, Ivan Marcikic, Wolfgang Tittel, Hugo Zbinden, Daniel Collins, and Nicolas Gisin, 2004, “Long Distance Quantum Teleportation in a Quantum Relay Configuration,” *Phys. Rev. Lett.* **92**, 047904.

Deutsch, David, Artur Ekert, Richard Jozsa, Chiara Macchiavello, Sandu Popescu, and Anna Sanpera, 1996, “Quantum Privacy Amplification and the Security of Quantum Cryptography over Noisy Channels,” *Phys. Rev. Lett.* **77**, 2818–2821.

Devetak, Igor, 2005, “The private classical capacity and quantum capacity of a quantum channel,” *IEEE Trans. Inf. Theory* **51**, 44–55.

Devitt, Simon J., Andrew D. Greentree, Ashley M. Stephens, and Rodney Van Meter, 2016, “High-speed quantum networking by ship,” *Sci. Rep.* **6**, 36163.

Dias, Josephine, and T. C. Ralph, 2017, “Quantum repeaters using continuous-variable teleportation,” *Phys. Rev. A* **95**, 022312.

Dideriksen, Karsten B., Rebecca Schmiegel, Michael Zugenmaier, and Eugene S. Polzik, 2021, “Room-temperature single-photon source with near-millisecond built-in memory,” *Nat. Commun.* **12**, 3699.

Dieks, D., 1982, “Communication by EPR devices,” *Phys. Lett.* **92A**, 271–272.

Dowling, Jonathan P., and Gerard J. Milburn, 2003, “Quantum technology: The second quantum revolution,” *Phil. Trans. R. Soc. A* **361**, 1655–1674.

Duan, L.-M., M. D. Lukin, J. I. Cirac, and P. Zoller, 2001, “Long-distance quantum communication with atomic ensembles and linear optics,” *Nature (London)* **414**, 413–418.

Dudin, Y. O., L. Li, and A. Kuzmich, 2013, “Light storage on the time scale of a minute,” *Phys. Rev. A* **87**, 031801.

Dudin, Y. O., A. G. Radnaev, Ran Zhao, J. Z. Blumoff, T. A. B. Kennedy, and Alex Kuzmich, 2010, “Entanglement of Light-Shift Compensated Atomic Spin Waves with Telecom Light,” *Phys. Rev. Lett.* **105**, 260502.

Dupuis, Frederic, Omar Fawzi, and Stephanie Wehner, 2015, “Entanglement sampling and applications,” *IEEE Trans. Inf. Theory* **61**, 1093–1112.

Dür, W., and H. J. Briegel, 2007, “Entanglement purification and quantum error correction,” *Rep. Prog. Phys.* **70**, 1381–1424.

Dür, W., H.-J. Briegel, J. I. Cirac, and P. Zoller, 1999, “Quantum repeaters based on entanglement purification,” *Phys. Rev. A* **59**, 169–181.

Dür, W., G. Vidal, and J. I. Cirac, 2000, “Three qubits can be entangled in two inequivalent ways,” *Phys. Rev. A* **62**, 062314.

Durand, Alrik, *et al.*, 2021, “Broad Diversity of Near-Infrared Single-Photon Emitters in Silicon,” *Phys. Rev. Lett.* **126**, 083602.

Eberhard, Phillippe H., and Ronald R. Ross, 1989, “Quantum field theory cannot provide faster-than-light communication,” *Found. Phys. Lett.* **2**, 127–149.

Ebert, M., M. Kwon, T. G. Walker, and M. Saffman, 2015, “Coherence and Rydberg Blockade of Atomic Ensemble Qubits,” *Phys. Rev. Lett.* **115**, 093601.

Economou, Sophia E., Netanel Lindner, and Terry Rudolph, 2010, “Optically Generated 2-Dimensional Photonic Cluster State from Coupled Quantum Dots,” *Phys. Rev. Lett.* **105**, 093601.

Egan, Laird, *et al.*, 2021, “Fault-tolerant control of an error-corrected qubit,” *Nature (London)* **598**, 281–286.

Einstein, A., B. Podolsky, and N. Rosen, 1935, “Can quantum-mechanical description of physical reality be considered complete?,” *Phys. Rev.* **47**, 777–780.

Eisaman, M. D., J. Fan, A. Migdall, and S. V. Polyakov, 2011, “Invited review article: Single-photon sources and detectors,” *Rev. Sci. Instrum.* **82**, 071101.

Eisert, J., K. Jacobs, P. Papadopoulos, and M. B. Plenio, 2000, “Optimal local implementation of nonlocal quantum gates,” *Phys. Rev. A* **62**, 052317.

Eisert, J., S. Scheel, and M. B. Plenio, 2002, “Distilling Gaussian States with Gaussian Operations Is Impossible,” *Phys. Rev. Lett.* **89**, 137903.

Ekert, Artur K., 1991, “Quantum Cryptography Based on Bell’s Theorem,” *Phys. Rev. Lett.* **67**, 661–663.

Éthier-Majcher, G., D. Gangloff, R. Stockill, E. Clarke, M. Hugues, C. Le Gall, and M. Atatüre, 2017, “Improving a Solid-State Qubit through an Engineered Mesoscopic Environment,” *Phys. Rev. Lett.* **119**, 130503.

European Commission, 2022, “The European Quantum Communication Infrastructure (EuroQCI) initiative,” <https://digital-strategy.ec.europa.eu/en/policies/european-quantum-communication-infrastructure-euroqci>.

Ewert, Fabian, Marcel Bergmann, and Peter van Loock, 2016, “Ultrafast Long-Distance Quantum Communication with Static Linear Optics,” *Phys. Rev. Lett.* **117**, 210501.

Ewert, Fabian, and Peter van Loock, 2014, “3/4-Efficient Bell Measurement with Passive Linear Optics and Unentangled Ancillae,” *Phys. Rev. Lett.* **113**, 140403.

Ewert, Fabian, and Peter van Loock, 2017, “Ultrafast fault-tolerant long-distance quantum communication with static linear optics,” *Phys. Rev. A* **95**, 012327.

Fern, Jesse, and K. Birgitta Whaley, 2008, “Lower bounds on the nonzero capacity of Pauli channels,” *Phys. Rev. A* **78**, 062335.

Fibre Optic Association, 2019, “FOA reference guide,” <https://www.thefoa.org/tech/ref/testing/test/loss.html>.

Fitzsimons, Joseph F., 2017, “Private quantum computation: An introduction to blind quantum computing and related protocols,” *npj Quantum Inf.* **3**, 23.

Fiurášek, Jaromír, 2002, “Gaussian Transformations and Distillation of Entangled Gaussian States,” *Phys. Rev. Lett.* **89**, 137904.

Fiurášek, Jaromír, 2010, “Distillation and purification of symmetric entangled Gaussian states,” *Phys. Rev. A* **82**, 042331.

Fowler, A. G., D. S. Wang, C. D. Hill, T. D. Ladd, R. Van Meter, and L. C. L. Hollenberg, 2010, “Surface Code Quantum Communication,” *Phys. Rev. Lett.* **104**, 180503.

Fröhlich, Bernd, James F. Dynes, Marco Lucamarini, Andrew W. Sharpe, Zhiliang Yuan, and Andrew J. Shields, 2013, “A quantum access network,” *Nature (London)* **501**, 69–72.

Fuchs, G. D., Guido Burkard, P. V. Klimov, and D. D. Awschalom, 2011, “A quantum memory intrinsic to single nitrogen-vacancy centres in diamond,” *Nat. Phys.* **7**, 789–793.

Fujii, Keisuke, and Katsuji Yamamoto, 2009, “Entanglement purification with double selection,” *Phys. Rev. A* **80**, 042308.

Fukui, Kosuke, Rafael N. Alexander, and Peter van Loock, 2021, “All-optical long-distance quantum communication with Gottesman-Kitaev-Preskill qubits,” *Phys. Rev. Res.* **3**, 033118.

Fukui, Kosuke, Akihisa Tomita, and Atsushi Okamoto, 2017, “Analog Quantum Error Correction with Encoding a Qubit into an Oscillator,” *Phys. Rev. Lett.* **119**, 180507.

Furrer, Fabian, and William J. Munro, 2018, “Repeaters for continuous-variable quantum communication,” *Phys. Rev. A* **98**, 032335.

Gangloff, D. A., G. Ethier-Majcher, C. Lang, E. V. Denning, J. H. Bodey, D. M. Jackson, E. Clarke, M. Hugues, C. Le Gall, and M. Atatüre, 2019, “Quantum interface of an electron and a nuclear ensemble,” *Science* **364**, 62.

Gao, W. B., Parisa Fallahi, Emre Togan, Javier Miguel-Sánchez, and Atac Imamoglu, 2012, “Observation of entanglement between a quantum dot spin and a single photon,” *Nature (London)* **491**, 426–430.

Gavinsky, Dmitry, 2012, “Quantum money with classical verification,” in *Proceedings of the IEEE 27th Conference on Computational Complexity, Porto, Portugal, 2012* (IEEE, New York), pp. 42–52, [10.1109/CCC.2012.10](https://doi.org/10.1109/CCC.2012.10).

Giedke, G., and J. I. Cirac, 2002, “Characterization of Gaussian operations and distillation of Gaussian states,” *Phys. Rev. A* **66**, 032316.

Gimeno-Segovia, Mercedes, 2016, “Towards practical linear optical quantum computing,” Ph.D. thesis (Imperial College London), [10.25560/43936](https://doi.org/10.25560/43936).

Gimeno-Segovia, Mercedes, Terry Rudolph, and Sophia E. Economou, 2019, “Deterministic Generation of Large-Scale Entangled Photonic Cluster State from Interacting Solid State Emitters,” *Phys. Rev. Lett.* **123**, 070501.

Giovannetti, Vittorio, Seth Lloyd, Lorenzo Maccone, and Peter W. Shor, 2003a, “Broadband channel capacities,” *Phys. Rev. A* **68**, 062323.

Giovannetti, Vittorio, Seth Lloyd, Lorenzo Maccone, and Peter W. Shor, 2003b, “Entanglement Assisted Capacity of the Broadband Lossy Channel,” *Phys. Rev. Lett.* **91**, 047901.

Gisin, Nicolas, Stefano Pironio, and Nicolas Sangouard, 2010, “Proposal for Implementing Device-Independent Quantum Key Distribution Based on a Heralded Qubit Amplifier,” *Phys. Rev. Lett.* **105**, 070501.

Giustina, Marissa, *et al.*, 2013, “Bell violation using entangled photons without the fair-sampling assumption,” *Nature (London)* **497**, 227–230.

Google Quantum AI, 2023, “Suppressing quantum errors by scaling a surface code logical qubit,” *Nature (London)* **614**, 676–681.

Görlitz, Johannes, *et al.*, 2020, “Spectroscopic investigations of negatively charged tin-vacancy centres in diamond,” *New J. Phys.* **22**, 013048.

Gottesman, Daniel, 1997, “Stabilizer codes and quantum error correction,” Ph.D. thesis (California Institute of Technology), [10.7907/rzr7-dt72](https://doi.org/10.7907/rzr7-dt72).

Gottesman, Daniel, 1999, “The Heisenberg representation of quantum computers,” in *Group22: Proceedings of the XXII International Colloquium on Group Theoretical Methods in Physics*, edited by S. P. Corney, R. Delbourgo, and P. D. Jarvis (International Press, Cambridge, MA), pp. 32–43.

Gottesman, Daniel, and Isaac L. Chuang, 1999, “Demonstrating the viability of universal quantum computation using teleportation and single-qubit operations,” *Nature (London)* **402**, 390.

Gottesman, Daniel, Thomas Jennewein, and Sarah Croke, 2012, “Longer-Baseline Telescopes Using Quantum Repeaters,” *Phys. Rev. Lett.* **109**, 070503.

Gottesman, Daniel, Alexei Kitaev, and John Preskill, 2001, “Encoding a qubit in an oscillator,” *Phys. Rev. A* **64**, 012310.

Greibich, A., A. Shabaev, D. R. Yakovlev, Al. L. Efros, I. A. Yugova, D. Reuter, A. D. Wieck, and M. Bayer, 2007, “Nuclei-induced frequency focusing of electron spin coherence,” *Science* **317**, 1896–1899.

Grice, W. P., 2011, “Arbitrarily complete Bell-state measurement using only linear optical elements,” *Phys. Rev. A* **84**, 042331.

Grosshans, Frederic, and Nicolas J. Cerf, 2004, “Continuous-Variable Quantum Cryptography Is Secure against Non-Gaussian Attacks,” *Phys. Rev. Lett.* **92**, 047905.

Guha, Saikat, 2011, “Structured Optical Receivers to Attain Super-additive Capacity and the Holevo Limit,” *Phys. Rev. Lett.* **106**, 240502.

Gündoğan, Mustafa, Jasminder S. Sidhu, Victoria Henderson, Luca Mazzarella, Janik Wolters, Daniel K. L. Oi, and Markus Krutzik, 2021, “Proposal for space-borne quantum memories for global quantum networking,” *npj Quantum Inf.* **7**, 128.

Gurudev Dutt, M. V., Jun Cheng, Yanwen Wu, Xiaodong Xu, D. G. Steel, A. S. Bracker, D. Gammon, Sophia E. Economou, Ren-Bao Liu, and L. J. Sham, 2006, “Ultrafast optical control of electron spin coherence in charged GaAs quantum dots,” *Phys. Rev. B* **74**, 125306.

Hadfield, R. H., 2009, “Single-photon detectors for optical quantum information applications,” *Nat. Photonics* **3**, 696–705.

Hasegawa, Yasushi, Rikizo Ikuta, Nobuyuki Matsuda, Kiyoshi Tamaki, Hoi-Kwong Lo, Takashi Yamamoto, Koji Azuma, and Nobuyuki Imoto, 2019, “Experimental time-reversed adaptive Bell measurement towards all-photonic quantum repeaters,” *Nat. Commun.* **10**, 378.

Hastings, Matthew B., 2009, “Superadditivity of communication capacity using entangled inputs,” *Nat. Phys.* **5**, 255–257.

Hein, M., J. Eisert, and H. J. Briegel, 2004, “Multipartite entanglement in graph states,” *Phys. Rev. A* **69**, 062311.

Hein, Marc, Wolfgang Dür, Jens Eisert, Robert Raussendorf, M. Nest, and H.-J. Briegel, 2006, “Entanglement in graph states and its applications,” in *Quantum Computers, Algorithms and Chaos*, edited by G. Casati, D. L. Shepelyansky, P. Zoller, and G. Benenti (IOS Press, Amsterdam), 10.3254/978-1-61499-018-5-115.

Hensen, B., *et al.*, 2015, “Loophole-free Bell inequality violation using electron spins separated by 1.3 kilometres,” *Nature (London)* **526**, 682–686.

Hermans, S. L. N., M. Pompili, H. K. C. Beukers, S. Baier, J. Borregaard, and R. Hanson, 2022, “Qubit teleportation between non-neighbouring nodes in a quantum network,” *Nature (London)* **605**, 663–668.

Herrera-Martí, David A., Austin G. Fowler, David Jennings, and Terry Rudolph, 2010, “Photonic implementation for the topological cluster-state quantum computer,” *Phys. Rev. A* **82**, 032332.

Heshami, Khabat, Duncan G. England, Peter C. Humphreys, Philip J. Bustard, Victor M. Acosta, Joshua Nunn, and Benjamin J. Sussman, 2016, “Quantum memories: Emerging applications and recent advances,” *J. Mod. Opt.* **63**, 2005–2028.

Higginbottom, Daniel B., *et al.*, 2022, “Optical observation of single spins in silicon,” *Nature (London)* **607**, 266–270.

Hilaire, Paul, Edwin Barnes, and Sophia E. Economou, 2021, “Resource requirements for efficient quantum communication using all-photonic graph states generated from a few matter qubits,” *Quantum* **5**, 397.

Hilaire, Paul, Edwin Barnes, Sophia E. Economou, and Frédéric Grosshans, 2021, “Error-correcting entanglement swapping using a practical logical photon encoding,” *Phys. Rev. A* **104**, 052623.

Hilaire, Paul, Yaron Castor, Edwin Barnes, Sophia E. Economou, and Frédéric Grosshans, 2023, “Linear optical logical Bell state measurements with optimal loss-tolerance threshold,” *PRX Quantum* **4**, 040322.

Hilaire, Paul, Leonid Vidro, Hagai S. Eisenberg, and Sophia E. Economou, 2023, “Near-deterministic hybrid generation of arbitrary photonic graph states using a single quantum emitter and linear optics,” *Quantum* **7**, 992.

Hillery, Mark, Vladimír Bužek, and André Berthiaume, 1999, “Quantum secret sharing,” *Phys. Rev. A* **59**, 1829.

Horgan, John, 2016, “Is the gravitational-wave claim true? And was it worth the cost?” <https://blogs.scientificamerican.com/> cross-check/is-the-gravitational-wave-claim-true-and-was-it-worth-the-cost.

Horodecki, Karol, Michał Horodecki, Paweł Horodecki, and Jonathan Oppenheim, 2005, “Secure Key from Bound Entanglement,” *Phys. Rev. Lett.* **94**, 160502.

Horodecki, Michał, Paweł Horodecki, and Ryszard Horodecki, 1999, “General teleportation channel, singlet fraction, and quasidistillation,” *Phys. Rev. A* **60**, 1888.

Horodecki, Ryszard, Paweł Horodecki, Michał Horodecki, and Karol Horodecki, 2009, “Quantum entanglement,” *Rev. Mod. Phys.* **81**, 865–942.

Hosseini, Mahdi, Ben M. Sparkes, Geoff Campbell, Ping K. Lam, and Ben C. Buchler, 2011, “High efficiency coherent optical memory with warm rubidium vapour,” *Nat. Commun.* **2**, 174.

Howarth, Josh, 2021, “80+ amazing IoT statistics (2022–2030),” <https://explodingtopics.com/blog/iot-stats>.

Hu, Peng, Hao Li, Lixing You, Heqing Wang, You Xiao, Jia Huang, Xiaoyan Yang, Weijun Zhang, Zhen Wang, and Xiaoming Xie, 2020, “Detecting single infrared photons toward optimal system detection efficiency,” *Opt. Express* **28**, 36884–36891.

Hu, Xiao-Min, *et al.*, 2020, “Experimental High-Dimensional Quantum Teleportation,” *Phys. Rev. Lett.* **125**, 230501.

Hu, Xiao-Min, *et al.*, 2021, “Long-Distance Entanglement Purification for Quantum Communication,” *Phys. Rev. Lett.* **126**, 010503.

Hucul, David, Ismail V. Inlek, Grahame Vittorini, Clayton Crocker, Shantanu Debnath, Susan M. Clark, and Christopher Monroe, 2015, “Modular entanglement of atomic qubits using photons and phonons,” *Nat. Phys.* **11**, 37–42.

Humphreys, Peter C., Norbert Kalb, Jaco P. J. Morits, Raymond N. Schouten, Raymond F. L. Vermeulen, Daniel J. Twitchen, Matthew Markham, and Ronald Hanson, 2018, “Deterministic delivery of remote entanglement on a quantum network,” *Nature (London)* **558**, 268–273.

Hwang, Won-Young, 2003, “Quantum Key Distribution with High Loss: Toward Global Secure Communication,” *Phys. Rev. Lett.* **91**, 057901.

Ikuta, Rikizo, Yoshiaki Kusaka, Tsuyoshi Kitano, Hiroshi Kato, Takashi Yamamoto, Masato Koashi, and Nobuyuki Imoto, 2011, “Wide-band quantum interface for visible-to-telecommunication wavelength conversion,” *Nat. Commun.* **2**, 537.

Ikuta, Rikizo, *et al.*, 2018, “Polarization insensitive frequency conversion for an atom-photon entanglement distribution via a telecom network,” *Nat. Commun.* **9**, 1997.

Illiano, Jessica, Marcello Caleffi, Antonio Manzalini, and Angela Sara Cacciapuoti, 2022, “Quantum internet protocol stack: A comprehensive survey,” *Comput. Networks* **213**, 109092.

Imoto, N., H. A. Haus, and Y. Yamamoto, 1985, “Quantum non-demolition measurement of the photon number via the optical Kerr effect,” *Phys. Rev. A* **32**, 2287.

Inlek, Ismail Volkan, Clayton Crocker, Martin Lichtman, Ksenia Sosnova, and Christopher Monroe, 2017, “Multispecies Trapped-Ion Node for Quantum Networking,” *Phys. Rev. Lett.* **118**, 250502.

Inoue, Kyo, Edo Waks, and Yoshihisa Yamamoto, 2002, “Differential Phase Shift Quantum Key Distribution,” *Phys. Rev. Lett.* **89**, 037902.

Iwasaki, Takayuki, *et al.*, 2015, “Germanium-vacancy single color centers in diamond,” *Sci. Rep.* **5**, 12882.

Jackson, Daniel M., Dorian A. Gangloff, Jonathan H. Bodey, Leon Zaporski, Clara Bachorz, Edmund Clarke, Maxime Hugues, Claire Le Gall, and Mete Atatüre, 2021, “Quantum sensing of a coherent single spin excitation in a nuclear ensemble,” *Nat. Phys.* **17**, 585–590.

Jacobs, B. C., T. B. Pittman, and J. D. Franson, 2002, “Quantum relays and noise suppression using linear optics,” *Phys. Rev. A* **66**, 052307.

Javadi, Alisa, *et al.*, 2018, “Spin-photon interface and spin-controlled photon switching in a nanobeam waveguide,” *Nat. Nanotechnol.* **13**, 398–403.

Ji, Jia-Wei, Yu-Feng Wu, Stephen C. Wein, Faezeh Kimiae Asadi, Roohollah Ghobadi, and Christoph Simon, 2022, “Proposal for room-temperature quantum repeaters with nitrogen-vacancy centers and optomechanics,” *Quantum* **6**, 669.

Jiang, Cong, Zong-Wen Yu, Xiao-Long Hu, and Xiang-Bin Wang, 2019, “Unconditional Security of Sending or Not Sending Twin-Field Quantum Key Distribution with Finite Pulses,” *Phys. Rev. Appl.* **12**, 024061.

Jiang, L., J. M. Taylor, N. Khaneja, and M. D. Lukin, 2007, “Optimal approach to quantum communication algorithms using dynamic programming,” *Proc. Natl. Acad. Sci. U.S.A.* **104**, 17291–17296.

Jiang, Liang, J. M. Taylor, Kae Nemoto, W. J. Munro, Rodney Van Meter, and M. D. Lukin, 2009, “Quantum repeater with encoding,” *Phys. Rev. A* **79**, 032325.

Jiang, Liang, Jacob M. Taylor, Anders S. Sørensen, and Mikhail D. Lukin, 2007, “Distributed quantum computation based on small quantum registers,” *Phys. Rev. A* **76**, 062323.

Joo, Jaewoo, Peter L. Knight, Jeremy L. O’Brien, and Terry Rudolph, 2007, “One-way quantum computation with four-dimensional photonic qudits,” *Phys. Rev. A* **76**, 052326.

Jozsa, Richard, 1994, “Fidelity for mixed quantum states,” *J. Mod. Opt.* **41**, 2315–2323.

Jozsa, Richard, Daniel S. Abrams, Jonathan P. Dowling, and Colin P. Williams, 2000, “Quantum Clock Synchronization Based on Shared Prior Entanglement,” *Phys. Rev. Lett.* **85**, 2010–2013.

Jungnickel, Dieter, 2005, *Graphs, Networks and Algorithms* (Springer, New York).

Kalb, Norbert, Andreas A. Reiserer, Peter C. Humphreys, Jacob J. W. Bakermans, Sten J. Kamerling, Naomi H. Nickerson, Simon C. Benjamin, Daniel J. Twitchen, Matthew Markham, and Ronald Hanson, 2017, “Entanglement distillation between solid-state quantum network nodes,” *Science* **356**, 928–932.

Kaneda, Fumihiro, and Paul G. Kwiat, 2019, “High-efficiency single-photon generation via large-scale active time multiplexing,” *Sci. Adv.* **5**, eaaw8586.

Katz, Or, and Ofer Firstenberg, 2018, “Light storage for one second in room-temperature alkali vapor,” *Nat. Commun.* **9**, 2074.

Kent, Adrian, 2011, “Unconditionally secure bit commitment with flying qudits,” *New J. Phys.* **13**, 113015.

Kent, Adrian, William J. Munro, and Timothy P. Spiller, 2011, “Quantum tagging: Authenticating location via quantum information and relativistic signaling constraints,” *Phys. Rev. A* **84**, 012326.

Khabiboulline, Emil T., Johannes Borregaard, Kristiaan De Greve, and Mikhail D. Lukin, 2019, “Optical Interferometry with Quantum Networks,” *Phys. Rev. Lett.* **123**, 070504.

Khatri, Sumeet, Anthony J. Brady, Renée A Desporte, Manon P. Bart, and Jonathan P. Dowling, 2021, “Spooky action at a global distance: Analysis of space-based entanglement distribution for the quantum internet,” *npj Quantum Inf.* **7**, 4.

Khatri, Sumeet, and Mark M. Wilde, 2020, “Principles of quantum communication theory: A modern approach,” *arXiv:2011.04672*.

Kilmer, Thomas, and Saikat Guha, 2019, “Boosting linear-optical Bell measurement success probability with predetection squeezing and imperfect photon-number-resolving detectors,” *Phys. Rev. A* **99**, 032302.

Kimble, H. J., 2008, “The quantum internet,” *Nature (London)* **453**, 1023–1030.

Kimiae Asadi, F., N. Lauk, S. Wein, N. Sinclair, C. O’Brien, and C. Simon, 2018, “Quantum repeaters with individual rare-earth ions at telecommunication wavelengths,” *Quantum* **2**, 93.

Knill, E., R. Laflamme, and G. J. Milburn, 2001, “A scheme for efficient quantum computation with linear optics,” *Nature (London)* **409**, 46–52.

Knill, Emanuel, and Raymond Laflamme, 1996, “Concatenated quantum codes,” *arXiv:quant-ph/9608012*.

Knill, Emanuel, and Raymond Laflamme, 1997, “Theory of quantum error-correcting codes,” *Phys. Rev. A* **55**, 900.

Koashi, M., 2009, “Simple security proof of quantum key distribution based on complementarity,” *New J. Phys.* **11**, 045018.

Koashi, Masato, and Nobuyuki Imoto, 1998, “No-Cloning Theorem of Entangled States,” *Phys. Rev. Lett.* **81**, 4264–4267.

Koashi, Masato, and Nobuyuki Imoto, 2002, “Operations that do not disturb partially known quantum states,” *Phys. Rev. A* **66**, 022318.

Kok, Pieter, W. J. Munro, Kae Nemoto, T. C. Ralph, Jonathan P. Dowling, and G. J. Milburn, 2007, “Linear optical quantum computing with photonic qubits,” *Rev. Mod. Phys.* **79**, 135–174.

Kok, Pieter, Colin P. Williams, and Jonathan P. Dowling, 2003, “Construction of a quantum repeater with linear optics,” *Phys. Rev. A* **68**, 022301.

Komar, Peter, Eric M. Kessler, Michael Bishof, Liang Jiang, Anders S Sørensen, Jun Ye, and Mikhail D. Lukin, 2014, “A quantum network of clocks,” *Nat. Phys.* **10**, 582–587.

Konig, Robert, Stephanie Wehner, and Jürg Wullschleger, 2012, “Unconditional security from noisy quantum storage,” *IEEE Trans. Inf. Theory* **58**, 1962–1984.

Konno, Shunya, *et al.*, 2023, “Propagating Gottesman-Kitaev-Preskill states encoded in an optical oscillator,” *arXiv:2309.02306*.

Kozlowski, Wojciech, Axel Dahlberg, and Stephanie Wehner, 2020, “Designing a quantum network protocol,” in *Proceedings of the 16th International Conference on Emerging Networking Experiments and Technologies, Barcelona, 2020* (Association for Computing Machinery, New York), pp. 1–16, [10.1145/3386367.3431293](https://doi.org/10.1145/3386367.3431293).

Kozlowski, Wojciech, Stephanie Wehner, R. V. Meter, Bruno Rijssman, Angela Sara Cacciapuoti, Marcello Caleffi, and Shota Nagayama, 2020, “Architectural principles for a quantum internet,” [10.17487/RFC9340](https://doi.org/10.17487/RFC9340).

Krastanov, Stefan, Victor V. Albert, and Liang Jiang, 2019, “Optimized entanglement purification,” *Quantum* **3**, 123.

Krutyanskiy, V., M. Meraner, J. Schupp, V. Krcmarsky, H. Hainzer, and B. P. Lanyon, 2019, “Light-matter entanglement over 50 km of optical fibre,” *npj Quantum Inf.* **5**, 72.

Krutyanskiy, Victor, Marco Canteri, Martin Meraner, James Bate, Vojtech Krcmarsky, Josef Schupp, Nicolas Sangouard, and Ben P. Lanyon, 2023, “Telecom-Wavelength Quantum Repeater Node Based on a Trapped-Ion Processor,” *Phys. Rev. Lett.* **130**, 213601.

Kwiat, P. G., 1997, “Hyper-entangled states,” *J. Mod. Opt.* **44**, 2173.

Lago-Rivera, Dario, Samuele Grandi, Jelena V. Rakonjac, Alessandro Seri, and Hugues de Riedmatten, 2021, “Telecom-heralded entanglement between multimode solid-state quantum memories,” *Nature (London)* **594**, 37–40.

Langenfeld, Stefan, Olivier Morin, Matthias Körber, and Gerhard Rempe, 2020, “A network-ready random-access qubits memory,” *npj Quantum Inf.* **6**, 86.

Langenfeld, Stefan, Philip Thomas, Olivier Morin, and Gerhard Rempe, 2021, “Quantum Repeater Node Demonstrating Unconditionally Secure Key Distribution,” *Phys. Rev. Lett.* **126**, 230506.

Lau, Hoi-Kwan, and Hoi-Kwong Lo, 2011, “Insecurity of position-based quantum-cryptography protocols against entanglement attacks,” *Phys. Rev. A* **83**, 012322.

Lauk, Nikolai, Neil Sinclair, Shabir Barzanjeh, Jacob P. Covey, Mark Saffman, Maria Spiropulu, and Christoph Simon, 2020, “Perspectives on quantum transduction,” *Quantum Sci. Technol.* **5**, 020501.

Laurenza, Riccardo, and Stefano Pirandola, 2017, “General bounds for sender-receiver capacities in multipoint quantum communications,” *Phys. Rev. A* **96**, 032318.

Lee, J. P., B. Villa, A. J. Bennett, R. M. Stevenson, D. J. P. Ellis, I. Farrer, D. A. Ritchie, and A. J. Shields, 2019, “A quantum dot as a source of time-bin entangled multi-photon states,” *Quantum Sci. Technol.* **4**, 025011.

Lee, J. P., L. M. Wells, B. Villa, S. Kalliakos, R. M. Stevenson, D. J. P. Ellis, I. Farrer, D. A. Ritchie, A. J. Bennett, and A. J. Shields, 2018, “Controllable Photonic Time-Bin Qubits from a Quantum dot,” *Phys. Rev. X* **8**, 021078.

Lee, Seung-Woo, Timothy C. Ralph, and Hyunseok Jeong, 2019, “Fundamental building block for all-optical scalable quantum networks,” *Phys. Rev. A* **100**, 052303.

Le Gall, François, Harumichi Nishimura, and Ansis Rosmanis, 2019, “Quantum advantage for the LOCAL model in distributed computing,” in *Proceedings of the 36th International Symposium on Theoretical Aspects of Computer Science (STACS 2019)*, Berlin, 2019, edited by Rolf Niedermeier and Christophe Paul (Schloss Dagstuhl-Leibniz-Zentrum fuer Informatik, Wadern, Germany), 10.4230/LIPIcs.STACS.2019.49.

Leghtas, Z., G. Kirchmair, B. Vlastakis, R. Schoelkopf, M. Devoret, and M. Mirrahimi, 2013, “Hardware-Efficient Autonomous Quantum Error Correction,” *Phys. Rev. Lett.* **111**, 120501.

Leon-Garcia, Alberto, and Martha Steenstrup, 2021, “The need for holistic network design,” *IEEE Commun. Mag.* **59**, 4–5.

Leung, Patrick M., and Timothy C. Ralph, 2006, “Quantum memory scheme based on optical fibers and cavities,” *Phys. Rev. A* **74**, 022311.

Levine, Harry, *et al.*, 2019, “Parallel Implementation of High-Fidelity Multiqubit Gates with Neutral Atoms,” *Phys. Rev. Lett.* **123**, 170503.

Li, Bikun, Sophia E. Economou, and Edwin Barnes, 2022, “Photonic resource state generation from a minimal number of quantum emitters,” *npj Quantum Inf.* **8**, 11.

Li, Hang, Jian-Peng Dou, Xiao-Ling Pang, Tian-Huai Yang, Chao-Ni Zhang, Yuan Chen, Jia-Ming Li, Ian A. Walmsley, and Xian-Min Jin, 2021, “Heralding quantum entanglement between two room-temperature atomic ensembles,” *Optica* **8**, 925–929.

Li, Linshu, Chang-Ling Zou, Victor V. Albert, Sreraman Muralidharan, S. M. Girvin, and Liang Jiang, 2017, “Cat Codes with Optimal Decoherence Suppression for a Lossy Bosonic Channel,” *Phys. Rev. Lett.* **119**, 030502.

Li, Wei, *et al.*, 2023, “Twin-Field Quantum Key Distribution without Phase Locking,” *Phys. Rev. Lett.* **130**, 250802.

Li, Ying, Sean D. Barrett, Thomas M. Stace, and Simon C. Benjamin, 2013, “Long range failure-tolerant entanglement distribution,” *New J. Phys.* **15**, 023012.

Li, Ying, Peter C. Humphreys, Gabriel J. Mendoza, and Simon C. Benjamin, 2015, “Resource Costs for Fault-Tolerant Linear Optical Quantum Computing,” *Phys. Rev. X* **5**, 041007.

Li, Zheng-Da, *et al.*, 2019, “Experimental quantum repeater without quantum memory,” *Nat. Photonics* **13**, 644–648.

Li, Zhuo, Li-Juan Xing, and Xin-Mei Wang, 2008, “Quantum generalized Reed-Solomon codes: Unified framework for quantum maximum-distance-separable codes,” *Phys. Rev. A* **77**, 012308.

Liao, Sheng-Kai, *et al.*, 2017, “Satellite-to-ground quantum key distribution,” *Nature (London)* **549**, 43.

Liao, Sheng-Kai, *et al.*, 2018, “Satellite-Relayed Intercontinental Quantum Network,” *Phys. Rev. Lett.* **120**, 030501.

Lidar, Daniel A., and Todd A. Brun, 2013, Eds., *Quantum Error Correction* (Cambridge University Press, Cambridge, England).

Lin, Jie, and Norbert Lütkenhaus, 2018, “Simple security analysis of phase-matching measurement-device-independent quantum key distribution,” *Phys. Rev. A* **98**, 042332.

Lindner, Netanel H., and Terry Rudolph, 2009, “Proposal for Pulsed On-Demand Sources of Photonic Cluster State Strings,” *Phys. Rev. Lett.* **103**, 113602.

Liorni, Carlo, Hermann Kampermann, and Dagmar Bruß, 2021, “Quantum repeaters in space,” *New J. Phys.* **23**, 053021.

Lita, Adriana E., Aaron J. Miller, and Sae Woo Nam, 2008, “Counting near-infrared single-photons with 95% efficiency,” *Opt. Express* **16**, 3032–3040.

Liu, Xiao, Jun Hu, Zong-Feng Li, Xue Li, Pei-Yun Li, Peng-Jun Liang, Zong-Quan Zhou, Chuan-Feng Li, and Guang-Can Guo, 2021, “Heralded entanglement distribution between two absorptive quantum memories,” *Nature (London)* **594**, 41–45.

Lo, Hoi-Kwong, 1997, “Insecurity of quantum secure computations,” *Phys. Rev. A* **56**, 1154.

Lo, Hoi-Kwong, 2000, “Classical-communication cost in distributed quantum-information processing: A generalization of quantum-communication complexity,” *Phys. Rev. A* **62**, 012313.

Lo, Hoi-Kwong, and H. F. Chau, 1999, “Unconditional security of quantum key distribution over arbitrarily long distances,” *Science* **283**, 2050–2056.

Lo, Hoi-Kwong, and Hoi Fung Chau, 1997, “Is Quantum Bit Commitment Really Possible?,” *Phys. Rev. Lett.* **78**, 3410.

Lo, Hoi-Kwong, and Hoi Fung Chau, 1998, “Why quantum bit commitment and ideal quantum coin tossing are impossible,” *Physica (Amsterdam)* **120D**, 177–187.

Lo, Hoi-Kwong, Marcos Curty, and Bing Qi, 2012, “Measurement-Device-Independent Quantum Key Distribution,” *Phys. Rev. Lett.* **108**, 130503.

Lo, Hoi-Kwong, Marcos Curty, and Kiyoshi Tamaki, 2014, “Secure quantum key distribution,” *Nat. Photonics* **8**, 595–604.

Lo, Hoi-Kwong, Xiongfeng Ma, and Kai Chen, 2005, “Decoy State Quantum Key Distribution,” *Phys. Rev. Lett.* **94**, 230504.

Lucamarini, M., Z. L. Yuan, J. F. Dynes, and A. J. Shields, 2018, “Overcoming the rate-distance limit of quantum key distribution without quantum repeaters,” *Nature (London)* **557**, 400–403.

Lukin, Daniil M., Melissa A. Giedry, and Jelena Vučković, 2020, “Integrated quantum photonics with silicon carbide: Challenges and prospects,” *PRX Quantum* **1**, 020102.

Luo, Yi-Han, *et al.*, 2019, “Quantum Teleportation in High Dimensions,” *Phys. Rev. Lett.* **123**, 070505.

Luong, David, Liang Jiang, Jungsang Kim, and Norbert Lütkenhaus, 2016, “Overcoming lossy channel bounds using a single quantum repeater node,” *Appl. Phys. B* **122**, 96.

Lütkenhaus, N., J. Calsamiglia, and K.-A. Suominen, 1999, “Bell measurements for teleportation,” *Phys. Rev. A* **59**, 3295.

Lvovsky, Alexander I., Barry C. Sanders, and Wolfgang Tittel, 2009, “Optical quantum memory,” *Nat. Photonics* **3**, 706–714.

Ma, Xiao-song, Stefan Zotter, Johannes Kofler, Thomas Jennewein, and Anton Zeilinger, 2011, “Experimental generation of single photons via active multiplexing,” *Phys. Rev. A* **83**, 043814.

Ma, Xiongfeng, and Mohsen Razavi, 2012, “Alternative schemes for measurement-device-independent quantum key distribution,” *Phys. Rev. A* **86**, 062319.

Ma, Xiongfeng, Pei Zeng, and Hongyi Zhou, 2018, "Phase-Matching Quantum Key Distribution," *Phys. Rev. X* **8**, 031043.

Ma, Yu, You-Zhi Ma, Zong-Quan Zhou, Chuan-Feng Li, and Guang-Can Guo, 2021, "One-hour coherent optical storage in an atomic frequency comb memory," *Nat. Commun.* **12**, 2381.

Maeda, Kento, Toshihiko Sasaki, and Masato Koashi, 2019, "Repeaterless quantum key distribution with efficient finite-key analysis overcoming the rate-distance limit," *Nat. Commun.* **10**, 3140.

Maiwald, Robert, Andrea Golla, Martin Fischer, Marianne Bader, Simon Heugel, Benoît Chalopin, Markus Sondermann, and Gerd Leuchs, 2012, "Collecting more than half the fluorescence photons from a single ion," *Phys. Rev. A* **86**, 043431.

Maring, Nicolas, Pau Farrera, Kutlu Kutluer, Margherita Mazzera, Georg Heinze, and Hugues de Riedmatten, 2017, "Photonic quantum state transfer between a cold atomic gas and a crystal," *Nature (London)* **551**, 485–488.

Marsili, F., *et al.*, 2013, "Detecting single infrared photons with 93% system efficiency," *Nat. Photonics* **7**, 210–214.

Martin, Leigh S., and K. Birgitta Whaley, 2019, "Single-shot deterministic entanglement between non-interacting systems with linear optics," *arXiv:1912.00067*.

Matsuo, Takaaki, Clément Durand, and Rodney Van Meter, 2019, "Quantum link bootstrapping using a RuleSet-based communication protocol," *Phys. Rev. A* **100**, 052320.

Matthiesen, Clemens, Martin Geller, Carsten H. H. Schulte, Claire Le Gall, Jack Hansom, Zhengyong Li, Maxime Hugues, Edmund Clarke, and Mete Atatüre, 2013, "Phase-locked indistinguishable photons with synthesized waveforms from a solid-state source," *Nat. Commun.* **4**, 1600.

Mayers, Dominic, 1997, "Unconditionally Secure Quantum Bit Commitment Is Impossible," *Phys. Rev. Lett.* **78**, 3414.

Mayers, Dominic, 2001, "Unconditional security in quantum cryptography," *J. Assoc. Comput. Mach.* **48**, 351–406.

Mayers, Dominic, and Andrew Yao, 1998, "Quantum cryptography with imperfect apparatus," in *Proceedings of the 39th Annual Symposium on Foundations of Computer Science (Cat. No. 98CB36280)*, Palo Alto, 1998 (IEEE, New York), pp. 503–509, [10.1109/SFCS.1998.743501](https://doi.org/10.1109/SFCS.1998.743501).

Mazurek, Paweł, Andrzej Grudka, Michał Horodecki, Paweł Horodecki, Justyna Łodyga, Łukasz Pankowski, and Anna Przysięzna, 2014, "Long-distance quantum communication over noisy networks without long-time quantum memory," *Phys. Rev. A* **90**, 062311.

McGuinness, Hayden J., Michael G. Raymer, Colin J. McKinstrie, and Stojan Radic, 2010, "Quantum Frequency Translation of Single-Photon States in a Photonic Crystal Fiber," *Phys. Rev. Lett.* **105**, 093604.

Menicucci, Nicolas C., Peter van Loock, Mile Gu, Christian Weedbrook, Timothy C. Ralph, and Michael A. Nielsen, 2006, "Universal Quantum Computation with Continuous-Variable Cluster States," *Phys. Rev. Lett.* **97**, 110501.

Michael, Marios H., Matti Silveri, R. T. Brierley, Victor V. Albert, Juha Salmilehto, Liang Jiang, and S. M. Girvin, 2016, "New Class of Quantum Error-Correcting Codes for a Bosonic Mode," *Phys. Rev. X* **6**, 031006.

Midgall, Alan L., D. Branning, and Stefania Castelletto, 2002, "Tailoring single-photon and multiphoton probabilities of a single-photon on-demand source," *Phys. Rev. A* **66**, 053805.

Miller, Johanna L., 2016, "Three groups close the loopholes in tests of Bell's theorem," *Phys. Today* **69**, No. 1, 14–16.

Minder, M., M. Pittaluga, G. L. Roberts, M. Lucamarini, J. F. Dynes, Z. L. Yuan, and A. J. Shields, 2019, "Experimental quantum key distribution beyond the repeaterless secret key capacity," *Nat. Photonics* **13**, 334–338.

Mirhosseini, Mohammad, Alp Sipahigil, Mahmoud Kalaei, and Oskar Painter, 2020, "Superconducting qubit to optical photon transduction," *Nature (London)* **588**, 599–603.

Mirrahimi, M., Z. Leghtas, Victor V. Albert, S. Touzard, R. Schoelkopf, L. Jiang, and M. Devoret, 2014, "Dynamically protected cat-qubits: A new paradigm for universal quantum computation," *New J. Phys.* **16**, 045014.

Mochon, Carlos, 2007, "Quantum weak coin flipping with arbitrarily small bias," *arXiv:0711.4114*.

Moehring, David L., Peter Maunz, Steve Olmschenk, Kelly C. Younge, Dzmitry N. Matsukevich, L.-M. Duan, and Christopher Monroe, 2007, "Entanglement of single-atom quantum bits at a distance," *Nature (London)* **449**, 68–71.

Munro, W. J., K. A. Harrison, A. M. Stephens, S. J. Devitt, and Kae Nemoto, 2010, "From quantum multiplexing to high-performance quantum networking," *Nat. Photonics* **4**, 792–796.

Munro, W. J., A. M. Stephens, S. J. Devitt, K. A. Harrison, and Kae Nemoto, 2012, "Quantum communication without the necessity of quantum memories," *Nat. Photonics* **6**, 777–781.

Munro, W. J., R. Van Meter, Sébastien G. R. Louis, and Kae Nemoto, 2008, "High-Bandwidth Hybrid Quantum Repeater," *Phys. Rev. Lett.* **101**, 040502.

Munro, William J., Koji Azuma, Kiyoshi Tamaki, and Kae Nemoto, 2015, "Inside quantum repeaters," *IEEE J. Sel. Top. Quantum Electron.* **21**, 78–90.

Munro, William J., Nicolo' Lo Piparo, Josephine Dias, Michael Hanks, and Kae Nemoto, 2022, "Designing tomorrow's quantum internet," *AVS Quantum Sci.* **4**, 020503.

Muralidharan, Sreraman, Jungsang Kim, Norbert Lütkenhaus, Mikhail D. Lukin, and Liang Jiang, 2014, "Ultrafast and Fault-Tolerant Quantum Communication across Long Distances," *Phys. Rev. Lett.* **112**, 250501.

Muralidharan, Sreraman, Linshu Li, Jungsang Kim, Norbert Lütkenhaus, Mikhail D. Lukin, and Liang Jiang, 2016, "Optimal architectures for long distance quantum communication," *Sci. Rep.* **6**, 20463.

Muralidharan, Sreraman, Chang-Ling Zou, Linshu Li, and Liang Jiang, 2018, "One-way quantum repeaters with quantum Reed-Solomon codes," *Phys. Rev. A* **97**, 052316.

Muralidharan, Sreraman, Chang-Ling Zou, Linshu Li, Jianming Wen, and Liang Jiang, 2017, "Overcoming erasure errors with multilevel systems," *New J. Phys.* **19**, 013026.

Murta, Gláucia, Federico Grasselli, Hermann Kampermann, and Dagmar Bruß, 2020, "Quantum conference key agreement: A review," *Adv. Quantum Technol.* **3**, 2000025.

Nadlinger, D. P., *et al.*, 2022, "Experimental quantum key distribution certified by Bell's theorem," *Nature (London)* **607**, 682–686.

Neu, Elke, Martin Fischer, Stefan Gsell, Matthias Schreck, and Christoph Becher, 2011, "Fluorescence and polarization spectroscopy of single silicon vacancy centers in heteroepitaxial nano-diamonds on iridium," *Phys. Rev. B* **84**, 205211.

Neu, Elke, David Steinmetz, Janine Riedrich-Möller, Stefan Gsell, Martin Fischer, Matthias Schreck, and Christoph Becher, 2011, "Single photon emission from silicon-vacancy colour centres in chemical vapour deposition nano-diamonds on iridium," *New J. Phys.* **13**, 025012.

Nguyen, C. T., *et al.*, 2019a, "An integrated nanophotonic quantum register based on silicon-vacancy spins in diamond," *Phys. Rev. B* **100**, 165428.

Nguyen, C. T., *et al.*, 2019b, "Quantum Network Nodes Based on Diamond Qubits with an Efficient Nanophotonic Interface," *Phys. Rev. Lett.* **123**, 183602.

Nickerson, Naomi H., Joseph F. Fitzsimons, and Simon C. Benjamin, 2014, “Freely Scalable Quantum Technologies Using Cells of 5-to-50 Qubits with Very Lossy and Noisy Photonic Links,” *Phys. Rev. X* **4**, 041041.

Nickerson, Naomi H., Ying Li, and Simon C. Benjamin, 2013, “Topological quantum computing with a very noisy network and local error rates approaching one percent,” *Nat. Commun.* **4**, 1756.

Nielsen, Michael A., 2004, “Optical Quantum Computation Using Cluster States,” *Phys. Rev. Lett.* **93**, 040503.

Nielsen, Michael A., and Isaac L. Chuang, 2010, *Quantum Computation and Quantum Information: 10th Anniversary Edition* (Cambridge University Press, Cambridge, England).

Niset, Julien, Jaromír Fiurášek, and Nicolas J. Cerf, 2009, “No-Go Theorem for Gaussian Quantum Error Correction,” *Phys. Rev. Lett.* **102**, 120501.

NIST, 2021, “Post-quantum cryptography,” <https://csrc.nist.gov/projects/post-quantum-cryptography>.

Niu, Daocheng, Yuxuan Zhang, Alireza Shabani, and Hassan Shapourian, 2023, “All-photonic one-way quantum repeaters with measurement-based error correction,” *npj Quantum Inf.* **9**, 106.

Noh, Kyungjoo, Victor V. Albert, and Liang Jiang, 2019, “Quantum capacity bounds of Gaussian thermal loss channels and achievable rates with Gottesman-Kitaev-Preskill codes,” *IEEE Trans. Inf. Theory* **65**, 2563–2582.

Noh, Kyungjoo, and Christopher Chamberland, 2020, “Fault-tolerant bosonic quantum error correction with the surface–Gottesman–Kitaev–Preskill code,” *Phys. Rev. A* **101**, 012316.

Noh, Kyungjoo, S. M. Girvin, and Liang Jiang, 2020, “Encoding an Oscillator into Many Oscillators,” *Phys. Rev. Lett.* **125**, 080503.

Olbrich, Fabian, Jonatan Höschele, Markus Müller, Jan Kettler, Simone Luca Portalupi, Matthias Paul, Michael Jetter, and Peter Michler, 2017, “Polarization-entangled photons from an InGaAs-based quantum dot emitting in the telecom C-band,” *Appl. Phys. Lett.* **111**, 133106.

Palyanov, Yuri N., Igor N. Kupriyanov, Yuri M. Borzdov, and Nikolay V. Surovtsev, 2015, “Germanium: A new catalyst for diamond synthesis and a new optically active impurity in diamond,” *Sci. Rep.* **5**, 14789.

Pan, Jian-Wei, Dik Bouwmeester, Harald Weinfurter, and Anton Zeilinger, 1998, “Experimental Entanglement Swapping: Entangling Photons That Never Interacted,” *Phys. Rev. Lett.* **80**, 3891–3894.

Pan, Jian-Wei, Sara Gasparoni, Rupert Ursin, Gregor Weihs, and Anton Zeilinger, 2003, “Experimental entanglement purification of arbitrary unknown states,” *Nature (London)* **423**, 417–422.

Pan, Jian-Wei, Christoph Simon, Časlav Brukner, and Anton Zeilinger, 2001, “Entanglement purification for quantum communication,” *Nature (London)* **410**, 1067.

Panayi, Christiana, Mohsen Razavi, Xiongfeng Ma, and Norbert Lütkenhaus, 2014, “Memory-assisted measurement-device-independent quantum key distribution,” *New J. Phys.* **16**, 043005.

Pang, Xiao-Ling, *et al.*, 2020, “A hybrid quantum memory–enabled network at room temperature,” *Sci. Adv.* **6**, eaax1425.

Pant, Mihir, Hari Krovi, Dirk Englund, and Saikat Guha, 2017, “Rate-distance tradeoff and resource costs for all-optical quantum repeaters,” *Phys. Rev. A* **95**, 012304.

Park, Jiho, Heonoh Kim, and Han Seb Moon, 2019, “Polarization-Entangled Photons from a Warm Atomic Ensemble Using a Sagnac Interferometer,” *Phys. Rev. Lett.* **122**, 143601.

Peev, Momtchil, *et al.*, 2009, “The SECOQC quantum key distribution network in Vienna,” *New J. Phys.* **11**, 075001.

Pegg, David T., Lee S. Phillips, and Stephen M. Barnett, 1998, “Optical State Truncation by Projection Synthesis,” *Phys. Rev. Lett.* **81**, 1604–1606.

Pichler, Hannes, Soonwon Choi, Peter Zoller, and Mikhail D. Lukin, 2017, “Universal photonic quantum computation via time-delayed feedback,” *Proc. Natl. Acad. Sci. U.S.A.* **114**, 11362–11367.

Pingault, Benjamin, David-Dominik Jarausch, Christian Hepp, Lina Klintberg, Jonas N. Becker, Matthew Markham, Christoph Becher, and Mete Atatüre, 2017, “Coherent control of the silicon-vacancy spin in diamond,” *Nat. Commun.* **8**, 15579.

Piparo, Nicoló Lo, Mohsen Razavi, and William J. Munro, 2017a, “Measurement-device-independent quantum key distribution with nitrogen vacancy centers in diamond,” *Phys. Rev. A* **95**, 022338.

Piparo, Nicoló Lo, Mohsen Razavi, and William J. Munro, 2017b, “Memory-assisted quantum key distribution with a single nitrogen-vacancy center,” *Phys. Rev. A* **96**, 052313.

Piparo, Nicoló Lo, Mohsen Razavi, and Christiana Panayi, 2015, “Measurement-device-independent quantum key distribution with ensemble-based memories,” *IEEE J. Sel. Top. Quantum Electron.* **21**, 138–147.

Pirandola, S., *et al.*, 2020, “Advances in quantum cryptography,” *Adv. Opt. Photonics* **12**, 1012–1236.

Pirandola, Stefano, 2016, “Capacities of repeater-assisted quantum communications,” [arXiv:1601.00966](https://arxiv.org/abs/1601.00966).

Pirandola, Stefano, 2019, “End-to-end capacities of a quantum communication network,” *Commun. Phys.* **2**, 51.

Pirandola, Stefano, Riccardo Laurenza, Carlo Ottaviani, and Leonardo Banchi, 2017, “Fundamental limits of repeaterless quantum communications,” *Nat. Commun.* **8**, 15043.

Pirker, Alexander, and Wolfgang Dür, 2019, “A quantum network stack and protocols for reliable entanglement-based networks,” *New J. Phys.* **21**, 033003.

Pittaluga, Mirko, Mariella Minder, Marco Lucamarini, Mirko Sanzaro, Robert I. Woodward, Ming-Jun Li, Zhiliang Yuan, and Andrew J. Shields, 2021, “600-km repeater-like quantum communications with dual-band stabilization,” *Nat. Photonics* **15**, 530–535.

Pittman, T. B., B. C. Jacobs, and J. D. Franson, 2001, “Probabilistic quantum logic operations using polarizing beam splitters,” *Phys. Rev. A* **64**, 062311.

Plenio, Martin B., and Shashank Virmani, 2007, “An introduction to entanglement measures,” *Quantum Inf. Comput.* **7**, 1–51.

Pompili, M., *et al.*, 2021, “Realization of a multinode quantum network of remote solid-state qubits,” *Science* **372**, 259–264.

Pompili, Matteo, *et al.*, 2022, “Experimental demonstration of entanglement delivery using a quantum network stack,” *npj Quantum Inf.* **8**, 121.

Portmann, Christopher, and Renato Renner, 2022, “Security in quantum cryptography,” *Rev. Mod. Phys.* **94**, 025008.

Pu, Yun-Fei, Sheng Zhang, Yu-Kai Wu, Nan Jiang, Wei Chang, Chang Li, and Lu-Ming Duan, 2021, “Experimental demonstration of memory-enhanced scaling for entanglement connection of quantum repeater segments,” *Nat. Photonics* **15**, 374–378.

Quantum Protocol Zoo, 2019, <https://wiki.veriqloud.fr>.

Quesada, N., L. G. Helt, J. Izaac, J. M. Arrazola, R. Shahrokhsahai, C. R. Myers, and K. K. Sabapathy, 2019, “Simulating realistic non-Gaussian state preparation,” *Phys. Rev. A* **100**, 022341.

Ralph, T. C., A. J. F. Hayes, and A. Gilchrist, 2005, “Loss-Tolerant Optical Qubits,” *Phys. Rev. Lett.* **95**, 100501.

Ralph, Timothy C., and A. P. Lund, 2009, “Nondeterministic noiseless linear amplification of quantum systems,” *AIP Conf. Proc.* **1110**, 155–160.

Rančić, Miloš, Morgan P. Hedges, Rose L. Ahlefeldt, and Matthew J. Sellars, 2018, “Coherence time of over a second in a telecom-compatible quantum memory storage material,” *Nat. Phys.* **14**, 50–54.

Raussendorf, R., J. Harrington, and K. Goyal, 2006, “A fault-tolerant one-way quantum computer,” *Ann. Phys. (Amsterdam)* **321**, 2242–2270.

Raussendorf, R., J. Harrington, and K. Goyal, 2007, “Topological fault-tolerance in cluster state quantum computation,” *New J. Phys.* **9**, 199.

Raussendorf, Robert, and Hans J. Briegel, 2001, “A One-Way Quantum Computer,” *Phys. Rev. Lett.* **86**, 5188–5191.

Raussendorf, Robert, and Jim Harrington, 2007, “Fault-Tolerant Quantum Computation with High Threshold in Two Dimensions,” *Phys. Rev. Lett.* **98**, 190504.

Razavi, M., M. Piani, and N. Lütkenhaus, 2009, “Quantum repeaters with imperfect memories: Cost and scalability,” *Phys. Rev. A* **80**, 032301.

Razavi, M., K. Thompson, H. Farmanbar, Ma. Piani, and Norbert Lütkenhaus, 2009, “Physical and architectural considerations in quantum repeaters,” *Proc. SPIE Int. Soc. Opt. Eng.* **7236**, 723603–723613.

Razavi, Mohsen, 2018, *An Introduction to Quantum Communications Networks* (Morgan & Claypool Publishers, San Rafael, CA).

Redjem, W., *et al.*, 2020, “Single artificial atoms in silicon emitting at telecom wavelengths,” *Nat. Electron.* **3**, 738–743.

Reichle, Rainer, Dietrich Leibfried, Emanuel Knill, Joseph Britton, R. B. Blakestad, John D. Jost, Christopher Langer, R. Ozeri, Signe Seidelin, and David J. Wineland, 2006, “Experimental purification of two-atom entanglement,” *Nature (London)* **443**, 838–841.

Reiserer, Andreas, Norbert Kalb, Gerhard Rempe, and Stephan Ritter, 2014, “A quantum gate between a flying optical photon and a single trapped atom,” *Nature (London)* **508**, 237–240.

Reiserer, Andreas, and Gerhard Rempe, 2015, “Cavity-based quantum networks with single atoms and optical photons,” *Rev. Mod. Phys.* **87**, 1379–1418.

Renner, Renato, 2008, “Security of quantum key distribution,” *Int. J. Quantum Inf.* **06**, 1–127.

Riedel, Daniel, Immo Söllner, Brendan J. Shields, Sebastian Starosielec, Patrick Appel, Elke Neu, Patrick Maletinsky, and Richard J. Warburton, 2017, “Deterministic Enhancement of Coherent Photon Generation from a Nitrogen-Vacancy Center in Ultrapure Diamond,” *Phys. Rev. X* **7**, 031040.

Riedl, Stefan, Matthias Lettner, Christoph Vo, Simon Baur, Gerhard Rempe, and Stephan Dürr, 2012, “Bose-Einstein condensate as a quantum memory for a photonic polarization qubit,” *Phys. Rev. A* **85**, 022318.

Riera-Sàbat, F., P. Sekatski, A. Pirker, and W. Dür, 2021, “Entanglement-Assisted Entanglement Purification,” *Phys. Rev. Lett.* **127**, 040502.

Rigovacca, Luca, Go Kato, Stefan Bäuml, Myungshik S. Kim, William J. Munro, and Koji Azuma, 2018, “Versatile relative entropy bounds for quantum networks,” *New J. Phys.* **20**, 013033.

Rivest, Ronald L., Adi Shamir, and Leonard Adleman, 1978, “A method for obtaining digital signatures and public-key cryptosystems,” *Commun. ACM* **21**, 120–126.

Roche, Calum, 2022, “How much money did CERN’s Large Hadron Collider cost to build and who paid for it?,” [https://en.as.com/latest\\_news/how-much-money-did-cerns-large-hadron-collider-cost-to-build-and-who-paid-for-it.n](https://en.as.com/latest_news/how-much-money-did-cerns-large-hadron-collider-cost-to-build-and-who-paid-for-it.n).

Rozpędek, Filip, Kenneth Goodenough, Jeremy Ribeiro, Norbert Kalb, V. Caprara Vivoli, Andreas Reiserer, Ronald Hanson, Stephanie Wehner, and David Elkouss, 2018, “Parameter regimes for a single sequential quantum repeater,” *Quantum Sci. Technol.* **3**, 034002.

Rozpędek, Filip, Kyungjoo Noh, Qian Xu, Saikat Guha, and Liang Jiang, 2021, “Quantum repeaters based on concatenated bosonic and discrete-variable quantum codes,” *npj Quantum Inf.* **7**, 102.

Rozpędek, Filip, Raja Yehia, Kenneth Goodenough, Maximilian Ruf, Peter C. Humphreys, Ronald Hanson, Stephanie Wehner, and David Elkouss, 2019, “Near-term quantum-repeater experiments with nitrogen-vacancy centers: Overcoming the limitations of direct transmission,” *Phys. Rev. A* **99**, 052330.

Ruf, Maximilian, Noel H. Wan, Hyeongrak Choi, Dirk Englund, and Ronald Hanson, 2021, “Quantum networks based on color centers in diamond,” *J. Appl. Phys.* **130**, 070901.

Russo, Antonio, Edwin Barnes, and Sophia E. Economou, 2018, “Photonic graph state generation from quantum dots and color centers for quantum communications,” *Phys. Rev. B* **98**, 085303.

Russo, Antonio, Edwin Barnes, and Sophia E. Economou, 2019, “Generation of arbitrary all-photonic graph states from quantum emitters,” *New J. Phys.* **21**, 055002.

Sabapathy, Krishna Kumar, Haoyu Qi, Josh Izaac, and Christian Weedbrook, 2019, “Production of photonic universal quantum gates enhanced by machine learning,” *Phys. Rev. A* **100**, 012326.

Salvail, Louis, Momtchil Peev, Eleni Diamanti, Romain Alléaume, Norbert Lütkenhaus, and Thomas Länger, 2010, “Security of trusted repeater quantum key distribution networks,” *J. Comput. Secur.* **18**, 61–87.

Sangouard, Nicolas, Romain Dubessy, and Christoph Simon, 2009, “Quantum repeaters based on single trapped ions,” *Phys. Rev. A* **79**, 042340.

Sangouard, Nicolas, Christoph Simon, Hugues de Riedmatten, and Nicolas Gisin, 2011, “Quantum repeaters based on atomic ensembles and linear optics,” *Rev. Mod. Phys.* **83**, 33–80.

Sasaki, M., *et al.*, 2011, “Field test of quantum key distribution in the Tokyo QKD network,” *Opt. Express* **19**, 10387–10409.

Sasaki, Masahide, Kentaro Kato, Masayuki Izutsu, and Osamu Hirota, 1998, “Quantum channels showing superadditivity in classical capacity,” *Phys. Rev. A* **58**, 146.

Sasaki, Toshihiko, Yoshihisa Yamamoto, and Masato Koashi, 2014, “Practical quantum key distribution protocol without monitoring signal disturbance,” *Nature (London)* **509**, 475–478.

Schaffner, Christian, 2010, “Simple protocols for oblivious transfer and secure identification in the noisy-quantum-storage model,” *Phys. Rev. A* **82**, 032308.

Schaibley, J. R., A. P. Burgers, G. A. McCracken, L.-M. Duan, P. R. Berman, D. G. Steel, A. S. Bracker, D. Gammon, and L. J. Sham, 2013, “Demonstration of Quantum Entanglement between a Single Electron Spin Confined to an InAs Quantum Dot and a Photon,” *Phys. Rev. Lett.* **110**, 167401.

Schön, C., E. Solano, F. Verstraete, J. I. Cirac, and M. M. Wolf, 2005, “Sequential Generation of Entangled Multiqubit States,” *Phys. Rev. Lett.* **95**, 110503.

Schrödinger, E., 1935, “Discussion of probability relations between separated systems,” *Math. Proc. Cambridge Philos. Soc.* **31**, 555–563.

Schwartz, Ido, Dan Cogan, Emma R. Schmidgall, Yaroslav Don, Liron Gantz, Oded Kenneth, Netanel H. Lindner, and David Gershoni, 2016, “Deterministic generation of a cluster state of entangled photons,” *Science* **354**, 434–437.

Scully, Marlan O., and M. Suhail Zubairy, 1997, *Quantum Optics* (Cambridge University Press, Cambridge, England).

Senellart, Pascale, Glenn Solomon, and Andrew White, 2017, “High-performance semiconductor quantum-dot single-photon sources,” *Nat. Nanotechnol.* **12**, 1026–1039.

Seshadreesan, Kaushik P., Hari Krovi, and Saikat Guha, 2020, “Continuous-variable quantum repeater based on quantum scissors and mode multiplexing,” *Phys. Rev. Res.* **2**, 013310.

Seshadreesan, Kaushik P., Masahiro Takeoka, and Mark M. Wilde, 2016, “Bounds on entanglement distillation and secret key agreement for quantum broadcast channels,” *IEEE Trans. Inf. Theory* **62**, 2849–2866.

Shaham, Roy, Or Katz, and Ofer Firstenberg, 2022, “Strong coupling of alkali-metal spins to noble-gas spins with an hour-long coherence time,” *Nat. Phys.* **18**, 506–510.

Sheng, Yu-Bo, and Fu-Guo Deng, 2010, “Deterministic entanglement purification and complete nonlocal Bell-state analysis with hyperentanglement,” *Phys. Rev. A* **81**, 032307.

Sheng, Yu-Bo, Lan Zhou, and Gui-Lu Long, 2013, “Hybrid entanglement purification for quantum repeaters,” *Phys. Rev. A* **88**, 022302.

Shibata, H., H. Takesue, T. Honjo, T. Akazaki, and Y. Tokura, 2010, “Single-photon detection using magnesium diboride superconducting nanowires,” *Appl. Phys. Lett.* **97**, 212504.

Shibata, Hiroyuki, Toshimori Honjo, and Kaoru Shimizu, 2014, “Quantum key distribution over a 72 db channel loss using ultralow dark count superconducting single-photon detectors,” *Opt. Lett.* **39**, 5078–5081.

Shor, Peter W., 1997, “Polynomial-time algorithms for prime factorization and discrete logarithms on a quantum computer,” *SIAM J. Comput.* **26**, 1484–1509.

Shor, Peter W., and John Preskill, 2000, “Simple Proof of Security of the BB84 Quantum Key Distribution Protocol,” *Phys. Rev. Lett.* **85**, 441–444.

Simon, C., *et al.*, 2010, “Quantum memories: A review based on the European integrated project ‘Qubit applications (QAP),’” *Eur. Phys. J. D* **58**, 1–22.

Sinclair, Neil, *et al.*, 2014, “Spectral Multiplexing for Scalable Quantum Photonics Using an Atomic Frequency Comb Quantum Memory and Feed-Forward Control,” *Phys. Rev. Lett.* **113**, 053603.

Sipahigil, Alp, Kay D. Jahnke, Lachlan J. Rogers, Tokuyuki Teraji, Junichi Isoya, Alexander S. Zibrov, Fedor Jelezko, and Mikhail D. Lukin, 2014, “Indistinguishable Photons from Separated Silicon-Vacancy Centers in Diamond,” *Phys. Rev. Lett.* **113**, 113602.

Slodička, L., G. Hétet, N. Röck, P. Schindler, M. Hennrich, and R. Blatt, 2013, “Atom-Atom Entanglement by Single-Photon Detection,” *Phys. Rev. Lett.* **110**, 083603.

Somaschi, N., *et al.*, 2016, “Near-optimal single-photon sources in the solid state,” *Nat. Photonics* **10**, 340–345.

Stace, Thomas M., Sean D. Barrett, and Andrew C. Doherty, 2009, “Thresholds for Topological Codes in the Presence of Loss,” *Phys. Rev. Lett.* **102**, 200501.

Stephenson, L. J., D. P. Nadlinger, B. C. Nichol, S. An, P. Drmota, T. G. Ballance, K. Thirumalai, J. F. Goodwin, D. M. Lucas, and C. J. Ballance, 2020, “High-Rate, High-Fidelity Entanglement of Qubits across an Elementary Quantum Network,” *Phys. Rev. Lett.* **124**, 110501.

Stinaff, Eric A., Michael Scheibner, Allan S. Bracker, Ilya V. Ponomarev, Vladimir L. Korenev, Morgan E. Ware, Matt F. Doty, Thomas L. Reinecke, and Dan Gammon, 2006, “Optical signatures of coupled quantum dots,” *Science* **311**, 636–639.

Stockill, Robert, M. J. Stanley, Lukas Huthmacher, E. Clarke, M. Hugues, A. J. Miller, C. Matthiesen, C. Le Gall, and Mete Atatüre, 2017, “Phase-Tuned Entangled State Generation between Distant Spin Qubits,” *Phys. Rev. Lett.* **119**, 010503.

Stucki, Damien, *et al.*, 2011, “Long-term performance of the SwissQuantum quantum key distribution network in a field environment,” *New J. Phys.* **13**, 123001.

Su, Daiqin, Casey R. Myers, and Krishna Kumar Sabapathy, 2019, “Conversion of Gaussian states to non-Gaussian states using photon-number-resolving detectors,” *Phys. Rev. A* **100**, 052301.

Sukachev, Denis D., Alp Sipahigil, Christian T. Nguyen, Mihir K. Bhaskar, Ruffin E. Evans, Fedor Jelezko, and Mikhail D. Lukin, 2017, “Silicon-Vacancy Spin Qubit in Diamond: A Quantum Memory Exceeding 10 ms with Single-Shot State Readout,” *Phys. Rev. Lett.* **119**, 223602.

Sun, Shuo, Hyochul Kim, Glenn S. Solomon, and Edo Waks, 2016, “A quantum phase switch between a single solid-state spin and a photon,” *Nat. Nanotechnol.* **11**, 539–544.

Takeoka, Masahiro, Saikat Guha, and Mark M. Wilde, 2014a, “Fundamental rate-loss tradeoff for optical quantum key distribution,” *Nat. Commun.* **5**, 5235.

Takeoka, Masahiro, Saikat Guha, and Mark M. Wilde, 2014b, “The squashed entanglement of a quantum channel,” *IEEE Trans. Inf. Theory* **60**, 4987–4998.

Takeoka, Masahiro, Kaushik P. Seshadreesan, and Mark M. Wilde, 2017, “Unconstrained Capacities of Quantum Key Distribution and Entanglement Distillation for Pure-Loss Bosonic Broadcast Channels,” *Phys. Rev. Lett.* **119**, 150501.

Tamaki, Kiyoshi, Marcos Curty, Go Kato, Hoi-Kwong Lo, and Koji Azuma, 2014, “Loss-tolerant quantum cryptography with imperfect sources,” *Phys. Rev. A* **90**, 052314.

Tamaki, Kiyoshi, Hoi-Kwong Lo, Chi-Hang Fred Fung, and Bing Qi, 2012, “Phase encoding schemes for measurement-device-independent quantum key distribution with basis-dependent flaw,” *Phys. Rev. A* **85**, 042307.

Tamaki, Kiyoshi, Hoi-Kwong Lo, Wenyuan Wang, and Marco Lucamarini, 2018, “Information theoretic security of quantum key distribution overcoming the repeaterless secret key capacity bound,” *arXiv:1805.05511*.

Taminiau, T. H., J. J. T. Wagenaar, T. Van der Sar, Fedor Jelezko, Viatcheslav V. Dobrovitski, and R. Hanson, 2012, “Detection and Control of Individual Nuclear Spins Using a Weakly Coupled Electron Spin,” *Phys. Rev. Lett.* **109**, 137602.

Tan, Ting Rei, John P. Gaebler, Yiheng Lin, Yong Wan, R. Bowler, D. Leibfried, and David J. Wineland, 2015, “Multi-element logic gates for trapped-ion qubits,” *Nature (London)* **528**, 380–383.

Tani, Seiichiro, Hirotada Kobayashi, and Keiji Matsumoto, 2005, “Exact quantum algorithms for the leader election problem,” in *Proceedings of the 22nd Annual Symposium on Theoretical Aspects of Computer Science, Stuttgart, 2005*, edited by Volker Diekert and B. Durand (Springer, New York), pp. 581–592, [10.1007/978-3-540-31856-9\\_48](https://doi.org/10.1007/978-3-540-31856-9_48).

Tanzilli, S., W. Tittel, M. Halder, O. Alibart, P. Baldi, N. Gisin, and H. Zbinden, 2005, “A photonic quantum information interface,” *Nature (London)* **437**, 116–120.

Tchebotareva, Anna, *et al.*, 2019, “Entanglement between a Diamond Spin Qubit and a Photonic Time-Bin Qubit at Telecom Wavelength,” *Phys. Rev. Lett.* **123**, 063601.

Terhal, Barbara M., 2015, “Quantum error correction for quantum memories,” *Rev. Mod. Phys.* **87**, 307–346.

Thomas, Philip, Leonardo Ruscio, Olivier Morin, and Gerhard Rempe, 2022, “Efficient generation of entangled multiphoton graph states from a single atom,” *Nature (London)* **608**, 677–681.

Togan, E., *et al.*, 2010, “Quantum entanglement between an optical photon and a solid-state spin qubit,” *Nature (London)* **466**, 730–734.

Tomm, Natasha, *et al.*, 2021, “A bright and fast source of coherent single photons,” *Nat. Nanotechnol.* **16**, 399–403.

Townsend, Kevin, 2022, "NIST post-quantum algorithm finalist cracked using a classical PC," <https://www.securityweek.com/nist-post-quantum-algorithm-finalist-cracked-using-classical-pc>.

Townsend, Paul D., 1997, "Quantum cryptography on multiuser optical fibre networks," *Nature (London)* **385**, 47–49.

Trényi, Róbert, Koji Azuma, and Marcos Curty, 2019, "Beating the repeaterless bound with adaptive measurement-device-independent quantum key distribution," *New J. Phys.* **21**, 113052.

Trusheim, Matthew E., *et al.*, 2020, "Transform-Limited Photons from a Coherent Tin-Vacancy Spin in Diamond," *Phys. Rev. Lett.* **124**, 023602.

Tzitrin, Ilan, 2018, "Local equivalence of complete bipartite and repeater graph states," *Phys. Rev. A* **98**, 032305.

Tzitrin, Ilan, J. Eli Bourassa, Nicolas C. Menicucci, and Krishna Kumar Sabapathy, 2020, "Progress towards practical qubit computation using approximate Gottesman-Kitaev-Preskill codes," *Phys. Rev. A* **101**, 032315.

Tzitrin, Ilan, Takaya Matsuura, Rafael N. Alexander, Guillaume Dauphinain, J. Eli Bourassa, Krishna K. Sabapathy, Nicolas C. Menicucci, and Ish Dhand, 2021, "Fault-tolerant quantum computation with static linear optics," *PRX Quantum* **2**, 040353.

Uppu, Ravitej, *et al.*, 2020, "Scalable integrated single-photon source," *Sci. Adv.* **6**, eabc8268.

Ursin, Rupert, *et al.*, 2007, "Entanglement-based quantum communication over 144 km," *Nat. Phys.* **3**, 481.

Vaidman, Lev, 2003, "Instantaneous Measurement of Nonlocal Variables," *Phys. Rev. Lett.* **90**, 010402.

van Leent, Tim, Matthias Bock, Robert Garthoff, Kai Redeker, Wei Zhang, Tobias Bauer, Benjamin Rosenfeld, Christoph Becher, and Harald Weinfurter, 2020, "Long-Distance Distribution of Atom-Photon Entanglement at Telecom Wavelength," *Phys. Rev. Lett.* **124**, 010510.

van Leent, Tim, *et al.*, 2022, "Entangling single atoms over 33 km telecom fibre," *Nature (London)* **607**, 69–73.

van Loock, P., T. D. Ladd, K. Sanaka, F. Yamaguchi, Kae Nemoto, W. J. Munro, and Y. Yamamoto, 2006, "Hybrid Quantum Repeater Using Bright Coherent Light," *Phys. Rev. Lett.* **96**, 240501.

Van Meter, Rodney, 2014, *Quantum Networking* (John Wiley & Sons, New York).

Van Meter, Rodney, Thaddeus D. Ladd, William J. Munro, and Kae Nemoto, 2009, "System design for a long-line quantum repeater," *IEEE/ACM Trans. Networking* **17**, 1002–1013.

Van Meter, Rodney, and Joe Touch, 2013, "Designing quantum repeater networks," *IEEE Commun. Mag.* **51**, 64–71.

Varnava, Michael, Daniel E. Browne, and Terry Rudolph, 2006, "Loss Tolerance in One-Way Quantum Computation via Counterfactual Error Correction," *Phys. Rev. Lett.* **97**, 120501.

Varnava, Michael, Daniel E. Browne, and Terry Rudolph, 2007, "Loss tolerant linear optical quantum memory by measurement-based quantum computing," *New J. Phys.* **9**, 203.

Varnava, Michael, Daniel E. Browne, and Terry Rudolph, 2008, "How Good Must Single Photon Sources and Detectors Be for Efficient Linear Optical Quantum Computation?," *Phys. Rev. Lett.* **100**, 060502.

Vasconcelos, Rui, Sarah Reisenbauer, Cameron Salter, Georg Wachter, Daniel Wirtitsch, Jörg Schmiedmayer, Philip Walther, and Michael Trupke, 2020, "Scalable spin-photon entanglement by time-to-polarization conversion," *npj Quantum Inf.* **6**, 9.

Vezvaei, Arian, Paul Hilaire, Matthew F. Doty, and Sophia E. Economou, 2022, "Deterministic Generation of Entangled Photonic Cluster States from Quantum Dot Molecules," *Phys. Rev. Appl.* **18**, L061003.

Volz, Jürgen, Markus Weber, Daniel Schlenk, Benjamin Rosenfeld, Johannes Vrana, Karen Saucke, Christian Kurtsiefer, and Harald Weinfurter, 2006, "Observation of Entanglement of a Single Photon with a Trapped Atom," *Phys. Rev. Lett.* **96**, 030404.

Waks, Edo, Assaf Zeevi, and Yoshihisa Yamamoto, 2002, "Security of quantum key distribution with entangled photons against individual attacks," *Phys. Rev. A* **65**, 052310.

Waldherr, Gerald, *et al.*, 2014, "Quantum error correction in a solid-state hybrid spin register," *Nature (London)* **506**, 204–207.

Wallnöfer, Julius, Frederik Hahn, Mustafa Gündoğan, Jasminder S. Sidhu, Fabian Wiesner, Nathan Walk, Jens Eisert, and Janik Wolters, 2022, "Simulating quantum repeater strategies for multiple satellites," *Commun. Phys.* **5**, 169.

Walls, Daniel F., and Gerard J. Milburn, 2007, *Quantum Optics* (Springer Science+Business Media, New York).

Wan, Noel H., *et al.*, 2020, "Large-scale integration of artificial atoms in hybrid photonic circuits," *Nature (London)* **583**, 226–231.

Wang, Hui, *et al.*, 2019, "Towards optimal single-photon sources from polarized microcavities," *Nat. Photonics* **13**, 770–775.

Wang, Pengfei, Chun-Yang Luan, Mu Qiao, Mark Um, Junhua Zhang, Ye Wang, Xiao Yuan, Mile Gu, Jingning Zhang, and Kihwan Kim, 2021, "Single ion qubit with estimated coherence time exceeding one hour," *Nat. Commun.* **12**, 233.

Wang, Shuang, De-Yong He, Zhen-Qiang Yin, Feng-Yu Lu, Chao-Han Cui, Wei Chen, Zheng Zhou, Guang-Can Guo, and Zheng-Fu Han, 2019, "Beating the Fundamental Rate-Distance Limit in a Proof-of-Principle Quantum Key Distribution System," *Phys. Rev. X* **9**, 021046.

Wang, Shuang, *et al.*, 2022, "Twin-field quantum key distribution over 830-km fibre," *Nat. Photonics* **16**, 154–161.

Wang, Xiang-Bin, 2005, "Beating the Photon-Number-Splitting Attack in Practical Quantum Cryptography," *Phys. Rev. Lett.* **94**, 230503.

Wang, Xiang-Bin, Zong-Wen Yu, and Xiao-Long Hu, 2018, "Twin-field quantum key distribution with large misalignment error," *Phys. Rev. A* **98**, 062323.

Wang, Ye, Mark Um, Junhua Zhang, Shuoming An, Ming Lyu, Jing-Ning Zhang, L.-M. Duan, Dahyun Yum, and Kihwan Kim, 2017, "Single-qubit quantum memory exceeding ten-minute coherence time," *Nat. Photonics* **11**, 646.

Wehner, Stephanie, Marcos Curty, Christian Schaffner, and Hoi-Kwong Lo, 2010, "Implementation of two-party protocols in the noisy-storage model," *Phys. Rev. A* **81**, 052336.

Wehner, Stephanie, David Elkouss, and Ronald Hanson, 2018, "Quantum internet: A vision for the road ahead," *Science* **362**, eaam9288.

Wells, L. M., Sokratis Kalliakos, Bruno Villa, D. J. P. Ellis, R. M. Stevenson, A. J. Bennett, Ian Farrer, D. A. Ritchie, and A. J. Shields, 2019, "Photon Phase Shift at the Few-Photon Level and Optical Switching by a Quantum Dot in a Microcavity," *Phys. Rev. Appl.* **11**, 061001.

Werner, Reinhard F., 2001, "All teleportation and dense coding schemes," *J. Phys. A* **34**, 7081.

Wiesner, Stephen, 1983, "Conjugate coding," *ACM SIGACT News* **15**, 78–88.

Wolf, Michael M., David Pérez-García, and Geza Giedke, 2007, "Quantum Capacities of Bosonic Channels," *Phys. Rev. Lett.* **98**, 130501.

Wootters, W. K., and W. H. Zurek, 1982, "A single quantum cannot be cloned," *Nature (London)* **299**, 802–803.

Wootters, William K., 1998, "Entanglement of Formation of an Arbitrary State of Two Qubits," *Phys. Rev. Lett.* **80**, 2245–2248.

Xie, Yuan-Mei, Yu-Shuo Lu, Chen-Xun Weng, Xiao-Yu Cao, Zhao-Ying Jia, Yu Bao, Yang Wang, Yao Fu, Hua-Lei Yin, and Zeng-Bing Chen, 2022, “Breaking the rate-loss bound of quantum key distribution with asynchronous two-photon interference,” *PRX Quantum* **3**, 020315.

Xu, Feihu, Marcos Curty, Bing Qi, and Hoi-Kwong Lo, 2015, “Measurement-device-independent quantum cryptography,” *IEEE J. Sel. Top. Quantum Electron.* **21**, 148–158.

Xu, Feihu, Xiongfeng Ma, Qiang Zhang, Hoi-Kwong Lo, and Jian-Wei Pan, 2020, “Secure quantum key distribution with realistic devices,” *Rev. Mod. Phys.* **92**, 025002.

Xu, Zhongxiao, Yuelong Wu, Long Tian, Lirong Chen, Zhiying Zhang, Zhihui Yan, Shujing Li, Hai Wang, Changde Xie, and Kunchi Peng, 2013, “Long Lifetime and High-Fidelity Quantum Memory of Photonic Polarization Qubit by Lifting Zeeman Degeneracy,” *Phys. Rev. Lett.* **111**, 240503.

Yamamoto, Takashi, Masato Koashi, and Nobuyuki Imoto, 2001, “Concentration and purification scheme for two partially entangled photon pairs,” *Phys. Rev. A* **64**, 012304.

Yamamoto, Takashi, Masato Koashi, Şahin Kaya Özdemir, and Nobuyuki Imoto, 2003, “Experimental extraction of an entangled photon pair from two identically decohered pairs,” *Nature (London)* **421**, 343–346.

Yang, Sheng-Jun, Xu-Jie Wang, Xiao-Hui Bao, and Jian-Wei Pan, 2016, “An efficient quantum light-matter interface with sub-second lifetime,” *Nat. Photonics* **10**, 381–384.

Yehia, Raja, Simon Neves, Eleni Diamanti, and Iordanis Kerenidis, 2022, “Quantum city: Simulation of a practical near-term metropolitan quantum network,” *arXiv:2211.01190*.

Yin, Juan, *et al.*, 2017, “Satellite-based entanglement distribution over 1200 kilometers,” *Science* **356**, 1140–1144.

Yu, Leo, *et al.*, 2015, “Two-photon interference at telecom wavelengths for time-bin-encoded single photons from quantum-dot spin qubits,” *Nat. Commun.* **6**, 8955.

Yu, Yong, *et al.*, 2020, “Entanglement of two quantum memories via fibres over dozens of kilometres,” *Nature (London)* **578**, 240–245.

Yu, Zong-Wen, Xiao-Long Hu, Cong Jiang, Hai Xu, and Xiang-Bin Wang, 2019, “Sending-or-not-sending twin-field quantum key distribution in practice,” *Sci. Rep.* **9**, 3080.

Zaidi, Hussain A., Chris Dawson, Peter van Loock, and Terry Rudolph, 2015, “Near-deterministic creation of universal cluster states with probabilistic Bell measurements and three-qubit resource states,” *Phys. Rev. A* **91**, 042301.

Zanin, Guilherme Luiz, Maxime J. Jacquet, Michele Spagnolo, Peter Schiavone, Irati Alonso Calafell, Lee A. Rozema, and Philip Walther, 2021, “Fiber-compatible photonic feed-forward with 99% fidelity,” *Opt. Express* **29**, 3425–3437.

Zaske, Sebastian, *et al.*, 2012, “Visible-to-Telecom Quantum Frequency Conversion of Light from a Single Quantum Emitter,” *Phys. Rev. Lett.* **109**, 147404.

Zeng, Pei, Hongyi Zhou, Weijie Wu, and Xiongfeng Ma, 2022, “Mode-pairing quantum key distribution,” *Nat. Commun.* **13**, 3903.

Zhan, Yuan, Paul Hilaire, Edwin Barnes, Sophia E. Economou, and Shuo Sun, 2023, “Performance analysis of quantum repeaters enabled by deterministically generated photonic graph states,” *Quantum* **7**, 924.

Zhan, Yuan, and Shuo Sun, 2020, “Deterministic Generation of Loss-Tolerant Photonic Cluster States with a Single Quantum Emitter,” *Phys. Rev. Lett.* **125**, 223601.

Zhang, Qiang, Xiao-Hui Bao, Chao-Yang Lu, Xiao-Qi Zhou, Tao Yang, Terry Rudolph, and Jian-Wei Pan, 2008, “Demonstration of a scheme for the generation of ‘event-ready’ entangled photon pairs from a single-photon source,” *Phys. Rev. A* **77**, 062316.

Zhang, Rui, Li-Zheng Liu, Zheng-Da Li, Yue-Yang Fei, Xu-Fei Yin, Li Li, Nai-Le Liu, Yingqiu Mao, Yu-Ao Chen, and Jian-Wei Pan, 2022, “Loss-tolerant all-photonic quantum repeater with generalized Shor code,” *Optica* **9**, 152–158.

Zhang, Wei, *et al.*, 2022, “A device-independent quantum key distribution system for distant users,” *Nature (London)* **607**, 687–691.

Zhong, Han-Sen, *et al.*, 2018, “12-Photon Entanglement and Scalable Scattershot Boson Sampling with Optimal Entangled-Photon Pairs from Parametric Down-Conversion,” *Phys. Rev. Lett.* **121**, 250505.

Zhong, Manjin, Morgan P. Hedges, Rose L. Ahlefeldt, John G. Bartholomew, Sarah E. Beavan, Sven M. Wittig, Jevon J. Longdell, and Matthew J. Sellars, 2015, “Optically addressable nuclear spins in a solid with a six-hour coherence time,” *Nature (London)* **517**, 177–180.

Zhong, Tian, and Philippe Goldner, 2019, “Emerging rare-earth doped material platforms for quantum nanophotonics,” *Nanophotonics* **8**, 2003–2015.

Zhong, Tian, Jonathan M. Kindem, Evan Miyazono, and Andrei Faraon, 2015, “Nanophotonic coherent light-matter interfaces based on rare-earth-doped crystals,” *Nat. Commun.* **6**, 8206.

Zhong, Xiaoqing, Jianyong Hu, Marcos Curty, Li Qian, and Hoi-Kwong Lo, 2019, “Proof-of-Principle Experimental Demonstration of Twin-Field Type Quantum Key Distribution,” *Phys. Rev. Lett.* **123**, 100506.

Zhong, Xiaoqing, Wenyuan Wang, Reem Mandil, Hoi-Kwong Lo, and Li Qian, 2022, “Simple Multiuser Twin-Field Quantum Key Distribution Network,” *Phys. Rev. Appl.* **17**, 014025.

Zhong, Xiaoqing, Wenyuan Wang, Li Qian, and Hoi-Kwong Lo, 2021, “Proof-of-principle experimental demonstration of twin-field quantum key distribution over optical channels with asymmetric losses,” *npj Quantum Inf.* **7**, 6.

Zhou, Lai, Jinping Lin, Yuan-Mei Xie, Yu-Shuo Lu, Yumang Jing, Hua-Lei Yin, and Zhiliang Yuan, 2023, “Experimental Quantum Communication Overcomes the Rate-Loss Limit Without Global Phase Tracking,” *Phys. Rev. Lett.* **130**, 250801.

Zhou, Lan, Wei Zhong, and Yu-Bo Sheng, 2020, “Purification of the residual entanglement,” *Opt. Express* **28**, 2291–2301.

Zhu, Hao-Tao, *et al.*, 2023, “Experimental Mode-Pairing Measurement-Device-Independent Quantum Key Distribution without Global Phase Locking,” *Phys. Rev. Lett.* **130**, 030801.

Zukowski, M., A. Zeilinger, M. A. Horne, and A. K. Ekert, 1993, “Event-Ready-Detectors Bell Experiment via Entanglement Swapping,” *Phys. Rev. Lett.* **71**, 4287.

Zwerger, M., H. J. Briegel, and W. Dür, 2014, “Hybrid architecture for encoded measurement-based quantum computation,” *Sci. Rep.* **4**, 5364.

Zwerger, M., H. J. Briegel, and W. Dür, 2016, “Measurement-based quantum communication,” *Appl. Phys. B* **122**, 50.

Zwerger, M., W. Dür, and H. J. Briegel, 2012, “Measurement-based quantum repeaters,” *Phys. Rev. A* **85**, 062326.

Zwerger, M., A. Pirker, V. Dunjko, H. J. Briegel, and W. Dür, 2018, “Long-Range Big Quantum-Data Transmission,” *Phys. Rev. Lett.* **120**, 030503.